ENGINEERING LEUKOCYTE INTEGRINS FOR THERAPEUTIC DEVELOPMENT AGAINST INFLAMMATORY DISEASES

A Dissertation

Presented to the Faculty of the Graduate School

of Cornell University

In Partial Fulfillment of the Requirements for the Degree of

Doctor of Philosophy

by

Sungkwon Kang

January 2012

ENGINEERING LEUKOCYTE INTEGRINS FOR THERAPEUTIC DEVELOPMENT AGAINST INFLAMMATORY DISEASES

Sungkwon Kang, Ph. D.

Cornell University 2012

Inflammation is considered as a hallmark of host defense against infections and injuries. On the flipside, prolonged and non-resolving chronic inflammation is also associated with various pathological conditions. In the immune and inflammatory responses, it is the leukocyte integrins and their physiologic ligands that provide the essential molecular basis for cell adhesion and recognition. As important as these molecules are in maintaining healthy immune system, aberrant activities have been implicated in dysregulated inflammation, making integrins and their ligands a major therapeutic target. In this dissertation, I have developed and applied protein engineering techniques for modulating structure and function of integrins and their ligands, and thereby rendering opportunities for therapeutic development.

Integrins have at least two distinct conformations, denoted as inactive or active. We have engineered the major ligand binding domains, or the inserted (I) domains, of leukocyte integrins into an activated state, competent for ligand binding. Possessing the ability to harness the I domains expressed in their inactive (wild-type) and active (high affinity mutants) states allowed us to discover neoepitope specific antibodies that preferentially bind to the active conformation of integrins. This was a streamlined process performed with the novel protein engineering platform, yeast surface two-hybrid, that we developed, which greatly facilitated the process of antigen engineering and novel antibody discovery. The discovered antibody potently inhibited

leukocyte migration on ligand coated surfaces. Such antibodies specific against active conformation of integrins may be safer and administered at lower dosages, and result in better clinical outcomes.

We also used the engineered I domains to create drug and gene delivery nanoparticles that mimic how leukocytes would bind and migrate selectively to inflammatory sites. More specifically, we used the I domain derived from the integrin lymphocyte function associated antigen-1 (LFA-1) for inflammation-specific accumulation of anti-inflammatory drugs, which otherwise would create systemic cytotoxicity. Delivery by the I domain was inflammation-specific because the physiological ligand of LFA-1, intercellular adhesion molecule-1 (ICAM-1) has a highly inducible expression on numerous cell types, including endothelial cells and immune cells. Specificity toward inflammation was dependent on the avidity of the I domain on delivery vehicles, and such optimally adjusted multimeric binding to ICAM-1 elicited rapid endocytosis. In this dissertation, I demonstrate that the use of the interaction between ICAM-1 and the engineered I domain provide a great opportunity to pierce through the barriers of gene delivery systems, with the addition of one more component for endosomal escape. Indeed, by using a cationic polymer previously known to elicit efficient endosomal escape, we were able to formulate nanoparticles that deliver genes like viruses, with improved gene transfer efficiency and for systemic applications. We anticipate that our virus-like particles may greatly contribute to a successful translation of such therapeutics into the clinics.

BIOGRAPHICAL SKETCH

Sungkwon is the second child born to a Korean family between Kwang Suk Kang and Se Ran Ahn in Lima, Peru in August of 1983. It was while they were stationed in the country to work at the Korean embassy. His sister, Keung Min, was four at the time. Sungkwon attended kindergarten and elementary school in Peru—he enjoyed his childhood there, playing in the pool with friends and out in the field hitting golf balls every weekend. His family moved back to Korea in October 1990, where he continued with elementary school till middle school. That is when he faced much competition in school for the first time, though he never cared to study hard. Fortunately, in 1999 his parents were once again stationed to work at the Korean embassy, this time in Bogotá, Colombia. Sungkwon attended a bilingual international high school, Colegio Nueva Granada, starting in 10^{th} grade. He enjoyed much of his time there of course, with the ecstatic feeling to be free from the arduous schooling in Korea. However, it was then in high school when he genuinely developed his interests in mathematics and science, influenced by his nerdy friends Brian Skinner and Richard Foster. He and his friends won the Best Senior Independent Study Award at the end of the senior year.

Sungkwon then decided to pursue his undergraduate studies in the United States, and attended Virginia Polytechnic Institute and State University (Virginia Tech) in 2002, with majors in mechanical engineering and applied computational mathematics. During the years as a college student at Virginia Tech, he also had professional experiences to work as an intern at e-Castle Electronics in 2003, and as a co-op engineer at Georgia-Pacific in 2005. Although his immediate interests within the fields of engineering was automation and robotics, he was eventually drawn into biomedical engineering and biotechnology. Amazed by how biological systems work

at the cellular and molecular level, he joined Dr. Yong Woo Lee's Vascular Biology Lab in 2005 and developed basic research skills. During the two years period at Dr. Lee's lab, he published numerous abstracts and presented at conferences, and by the time of graduation in 2007, he contributed as a second author in a peer reviewed journal paper. Sungkwon came to Cornell in 2007 and has worked with Dr. Moonsoo Jin ever since, on various protein engineering projects and drug/gene delivery systems, and has had productive Ph.D. years. Sungkwon was awarded a Graduate Research Award from the Biomedical Engineering Society in 2008. He won a Predoctoral Fellowship Award from the American Heart Association in 2010. He was also awarded a Mogam Science Scholarship in the same year. Since coming to Cornell, he has had the opportunity to publish one first authored paper and three second authored papers, and he will soon publish two more first authored papers. From January 2012 he is situated in Korea and will work for LG Life Sciences as an assistant research manager.

Dedicated to Mom and Dad, and to my sister.

For their constant love and sacrifice.

ACKNOWLEDGMENTS

First and foremost, I would like to express my deepest and sincerest appreciation to my advisor, Dr. Moonsoo Jin, for everything he has done for me. Dr. Jin is a thorough, self-critical, and enthusiastic scientist who believes nothing is impossible, and I hope I have acquired these traits for my future career. Looking back over the years of my training, I can only find how much I have grown intellectually and personally since the first day of joining his lab. Every conversation was a new lesson to learn and every lecture was an eye-opening experience for me. I have been constantly amazed and inspired by his attentiveness, perseverance, and the ability to connect on a broad range of topics, spanning many disciplines. I thank him for all that I have learned from him, and most importantly of course, for I have learned how to learn, and learn very well, all of which will undoubtedly make the rest of my life much richer and fuller in so many different ways.

I would also like to thank my committee members, Drs. Matthew DeLisa and John Parker, for all the help they have provided during my training. I am also indebted to Dr. Peter Doerschuk, the tallest man with the most delightful laughter in the hallway, for all the encouragements and cheers I have had. I would like to extend a special thank you to Belinda for the superfast administrative support and the warmest welcomes whenever I dropped by her office.

I have had the luxury to work with many talented lab members; Jin lab is the place where I have constantly tested my limits every day and night for months and years, and it is with them I have been able to endure the seemingly everlasting challenges. I have learned a great deal from the post docs, Xuebo, Ling, Taehyun, and Roisin, and without their technical help and fruitful discussions, I would not have had the success I have today. I also thank my dear labmates, Zoe, Spencer, Fai, Yvonne,

Richard, and Yogi, for all their help and support. I have great memories because of all the fun moments I have shared with Tricia, Marina, Leslie, Brian, Dave, Milly and Kristin. Our lab was such a fun place to work because it was also a place to befriend fellow students—I owe a big thank you to Nikolai, Nina, Greg, Tanwi, Turner, Susan, Gig, Andrew, Kathleen, Ada, Jared, Yoshi, and Marjan for being wonderful and encouraging. I am especially grateful and indebted to Kevin—it is more than probable that I could not have finished much of the work presented in this dissertation without his diligent help. I am also thankful to our forever neighbor, Dr. Fischbach and her lab members, Scott, Bo Ri, Young Hye, Dan, Emily, Sid, David, and Maureen. I must confess that I have many times sneaked and stolen much coffee from Dr. Schaffer's lab—the high quality illy coffee has definitely been a major source of fuel for my lab work.

I would like to thank my other half, Na Young, for all the love and support she has given me. She has taught me that there is more to life than work and success; even during the busiest days we always had so much fun; she and I were always together, from the morning to the evening, for every meal and for any free snack, anytime and everywhere in the building, on campus and off campus. I have learned so much from her to become a better person every day, and I am thankful that she has been way more than my other half to me.

Finally, I would like to acknowledge the financial support from the American Heart Association.

TABLE OF CONTENTS

LIST OF FIGURES

LIST OF TABLES

CHAPTER 1

INTRODUCTION

Inflammation, integrins, and therapeutics

Inflammation is arguably one of the most important host defenses to injuries and infections occurring in vascularized tissues. Inflammation is characterized by swelling and redness of tissues that are often associated with heat, pain, and loss of function. In response to injuries and infections, a complex conglomerate of biochemical signals is released from the damaged tissue, which initiates and maintains the inflammatory reactions to heal the afflicted site or to remove the infecting agents (Fig. 1.1). Initial signals include the secretion of pro-inflammatory chemokines and cytokines that regulate the expression of various adhesion molecules and extracellular proteases as well as the activation of cell surface receptors [1-4]. All of these responses in concert attract white blood cells or leukocytes, the major immune cells that defend our body against infectious foreign materials, specifically at the site of injuries (Fig. 1.1) [5-6]. Following the responses initiated by pro-inflammatory mediators is the anti-inflammatory responses that abate those cellular activities, once the tissue damages are tamed under control. When the balance between pro- and anti-inflammatory responses is disrupted, such as in the case of prolonged and dysregulated chronic inflammation, this non-resolving host response can lead to debilitating pathological conditions [7-11].

Like many other immune responses, the inflammatory response is the result of complex cell-cell communications existing in many different types of cells in our body. Leukocyte adhesion and migration through the endothelial lining of blood

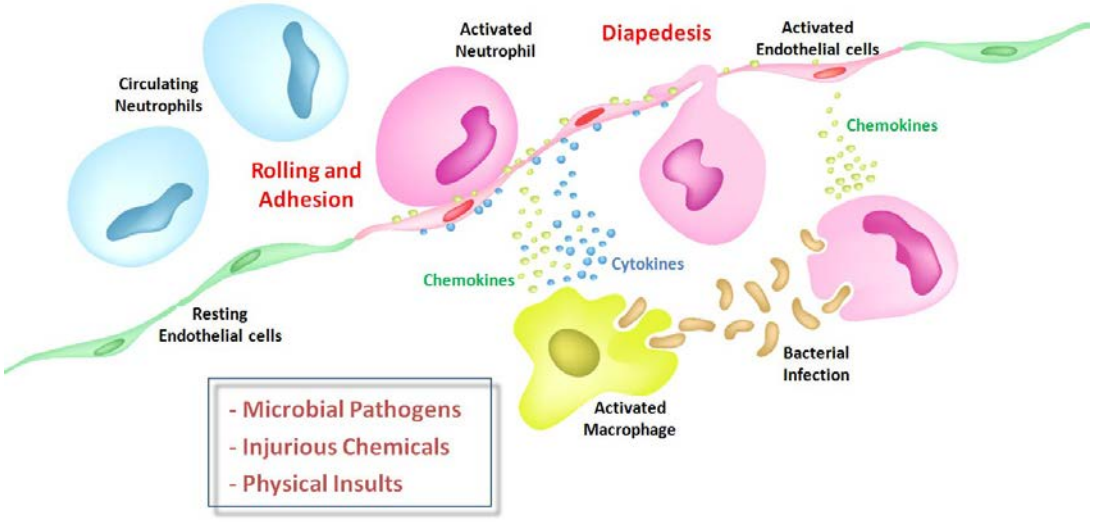

Figure 1.1. The inflammatory response of vascularized tissue.

Irritated inflammatory tissue recruits leukocytes, such as neutrophils and monocyte/macrophages through activated endothelial cells, involving the steps of rolling, strengthening of adhesion, intramural crawling, and paracellular and transcellular migration (diapedesis). Subsequently, migrated leukocytes secrete pro-inflammatory cytokines and chemokines that further activates the surrounding tissue to recruit more immune cells. (Illustration designed and rendered by Sungkwon Kang)

vessels [5-6, 12] is a representative event of such cell-cell interactions in inflammation, as it was observed and recognized more than 100 years ago by intravital microscopy [13]. However, the underlying molecular interactions of how cells adhere to one another, a process that also occurs at the immunological synapse or in the formation of organs, were little understood until the 1970's. In fact, it was the advent of the use of monoclonal antibodies for biochemical studies and various other techniques developed in molecular biology that have exponentially expanded our understanding of how cells recognize other cells at the molecular level. Indeed, only after monoclonal antibodies have various discoveries been made of novel antigens and receptors that regulate the host immune and inflammatory responses. One of the first molecules discovered was the antigen presentation and T cell receptor recognition between target cells and killer lymphocytes. Later, lymphocyte function associated antigen-1 (LFA-1; $\alpha_L\beta_2$) was discovered as the molecule that supports the important cell adhesion involved in those immunological and inflammatory responses of the killer lymphocytes [14-16]. LFA-1 was characterized as a noncovalently associated heterodimer between α and β polypeptides [17-19], and together with other homologous molecules it was later classified as a member of integrin family. The counter-receptor for LFA-1 was subsequently discovered and was named as intercellular adhesion molecule-1 (ICAM-1) [20]. The interaction between LFA-1 and ICAM-1 was found to be required for the firm adhesion of leukocytes to inflamed endothelial cells, together with other cell surface molecules such as selectins that mediate the initial rolling onto the vessel wall [5-6, 12-13, 21]. More detailed functions of integrins were also revealed along the way: integrins on leukocytes requires activation for firm adhesion to their ligands, triggered by chemoattractants that bind to G protein-coupled receptors [22]. Thus far, 18 distinct α subunits and 8 β subunits have been characterized, different pairings of which can

generate at least 24 unique integrins [23-24]. A subset of integrins predominantly found on leukocytes has been denoted as leukocyte integrins (Fig. 1.2), which includes LFA-1 and two others, macrophage differentiation antigen-1 (Mac-1; $\alpha_M\beta_2$) and very late activation antigen-4 (VLA-4; $\alpha_4\beta_1$) [25-27].

As important as integrins are for the maintenance of healthy immune and inflammatory responses, leukocyte infiltration mediated by integrins and ligands have been linked to pathological conditions of various diseases [25]. The immunologic defects in patients with leukocyte adhesion deficiency I are mainly caused by loss-of-function mutations in the β_2 subunit, a polypeptide chain commonly shared by LFA-1 and Mac-1 integrins [28]. Under various pathological conditions, on the other hand, leukocyte recruitment can be dysregulated by aberrant activation of integrins that cause tissue damages, eventually leading to irreversible tissue necrosis and loss of functionality. This includes the events of ischemia and reperfusion injury such as stroke and myocardial ischemia and infarction, and various autoimmune disorders including psoriasis, multiple sclerosis, and rheumatoid arthritis [29]. Moreover, pathogenesis of various diseases commonly associated with non-resolving chronic inflammation, such as inflammatory bowel disease and atherosclerosis, has been closely associated with abnormal immune cell activities that largely depend on the interaction of leukocyte integrins [7-8, 25, 30-31]. More recently, inflammation has been widely accepted as a critical component of cancer initiation, progression, and metastasis (Fig. 1.3) [11, 32-33], though the question of whether it directly causes or indirectly aids the processes involved in the development of cancer is still under investigation. Nonetheless, important roles of inflammation in cancer have been elucidated, and have been implicated in the promotion of angiogenesis and neoplastic proliferation (Fig. 1.3) [34-36]. Furthermore, cancer cells can co-opt different types

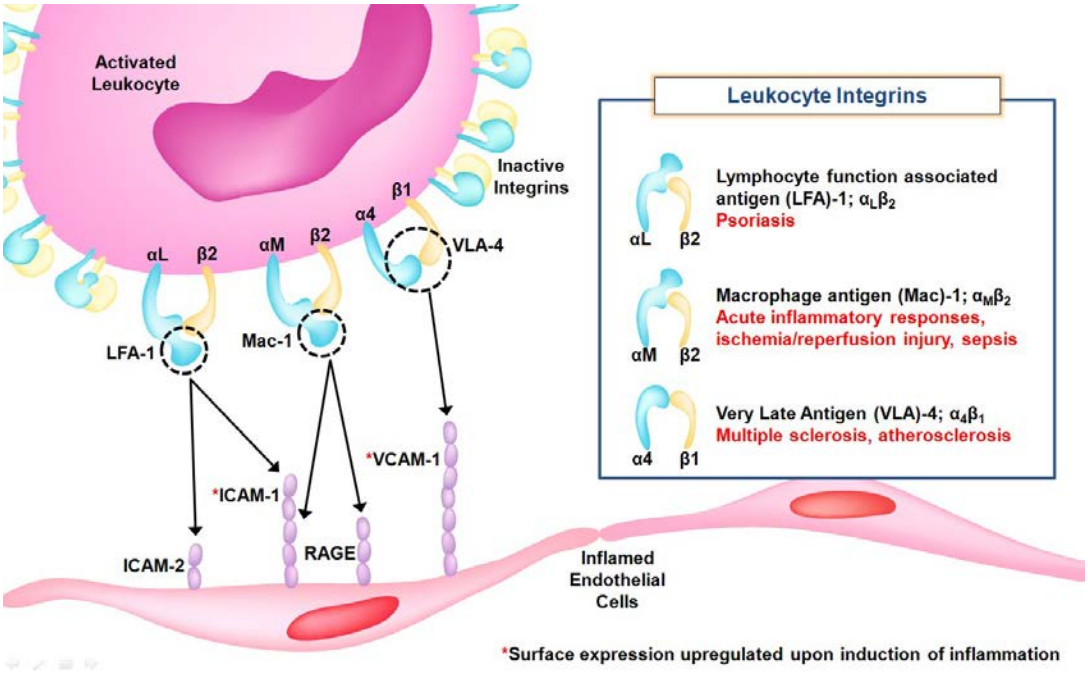

Figure 1.2. Leukocyte integrins and the physiologic ligands.

Three major leukocyte integrins include lymphocyte function associated antigen-1 (LFA-1), macrophage antigen-1 (Mac-1), and very late antigen-4 (VLA-4). Activated integrins bind to their physiologic ligands through the top of the extended form, indicated with dotted circles. LFA-1 binds to ICAM-1 and -2. Mac-1 binds to ICAM-1 and RAGE (receptor for advanced glycation products). VLA-4 binds to VCAM-1. The expression of ICAM-1 and VCAM-1 are upregulated on inflamed endothelial cells. (Illustration designed and rendered by Sungkwon Kang)

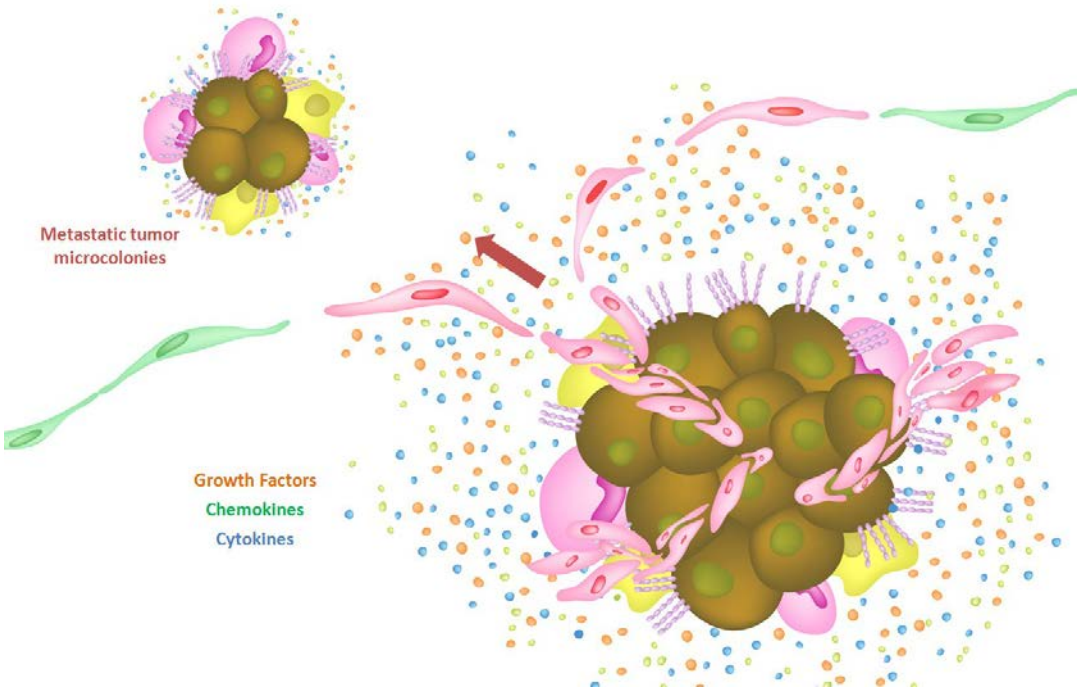

Figure 1.3. Inflammation and cancer.

A conglomerate of inflammatory biochemical signals are released from tumors and its stroma, including growth factors (orange), chemokines (green), and cytokines (blue), that together promote angiogenesis, neoplastic proliferation. Cancer cells can co-opt cell adhesion molecules for extravasation and invasion. Neovasculatures provide an egress route for metastatic tumor microcolonies. (Illustration designed and rendered by Sungkwon Kang)

of leukocytes to exploit integrins and other adhesion molecules for extravasation and invasion (Fig. 1.3) [37-38].

For these various reasons, leukocyte integrins are of particular interests for the development of antagonists as therapeutics against many different clinical disorders [25]. Antibodies against leukocyte integrins are currently being used in the clinic as therapeutics against diverse conditions of immune and inflammatory dysfunctions, including psoriasis [39], multiple sclerosis [40], and inflammatory bowel disease [41]. Psoriasis is a common skin disorder characterized by sharply demarcated chronic skin inflammation often covered by white skin scales. This is the result of autoimmune response of infiltrating leukocytes, such as macrophages, lymphocytes, and neutrophils, into the epidermal layer [39, 42]. Importance of LFA-1 integrin in leukocyte recruitment led to the development of a function-blocking antibody named efalizumab [43-44], which was approved for clinical use by the Food and Drug Administration (FDA) in 2003 with the trade name Raptiva (Genentech). Efalizumab is directed against the major ligand binding domain in the α_L chain of LFA-1 integrin, used for moderate and severe cases of psoriasis. Another example of an antibody against leukocyte integrins is natalizumab [40, 45], approved by FDA in 2004 for the treatment of multiple sclerosis with the trade name Tysabri (Biogen). Multiple sclerosis is a chronic inflammatory neurologic disorder characterized by lesions in the white matter in the brain, which eventually disables many patients. Similarly, multiple sclerosis is also an autoimmune disorder of leukocytes, mediated by the interaction between VLA-4 and its ligands such as vascular-cell adhesion molecule-1 (VCAM-1) and mucosal addressin-cell adhesion molecule-1 (MAdCAM-1) [46]. This is because the interaction of VLA-4 with VCAM-1 and MAdCAM-1 is required for leukocytes to enter the central nervous system and the intestine, respectively. Natalizumab inhibits the entry of those leukocytes into the brain and spinal cord by

binding to the α_4 chain of VLA-4 and thereby decreasing lesion formations. As integrins mediate leukocyte entry into the intestine, natalizumab has also shown efficacy against Crohn's disease, which is a type of inflammatory bowel disease [47].

Structure and function of integrins and its ligands

The ability of immunocompetent cells to reach sites of infection and inflammation is one of the most important functions of the immune system. All circulating blood leukocytes and their associated functions, such as neutrophil recruitment, lymphocyte recirculation, and monocyte trafficking, require adhesion and transmigration through blood vessel walls. Constant extravasation of blood leukocytes, which involves steps of rolling, strengthening of adhesion, intraluminal crawling, and paracellular and transcellular migration, is required for proper immune surveillance and prompt development of inflammatory responses [48]. Integrins are the major cell receptors that mediate firm leukocyte arrest to the adhesion molecules and function as traction sites over which they migrate [49-50].

Integrins are non-covalently associated αβ heterodimeric cell surface receptors (Fig. 1.4). Upon activation by intracellular signals, integrins exhibit global conformational rearrangements in the extracellular domains, a process resembles a switchblade extension (Fig. 1.4) [24]. Integrins in an inactive state exist in a bent conformation with the ‘headpiece’ folded over the ‘tailpiece’ [51-53]. The global conformational change of the extracellular portion of integrins from low to high affinity binding to ligands involves the switchblade-like extension of the head [54], and the separation of the α and β subunits at their cytoplasmic, transmembrane, and leg domains (Fig. 1.4). The ‘head’ in integrin directly interacts with diverse cell surface and extracellular ligands, with its affinity regulated by allostery. Dynamic

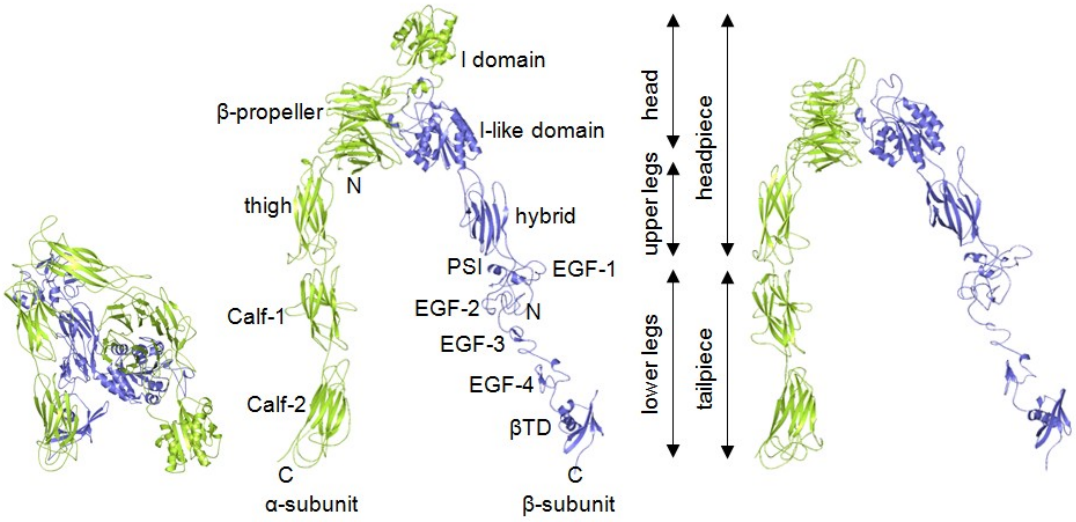

Figure 1.4. Global conformational rearrangements of integrin.

Inactive integrin exists in a bent conformation with the headpiece folded over the tailpiece. Active integrin exhibits the switchblade-like extension and the separation of the α (green) and β (blue) subunits at their cytoplasmic, transmembrane, and leg domains. Two types of integrins, I domain containing and non-I domain containing, are shown in ribbon diagram with detailed structural features. Model structures were constructed based on the crystal structures of integrin $\alpha_{IIb}\beta_3$ and $\alpha_v\beta_3$ [51-53]. Ribbon diagrams were made using PyMOL (DeLano, W.L.).

and large-scale quaternary structural rearrangement of integrins in the extracellular, transmembrane, and cytoplasmic domains transmit signals bidirectionally across the plasma membrane.

During the structural rearrangements from bent to extended conformations, integrins exhibit three distinct conformational or affinity states. These conformational states are bent conformer, extended conformer with a closed headpiece, and extended conformer with an open headpiece, representing the low, intermediate, and high affinity states to ligands, respectively [55]. The distinct affinity states were elucidated by electron microscopy (EM) studies from which integrins were found to exist predominantly in bent conformation, representing physiologically relevant low affinity state [56]. At the bent conformational state, integrins have numbers of intra- and intersubunit interfaces. Some of the major intrasubunit interfaces include β- propeller/thigh and thigh/Calf-1 domains in the α subunit, I-like/hybrid domains in the β subunit. Intersubunit interfaces are formed between β-propeller/I-like, Calf-1/EGF-3, Calf-2/EGF-4, and Calf-2/βTD domains of each subunit [57]. Integrin can be activated upon addition of Mn^{2+} which induces a mixture of all three conformational states observed in EM studies. Disulfide bond studies showed that integrin locked in the bent conformation is unable to bind ligands with high affinity, providing evidence that the extension of the ectodomain is a prerequisite event for regulation of affinity and ligand binding [58]. Once extended, separation of the integrin leg domains can also further regulate affinity states. Previous studies of integrins with a releasable clasp, connecting the two C-termini of the α and β subunits, showed that extended conformers with clasp (α and β legs restrained from separation) and clasp released resulted in intermediate and high affinity states, respectively [54, 58]. Upon extension, the domains in the headpiece and the tailpiece of the α subunit stay relatively unchanged whereas the β subunit

headpiece extends between the I-like and hybrid domains and the tailpiece shows highly flexible structural variation [54].

Global structural rearrangements of integrins that transmit interdomain conformational shifts eventually lead to the allosteric activation of the major ligand binding domains in the head of integrins. Of eighteen α subunits, nine contain a domain called the inserted (I) domain. The I domain is the major ligand-binding site for those integrins containing the I domain (Fig. 1.5). All 8 β subunits contain a domain called the I-like domain (Fig. 1.5), which is structurally homologous to the I domain. In integrins lacking the I domain, the β-propeller domain in the α subunit and the I-like domain in the β subunit provide the binding site for ligands. The metal ion and the neighboring residues at the top of the I or I-like domains, termed the metal-ion dependent adhesion site (MIDAS), is the major interaction site with the ligands (Fig. 1.5). Both the I and the I-like domains exhibit allostery in the conformational change from inactive to active states, where the downward displacement of the C-terminal α7-helix induces the high affinity conformation of the MIDAS [52]. There are two additional metal binding sites in the I-like domains, termed ADMIDAS (adjacent to MIDAS) and SyMBS (synergistic metal ion binding site) at either side of the MIDAS, which play negative and positive regulatory roles in the MIDAS activation, respectively (Fig. 1.5) [59]. The extension of the integrin head swings out the hybrid domain, which pulls down the α7-helix to induce high affinity conformation in the I-like domain. In I domain containing integrins, the activation of the I-like domain in turn pulls down an acidic residue at the C-terminal α7-helix of the I domain to trigger the activation of the I domain [60].

The most biologically important physiologic ligands of leukocyte integrins are ICAM-1 and VCAM-1. Expression of these cell adhesion molecules is upregulated in a range of cell types during the course of acute and chronic inflammation, and is

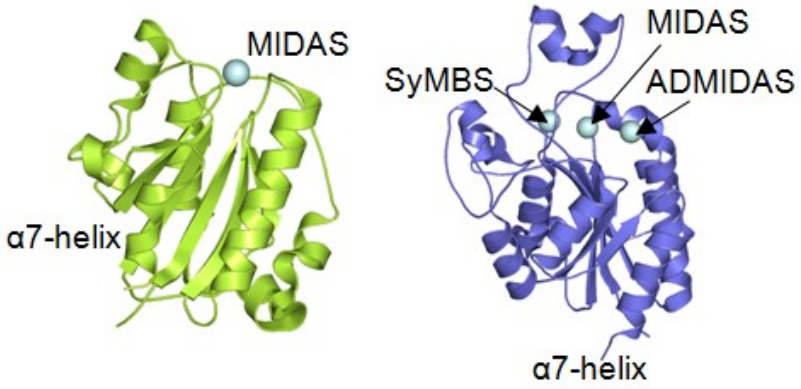

Figure 1.5. Metal ion binding sites of α I domain and β I-like domains.

The metal ion at the top of the I (green) or I-like (blue) domains, termed the metal-ion dependent adhesion site (MIDAS), is the major interaction site with the ligands. There are two additional metal binding sites in the I-like domains, termed ADMIDAS (adjacent to MIDAS) and SyMBS (synergistic metal ion binding site) at either side of the MIDAS. Both the I and the I-like domains exhibit allostery in the conformational change from inactive to active states, where the downward displacement of the C-terminal α7-helix induces high affinity conformation of the MIDAS. Ribbon diagrams for the structures of the I domain and the I-like domain [52] were made using PyMOL (DeLano, W.L.).

induced by chemokines and cytokines as well as injurious chemicals and endotoxins [61-62]. Although constitutively expressed at low levels on cell surfaces, adhesiveness to immune cells does not arise until rapid upregulation and dense expression of ICAM-1 are elicited. Expression of VCAM-1, on the other hand, is more tightly regulated and is detected mainly at areas of inflammation, but with much lower cell surface density [63]. Upregulation of ICAM-1 and VCAM-1 expression is mediated by the activity of nuclear factor kappa B (NF-κB), the major transcription factor that modulates most inflammatory responses [64-65]. Because ICAM-1 and VCAM-1 mediate recruitment of lymphocytes and myeloid cells, these cell adhesion molecules are also important therapeutic targets to inhibit immune cell migration in inflammatory diseases. Moreover, regardless of their positive and negative roles in the pathogenesis of inflammatory diseases, localized and highly upregulated expression at the sites of disease makes ICAM-1 and VCAM-1 attractive targets for site-directed therapeutic drug/gene delivery systems. In addition, multivalent receptor-mediated clustering of ICAM-1 and VCAM-1 induces rapid clathrin-independent endocytosis [66], rendering these molecules ideal target for intracellular drug delivery.

ICAM-1 and VCAM-1 are members of the immunoglobulin superfamily (IgSF), having five and seven heavily glycosylated extracellular ectodomains, respectively. The first N-terminal domain (D1) of ICAM-1 binds LFA-1 integrin, by means of the Glu-34 side chain of ICAM-1 D1 which docks into the top of the I domain, completing the metal ion coordination of the MIDAS. ICAM-1 is also subverted as a receptor for major human rhinoviruses, which bind the N-terminal face of D1, distinct from the binding site of LFA-1 I domain. The third domain (D3) of ICAM-1 interacts with Mac-1 integrin. The efficiency of their interaction has been hypothesized to be regulated by the extent of N-linked glycosylation levels in the

nearby region. Similarly, VCAM-1 has an N-terminal extracellular domain with VLA-4 integrin binding motifs in domains 1 and 4. The detailed structural basis of how VCAM-1 binds to VLA-4 is not yet known. However, based on mutational studies on VCAM-1 and other relevant integrin structural studies, it is speculated that the acidic residue (Asp-40) in VCAM-1 D1, a part of the integrin binding motif Q38IDSPL, would coordinate to the MIDAS of the I-like domain in β_1 chain of VLA-4.

Inflammation and atherosclerosis

Pathological consequences of atherosclerosis, such as myocardial infarction and cerebral infarction, overwhelmingly contribute to the incidence of mortality and morbidity. High mortality rate of atherosclerotic diseases lies in the asymptomatic nature of vascular lesions which develop as lipids and fibrous elements accumulate in the intima of elastic arteries. Indeed, the development of atherosclerotic plaques, beginning with fatty acid streaks, through stages of atheromas, and fibroatheromas, to complicated and vulnerable lesions, can progress asymptomatically over several decades. On the contrary, the final obstructive event causes sudden and irreversible tissue damages when vulnerable plaques rupture and release fibrofatty thrombi that occlude downstream arteries. Because seemingly healthy individuals can develop vulnerable lesions and become victims of acute life-threatening complications, halting and even reversing disease progression at early stages of atherosclerosis have been considered important.

Atherosclerotic lesions are characterized by asymmetric local thickenings of the three concentric aortic vascular layers—intima, media, and adventitia—which include endothelial cells, smooth muscle cells, and extracellular matrix (Fig. 1.6).

Progression of atherosclerotic lesions, from its inception to the development of complications, is closely associated with various hallmarks of chronic inflammatory conditions [8, 30-31, 67]. In particular, activation of endothelial cells followed by subsequent recruitment and intimal/adventitial retention of immune cells play a central role in atherogenesis. Pathophysiological stimuli, mainly involving hemodynamic strain and infiltrating low-density lipoprotein (LDL) cholesterol, trigger local activation of endothelial cells, which in turn upregulate the expression of cell adhesion molecules [68-69]. Important molecules include ICAM-1, VCAM-1, P-selectin, and E-selectin that collectively provide a sticky surface for activated immune cells to adhere and thus allow them to migrate into the atherosclerotic lesions [61]. Upregulated expression of these molecules and active recruitment of immune cells in atherosclerosis are observed at both the arterial luminal endothelium and the angiogenic in-plaque neovasculature stemming from normal vasa vasorum [70]. Most accumulated B and T lymphocytes, and myeloid cells, which include monocyte-derived macrophages, foam cells, and dendritic cells, aggravate plaque development. Especially macrophages and foam cells exacerbate atherosclerosis via prolonged secretion of cytokines and chemokines, production of pro-inflammatory mediators, promotion of in-plaque angiogenesis and smooth muscle cell/immune proliferation, and intimal retention of lipoproteins (Fig. 1.6) [30-31, 71-72]. Moreover, pro-inflammatory mediators, elicit the production of reactive oxygen species (ROS) and oxidative modification of LDL (e.g. oxLDL). This inhibits normal egress of macrophages and lipid-laden foam cells from the lesions and thereby worsens plaque growth (Fig. 1.6) [73-74].

Because all stages of atherosclerosis are critically dependent on immune and inflammatory mechanisms, subverting these processes has therapeutic potential both *in vitro* and *in vivo*. Blocking immune cell adhesion in mouse models of

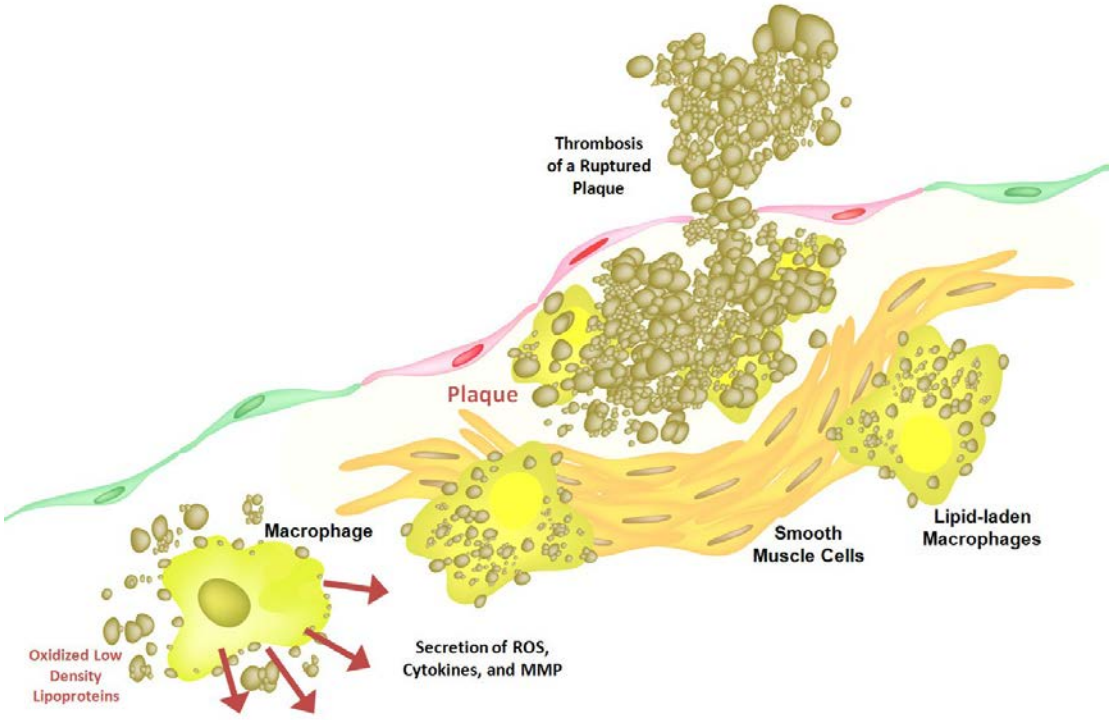

Figure 1.6. Inflammation and atherosclerosis.

Atherosclerotic lesions are characterized by asymmetric local thickenings of the aortic vascular layers that include endothelial cells, smooth muscle cells, and extracellular matrix. Infiltrating oxidized low-density lipoprotein (oxLDL) cholesterol triggers local activation of endothelial cells. Especially lipid-laden macrophages exacerbate atherosclerosis via prolonged secretion of cytokines and chemokines, matrix metalloproteinases (MMP), and reactive oxygen species (ROS). These pro-inflammatory mediators inhibit normal egress of lipid-laden foam cells into regional lymph nodes. Retention of macrophages in the intima eventually leads to rupturing of plaques, causing thrombosis in the downstream vessels. (Illustration designed and rendered by Sungkwon Kang)

atherosclerosis reduced lesion development [75-78], supporting the idea that inhibition of immune and inflammatory responses that aggravate disease progression can be an effective therapeutic strategy. Previous studies have shown that immunosuppressive glucocorticoids inhibit in-plaque neovascularization and immune cell proliferation, which resulted in suppression of intimal growth [79-81]. Moreover, applying antioxidants or inhibitors of nicotinamide adenine dinucleotide phosphate (NADPH) oxidase, which reduce oxidative stress induced by ROS and oxLDL, restores efficient emigration of foam cells into lymph nodes and results in plaque regression [73, 82-83]. However, despite the elucidation of the prevailing inflammatory responses at the site of atherosclerotic lesions and the corresponding development of various drugs, current therapeutic strategies have not integrated important advances in the field. Furthermore, systemic treatment of antioxidants and immunosuppressive drugs are associated with cytotoxic side effects and their low doses often fail to cause any therapeutic effect against intermediate and advanced lesions [84-85].

Integrin engineering for active conformation-specific antibody discovery

For biochemical and structural studies, integrins have been recombinantly expressed in a range of bacterial, yeast, insect, and mammalian cell expression systems, modularly or in their entirety. Studies with modularly expressed domains have provided with more detailed analyses of structural regulations and functions in the context of the entire global conformational changes. Especially the expression of major ligand binding domains (i.e. I domain or β-propeller/I-like domains) [86-88] have been of particular interest as it contains the interface for ligand binding and undergoes allosteric activation by switchblade-like extension of integrins. However,

because integrins are activated for higher affinity to ligands by the aforementioned global conformational rearrangements of the extracellular domains [54], modularly expressed major ligand binding domains are most often expressed in their inactive states. To understand the structural basis of integrin activation, previous studies have used various mutational techniques to stabilize these modular domains in activated states [89-90], competent for high affinity ligand binding.

The structural basis of allosteric switching of the I domain has been studied extensively. Early evidence of allosteric activation of I domains came from the first crystal structure of the I domain of α_M [91-92]. Further mutational studies for I domain activation was performed with various protein expression systems, including studies where cysteine disulfide bridge mutations in the I domain were designed to anchor the α7-helix in an active conformation [87, 90]. Some other studies demonstrated that single point mutations, can lead to higher affinity of the I domains. The structural basis of allosteric activation of integrins that do not possess I domains has also been investigated. In these studies, integrin headpieces were modularly expressed and crystallized in the presence of high affinity ligand-mimetic compounds to promote the active conformation [52, 94]. Other biochemical functional studies have demonstrated that these modular domains can be engineered for higher affinity by introducing N-linked glycosylation sites [95], at intra- and intersubunit interfaces to obstruct the bent conformer and thereby promote the extension of the integrin legs for activation. Also, as demonstrated with the I domains, I-like domains were also subject to cysteine disulfide bond mutations and point mutations for more stable and higher affinity interaction with ligands [59, 96].

One of the most powerful tools for I domain engineering into a high affinity conformation is directed evolution [89], an approach based on random mutagenesis

coupled with functional screening. One system uses baker's yeast, *Saccharomyces cerevisiae*, to display a protein of interest on the cell surface [97]. This allows direct analysis of the protein by conformation specific antibodies and physiologic ligands for structural and functional studies. Proteins are expressed as a fusion to agglutinin protein Aga2p, which forms disulfide bonds with cell surface protein Aga1p and is transported to the outermost cell wall. Construction of yeast libraries (functional size typically up to 10^8) is enabled by the ability of yeast cells to carry out highly efficient *in vivo* homologous recombination. The first application of directed evolution on integrin was the LFA-1 I domain, from which selected mutations led to an I domain with an affinity 200,000-fold higher to ICAM-1 than the wild-type [89]. The advantage of using directed evolution is that proteins that undergo complex allostery, such as the I domain, can be engineered for activation without *a priori* structural knowledge. The affinity of the LFA-1 I domain mutants for ICAM-1 varied depending on the position of the identified hot spots as well as the selection of amino acid substitution.

The ability to express integrins stabilized in inactive (wild-type) and active (high affinity mutants) conformations provides a strategy to screen antibodies that can specifically bind only to the active conformation [98-99]. Such antibodies could specifically target the subset of leukocytes that undergo aberrant activation under pathological conditions and might have therapeutic utility if it antagonized binding of the integrin to it its ligand [99-102]. Integrins in both active and inactive states are present on the surface of individual neutrophils. Integrins in their active form are found at the leading edge of the cell and inactive forms are found at the trailing edge [49-50]. Active conformation-specific antibodies were found by screening a human antibody phage library against an LFA-1 I domain engineered for high affinity with

subtractive panning against the wild-type [98-99]. The discovered antibody, named AL-57, is a ligand-mimetic, metal ion-dependent, activation specific antibody.

In this dissertation, I have documented my efforts to develop more efficient platforms for protein engineering and novel antibody discovery, based on our knowledge of integrin functions and structures. I first developed a novel yeast surface display system which expresses two proteins simultaneously. One protein is anchored on the yeast surface (bait) and the other is secreted as a soluble protein (prey). The system is designed such that only when the two proteins interact can peptide tags appended to the soluble protein would be detected by fluorescently labeled antibodies. We named the system as yeast surface two-hybrid (YS2H). Using YS2H, we demonstrated the directed evolution of LFA-1 I domain (mutagenesis library expressed as anchored bait) into high affinity states using AL-57 (expressed as a soluble prey) as a selective pressure. Along the way, we also developed a strategy to facilitate the discovery of antibodies that can bind to previously unknown epitopes. With this method we discovered antibodies that preferentially bind to the active conformation, but not to the wild-type, of Mac-1 I domain. This was a streamlined process starting with the engineering of Mac-1 I domain for high affinity conformation, and using the antigen to pan a phage human antibody library for the discovery of such conformation-specific antibody.

Integrin engineering for inflammation-specific targeted therapeutic delivery

Novel engineered drug delivery systems promise to greatly enhance the pharmacokinetics, bioavailability, and biodistribution of conventional ("free") drugs [103]. These delivery systems are particulate carriers, composed primarily of lipids,

polymers, or proteins, that encapsulate or associate with various therapeutics including small molecule drugs, siRNAs, and plasmids. One of the first drug carrier based therapeutics to be approved by the FDA for clinical use was the doxorubicin hydrochloride liposomes (Doxil) for the treatment of ovarian cancer and multiple myeloma [104]. The advantage of encapsulating the chemotherapy drug doxorubicin in liposomes is that it prolongs the circulation time, while tumors with fenestrated vascular endothelium would allow the preferential accumulation of these drug carriers, a mechanism called the enhanced permeation-retention effect. As opposed to the passive delivery of therapeutics, there has also been considerable interest in developing immunotargeting or site-directed carriers, most of which are designed for ligand/receptor interaction specific delivery of the payload [103]. This allows the therapeutics to actively accumulate at the site of disease, depending on the presence of target antigens, thereby significantly minimizing the required effective dosage, and the associated cytotoxicity and unwanted side effects.

Integrins have often been targeted by numerous delivery systems. Previous studies have demonstrated the delivery of drug/siRNA/gene carriers targeted by antibodies directed to integrins [105]. One of the best established paradigms in integrin biology is the recognition of proteins ligands through Arg-Gly-Asp (RGD) sequences, recognized by eight vertebrate integrins including $\alpha_{IIb}\beta_3$ and $\alpha_v\beta_3$. Because of the simplicity of this targeting moiety, RGD peptides have been extensively used in various integrin directed delivery systems [106]. The RGD motif allows a stringent targeting to those cells with activated conformations of those integrins. More complex molecules were also used for targeted delivery, such as the use of the activation-specific antibody AL-57 for the delivery of siRNA only to activated leukocytes [107]. Physiologic ligands of integrins, including cell adhesion molecules such as ICAM-1 and VCAM-1, have also been extensively targeted for

drug/gene delivery [108-110]. Because the expression of VCAM-1 and ICAM-1are highly upregulated at the sites of inflammatory disease, these surface molecules have become attractive targets. Moreover, multimeric clustering of these molecules promotes rapid endocytosis, allowing delivery systems to reach into the cytosol of target cells, which is an important trait for gene delivery systems [66].

In this dissertation, I demonstrate the application of the high affinity LFA-1 I domain for targeted delivery to overexpressed ICAM-1, to specifically target inflammation. I used liposomes to encapsulate a potent anti-inflammatory drug, which was functionalized with LFA-1 I domain for targeted delivery. I found that, by fine-tuning the surface density of targeting moieties, liposomes preferentially accumulated in inflamed cells that upregulated the expression of ICAM-1 with minimal or inefficient delivery to resting cells. In this study, I demonstrate that the extent of the avidity interaction between the targeting moieties of drug carriers and the target antigens on cell surfaces is an important design criterion for efficient drug delivery systems.

As a follow up study, I also attempted to deliver nucleic acid payloads such as siRNA or plasmid DNA using the same interaction between the LFA-1 I domain and ICAM-1. My first approach was to design a fusion protein between the high affinity LFA-1 I domain and a double stranded RNA-binding domain for targeted delivery of siRNA. Although the delivery scheme was efficient in eliciting endocytosis into cells, I failed to observe efficient gene silencing. Also, other schemes using short peptides such as 9 arginine or protamine fragments for association with nucleic acids did not result in satisfactory gene transfer efficiency. I hypothesized that ICAM-1 clustering-mediated endocytosis was not sufficient for successful delivery of nucleic acid payloads, and sought a means to promote the

endosomal escape of the cargo. Satisfactory gene transfer efficiency was achieved when we used polyethyleneimine (PEI), a cationic polymer based transfection agent, known to elicit endosomal escape by a mechanism termed as the proton sponge effect [111]. I functionalized PEI by expressing the I domain as a fusion to a polyanionic peptide with 18 randomly ordered glutamic and aspartic acids. Multimeric clustering of ICAM-1 mediated by the I domains attached to the gene carrier promoted rapid endocytosis. Within late endosomes, PEI aided the endosomal escape and efficient delivery of the gene payloads.

Dissertation outline

Chapter 2 describes the development of the YS2H, an improved version of the yeast surface display system for protein engineering and direct readout of protein-protein interaction. I show that the signal strength detected from the tag appended to the soluble protein is indicative of the affinity to the surface anchored protein. As mentioned above, in this chapter I demonstrate the application of directed evolution to engineer the LFA-1 I domain via the selective pressure imposed by the activation-specific antibody AL-57. I also demonstrate the isolation of single chain-only antibodies against botulinum neurotoxin using YS2H.

Chapter 3 documents the strategy I applied to discover novel antibodies against short-lived neoepitopes exposed during integrin I domain allostery. As briefly described in the previous sections, we first engineered the Mac-1 I domain into an active conformation, which was then used for screening of a human antibody phage library. The antibody isolated in this study was indeed activation specific, and potently inhibited the migration of inflamed neutrophils on fibronectin coated surfaces.

Chapter 4 reports the crystal structure of the complex between LFA-1 I domain and ICAM-1 D1, engineered for high affinity and native folding, respectively. This chapter shows that protein engineering is not only for therapeutic development, but can also lead to deeper understanding how these molecules fold and function. The complex structure in this study revealed that the engineered LFA-1 I domain for high affinity was indeed found with the α7-helix in an open conformation. We also verified that the mutations discovered in D1, which resulted in functional expression of the protein, promoted folding close to the wild-type structure that enabled the retention of the interaction with the LFA-1 I domain.

Chapter 5 demonstrates a possible clinical use of the engineered LFA-1 I domain for targeted delivery. In this study, I used the high affinity I domain to target liposomes encapsulating anti-inflammatory drug to overexpressed ICAM-1 on inflamed cells. Also, I demonstrate that the extent of multimeric avidity binding of the drug carriers to the target cells has to be precisely adjusted for efficient carrier binding and drug delivery. I also show that specific delivery of anti-inflammatory drug protects cells from recurring inflammatory injuries by inhibiting the expression of various pro-inflammatory mediators in both endothelial cells and immune cells.

Chapter 6 presents my latest work to develop a novel systemic and targeted gene delivery system. By expressing the engineered LFA-1 I domain with a polyanionic peptide, I was able to functionalize a cationic transfection reagent for targeted gene delivery system. Because ICAM-1 expression is localized at inflammatory sites, I was also able to specifically deliver genes to inflamed tissues. Multimeric interactions between LFA-1 I domain and ICAM-1 triggered a rapid entry of the delivery vehicles into cells. I also showed that receptor-mediated gene delivery produced significantly less cytotoxic effects than with conventional transfection.

Chapter 7 provides an overall conclusion of the work presented in this dissertation, as well as suggestions for future research directions.

Appendix 1 documents the engineering of β_1 I-like domain, additional work I have accomplished along the efforts on engineering integrin α I domains.

REFERENCES

1. Proost P, Wuyts A, van Damme J. The role of chemokines in inflammation. Int J Clin Lab Res. 1996;26(4):211-23.

2. Li QT, Verma IM. NF-kappa B regulation in the immune system. Nat Rev Immunol. 2002;2(10):725-34.

3. Nathan C. Points of control in inflammation. Nature. 2002;420(6917):846-52.

4. Charo IF, Ransohoff RM. Mechanisms of disease - The many roles of chemokines and chemokine receptors in inflammation. New Engl J Med. 2006;354(6):610-21.

5. Springer TA. Traffic Signals for Lymphocyte Recirculation and Leukocyte Emigration - the Multistep Paradigm. Cell. 1994;76(2):301-14.

6. Springer TA. Traffic Signals on Endothelium for Lymphocyte Recirculation and Leukocyte Emigration. Annu Rev Physiol. 1995;57:827-72.

7. Nathan C, Ding AH. Nonresolving Inflammation. Cell. 2010;140(6):871-82.

8. Libby P. Inflammation in atherosclerosis. Nature. 2002;420(6917):868-74.

9. Hotamisligil GS. Inflammation and metabolic disorders. Nature. 2006;444(7121):860-7.

10. Glass CK, Saijo K, Winner B, Marchetto MC, Gage FH. Mechanisms underlying inflammation in neurodegeneration. Cell. 2010;140(6):918-34.

11. Coussens LM, Werb Z. Inflammation and cancer. Nature. 2002;420(6917):860-7.

12. von Andrian UH, Chambers JD, McEvoy LM, Bargatze RF, Arfors KE, Butcher EC. Two-step model of leukocyte-endothelial cell interaction in inflammation: distinct roles for LECAM-1 and the leukocyte beta 2 integrins in vivo. Proc Natl Acad Sci U S A. 1991;88(17):7538-42.

13. Lawrence MB, Springer TA. Leukocytes Roll on a Selectin at Physiological Flow-Rates - Distinction from and Prerequisite for Adhesion through Integrins. Cell. 1991;65(5):859-73.

14. Kurzinger K, Reynolds T, Germain RN, Davignon D, Martz E, Springer TA. A Novel Lymphocyte Function-Associated Antigen (Lfa-1) - Cellular-Distribution, Quantitative Expression, and Structure. J Immunol. 1981;127(2):596-602.

15. Davignon D, Martz E, Reynolds T, Kurzinger K, Springer TA. Monoclonal-Antibody to a Novel Lymphocyte Function-Associated Antigen (Lfa-1) - Mechanism of Blockade of Lymphocyte-T-Mediated Killing and Effects on Other T and B-Lymphocyte Functions. J Immunol. 1981;127(2):590-5.

16. Davignon D, Martz E, Reynolds T, Kurzinger K, Springer TA. Lymphocyte Function-Associated Antigen-1 (Lfa-1) - a Surface-Antigen Distinct from Lyt-2,3 That Participates in Lymphocyte-T-Mediated Killing. P Natl Acad Sci-Biol. 1981;78(7):4535-9.

17. Kurzinger K, Ho MK, Springer TA. Structural homology of a macrophage differentiation antigen and an antigen involved in T-cell-mediated killing. Nature. 1982;296(5858):668-70.

18. Kurzinger K, Springer TA. Purification and structural characterization of LFA-1, a lymphocyte function-associated antigen, and Mac-1, a related macrophage differentiation antigen associated with the type three complement receptor. J Biol Chem. 1982;257(20):12412-8.

19. Sanchez-Madrid F, Simon P, Thompson S, Springer TA. Mapping of antigenic and functional epitopes on the alpha- and beta-subunits of two related mouse glycoproteins involved in cell interactions, LFA-1 and Mac-1. J Exp Med. 1983;158(2):586-602.

20. Rothlein R, Dustin ML, Marlin SD, Springer TA. A human intercellular adhesion molecule (ICAM-1) distinct from LFA-1. J Immunol. 1986;137(4):1270-4.

21. Dustin ML, Springer TA. Lymphocyte function-associated antigen-1 (LFA-1) interaction with intercellular adhesion molecule-1 (ICAM-1) is one of at least three mechanisms for lymphocyte adhesion to cultured endothelial cells. J Cell Biol. 1988;107(1):321-31.

22. Dustin ML, Springer TA. T-Cell Receptor Cross-Linking Transiently Stimulates Adhesiveness through Lfa-1. Nature. 1989;341(6243):619-24.

23. Luo BH, Carman CV, Springer TA. Structural basis of integrin regulation and signaling. Annu Rev Immunol. 2007;25:619-47.

24. Shimaoka M, Takagi J, Springer TA. Conformational regulation of integrin structure and function. Annu Rev Bioph Biom. 2002;31:485-516.

25. Yonekawa K, Harlan JM. Targeting leukocyte integrins in human diseases. J Leukocyte Biol. 2005;77(2):129-40.

26. Harris ES, McIntyre TM, Prescott SM, Zimmerman GA. The leukocyte integrins. Journal of Biological Chemistry. 2000;275(31):23409-12.

27. Gahmberg CG, Valmu L, Fagerholm S, Kotovuori P, Ihanus E, Tian L, et al. Leukocyte integrins and inflammation. Cell Mol Life Sci. 1998;54(6):549-55.

28. Springer TA, Thompson WS, Miller LJ, Schmalstieg FC, Anderson DC. Inherited Deficiency of the Mac-1, Lfa-1, P150,95 Glycoprotein Family and Its Molecular-Basis. Journal of Experimental Medicine. 1984;160(6):1901-18.

29. Bevilacqua MP, Nelson RM, Mannori G, Cecconi O. Endothelial-leukocyte adhesion molecules in human disease. Annu Rev Med. 1994;45:361-78.

30. Hansson GK, Robertson AK, Soderberg-Naucler C. Inflammation and atherosclerosis. Annu Rev Pathol. 2006;1:297-329.

31. Galkina E, Ley K. Immune and inflammatory mechanisms of atherosclerosis (*). Annu Rev Immunol. 2009;27:165-97.

32. Grivennikov SI, Greten FR, Karin M. Immunity, inflammation, and cancer. Cell. 2010;140(6):883-99.

33. Balkwill F, Mantovani A. Inflammation and cancer: back to Virchow? Lancet. 2001;357(9255):539-45.

34. Schoppmann SF, Birner P, Stockl J, Kalt R, Ullrich R, Caucig C, et al. Tumor-associated macrophages express lymphatic endothelial growth factors and are related to peritumoral lymphangiogenesis. Am J Pathol. 2002;161(3):947-56.

35. Ono M, Torisu H, Fukushi J, Nishie A, Kuwano M. Biological implications of macrophage infiltration in human tumor angiogenesis. Cancer Chemother Pharmacol. 1999;43 Suppl:S69-71.

36. Torisu H, Ono M, Kiryu H, Furue M, Ohmoto Y, Nakayama J, et al. Macrophage infiltration correlates with tumor stage and angiogenesis in human malignant melanoma: possible involvement of TNFalpha and IL-1alpha. Int J Cancer. 2000;85(2):182-8.

37. Scholl SM, Pallud C, Beuvon F, Hacene K, Stanley ER, Rohrschneider L, et al. Anti-colony-stimulating factor-1 antibody staining in primary breast adenocarcinomas correlates with marked inflammatory cell infiltrates and prognosis. J Natl Cancer Inst. 1994;86(2):120-6.

38. Shacter E, Weitzman SA. Chronic inflammation and cancer. Oncology (Williston Park). 2002;16(2):217-26, 29; discussion 30-2.

39. Nestle FO, Kaplan DH, Barker J. Mechanisms of Disease: Psoriasis. New Engl J Med. 2009;361(5):496-509.

40. Frohman EM, Racke MK, Raine CS. Medical progress: Multiple sclerosis - The plaque and its pathogenesis. New Engl J Med. 2006;354(9):942-55.

41. Abraham C, Cho JH. MECHANISMS OF DISEASE Inflammatory Bowel Disease. New Engl J Med. 2009;361(21):2066-78.

42. Schon MP, Boehncke WH. Medical progress - Psoriasis. New Engl J Med. 2005;352(18):1899-912.

43. Hildreth JEK, Gotch FM, Hildreth PDK, Mcmichael AJ. A Human Lymphocyte-Associated Antigen Involved in Cell-Mediated Lympholysis. Eur J Immunol. 1983;13(3):202-8.

44. Kupper TS. Immunologic targets in psoriasis. New Engl J Med. 2003;349(21):1987-90.

45. Ransohoff RM. Natalizumab for multiple sclerosis. New Engl J Med. 2007;356(25):2622-9.

46. von Andrian UH, Engelhardt B. alpha(4) integrins as therapeutic targets in autoimmune disease. New Engl J Med. 2003;348(1):68-72.

47. Ghosh S, Goldin E, Gordon FH, Malchow HA, Rask-Madsen J, Rutgeerts P, et al. Natalizumab for active Crohn's disease. New Engl J Med. 2003;348(1):24-32.

48. Ley K, Laudanna C, Cybulsky MI, Nourshargh S. Getting to the site of inflammation: the leukocyte adhesion cascade updated. Nat Rev Immunol. 2007;7(9):678-89.

49. Semmrich M, Smith A, Feterowski C, Beer S, Engelhardt B, Busch DH, et al. Importance of integrin LFA-1 deactivation for the generation of immune responses. Journal of Experimental Medicine. 2005;201(12):1987-98.

50. Morin NA, Oakes PW, Hyun YM, Lee DY, Chin EY, King MR, et al. Nonmuscle myosin heavy chain IIA mediates integrin LFA-1 de-adhesion during T lymphocyte migration. Journal of Experimental Medicine. 2008;205(1):195-205.

51. Xiong JP, Stehle T, Zhang RG, Joachimiak A, Frech M, Goodman SL, et al. Crystal structure of the extracellular segment of integrin alpha V beta 3 in complex with an Arg-Gly-Asp ligand. Science. 2002;296(5565):151-5.

52. Xiao T, Takagi J, Coller BS, Wang JH, Springer TA. Structural basis for allostery in integrins and binding to fibrinogen-mimetic therapeutics. Nature. 2004;432(7013):59-67.

53. Xiong JP, Stehle T, Diefenbach B, Zhang RG, Dunker R, Scott DL, et al. Crystal structure of the extracellular segment of integrin alpha V beta 3. Science. 2001;294(5541):339-45.

54. Takagi J, Petre BM, Walz T, Springer TA. Global conformational rearrangements in integrin extracellular domains in outside-in and inside-out signaling. Cell. 2002;110(5):599-611.

55. Shimaoka M, Springer TA. Therapeutic antagonists and conformational regulation of integrin function. Nat Rev Drug Discov. 2003;2(9):703-16.

56. Nishida N, Xie C, Shimaoka M, Cheng YF, Walz T, Springer TA. Activation of leukocyte beta(2) integrins by conversion from bent to extended conformations. Immunity. 2006;25(4):583-94.

57. Arnaout MA. Integrin structure: new twists and turns in dynamic cell adhesion. Immunol Rev. 2002;186:125-40.

58. Zhu JQ, Boylan B, Luo BH, Newman PJ, Springer TA. Tests of the extension and deadbolt models of integrin activation. Journal of Biological Chemistry. 2007;282(16):11914-20.

59. Chen JF, Salas A, Springer TA. Bistable regulation of integrin adhesiveness by a bipolar metal ion cluster. Nat Struct Biol. 2003;10(12):995-1001.

60. Yang W, Shimaoka M, Salas A, Takagi J, Springer TA. Intersubunit signal transmission in integrins by a receptor-like interaction with a pull spring. Proc Natl Acad Sci U S A. 2004;101(9):2906-11.

61. Galkina E, Ley K. Vascular adhesion molecules in atherosclerosis. Arterioscler Thromb Vasc Biol. 2007;27(11):2292-301.

62. Doran AC, Meller N, McNamara CA. Role of smooth muscle cells in the initiation and early progression of atherosclerosis. Arterioscler Thromb Vasc Biol. 2008;28(5):812-9.

63. Nakashima Y, Raines EW, Plump AS, Breslow JL, Ross R. Upregulation of VCAM-1 and ICAM-1 at atherosclerosis-prone sites on the endothelium in the ApoE-deficient mouse. Arterioscl Throm Vas. 1998;18(5):842-51.

64. Collins T, Cybulsky MI. NF-kappa B: pivotal mediator or innocent bystander in atherogenesis? Journal of Clinical Investigation. 2001;107(3):255-64.

65. Gareus R, Kotsaki E, Xanthoulea S, van der Made I, Gijbels MJ, Kardakaris R, et al. Endothelial cell-specific NF-kappaB inhibition protects mice from atherosclerosis. Cell Metab. 2008;8(5):372-83.

66. Muro S, Gajewski C, Koval M, Muzykantov VR. ICAM-1 recycling in endothelial cells: a novel pathway for sustained intracellular delivery and prolonged effects of drugs. Blood. 2005;105(2):650-8.

67. Hansson GK. Inflammation, atherosclerosis, and coronary artery disease. N Engl J Med. 2005;352(16):1685-95.

68. Dai G, Kaazempur-Mofrad MR, Natarajan S, Zhang Y, Vaughn S, Blackman BR, et al. Distinct endothelial phenotypes evoked by arterial waveforms derived from atherosclerosis-susceptible and -resistant regions of human vasculature. Proc Natl Acad Sci U S A. 2004;101(41):14871-6.

69. Skalen K, Gustafsson M, Rydberg EK, Hulten LM, Wiklund O, Innerarity TL, et al. Subendothelial retention of atherogenic lipoproteins in early atherosclerosis. Nature. 2002;417(6890):750-4.

70. O'Brien KD, McDonald TO, Chait A, Allen MD, Alpers CE. Neovascular expression of E-selectin, intercellular adhesion molecule-1, and vascular cell adhesion molecule-1 in human atherosclerosis and their relation to intimal leukocyte content. Circulation. 1996;93(4):672-82.

71. Osterud B, Bjorklid E. Role of monocytes in atherogenesis. Physiol Rev. 2003;83(4):1069-112.

72. Saha P, Modarai B, Humphries J, Mattock K, Waltham M, Burnand KG, et al. The monocyte/macrophage as a therapeutic target in atherosclerosis. Curr Opin Pharmacol. 2009;9(2):109-18.

73. Park YM, Febbraio M, Silverstein RL. CD36 modulates migration of mouse and human macrophages in response to oxidized LDL and may contribute to macrophage trapping in the arterial intima. J Clin Invest. 2009;119(1):136-45.

74. Sadat U, Gillard JH, Varty K. CD36 modulation in the subintimal trapping and LDL-mediated migration of macrophages. Expert Rev Cardiovasc Ther. 2009;7(6):587-90.

75. Dong ZM, Brown AA, Wagner DD. Prominent role of P-selectin in the development of advanced atherosclerosis in ApoE-deficient mice. Circulation. 2000;101(19):2290-5.

76. Barringhaus KG, Phillips JW, Thatte JS, Sanders JM, Czarnik AC, Bennett DK, et al. alpha(4)beta(1) integrin (VLA-4) blockade attenuates both early and late leukocyte recruitment and neointimal growth following carotid injury in apolipoprotein E (-/-) mice. J Vasc Res. 2004;41(3):252-60.

77. Patel SS, Thiagarajan R, Willerson JT, Yeh ETH. Inhibition of alpha(4) integrin and ICAM-1 markedly attenuate macrophage homing to atherosclerotic plaques in ApoE-deficient mice. Circulation. 1998;97(1):75-81.

78. Nageh MF, Sandberg ET, Marotti KR, Lin AH, Melchior EP, Bullard DC, et al. Deficiency of inflammatory cell adhesion molecules protects against atherosclerosis in mice. Arterioscl Throm Vas. 1997;17(8):1517-20.

79. Joner M, Morimoto K, Kasukawa H, Steigerwald K, Merl S, Nakazawa G, et al. Site-Specific Targeting of Nanoparticle Prednisolone Reduces In-Stent Restenosis in a Rabbit Model of Established Atheroma. Arterioscl Throm Vas. 2008;28(11):1960-U113.

80. Winter PM, Neubauer AM, Caruthers SD, Harris TD, Robertson JD, Williams TA, et al. Endothelial alpha(v)beta(3) integrin-targeted fumagillin nanoparticles inhibit angiogenesis in atherosclerosis. Arterioscl Throm Vas. 2006;26(9):2103-9.

81. Kolodgie FD, John M, Khurana C, Farb A, Wilson PS, Acampado E, et al. Sustained reduction of in-stent neointimal growth with the use of a novel systemic nanoparticle paclitaxel. Circulation. 2002;106(10):1195-8.

82. Curtiss LK. Reversing atherosclerosis? N Engl J Med. 2009;360(11):1144-6.

83. Fan E, Zhang L, Jiang S, Bai Y. Beneficial effects of resveratrol on atherosclerosis. J Med Food. 2008;11(4):610-4.

84. Rhen T, Cidlowski JA. Antiinflammatory action of glucocorticoids--new mechanisms for old drugs. N Engl J Med. 2005;353(16):1711-23.

85. Crowell JA, Korytko PJ, Morrissey RL, Booth TD, Levine BS. Resveratrol-associated renal toxicity. Toxicol Sci. 2004;82(2):614-9.

86. Shimaoka M, Lu C, Salas A, Xiao T, Takagi J, Springer TA. Stabilizing the integrin alpha M inserted domain in alternative conformations with a range of engineered disulfide bonds. Proc Natl Acad Sci U S A. 2002;99(26):16737-41.

87. Shimaoka M, Xiao T, Liu JH, Yang Y, Dong Y, Jun CD, et al. Structures of the alpha L I domain and its complex with ICAM-1 reveal a shape-shifting pathway for integrin regulation. Cell. 2003;112(1):99-111.

88. Takagi J, Erickson HP, Springer TA. C-terminal opening mimics 'inside-out' activation of integrin alpha5beta1. Nat Struct Biol. 2001;8(5):412-6.

89. Jin M, Song G, Carman CV, Kim YS, Astrof NS, Shimaoka M, et al. Directed evolution to probe protein allostery and integrin I domains of 200,000-fold higher affinity. Proc Natl Acad Sci U S A. 2006;103(15):5758-63.

90. Shimaoka M, Lu C, Palframan RT, von Andrian UH, McCormack A, Takagi J, et al. Reversibly locking a protein fold in an active conformation with a disulfide bond: integrin alphaL I domains with high affinity and antagonist activity in vivo. Proc Natl Acad Sci U S A. 2001;98(11):6009-14.

91. Lee JO, Rieu P, Arnaout MA, Liddington R. Crystal structure of the A domain from the alpha subunit of integrin CR3 (CD11b/CD18). Cell. 1995;80(4):631-8.

92. Lee JO, Bankston LA, Arnaout MA, Liddington RC. Two conformations of the integrin A-domain (I-domain): a pathway for activation? Structure. 1995;3(12):1333-40.

93. McCleverty CJ, Liddington RC. Engineered allosteric mutants of the integrin alphaMbeta2 I domain: structural and functional studies. Biochem J. 2003;372(Pt 1):121-7.

94. Springer TA, Zhu J, Xiao T. Structural basis for distinctive recognition of fibrinogen gammaC peptide by the platelet integrin alphaIIbbeta3. J Cell Biol. 2008;182(4):791-800.

95. Luo BH, Springer TA, Takagi J. Stabilizing the open conformation of the integrin headpiece with a glycan wedge increases affinity for ligand. Proc Natl Acad Sci U S A. 2003;100(5):2403-8.

96. Luo BH, Takagi J, Springer TA. Locking the beta(3) integrin I-like domain into high and low affinity conformations with disulfides. Journal of Biological Chemistry. 2004;279(11):10215-21.

97. Boder ET, Wittrup KD. Yeast surface display for screening combinatorial polypeptide libraries. Nat Biotechnol. 1997;15(6):553-7.

98. Huang LL, Shimaoka M, Rondon IJ, Roy I, Chang Q, Po M, et al. Identification and characterization of a human monoclonal antagonistic antibody AL-57 that preferentially binds the high-affinity form of lymphocyte function-associated antigen-1. J Leukocyte Biol. 2006;80(4):905-14.

99. Shimaoka M, Kim M, Cohen EH, Yang W, Astrof N, Peer D, et al. AL-57, a ligand-mimetic antibody to integrin LFA-1, reveals chemokine-induced affinity up-regulation in lymphocytes. P Natl Acad Sci USA. 2006;103(38):13991-6.

100. Eisenhardt SU, Schwarz M, Schallner N, Soosairajah J, Bassler N, Huang DX, et al. Generation of activation-specific human anti-alpha(M)beta(2) single-chain antibodies as potential diagnostic tools and therapeutic agents. Blood. 2007;109(8):3521-8.

101. Schwarz M, Meade G, Stoll P, Ylanne J, Bassler N, Chen YC, et al. Conformation-specific blockade of the integrin GPIIb/IIIa - A novel antiplatelet

strategy that selectively targets activated platelets. Circulation Research. 2006;99(1):25-33.

102. Schwarz M, Rottgen P, Takada Y, Le Gall F, Knackmuss S, Bassler N, et al. Single-chain antibodies for the conformation-specific blockade of activated platelet integrin alpha(IIb)beta(3) designed by subtractive selection from naive human phage libraries. Faseb J. 2004;18(12):1704-+.

103. Allen TM, Cullis PR. Drug delivery systems: entering the mainstream. Science. 2004;303(5665):1818-22.

104. Juliano R. Clinical implications of basic research: Bugging tumors to put drugs on target. New Engl J Med. 2007;356(9):954-5.

105. Peer D, Park EJ, Morishita Y, Carman CV, Shimaoka M. Systemic leukocyte-directed siRNA delivery revealing cyclin D1 as an anti-inflammatory target. Science. 2008;319(5863):627-30.

106. Arap W, Pasqualini R, Ruoslahti E. Cancer treatment by targeted drug delivery to tumor vasculature in a mouse model. Science. 1998;279(5349):377-80.

107. Peer D, Zhu PC, Carman CV, Lieberman J, Shimaoka M. Selective gene silencing in activated leukocytes by targeting siRNAs to the integrin lymphocyte function-associated antigen-1. P Natl Acad Sci USA. 2007;104(10):4095-100.

108. Muzykantov VR. Targeting of superoxide dismutase and catalase to vascular endothelium. J Control Release. 2001;71(1):1-21.

109. Muro S, Dziubla T, Qiu WN, Leferovich J, Cui X, Berk E, et al. Endothelial targeting of high-affinity multivalent polymer nanocarriers directed to intercellular adhesion molecule 1. J Pharmacol Exp Ther. 2006;317(3):1161-9.

110. Kelly KA, Allport JR, Tsourkas A, Shinde-Patil VR, Josephson L, Weissleder R. Detection of vascular adhesion molecule-1 expression using a novel multimodal nanoparticle. Circulation Research. 2005;96(3):327-36.

111. Akinc A, Thomas M, Klibanov AM, Langer R. Exploring polyethylenimine-mediated DNA transfection and the proton sponge hypothesis. J Gene Med. 2005;7(5):657-63.

CHAPTER 2

YEAST SURFACE TWO-HYBRID FOR QUANTITATIVE *IN VIVO* DETECTION OF PROTEIN-PROTEIN INTERACTIONS VIA THE SECRETORY PATHWAY

Summary

A quantitative *in vivo* method for detecting protein-protein interactions will enhance our understanding of protein interaction networks and facilitate affinity maturation as well as designing new interaction pairs. We have developed a novel platform, dubbed "yeast surface two-hybrid (YS2H)," to enable a quantitative measurement of pairwise protein interactions via the secretory pathway by expressing one protein (bait) anchored to the cell wall and the other (prey) in soluble form. In YS2H, the prey is released either outside of the cells or remains on the cell surface by virtue of its binding to the bait. The strength of their interaction is measured by antibody binding to the epitope tag appended to the prey or direct readout of split green fluorescence protein (GFP) complementation. When two alpha-helices forming coiled coils were expressed as a pair of prey and bait, the amount of the prey in complex with the bait progressively decreased as the affinity changes from 100 pM to 10 μM. With GFP complementation assay, we were able to discriminate a 6-log difference in binding affinities in the range of 100 pM to 100 μM. The affinity estimated from the level of antibody binding to fusion tags was in good agreement with that measured in solution using a surface plasmon resonance technique. In

This chapter was originally published in the Journal of Biological Chemistry (Hu, X., Kang, S., Chen, X., Shoemaker, C.B., and Jin, M.M. *Journal of Biological Chemistry.* 2009;284(24):16369-76. © 2009 the American Society for Biochemistry and Molecular Biology.), and is reprinted with permission. Kang S contributed to the application of YS2H platform for directed evolution of integrin LFA-1 I domain. This included the experiments and writings related to Fig. 2.4, Fig. 2.5, Fig. 2.6, and Table 2.2.

contrast, the level of GFP complementation linearly increased with the on-rate of coiled coil interactions, likely because of the irreversible nature of GFP reconstitution. Furthermore, we demonstrate the use of YS2H in exploring the nature of antigen recognition by antibodies and activation allostery in integrins and in isolating heavy chain-only antibodies against botulinum neurotoxin.

Introduction

Protein-protein interactions are essential to virtually every cellular process, and their understanding is of great interest in basic science as well as in the development of effective therapeutics. Existing techniques to detect and screen pairs of interacting proteins *in vivo* include the yeast two-hybrid system [1] and protein-fragment complementation assay (PCA) [2-6], where the association of two interacting proteins either turns on a target gene that is necessary for cell survival or leads to the reconstitution of enzymes or green fluorescence protein (GFP) or its variants. The application of protein-protein interactions that are probed with yeast two-hybrid and PCA has been focused mainly on the interactions occurring in the nucleus or cytosol. To study interactions among secretory proteins and membrane-associated proteins, a variant of yeast two-hybrid has been developed for detecting protein-protein interactions occurring in the secretory pathway [7-8]. However, most existing methods are designed to map connectivity information for pairwise interactions and are not suitable for measuring the affinity between two interacting proteins, comparing interaction strength of different pairs, or ranking multiple binders to the interaction "hub" according to their binding affinity.

Quantitative estimation of protein-protein interactions *in vivo* will require the amount of the complex to be directly measured or the level of reconstituted reporters

to be directly proportional to the strength of the interactions. To achieve quantitative analysis of protein interactions in eukaryotic expression system, we have designed a yeast surface two-hybrid (YS2H) system that can express a pair of proteins, one protein as a fusion to a yeast cell wall protein, agglutinin, and the other in a secretory form. When two proteins interact in this system, they associate in the secretory pathway, and the prey that would otherwise be released into the media is captured on the surface by the bait. We have devised two different schemes to quantitatively estimate the affinity of two interacting molecules: flow cytometric detection of antibody binding to the epitope tags fused to the prey and the bait, and the GFP readout from the complementation of split GFP fragments fused to the prey and the bait. They are induced under a bi-directional promoter to promote a synchronized and comparable level of expression.

Herein we demonstrate the quantitative nature of YS2H in predicting the affinity between two interacting proteins, particularly in the range of 100 pM to 10 μM. This feature allowed us to examine specific interactions between antigen and antibody, to identify hot spots of allosteric activation in integrins, and to isolate camelid heavy chain-only antibodies against botulinum neurotoxin as components of therapeutic agents to treat botulism [9]. With the incorporation of PCA technique into the YS2H, our system may be developed into an *in vivo* tool to measure the kinetics of protein-protein interactions. Potential applications of YS2H include affinity maturation of antibodies, differentiation of weak to high affinity binders to the hub protein in interaction networks, and confirmation of hypothetical interacting pairs of proteins in a high throughput manner.

Experimental Procedures

YS2H vector design

Plasmid pCTCON was used as a backbone for constructing the YS2H vector (see Fig. 2.1a). A PCR fragment containing GAL10 promoter, AGA2, eGFP gene, FLAG tag, and terminator was inserted into the pCTCON by AgeI/KpnI sites. To express prey proteins as secretory forms, AGA2 sequence under the GAL1 promoter was removed by replacing an EcoRI/BamHI fragment with the fragment consisting of a signal sequence, either that of Aga2 or α-1 mating factor, and prey. The cDNA coding for the variable domains of AL-57 was obtained from the expression plasmid (a kind gift from Dr. Shimaoka at Harvard Medical School). The variable domains of TS1/22 were cloned from the hybridoma (ATCC). VH and VL cDNAs were connected with four repeats of a Gly-Gly-Gly-Gly-Ser linker sequence to produce scFv.

Yeast transformation, magnetic affinity cell sorting, and library construction

The plasmid encoding a specific pair of prey and bait proteins was introduced into yeast cells using a commercial reagent (Frozen-EZ Yeast Transformation II Kit, Zymo Research). Transformed yeast cells were grown in a solid medium plate for 48 h. A mutagenesis library of LFA-1 I domain was constructed by electroporation of a mixture of a MluI/NcoI linearized vector and error-prone PCR products of the I domain (Asn-129-Thr-318) into yeast, as described previously [10]. After transformation, the yeast libraries were grown in selective dextrose liquid medium at 30 °C with shaking for 24 h and induced in selective galactose media for 24–48 h at room temperature with shaking. To construct the variable domain of heavy chain from heavy chain-only antibody (VHH) yeast library, cDNA encoding VHH library was amplified by PCR using the primers shown in Table 2.1, which were designed based on the primers used by Maass et al. [11]. VHH cDNA PCR product was first ligated

into the YS2H vector using NheI/BamHI sites and then was transformed into XL1-Blue (Stratagene) by electroporation. The plasmids extracted from ~5×10^6 colonies were transformed into EBY100 by a lithium acetate method [12]. A single colony of EBY100 from fresh plate was inoculated into 10 ml of YPDA medium and cultured at 30 °C with shaking at 225 rpm for 16 h. The cells were then inoculated into 100 ml of YPDA at 0.5 A_{600} and cultured for another 4 h until A_{600} reaches 2. The cells were washed twice in water and resuspended in 10.8 ml of transformation mix buffer (7.2 ml of 50% polyethylene glycol, 1.1 ml of 1 M LiAc, 1.5 ml of 2 mg/ml single strand carrier DNA, and 150 μg of library plasmid in 1.0 ml water). The mixture was then incubated at 42 °C for 50 min. After incubation, the cells were cultured into 100 ml of selective dextrose liquid medium for 24 h and induced in selective galactose medium for 24–48 h. Library construction by homologous recombination or the lithium acetate method produced a library size of 10^6–10^7. The libraries of LFA-1 I domain and VHH were sorted with anti-Myc antibody using magnetic affinity cell sorting as described previously [10].

Immunofluorescence flow cytometry

Antibodies used in this study were the anti-c-Myc antibody 9E10 (ATCC), anti-FLAG, and phycoerythrin-labeled goat polyclonal anti-murine antibodies (Santa Cruz Biotechnology, Santa Cruz, CA). To measure the surface expression of specific prey and bait proteins using flow cytometry, one to five colonies from solid medium plate were inoculated together to obtain averaged values. After induction, the cells were harvested, washed in 100 μl of the labeling buffer (phosphate-buffered saline with 0.5% bovine serum albumin), and then incubated with ligands at 10 μg/ml in

Table 2.1. DNA sequences of forward (f) and reverse (r) primers are shown.

Product	Primers
E5	f:5'AGCTGCTAGCGAAGTTTCTGCTTTGGAAAAGGAAGTTTCTGCTTTGGAAAAGGAAGTTTCTGCCTTAGAGAAAGAGGTCTCC-3' r:5'CACCACTAGTCTTTTCCAAAGCAGAAACTTCCTTTTCCAAAGCGGAGACCTCTTTCTCTAAGGC -3'
K5	f:5'CACCATCGATTTCCTTCAAAGCAGAAACCTTTTCCTTCAAAGCAGAAACCTTTTCCTTCAAAGCGGAGACTTTCTCTTTTAATGCACT -3' r:5'CTCGACGCGTGGTGGTGGTGGTTCTGGTGGTGGTGGTTCTAAGGTTTCTGCTTTGAAGGAAAAGGTTAGTGCATTAAAAGAGAAAGTCTCC -3'
LFA-1 I domain	f:5'- TTGTGTCGACAACGTAGACCTGGTATTTCT-3' r:5'-CCATGGAGTCAGGTCCTGTTTGCTTG-3'
AL57	f:5'-GGATGCTAGCGAAGTTCAATTGTTAGAGTC-3' r:5'- GGTCGGATCCAGTTCGTTTGATTTCCACC-3'
TS1/22	f: 5'- AGCAGCTAGCCAGGTTCACCTGCAGCAATC -3' r: 5'- CACCACTAGTAGCCCGTTTCAGCTCCAGC -3'
BoNT/A-LC	f:5'-CGTTGTCGACCAATTCGTTAACAAGCAGTTCAAC-3' r:5'- AGTCCCATGGTTTGCTCGTTATAATGCCTCTAAC-3'
BoNT/B-LC	f:5'-CGTTGTCGACCCGGTGACGATCAACAACTTC-3' r:5'-AGTCCCATGGAACGCTCTTACACATTTGGATTT-3'
VHH-B8 &G6	f:5'-AGCTGCTAGCGCATGCCAGGCTCATGTCCAGCTGC-3; r:5'-GTTCGGATCCACTAGTTGGTTGTGGTTTTGGTGTCTTGG-3'
VHH library	f:5'-AGCTGCTAGCCAGRCTSAGKTGCAGCTCGTGGAG-3' r-I:5'-TGGTGGATCCTTGTGGTTTTGGTGTCTTGGG-3' r-II:5'-TGGTGGATCCGGGGTCTTCGCTGTGGTGCG-3'

50 μl of the labeling buffer for 20 min with shaking at 30 °C. The cells were then washed and incubated with secondary antibodies at 5 μg/ml in 50 μl of the labeling buffer for 20 min at 4 °C. Finally, the cells were washed once in 100 μl and suspended in 100 μl of the labeling buffer for flow cytometry (FACScan, BD Biosciences). For detecting TS1/22 binding (see Fig. 2.4b), goat polyclonal anti-murine antibody was used as a primary antibody.

Protein expression

The I domains were expressed in Escherichia coli BL21 DE3 (Invitrogen) as inclusion bodies and refolded and purified by an S75 size exclusion column connected to fast protein liquid chromatography (GE Healthcare) [10]. AL-57 as a single-chain format (scFv AL-57) was expressed using the protocol for I domain production, except that 3 mM cystamine and 6 mM cysteamine were added to the refolding buffer. Full-length BoNT/A and BoNT/B-LC encoding DNA (amino acids 1–448 of A-LC and 1–440 of B-LC) were synthesized employing codons optimal for expression in E. coli. A-LC and B-LC containing hexahistidine tags at both termini were produced using a pET14b vector. To express VHHs in soluble forms, we inserted VHH cDNA into the pET20b expression vector (Novagen). Soluble VHH was expressed in E. coli BL21 DE3, extracted by sonication, and purified using a nickel nitrilotriacetic acid column. Eluted VHHs were then injected into an S75 size exclusion column for further purification.

SPR analysis

A protein-coupled or a control mock-coupled CM5 sensor chip was prepared using an amine coupling kit (BIAcore, Piscataway, NJ), as described previously [10]. SPR was measured using a Biacore (BIA2000). I domains were injected over the chip

in 20 mM Tris-HCl, pH 8.0, 150 mM NaCl, 10 mM MgCl2 at a flow rate of 10 μl/min at room temperature. VHHs were injected over the chip in 20 mM Tris-HCl, pH 8.0, 150 mM NaCl at a flow rate of 10 μl/min at room temperature. The chip surface was regenerated by flowing 20 μl of 10 mM Tris-glycine, pH 1.5 buffer.

Results

The design of the YS2H

YS2H is built on a yeast display system [13-14], which expresses, under the control of the GAL1 promoter, a protein of interest as a fusion to Aga2. Aga2 connects to the β-glucan linked Aga1 to form a cell wall protein called agglutinin. To extend this methodology to the expression of a pair of proteins, we have inserted into the yeast display vector, pCTCON [13], an additional expression cassette under the GAL10 promoter [15]. We observed comparable expression of eGFP by GAL1 and GAL10 promoters using two different plasmids that were constructed to express eGFP under either GAL1 or GAL10 promoters (data not shown). The final YS2H vector (Fig. 2.1a) was designed to express the bait protein under the GAL10 promoter as a fusion to Aga2 and the prey protein under the GAL1 promoter without Aga2 fusion. The signal sequence used is either that of Aga2 (for the data in Figs. 2.2 and 2.3) or the α-1 mating factor (for the data in Figs. 2.4–2.6) [16]. The expression level of prey proteins with α-1 mating factor was comparable with those containing Aga2 signal sequence (data not shown). FLAG and Myc tags are fused to the C-terminal of the bait and prey proteins, respectively, and are used to examine the surface expression of the bait and the amount of the prey that is bound to the bait (Fig. 2.1b). To incorporate the PCA technique into the YS2H system, we inserted the sequence encoding enhanced

Figure 2.1. Design of the YS2H system.

(a) A map of the YS2H vector is drawn with restriction enzyme sites and genes labeled. The bait protein is expressed as a fusion to Aga2 on cell surface, whereas the prey protein is expressed as a secretory form. (b&c) Schematic diagrams of the expression cassette and protein-protein interactions (acid base coiled coils) via the secretory pathway are depicted. The prey bound to the bait is detected by antibody binding to the Myc tag (b) or by direct GFP readout from split GFP complementation (c). FLAG (DYKDDDDK) and Myc (EQKLISEEDL) epitope tags are fused to the C-terminal of the bait and prey proteins, respectively, and are used to measure the surface expression of the bait and the amount of the prey that is bound to the bait. (d) The deletion of signal sequence for the prey and bait proteins leads to their expression in the cytosol.

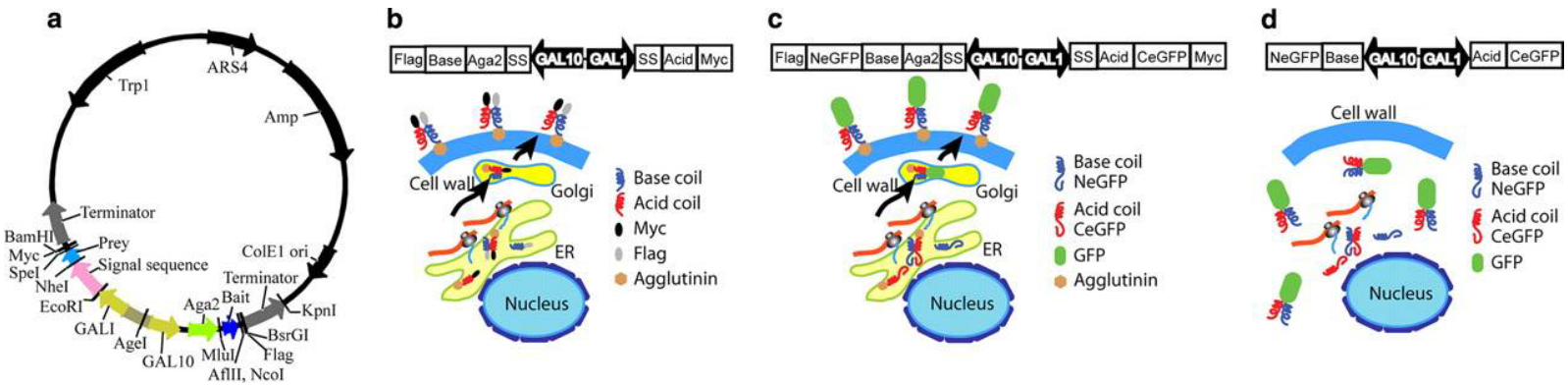
a
ARS4
Trp1
Amp
Terminator
BamHI
Prey
Myc
Signal sequence
SpeI
NheI
EcoRI
GALI
AgeI
GAL10
ColE1 ori
Terminator
Aga2
Bait
KpnI
BsrGI
MluI
Flag
AflII, NcoI
b
Flag Base Aga2 SS GAL10 GAL1 SS Acid Myc
Cell wall
Golgi
ER
Nucleus
Base coil
Acid coil
Myc
Flag
Agglutinin
c
Flag NeGFP Base Aga2 SS GAL10 GAL1 SS Acid CeGFP Myc
Cell wall
Golgi
ER
Nucleus
Base coil NeGFP
Acid coil CeGFP
GFP
Agglutinin
d
NeGFP Base GAL10 GAL1 Acid CeGFP
Cell wall
Nucleus
Base coil NeGFP
Acid coil CeGFP
GFP

eGFP fragments [3] downstream of the bait (NeGFP contains residues Val-2 to Ala-155) and the prey (CeGFP with Asp-156 to Lys-239) to monitor their interaction by GFP readout (Fig. 2.1c). The deletion of the secretory signal sequence of the prey and bait proteins causes this pair to express in the cytosol (Fig. 2.1d), which can be used to compare protein-protein interactions occurring in the secretory pathway versus cytosol.

The validation of the yeast surface two-hybrid system using coiled coil interaction

To validate that antibody binding to the Myc tag or GFP readout correlates with the strength of molecular interactions in YS2H, we expressed five pairs of acid (E*n*) and base (K*n*) α-helices of varying heptad repeats (*n*) that associate into coiled coils (Fig. 2.2). These coiled coils have been designed de novo to have affinities (K_D) in the range of 100 pM (E5/K5) to 100 μM (E3/K3) with higher affinity for longer helices through hydrophobic interactions at the interface and electrostatic attraction between the oppositely charged residues from each helix [17]. Myc expression (mean fluorescence intensity (MFI), measured by antibody binding to Myc tag) exhibited a strong correlation with the interaction affinity within the range of 100 pM to 10 μMK_D for E5-K5 to E5-K3 (Figs. 2.2b and 2.3a). With GFP complementation, this correlation extended beyond 10 μMK_D, and the difference between E5-K3 and E3-K3, corresponding to the affinity range of 10 μM to 100 μM, was clearly discernible (Figs. 2.2c and 2.3b). The Myc expression and GFP complementation were close to the level of background when the acid coil (K3 in Fig. 2.2, b and c) was deleted, indicating a lack of spontaneous complementation of the two split GFP. The level of surface expression of the bait protein measured by antibody binding to the FLAG tag was relatively invariant (Fig. 2.2, b and c), supporting the idea that the difference in the amount of the prey protein is solely due to the difference in its affinity to the bait.

Figure 2.2. Detection of coiled coil interactions by epitope expression and GFP complementation.

(a) A schematic diagram (adapted from the Fig. 1 by De Crescenzo et al. [17]) of the acid (E*n*)-base (K*n*) coiled coils with n indicating the number of heptad repeats. (b&c) The detection of coiled coil interactions by antibody binding to Myc tag (b) or direct GFP readout (c) using flow cytometry. Antibody binding to the FLAG tag measures the level of the base coil expression on cell surface. (d) Shown are the plots of GFP complementation caused by the coiled coil interactions occurring inside the cells. The numbers in each plot (b–d) indicate the MFI of an entire population shown in filled histogram. The thin lines represent the histograms of uninduced clones. The pairs of bait and prey are denoted for each column as bait:prey. The labels K3 and E3 indicate that the other coil is deleted from the expression vector.

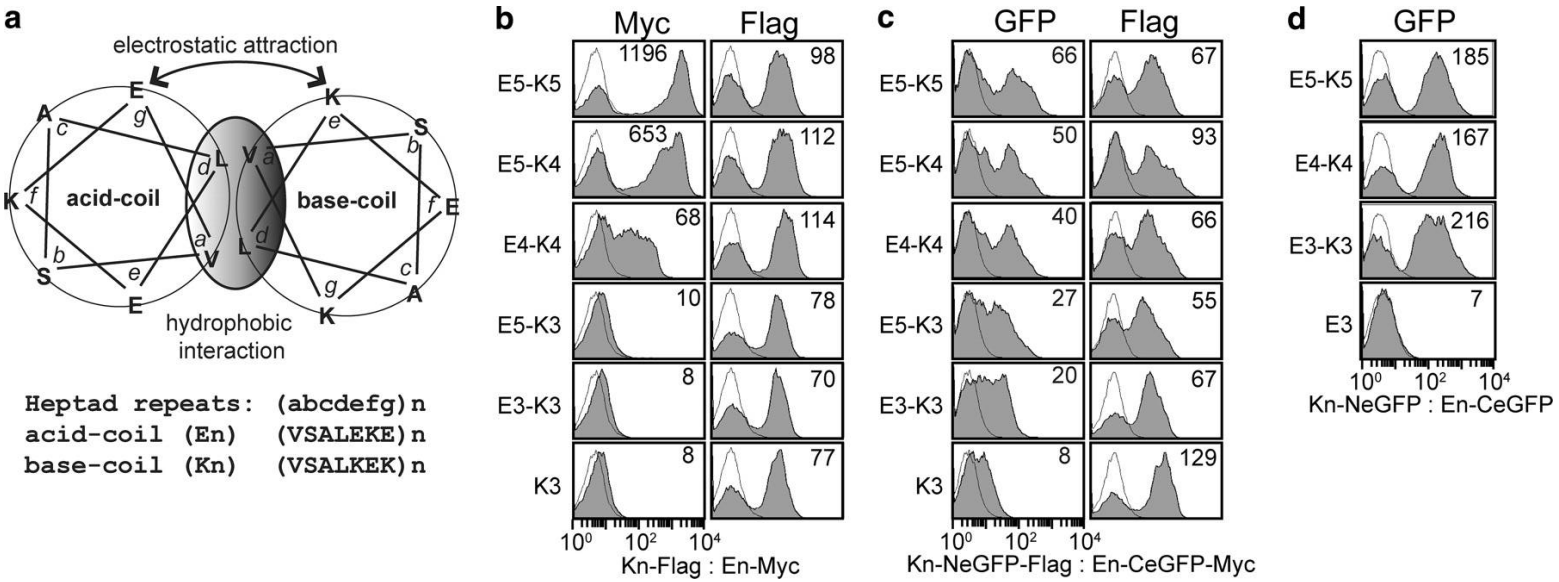

Heptad repeats: (abcdefg)n
acid-coil (En) (VSALEKE)n
base-coil (Kn) (VSALKEK)n

In contrast to a quantitative correlation between the strength of protein-protein interactions and GFP complementation, the acid and base coil interactions occurring in the cytosol (expression of the coils without secretory signal sequence) led to the complementation of split GFP that lacks correlation with the strength of coiled coil interactions (Figs. 2.2d and 2.3c). However, GFP complementation for these pairs was still due to specific interaction between acid and base coils, evidenced by the absence of fluorescence when the base coil was deleted from NeGFP (Fig. 2.2d).

YS2H detects specific interactions of antibodies and antigens

To investigate a potential use of YS2H for antibody discovery, we first examined whether YS2H can detect specific interactions of known pairs of antigen and antibody. As a model system, we chose a ligand-binding domain of the integrin LFA-1, known as the Inserted or I domain, and monoclonal antibodies specific to LFA-1 I domain (Fig. 2.4). The I domain exists in two distinct conformations that correspond to low and high affinity states to its ligand, intercellular adhesion molecule-1 (ICAM-1) (Fig. 2.5, a and b). Although the I domain in isolation is predominantly in an inactive, low affinity conformation, the mutations that would favor the active conformation were found to induce high affinity binding of the I domain to the ICAM-1. For example, the mutations of K287C and K294C (high affinity or HA I domain) designed to stabilize by disulfide bond the position of the α7-helix into active conformation led to an increase in the affinity to ICAM-1 by 10,000-fold over the wild-type I domain [18].

The antibodies that were expressed as scFv formats include the activation-insensitive antibody (TS1/22) [19], binding to both inactive and active I domains, and the activation-dependent antibody (AL-57) [10, 20], which binds only to the active

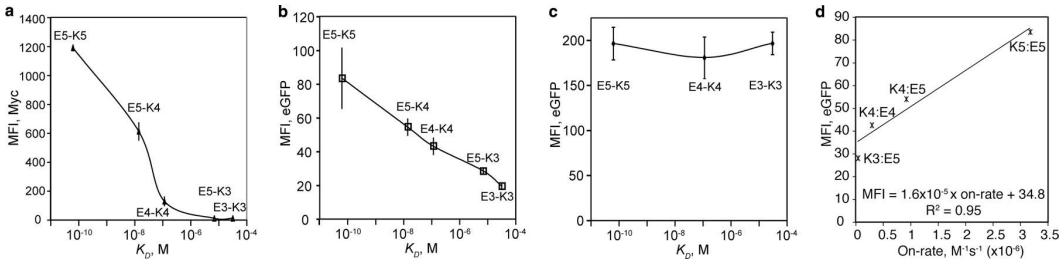

Figure 2.3. Affinity estimation by YS2H.

The correlation of the affinity measured by SPR [17] with the detection by epitope tag or direct readout of GFP complementation caused by coiled coil interactions occurring in the secretory pathway (a–d) or in the cytosol (c). The data are from three independent experiments involving different clones (means ± S.E.). The smooth solid lines are drawn by connecting data points. d, the MFI of eGFP complementation from the coiled coil interactions is plotted as a function of their on-rate, measured by SPR [17]. The solid line represents a least square fit to the data points.

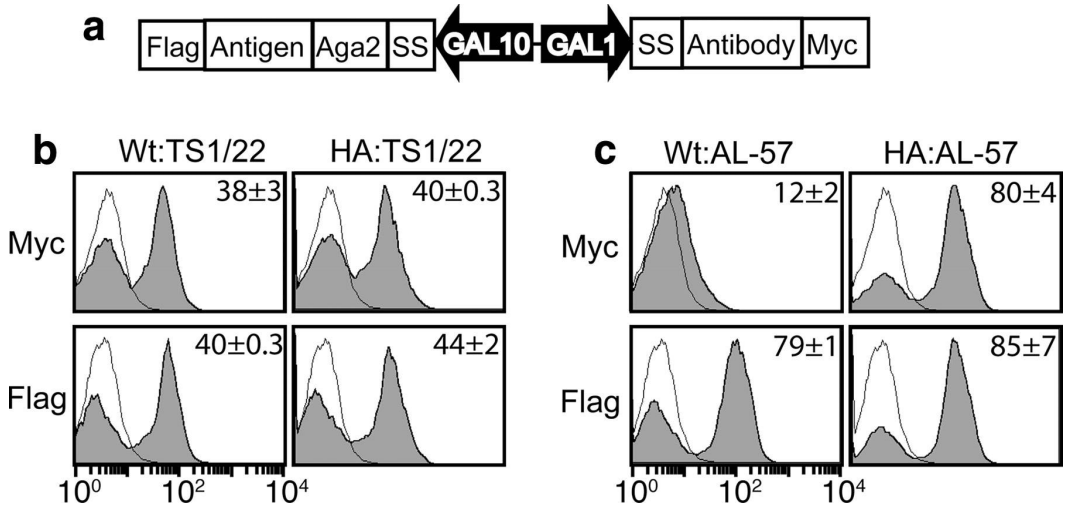

Figure 2.4. Detection of specific interactions between antibodies and antigens in YS2H.

(a) Schematic diagram of the expression cassette used to study antigen (bait) and antibody (prey) interactions. (b&c) Shown are the histograms of the interactions of the wild-type and the high affinity (HA) I domains as baits and activation-insensitive antibody, TS1/22 (b) activation-specific antibody, AL-57 (c) as preys. Filled histograms are of antibody binding to Myc and FLAG tags to the induced clones. Thin black lines represent antibody binding to uninduced clones as controls. The numbers in each plot indicate the means ± S.E. of the MFI of the filled histograms from three independent measurements.

Figure 2.5. Discovery of allosteric activation in the I domain.

(a) Cartoon diagrams of low (inactive) and high affinity (active) conformations of the LFA-1 I domains. The regions that are structurally conserved between two states are colored gray. The regions that differ structurally are colored in magenta and yellow for the inactive and the active conformations, respectively. The metal ions in the metal ion-dependent adhesion site are shown as spheres. The N and C termini and α7-helix are labeled. (b) The structure of the I domain is shown in complex with the first domain of ICAM-1 (D1). Gray spheres with a white center display the positions for the hot spots for allosteric activation found in our previous study [10]. The metal ion and three oxygen atoms of water molecules are depicted as spheres. The residues that coordinate to the metal ion are shown in stick models. The structures of the I domains and the complex of I domain with the ICAM-1 were modeled based on the crystal structures, as described previously [31]. (c) Myc expression of the I domain library before sort and after first and second sort are shown. The numbers indicate the percentage of the clones within the gated region. Antibody binding was measured with 10 mM MgCl2 or no metal ions with 10 mM EDTA. (d) Two activating mutations from the second sort were of F265S and L295P. The numbers in each plot indicate means ± S.E. of the MFI of the filled histograms from three independent measurements. (e&f) SPR measurements of L295P (e) and F265S (f) binding to scFv AL-57. I domains were injected over the scFv AL-57-coated chip as a series of 2-fold dilutions beginning at 500 nM.

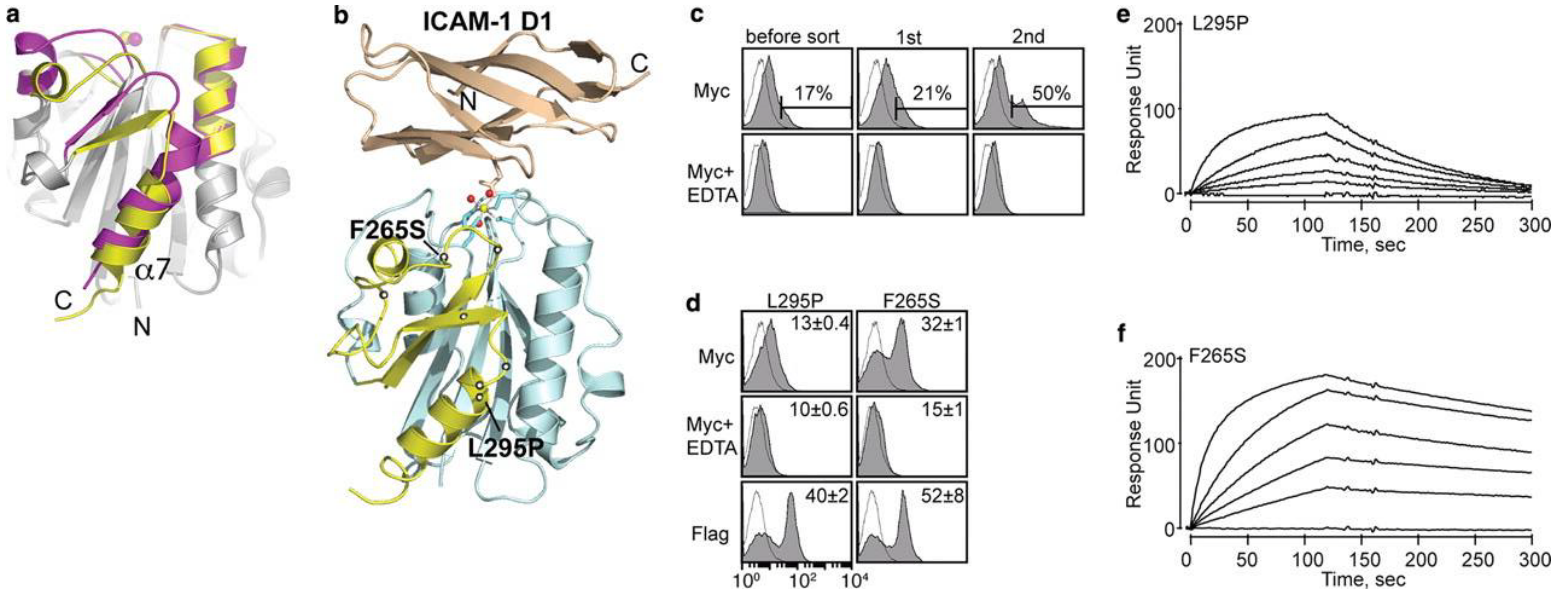
a
α7
C
N
b
ICAM-1 D1
C
N
F265S
L295P
c
before sort
1st
2nd
Myc
17%
21%
50%
Myc+
EDTA
d
L295P
F265S
Myc
13±0.4
32±1
Myc+
EDTA
10±0.6
15±1
Flag
40±2
52±8
10⁰
10²
10⁴
e
L295P
Response Unit
200
100
0
0
50
100
150
200
250
300
Time, sec
f
F265S
Response Unit
200
100
0
0
50
100
150
200
250
300
Time, sec

I domain. The interaction between antigen and antibody was measured by the detection of Myc tag fused to the antibody at the C terminus (Fig. 2.4). A tag-based assay was chosen instead of GFP complementation because it was found that the I domain fused to NeGFP did not express (no antibody binding to FLAG tag), presumably because of the quality control machinery in protein secretion [21] that prohibits misfolded proteins to be secreted (data not shown). This is in contrast to the expression of split GFP with a fusion of short coils, e.g. K3-NeGFP in Fig. 2.2c. Therefore, it appears that when NeGFP is fused to the I domain that by itself requires proper folding for secretion, the I domain fusion to NeGFP becomes completely misfolded and does not pass the quality control for secretion.

Myc tag expression in YS2H was in agreement with the specificities of monoclonal antibody AL-57 and TS1/22 against the LFA I domain; although the clones expressing TS1/22 displayed Myc expression either with the wild-type or with the HA I domains as antigens (Fig. 2.4b), the AL-57 clones exhibited Myc expression only with the HA I domain (Fig. 2.4c).

Discovery of activating mutations in the LFA-1 I domain

Next, we examined the ability of our system in isolating activating mutations in antigens that exhibit two different activation states. With the expression of AL-57 scFv and the error-prone PCR products of the wild-type I domain in YS2H, yeast library was constructed and sorted with anti-Myc antibody using a magnetic affinity cell sorter. With successive sorting, there was a gradual increase in the percentage of the population of cells that showed Myc expression above the background level (Fig. 2.5c). After two rounds of sorting, the cells were plated to yield individual clones, from which four clones were sequenced and tested for Myc expression. Of the four, three contained a mutation of F265S, and one contained L295P (Fig. 2.5d). These two

mutations belonged to a long list of activation hot spots that were identified in our previous study [10], where a large number of yeast cells were sorted and analyzed for their binding to exogenous AL-57 or ICAM-1-Fcγ.

The mutations of L295P and F265S were previously found to contribute to an increase in the binding of the I domain to ICAM-1 at 6 and 152%, respectively, of the HA I domain binding to ICAM-1 [10]. To directly measure the affinity of scFv AL-57 to I domain variants, we used a SPR technique (Fig. 2.5, e and f). A first order Langmuir adsorption equation was fitted to the sensograms to obtain the kinetic and equilibrium binding constants. The equilibrium dissociation constants (K_D) of L295P and F265S to scFv AL-57 were 243 and 15.7 nM, respectively, in agreement with higher Myc expression with F265S in our system. AL-57 binding to the LFA-1 I domain depends on the presence of metal ions at the top of the I domain, known as the metal ion-dependent adhesion site (Fig. 2.5b) [22]. This was also confirmed by the decrease in the Myc tag expression when EDTA was added at 10 mM to the cells during labeling (Fig. 2.5, c and d).

Antibody discovery: VHH against botulinum neurotoxin protease

Approximately half of the IgGs in camelid sera are heavy chain-only antibodies devoid of light chains [11, 23]. Because of the lack of light chains, antigenic specificity of the heavy chain-only antibodies is limited to a variable domain of the heavy chain. We are seeking VHH agents that bind and inhibit the LC protease domains of Botulinum neurotoxins (BoNTs) as components in therapeutic agents for the treatment of botulism. In prior work (Maass et al. [11], we immunized alpacas with BoNT LCs of serotype A (A-LC) followed by serotype B (B-LC). We then used phage display techniques to identify VHHs from these alpacas with affinity for the BoNT LC

Figure 2.6. Detection of VHH binding to BoNT LC protease.

(a) Specific binding of the VHHs against A-LC and B-LC was confirmed in YS2H by Myc expression. (b) New VHHs against B-LC protease were isolated by YS2H. The numbers in each plot indicate means ± S.E. of the MFI of the filled histograms from three independent measurements. (c&d) SPR measurements of B8 (c) and G6 (d) binding to BoNT/A-LC. A-LC was injected at a series of 2-fold dilutions beginning at 160 nM to the B8-coated and 400 nM to the G6-coated chip. (e) Cysteines are highlighted in yellow for the pair that forms a conserved disulfide bond or in orange that forms extra disulfide bonds. The framework region (FR) and complementarity determining regions (CDR) are noted.

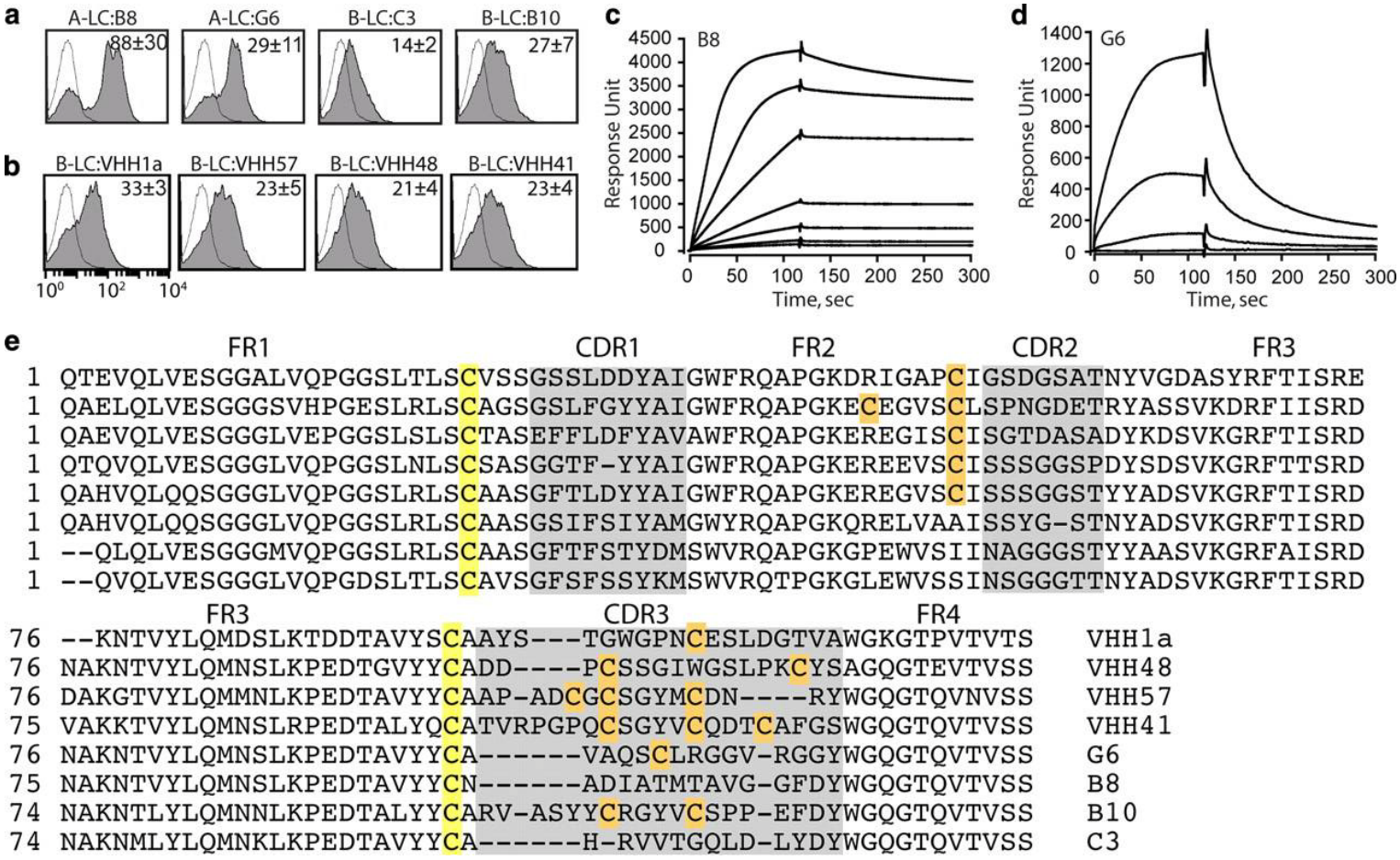
a
A-LC:B8
88±30
A-LC:G6
29±11
B-LC:C3
14±2
B-LC:B10
27±7
b
B-LC:VHH1a
33±3
B-LC:VHH57
23±5
B-LC:VHH48
21±4
B-LC:VHH41
23±4
10^0 10^2 10^4
c
B8
Response Unit
Time, sec
d
G6
Response Unit
Time, sec
e
FR1 CDR1 FR2 CDR2 FR3
1 QTEVQLVESGGALVQPGGSLTLSCVSSGSSLDDYAIGWFRQAPGKDRIGAPCIGSDGSATNYVGDASYRFTISRE
1 QAELQLVESGGGSVHPGESLRLSCAGSGSLFGYYAIGWFRQAPGKECEGVSCLSPNGDETRYASSVKDRFIISRD
1 QAEVQLVESGGGLVEPGGSLSLSCTASEFFLDFYAVAWFRQAPGKEREGISCISGTDASADYKDSVKGRFTISRD
1 QTQVQLVESGGGLVQPGGSLNLSCSASGGTF-YYAIGWFRQAPGKEREEVSCISSSGGSPDYSDSVKGRFTTSRD
1 QAHVQLQQSGGGLVQPGGSLRLSCAASGFTLDYYAIGWFRQAPGKEREGVSCISSSGGSTYYADSVKGRFTISRD
1 QAHVQLQQSGGGLVQPGGSLRLSCAASGSIFSIYAMGWYRQAPGKQRELVAAISSYG-STNYADSVKGRFTISRD
1 --QLQLVESGGGMVQPGGSLRLSCAASGFTFSTYDMSWVRQAPGKGPEWVSIINAGGGSTYYAASVKGRFAISRD
1 --QVQLVESGGGLVQPGDSLTLSCAVSGFSFSSYKMSWVRQTPGKGLEWVSSINSGGGTTNYADSVKGRFTISRD
FR3 CDR3 FR4
76 --KNTVYLQMDSLKTDDTAVYSCAAYS---TGWGPNCESLDGTVAWGKGTPVTVTS VHH1a
76 NAKNTVYLQMNSLKPEDTGVYYCADD----PCSSGIWGSLPKCYSAGQGTEVTVSS VHH48
76 DAKGTVYLQMMNLKPEDTAVYYCAAP-ADCGCSGYMCDN----RYWGQGTQVNVSS VHH57
75 VAKKTVYLQMNSLRPEDTALYQCATVRPGPQCSGYVCQDTCAFGSWGQGTQVTVSS VHH41
76 NAKNTVYLQMNSLKPEDTAVYYCA------VAQSCLRGGV-RGGYWGQGTQVTVSS G6
75 NAKNTVYLQMNSLKPEDTAVYYCN------ADIATMTAVG-GFDYWGQGTQVTVSS B8
74 NAKNTLYLQMNNLKPEDTALYYCARV-ASYYCRGYVCSPP-EFDYWGQGTQVTVSS B10
74 NAKNMLYLQMNKLKPEDTAVYYCA------H-RVVTGQLD-LYDYWGQGTQVTVSS C3

proteases. We selected two A-LC binding VHHs (B8 and G6) and two B-LC binding VHHs (B10 and C3) for testing with the YS2H system (Fig. 2.6a). Myc tag expression was found to be highest in the clone expressing VHH-B8 and BoNT/A-LC, whereas the binding level of the other VHHs was lower with MFI ranges from 14 to 29.

To confirm that the level of Myc expression correlates with the solution affinity of VHH to LC, we used a SPR technique (Fig. 2.6, c and d). A series of 2-fold dilutions of A-LC was injected into a chip coated with B8 and G6. The K_D values of B8 and G6 to BoNT/A-LC were estimated to be 2.3 and 230 nM, respectively. The 100-fold difference in the affinity was mainly due to the 34-fold difference in the dissociation rate ($k_{off} = 5.18 \times 10^{-4}$ s^{-1} for B8 versus 1.82×10^{-2} s^{-1} for G6), with the association rate differing by only 3-fold ($k_{on} = 2.26 \times 10^5 M^{-1}$ s^{-1} for B8 versus $7.61 \times 10^4 M^{-1}$ s^{-1} for G6).

To validate the use of YS2H for antibody discovery, a yeast antibody library was constructed by transforming cells with the alpaca immune cDNA library as prey and the BoNT/B-LC gene as bait. Yeast cells enriched after two rounds of magnetic affinity cell sorting with anti-Myc antibody began to show an increase in Myc tag expression (data not shown). Of 30 clones that were tested individually, 14 clones displayed positive expression of Myc tag. Eleven of these 14 clones were found to be unique clones, including B10 and C3, which were originally isolated by phage display. Anti-Myc antibody binding of the newly isolated nine clones was in the range of 21–33 MFI units, which is lower than that of B8 binding to A-LC (Myc expression of four selected clones are shown in Fig. 2.5b). Overall, anti-B-LC VHHs isolated by both the phage display and YS2H were low affinity binders (K_D = 100 nM to 1 μM), suggesting a lack of the high affinity binders to B-LC protease in alpaca immune library.

Sequence analysis of the VHHs identified by phage or YS2H revealed that VHHs contain two, four, or six cysteines, which would result in up to two extra

disulfide bonds in addition to the one that is conserved in all immunoglobulin fold domains (Fig. 2.6e). We found that of the nine VHHs newly isolated by our YS2H system, three VHHs contain six cysteines, and the other six VHHs contain four cysteines. In contrast, either two or four cysteines were dominant in VHHs that were isolated by phage display. The VHHs identified by a phage display system may be limited to those that fold properly in a bacterial expression system. VHHs containing extra disulfides may fold improperly in bacteria, whereas the formation of correct disulfide bonds is much less problematic in yeast.

Discussion

Here we demonstrate that our novel system, YS2H, is highly efficient in the detection and discovery of protein-protein interactions. The quantitative nature of YS2H is from the fact that protein-protein interactions occur via a secretory pathway, and the amount of the prey protein in complex with the bait is determined by the equilibrium affinity between the two. With the use of a PCA technique, our system may be designed to discriminate different pairs of protein-protein interactions according to their kinetics of binding.

The utility of *in vivo* methods for quantitative estimation of binding affinity extends to the cases where one aims to increase the affinity of weak interactions between antigen and antibody and to engineer high affinity ligands and receptors that can potentially serve as agonists or antagonists. As an example, a prokaryotic system capable of co-expression of antigens anchored on the inner membrane of bacteria and single chain variable fragments (scFv) as soluble form was efficient in affinity screening and maturation [24]. Therefore, co-expression of antigen and antibody through eukaryotic secretory system will further enable screening of antibody libraries

against the proteins that require eukaryotic folding machinery or that undergo post-translational modifications.

The amount of the prey bound to the bait in our system follows the Langmuir binding isotherm model. With the expression system used in this study, the concentration of prey proteins released into the media is far larger than that of the bait proteins, which is fused to Aga2. Under the mating conditions, the number of agglutinin goes up to 10,000 copies/cell [25], which approximates the concentration of the bait proteins to be 1.7 nM at 10^8 cells/1 ml of culture medium. The Langmuir equation is then given by [bait:prey]/[bait] = [prey]/([prey] + K_D) where [bait:prey], [bait], and [prey] denote the concentrations of the bait in complex with the prey, the bait, and the prey, respectively. By replacing [bait:prey] and [bait] with antibody binding to Myc (MFI_Myc) and FLAG tag (MFI_FLAG), respectively, and taking into consideration of the MFI ratio (α) of anti-Myc to anti-FLAG antibody binding to equal copies of Myc and FLAG tags, the Langmuir equation rearranges into 1/MFI_Myc = α^{-1} (1+ K_D/[prey])/MFI_FLAG. From this equation (with measured values of α = 15 and [prey] = 10 nM), the K_D values predicted for coiled coil interactions (E5-K5, E5-K4, E4-K4, and E5-K3) closely approximated the K_D values measured by SPR [17] (Table 2.2). The quantitative nature of YS2H in measuring protein-protein interactions extends to antigen and antibody interactions. The binding affinity of scFv TS1/22 to the wild-type and HA I domain, scFv AL-57 to the HA I domain, and the F265S ranged between 148 and 237 nMK_D, whereas it was 440 nM for the binding of L295P to scFv AL-57. SPR measurement of the binding of I domain variants to scFv AL-57 estimated that although F265S and HA I domains have comparable affinity to scFv AL-57, L295P showed much lower affinity (Fig. 2.5, e and f, and Table 2.2). Predicted affinity for VHH-B8 and VHH-G6 binding to A-LC is 38 and 143 nM, compared with the measured K_D of 2.3 and 230 nM, respectively.

Table 2.2. Comparison of equilibrium dissociation constants (K_D) predicted from YS2H versus directly measured using surface plasmon resonance.

Interaction pairs	Predicted from YS2H (means ± S.E.)	SPR measurements
	nM	nM
E3-K3	1269.5 ± 53	32000 ± 3000[a]
E5-K3	1292.8 ± 37	7000 ± 800[a]
E4-K4	150.7 ± 48	116 ± 8[a]
E5-K4	18.3 ± 3	14 ± 1[a]
E5-K5	0.49 ± 0.2	0.063 ± 0.005[a]
HA-AL57	150.9 ± 8	32.6 ± 0.28[b]
F265S-AL57	237.4 ± 11.6	15.7 ± 0.03[b]
L295P-AL57	439.7 ± 13.6	243 ± 3.9[b]
VHH-B8-A-LC	38.2 ± 13.3	2.3 ± 0.08[b]
VHH-G6-A-LC	143.0 ± 41.9	230 ± 1.3[b]

[a]The values are from the paper by De Crescenzo et al. [17]. Shown are the means ± 95% confidence interval.

[b]The values are measured from this study. Shown are the means ± S.E., estimated from BIAevaulation software from Biacore.

Overall, the affinity predicted by the level of antibody binding to Myc and FLAG tag in our system agreed well with the measured affinity in the range of 1 nM to 1 μMK_D (Table 2.2).

Although antibody binding to the Myc tag for protein-protein interactions higher than 10 μMK_D reduced to the level of background (Fig. 2.3a), the detection by GFP complementation spanned a larger range of affinities, exhibiting a linear decrease in the fluorescence with an increase in K_D in log scale (Fig. 2.3b). This is attributed to the fact that reconstituted GFP does not dissociate (or complementation is irreversible), such that the complemented GFP is functional whether or not the prey and the bait exist as a complex on the cell surface. Therefore, the dominant factor that determines GFP reconstitution will be the rate at which two coils associate (on-rate) to initiate split GFP assembly. Notably, when the MFI of reconstituted GFP was plotted against the measured on-rates [17] for E5-K5, E5-K4, E4-K4, and E5-K3 (on-rate is unavailable for E3-K3), a liner trend was obtained with a R^2 value of 0.95 (Fig. 2.3d). However, the use of GFP complementation was limited to the study of coiled coil interactions, because the I domain fused to the split GFP did not express on the surface. Therefore, to apply a PCA technique to detect diverse protein-protein interactions through the secretory pathway, split GFP needs to be optimized not to interfere with the folding of the bait and prey proteins. The additional parameter to be optimized is the length of the linker connecting split GFP to the proteins to enable GFP complementation for a wide range of size variation in proteins and topological variation between the binding interface and the GFP fusion site [6].

The fact that GFP complementation occurs by protein-protein interaction through the secretion process explains its quantitative correlation with the strength of protein-protein interactions. This is in contrast to a previous finding [4] that GFP complementation from protein interactions occurring in the cytosol only indicates the

presence of the interaction, and fluorescence intensity is relatively invariant with the affinity of two proteins. Indeed, when the two coils were expressed in the cytosol with the deletion of the secretory signal sequence, we found that overall fluorescent intensity was higher, and the complementation of split GFP lacked correlation with the strength of coiled coil association (Figs. 2.2d and 2.3c). Because of the irreversible complementation of split GFP, after 24–48 h of induction, it is the concentration of two interacting proteins in the cytosol that determines the GFP complementation rather than their interaction strength.

Systems such as ribosomal [26], phage [27], and yeast [14] displays provide efficient means to couple genotype and phenotype and to screen library for protein engineering and antibody discovery. A typical screening process of antibody libraries requires exogenous antigens in their soluble form. Co-expression of two proteins within the same display system, e.g. the fusion of antigen and antibody into split phage coat protein [28] and the expression of antigen and antibody in bacterial periplasm as bait and prey proteins [24], can be particularly useful if target antigens are hard to express or unstable in solution. Our new system will offer a method to select antibodies against antigens that need to be expressed in eukaryotes. Other applications of YS2H may include expression of heterodimeric proteins, as demonstrated by similar platforms for expression of heterodimeric mammalian proteins such as major histocompatibility complex II α and β subunits [29] and antibodies in Fab format [30]. The use of our system to quantify and discover protein-protein interactions is not necessarily limited to the study of secretory proteins, because many proteins in nonsecretory cellular compartments or cytosol will maintain native conformations and interactions.

An *in vivo* tool to map protein interactions has generated a large set of protein interactions, particularly among yeast proteins [6]. The readouts from the assays such

as yeast two-hybrid and PCA are of cell growth caused by the expression of auxotrophic markers or reconstitution of enzymes and fluorescent proteins and are suitable for determining the presence or absence of protein interactions. In the case of protein network "hubs" in the binary protein interactome, i.e. the proteins interacting with a large number protein partners, the information on the strength of pairwise interactions may provide an important insight into the flow of biological signals orchestrated by the protein hubs. Our newly developed YS2H system is well poised to implement such tasks. For example, in YS2H the hub proteins and known interacting partners are expressed as a pair of the bait and the prey, respectively, and the strength of pairwise interactions can be quantitatively estimated by antibody binding to fusion tags. Additionally, one can discover unknown interaction partners by expressing a library of hypothetical interacting partners in YS2H.

REFERENCES

1. Fields S, Song O. A novel genetic system to detect protein-protein interactions. Nature. 1989;340(6230):245-6.

2. Ghosh I, Hamilton AD, Regan L. Antiparallel leucine zipper-directed protein reassembly: Application to the green fluorescent protein. J Am Chem Soc. 2000;122(23):5658-9.

3. Hu CD, Chinenov Y, Kerppola TK. Visualization of interactions among bZip and Rel family proteins in living cells using bimolecular fluorescence complementation. Mol Cell. 2002;9(4):789-98.

4. Magliery TJ, Wilson CGM, Pan WL, Mishler D, Ghosh I, Hamilton AD, et al. Detecting protein-protein interactions with a green fluorescent protein fragment reassembly trap: Scope and mechanism. J Am Chem Soc. 2005;127(1):146-57.

5. Remy I, Michnick SW. Mapping biochemical networks with protein-fragment complementation assays. Methods Mol Biol. 2004;261:411-26.

6. Tarassov K, Messier V, Landry CR, Radinovic S, Serna Molina MM, Shames I, et al. An in vivo map of the yeast protein interactome. Science. 2008;320(5882):1465-70.

7. Stagljar I, Fields S. Analysis of membrane protein interactions using yeast-based technologies. Trends Biochem Sci. 2002;27(11):559-63.

8. Nyfeler B, Michnick SW, Hauri HP. Capturing protein interactions in the secretory pathway of living cells. P Natl Acad Sci USA. 2005;102(18):6350-5.

9. Arnon SS. Botulinum toxin as a biological weapon: Medical and public health management (vol 285, pg 1059, 2001). Jama-J Am Med Assoc. 2001;285(16):2081-.

10. Jin M, Song G, Carman CV, Kim YS, Astrof NS, Shimaoka M, et al. Directed evolution to probe protein allostery and integrin I domains of 200,000-fold higher affinity. P Natl Acad Sci USA. 2006;103(15):5758-63.

11. Maass DR, Sepulveda J, Pernthaner A, Shoemaker CB. Alpaca (Lama pacos) as a convenient source of recombinant camelid heavy chain antibodies (VHHs). J Immunol Methods. 2007;324(1-2):13-25.

12. Gietz RD, Schiestl RH. Large-scale high-efficiency yeast transformation using the LiAc/SS carrier DNA/PEG method. Nat Protoc. 2007;2(1):38-41.

13. Colby DW, Kellogg BA, Graff CP, Yeung YA, Swers JS, Wittrup KD. Engineering antibody affinity by yeast surface display. Method Enzymol. 2004;388:348-58.

14. Boder ET, Wittrup KD. Yeast surface display for screening combinatorial polypeptide libraries. Nat Biotechnol. 1997;15(6):553-7.

15. Johnston M, Davis RW. Sequences That Regulate the Divergent Gal1-Gal10 Promoter in Saccharomyces-Cerevisiae. Mol Cell Biol. 1984;4(8):1440-8.

16. Egel-Mitani M, Hansen MT, Norris K, Snel L, Fiil NP. Competitive expression of two heterologous genes inserted into one plasmid in Saccharomyces cerevisiae. Gene. 1988;73(1):113-20.

17. De Crescenzo G, Litowski JR, Hodges RS, O'Connor-McCourt MD. Real-time monitoring of the interactions of two-stranded de novo designed coiled-coils: effect of chain length on the kinetic and thermodynamic constants of binding. Biochemistry. 2003;42(6):1754-63.

18. Shimaoka M, Xiao T, Liu JH, Yang Y, Dong Y, Jun CD, et al. Structures of the alpha L I domain and its complex with ICAM-1 reveal a shape-shifting pathway for integrin regulation. Cell. 2003;112(1):99-111.

19. Sanchez-Madrid F, Krensky AM, Ware CF, Robbins E, Strominger JL, Burakoff SJ, et al. Three distinct antigens associated with human T-lymphocyte-mediated cytolysis: LFA-1, LFA-2, and LFA-3. Proc Natl Acad Sci U S A. 1982;79(23):7489-93.

20. Huang L, Shimaoka M, Rondon IJ, Roy I, Chang Q, Po M, et al. Identification and characterization of a human monoclonal antagonistic antibody AL-57 that preferentially binds the high-affinity form of lymphocyte function-associated antigen-1. J Leukoc Biol. 2006;80(4):905-14.

21. Hagihara Y, Kim PS. Toward development of a screen to identify randomly encoded, foldable sequences. Proc Natl Acad Sci U S A. 2002;99(10):6619-24.

22. Shimaoka M, Kim M, Cohen EH, Yang W, Astrof N, Peer D, et al. AL-57, a ligand-mimetic antibody to integrin LFA-1, reveals chemokine-induced affinity up-regulation in lymphocytes. Proc Natl Acad Sci U S A. 2006;103(38):13991-6.

23. Hamers-Casterman C, Atarhouch T, Muyldermans S, Robinson G, Hamers C, Songa EB, et al. Naturally occurring antibodies devoid of light chains. Nature. 1993;363(6428):446-8.

24. Jeong KJ, Seo MJ, Iverson BL, Georgiou G. APEx 2-hybrid, a quantitative protein-protein interaction assay for antibody discovery and engineering. Proc Natl Acad Sci U S A. 2007;104(20):8247-52.

25. Dranginis AM, Rauceo JM, Coronado JE, Lipke PN. A biochemical guide to yeast adhesins: glycoproteins for social and antisocial occasions. Microbiol Mol Biol Rev. 2007;71(2):282-94.

26. Hanes J, Pluckthun A. In vitro selection and evolution of functional proteins by using ribosome display. P Natl Acad Sci USA. 1997;94(10):4937-42.

27. Smith GP. Filamentous Fusion Phage - Novel Expression Vectors That Display Cloned Antigens on the Virion Surface. Science. 1985;228(4705):1315-7.

28. Krebber C, Spada S, Desplancq D, Krebber A, Ge LM, Pluckthun A. Selectively-infective phage (SIP): A mechanistic dissection of a novel in vivo selection for protein-ligand interactions. J Mol Biol. 1997;268(3):607-18.

29. Boder ET, Bill JR, Nields AW, Marrack PC, Kappler JW. Yeast surface display of a noncovalent MHC class II heterodimer complexed with antigenic peptide. Biotechnol Bioeng. 2005;92(4):485-91.

30. van den Beucken T, Pieters H, Steukers M, van der Vaart M, Ladner RC, Hoogenboom HR, et al. Affinity maturation of Fab antibody fragments by fluorescent-activated cell sorting of yeast-displayed libraries. Febs Lett. 2003;546(2-3):288-94.

31. Jin M, Andricioaei L, Springer TA. Conversion between three conformational states of integrin I domains with a C-terminal pull spring studied with molecular dynamics. Structure. 2004;12(12):2137-47.

CHAPTER 3

COMBINATORIAL LIBRARIES AGAINST LIBRARIES FOR SELECTING NEOEPITOPE ACTIVATION-SPECIFIC ANTIBODIES

Summary

A systematic approach to the discovery of conformation-specific antibodies or those that recognize activation-induced neoepitopes in signaling molecules and enzymes will be a powerful tool in developing antibodies for basic science and therapy. Here, we report the isolation of antibody antagonists that preferentially bind activated integrin Mac-1 ($\alpha_M\beta_2$) and are potent in blocking neutrophil adhesion and migration. A novel strategy was developed for this task, consisting of yeast surface display of Mac-1 inserted (I) domain library, directed evolution to isolate active mutants of the I domain, and screening of phage display of human antibody library against the active I domain in yeast. Enriched antibody library was then introduced into yeast surface two-hybrid system for final quantitative selection of antibodies from monomeric antigen–antibody interaction. This led to highly efficient isolation of intermediate to high affinity antibodies, which preferentially reacted with the active I domain, antagonized the I domain binding to intercellular adhesion molecule (ICAM) -1, complement C3 fragment iC3b, and fibronectin, and potently inhibited neutrophil migration on fibrinogen. The strategy demonstrated herein can be broadly applicable

---

This chapter was originally published in the Proceedings of the National Academy of Sciences U.S.A., (Hu, X., Kang, S., Lefort, C., Kim, M., Jin, M.M. *Proceedings of the National Academy of Sciences U.S.A.* 2010;107(14):6252-7. © 2010 National Academy of Sciences, U.S.A.), and is reprinted with permission. Kang S contributed to the engineering of Mac-1 I domain by cell surface adhesion sorting against HeLa cells, and the assays related to the inhibition of neutrophil migration using AM01. This included the experiments and writings related to Fig. 3.1, Fig 3.2, Fig. 3.3, Table 3.1, Fig. 3.6, Fig. 3.8, Table 3.2, Table 3.3, and Fig 3.9.

to developing antibodies against modular domains that switch between inactive and active conformations, particularly toward the discovery of antibody antagonists in therapeutic and diagnostic applications.

Introduction

Conformational change of proteins is essential to affinity regulation in cell signaling molecules, interactions of viral proteins with host receptors, and proteins with enzymatic activity [1]. Antibodies that can recognize the activation-induced epitopes ("neoepitope") may in turn cause activation and/or probe different activation states of the molecules. In contrast to conformation-insensitive antibodies, neoepitope-specific antibodies may be used to diagnose activation state of cells and to deliver therapeutic agents to specific cells [2-3]. Some antibodies produced by animal immunization are specific to active conformation of antigens [4-6]. Alternative to screening hybridoma antibodies for conformation- or activation-specific properties, *in vitro* methods can be used to isolate antibodies by repeated cycles of selection and depletion (subtractive panning) against wanted and unwanted antigens, respectively [7-9]. In this regard, phage display systems of naïve, immunized, or synthetic antibody libraries [10-11] have been most successful in selection of human antibodies against purified proteins, surface molecules of mammalian cells, or a library of antigens in yeast cells.

Complex linkage between conformation and affinity regulation exists in integrins, which are transmembrane heterodimers consisting of noncovalently associated α and β subunits [12]. As leukocyte infiltration into the tissue requires activation of integrins, integrins expressed in leukocytes are important therapeutic targets in autoimmune and inflammation-related diseases. This is evidenced by the

fact that antibody antagonists targeting leukocyte-specific integrins such as lymphocyte function-associated antigen (LFA)-1 ($\alpha_L\beta_2$), Mac-1 ($\alpha_M\beta_2$), $\alpha_{IIb}\beta_3$, and $\alpha_4\beta_1/\alpha_4\beta_7$ have been approved or are under preclinical and clinical studies [13-15]. To reduce potential unwanted side effects caused by indiscriminate binding of antibodies to integrins, systematic *in vitro* approaches have been utilized to produce antibodies that are more specific to activated integrins [8-9, 16]. For example, a series of subtractive panning of phage library against different forms of Mac-1 expressed in mammalian cells [9] or the inserted (I) domain of LFA-1 [2, 8] have been used to isolate single chain antibodies that preferentially react with activated integrins.

The I domain, a major ligand binding site in the I domain-containing integrins, exists in multiple conformations of low to high affinity to ligands, which is coupled to the transition from an inactive to an active state of integrins [17-19]. Antibodies specific to the high affinity conformation of the I domain, therefore, may also be specific to active integrins in cells. Due to the fact that I domain is the ligand binding site, such antibodies will likely be activation-specific antagonists. Similar to the previous approach of selecting antibody library against antigen library [11], we examined if protein domains displayed on the surface of yeast and engineered for high affinity by directed evolution can be used to screen phage clones. We first isolated activating mutations by screening a yeast library of Mac-1 I domains against HeLa cells expressing ligands for Mac-1. Then phage library were panned against the active I domain in yeast, where the enrichment of reactive phage clones was monitored by flow cytometry. From enriched phage libraries, cDNAs encoding single chain fragment variable (scFv) antibody and active Mac-1 I domain were introduced as a pair of the bait and prey proteins into the yeast surface two-hybrid system (YS2H) [20] that was designed for quantitative estimation of protein–protein interactions. Antibodies selected from two steps of phage binding to yeast and antigen–antibody

interactions in YS2H were found to react with the active Mac-1 I domain and be potent in blocking neutrophil adhesion and migration. The streamlined process of antigen display and engineering in yeast display system [21], phage panning directly with antigens displayed in yeast, and quantitative selection of antibodies in YS2H can be adapted to the discovery of neoepitope-specific antibodies against other mammalian proteins.

Experimental Procedures

Construction of random mutagenesis library of Mac-1 I domain

To generate random mutagenesis library, 2 μM each of nucleotide analogues of 8-oxo-2′-deoxyguanosine-5′-triphosphate and (8-oxo-dGTP, TriLink) and 2′-deoxy-pnucleoside-5′-triphosphate (dPTP, TriLink) mixed in 200 μM of dNTP were used to PCR amplify cDNA encoding Asp132—Thr322 of the Mac-1 I domain. 15 μg of PCR product and 4 μg of linearized pCTCON digested at NheI and BamHI sites were mixed in 5 μl water for high-efficiency yeast transformation. The cDNA library-vector mixture was added to a cuvette containing freshly prepared 3×10^8 yeast competent cells in 50 μl of 10 mM Tris (pH 7.5), 270 mM sucrose, and 1 mM $MgCl_2$. Electroporation was performed according to the published protocol [22]. Transformation efficiency was approximately 4%, estimated by the number of colonies on selective dextrose (SD) medium (20 g⁄L dextrose, 6.7 g⁄L Difco yeast nitrogen base, 5 g⁄L Bacto casamino acids, 5.4 g⁄L Na_2HPO_4, 8.56 g⁄L $NaH_2PO_4 \cdot H_2O$) with 2% (wt/vol) agar. The Mac-1 I domain library cells were grown in SD media for 24 h at 30 °C with shaking, induced in SG media (20 g⁄L galactose, 6.7 g⁄L Difco yeast nitrogen base, 5 g⁄L Bacto casamino acids, 5.4 g⁄L Na_2HPO_4, 8.56 g⁄L

$NaH_2PO_4 \cdot H_2O$) for 24 h at 30 °C with shaking, and screened for binding to HeLa cell monolayers. HeLa cells were grown to full confluency on a 24-well plate and were washed once with washing buffer (PBS, 0.5% BSA, 10 mM $MgCl_2$). A total of 5×10^7 yeast cells from the library of Mac-1 I domain were washed once with washing buffer, resuspended in 300 µl of washing buffer, and applied to the confluent HeLa cells in 24-well plate. Yeast cells were first allowed to settle down for at least 2 h at RT. The yeast cells were then washed off from HeLa cells by gentle shaking of the 24-well plate on an orbital shaker for 15 min. The washing cycle was repeated until uninduced yeast cells were completely washed off from HeLa cells. Yeast cells that remained adhered to HeLa cells were then collected with elution buffer (PBS, 0.5% BSA, 10 mM EDTA). The collected yeast cells were centrifuged and resuspended in SD medium, allowed to grow for 24 h, and induced in SG medium for 24 h. The yeast library underwent two rounds of sorting, after which enriched yeast cells were grown in SD plate. Individual clones from the plate were tested for binding to HeLa cells, similarly as described for library sorting. Microscopic images of yeast clones that remained bound on the surface of HeLa cells were acquired with a CCD camera (Spot Insight, Diagnostic Instruments) at 4 random spots. The acquired images were processed by Image-Pro Plus (Media Cybernetics) for automated cell counts. From the yeast clones the plasmids were extracted using Zymoprep II Yeast Plasmid Miniprep Kit (Zymo Research) for DNA sequencing of the Mac-1 I domain.

Quantitative screening of antibody library in YS2H

To screen antibodies based on monomeric antigen–antibody interactions in yeast, the cDNA encoding scFv was PCR-amplified from the phagemid belonging to the library after the second and the fourth round sorting. Then, scFv and the F302L cDNAs were inserted into the YS2H vector as the prey and the bait, respectively. Two

different tags (Myc and Flag) were used for immunofluorescence staining. In YS2H, Flag tag is fused to the I domain at the C-terminal and used to measure the level of antigen expression, and Myc tag is placed at the C-terminal of scFv and used to estimate the affinity between the I domain and scFv. The level of tag expression was measured by the binding of antiFlag monoclonal antibody and antiMyc antibody used at 5 μg⁄mL in PBS with 0.5% BSA and 10 mM $MgCl_2$. From mean fluorescence intensity (MFI) values of flag and myc tag expression, the affinity between antibody and the I domain was predicted using the first-order Langmuir equation, given by [bait : prey]/[bait] = [prey]/([prey] + K_D) or $1/MFI_{Myc} = \alpha^{-1} (1 + K_D/[prey])/MFI_{Flag}$, where α is the MFI ratio of antiMyc to antiFlag antibody binding to equal copies of Myc and Flag tags and [prey] = 10 nM [20].

Expression of the Mac-1 I domains and scFv

Wild-type Mac-1 I domain (Asp132-Ala318) and the mutants of F302L and I316G with six histidine (His tag) at the C-terminal were cloned into pET20b (EMD Chemicals). The scFvs in the phagemid vector, pIT2 were cloned into pET20b with His and Myc tags fused at the C-terminal. These proteins were expressed as soluble forms and purified by Nickel-nitrilotriacetic acid (NTA) column. Both proteins were expressed in BL21(DE3) (Invitrogen) as soluble proteins. BL21-transformed cells were grown at OD_{600} to 0.4, to which 1 mM isopropyl β-D-1-thiogalactopyranoside was added. Cells were induced to express protein at 30 °C by culturing for 6 hours with shaking at 250 rpm. After induction, cells were spun down, resuspended in binding buffer (50 mM sodium phosphate at pH 8.0, 300 mM sodium chloride, and 10 nM imidazole), sonicated to break the cell wall, and spun at 10,000 g for 15 min to remove cell debris. Proteins in the supernatant were purified with NTA column followed by gel filtration chromatography using Superdex 75 column connected to

AKTA Purifier (GE Healthcare). By comparing to the molecular weight markers for gel filtration chromatography (Sigma–Aldrich), the molecular weight of single-chain antibodies (AM01 and AM17) was estimated to be 25–30 kDa, indicating these antibodies exist as monomer in solution. The purity and the size of proteins were confirmed by sodium dodecyl sulfate polyacrylamide gel electrophoresis.

Surface plasmon resonance (SPR) analysis

CM5 sensor chip was prepared using an amine coupling kit (BIAcore) to immobilize Mac-1 ligands (inactivated complement component 3b (iC3b, EMD Biosciences), fibronectin (Invitrogen), and ICAM-1) or antibodies against Mac-1 (AM01, CBRM1/5 [4], and mAb44 [23]). SPR was measured using Biacore (BIA2000) as described previously [22]. To measure the affinity of I domain variants to Mac-1 ligands or antibodies, the I domains were injected over the chip in injection buffer (20 mM Tris HCl, pH 8.0, 150 mM NaCl, 10 mM $MgCl_2$) at a flow rate of 10 μl/ min at RT. To examine the potency of antibodies in blocking I domain binding to ligands, the I domains at 200 nM were preincubated with antibodies (AM01, CBRM1/5, and mAb44) at 62.5—1000 nM (per valency using the values of 30 kDa for scFv and 75 kDa for immunoglobulins) for 15–30 minutes at RT and the mixture was injected over the chip coated with Mac-1 ligands. The chip surface was regenerated by flowing 20 μl of 10 mM Tris-glycine, pH 2.0 buffer. The IC20 values of the antagonists in blocking Mac-1 binding to ICAM-1, fibronectin, and iC3b were determined by fitting the equation $A = A_{MAX} - (A_{MAX}/[1 + IC_{50}/L])$ to the data (GraphPad Prism), where "A" is the sensogram data and "L" is the molar concentration of inhibitors.

Antibody binding to neutrophils

To separate neutrophils, 20 mL of whole blood were drawn from volunteers (under the permission of Cornell Institutional Review Board), cooled down to RT, and loaded on top of 20 mL of 1-Step® Polymorphs (Accurate Chemical and Scientific Corporation). The gradient was centrifuged at 500 g for 30 min at 22 °C. After centrifuge, neutrophils in the polymorphonuclear fraction were taken out and washed with Hank's balanced salt solution without calcium and magnesium ions (Invitrogen). Purified neutrophils were suspended in PBS, 0.5% BSA with 1 mM $MgCl_2$, 1 mM $MgCl_2$ plus1 mM EGTA, or 1 mM EDTA, incubated with single-chain antibodies at RT for 10 min, washed, and then fixed with 3.7% formaldehyde for 10 min. Then neutrophils were incubated in respective labeling buffer with 5 μg⁄mL antiHis antibody on ice for 45 min, washed, and subsequently incubated with 5 μg⁄mL goat antimouse antibody conjugated with PE. The cells were washed and resuspended in PBS for flow cytometry analysis.

Immunofluorescence flow cytometry

Antibodies used in this study were the anti- Myc antibody 9E10 (ATCC), antiFlag (Genscript), and phycoerythrin-labeled goat polyclonal antimurine antibodies (Santa Cruz Biotechnology). After induction, yeast cells were harvested, washed in 100 μl of the labeling buffer (PBS containing 0.5% BSA with 10 mM $MgCl_2$ or 10 mM EDTA), and then incubated with ligands in 50 μl of the labeling buffer for 20 min with shaking at 30 °C. Cell were then washed and incubated with secondary antibodies at 5 μg⁄mL in 50 μl of the labeling buffer for 20 min at 4 °C. Finally, cells were washed once in 100 μl and suspended in 100 μl of the labeling buffer for flow cytometry (Epics XL flow cytometer, Beckman Coulter).

Adhesion inhibition assay

The 96-well V-bottom plate (Greiner) was coated with fibrinogen (100 μg⁄mL) or 2% BSA in PBS, pH 7.4 overnight at 4 °C, and washed three times before incubation with neutrophils. Neutrophils were suspended in PBS at 10^7 cells⁄mL with 1 mM $MgCl_2$ or 1 mM $MgCl_2$ and 1 mM EGTA to induce active conformation of Mac-1[24]. To this mixture, antibodies at 20 μg⁄mL and 2,7-bis-(2-carboxyethyl)-5-(and-6)-carboxyfluorescein acetoxymethyl ester (BCECF-AM) at 2 μg⁄mL were added. After 15 min incubation at RT, neutrophils were washed in PBS with 1 mM $MgCl_2$ plus with or without 1 mM EGTA and added to the V-bottom wells, and the plate was then subjected to centrifugation at 55 g for 1 min to cause nonadherent or weakly bound cells but not strongly adherent cells to accumulate at the tip of the V-bottom well [22]. The number of nonadhered cells was measured by a fluorescent plate reader (Synergy HT, Biotek). To detach all the adherent cells to measure the fluorescence from the total number of cells in each well, the plate was centrifuged at 873 g for 20 min.

Neutrophil adhesion and migration inhibition assay

The 96-well V-bottom plate (Greiner) assay [22] was used to measure the potency of antibodies in blocking neutrophil binding to fibrinogen (100 μg/mL). The percent relative inhibition by antibodies was calculated as 100× (F_antibody - F_BSA) / (F_max - F_BSA), where F_antibody, F_BSA, and F_max correspond to the level of BCECF-AM fluorescence from the neutrophils incubated with antibody and BSA, and with maximum centrifugation (873 g), respectively. Cell migration assay was carried out as previously described [25]. In brief, delta T dish (Fisher Scientific) was coated with 100 μg⁄mL fibrinogen (Sigma) in PBS, pH7.4 at 4 °C overnight and washed three times with PBS containing 1 mM $MgCl_2$ and 1 mM $CaCl_2$. 5×10^5 neutrophils were diluted in 1 ml L-15 media (Gibco), to which antibodies were added at 20 μg⁄mL.

After incubation at room temperature for 15 min, neutrophils were transferred to the delta T dish and prewarmed to 37 °C for 5 min. The images of neutrophil migration were recorded for 20 minutes on every 10 seconds using Nikon TE-2000U inverted microscope. During 20 min recording, 10 nM formyl-Met-Leu-Pro (fMLP) was added at 1 min after neutrophils were added to the dish. From the recorded differential interference contrast (DIC) microscopic images, the frames of the last 12 minute interval were chosen for analysis. The movie was contrast enhanced for automated object tracking using Image-Pro Plus to trace the migration path of individual cells. Only the neutrophils present in the image field for the entire 12-minute of the movie were included in analysis.

Selection of reactive phage clones

A phage library (2×10^{13} colony forming unit) of human single chain (scFv) antibody (Tomlison I/J phage libraries [26]) was incubated in 3 mL PBS containing 1 mM $MgCl_2$ and 2% instant nonfat dry milk (Carnation) for 30 min at RT, followed by 30 min incubation at RT with 10^7 yeast cells expressing unrelated proteins (heat shock factor 1) in 3 mL PBS containing 1 mM $MgCl_2$. After incubation, cells were spun down and the supernatant containing unbound phage clones was adjusted with 10 mM $MgCl_2$, to which 10^7 yeast cells expressing the active Mac-1 I domain (F302L) were added. After 30 min incubation at RT, yeast cells were spun down, washed with PBS with 10 mM $MgCl_2$, and the pellet was treated with 1 mg/mL trypsin for 10 min at RT to release bound phage from yeast cells. Phage clones eluted into the supernatant were used to infect Escherichia coli (TG1) to produce the next round of phage library. The binding of phage clones to yeast cells was monitored by immunofluorescence flow cytometry using antibodies against His-tag placed between single chain antibody and pIII coat protein.

Results

Overview of antibody selection strategy

Various mammalian proteins have been expressed functionally in yeast as a fusion to a cell wall protein called agglutinin [20, 27-30]. To isolate mutations that induce active conformation, a mutagenesis library of the Mac-1 I domain was sorted against HeLa cells, which express ICAM-1 and other ligands for Mac-1 (Fig 3.1). Against yeast cells expressing active mutant of Mac-1 I domain, a phage library of human single chain antibody (scFv) was panned to select for activation-specific antibodies. Using immunofluorescence flow cytometry, phage binding to yeast cells was monitored by antibody binding to the His tag, which is placed between the scFv and the phage coat protein, pIII. With successive sorting, the enrichment of reactive phage clones led to an increase in antiHis antibody binding. Next, the scFv cDNA library amplified from enriched phage clones was then introduced into the YS2H vector, where the affinity between antigen and antibody can be estimated by the flow cytometry measurement of antitag antibody binding. Final selection of antibodies in the YS2H enabled quantitative assessment of candidate antibodies according to their 1:1 binding affinity to the antigen.

Selection of active Mac-1 I domain by directed evolution

The I domain in integrin Mac-1 exists at low and high affinity conformation, which is stabilized in inactive and active state of full-length Mac-1, respectively. To isolate mutations that would induce high affinity conformation of the I domain, we constructed a mutagenesis library of the I domain (Asp132—Thr322) in yeast display and sorted yeast cells by their binding to HeLa cells. Whereas yeast cells expressing the wild-type I domain were easily washed out from HeLa, the number of bound yeast

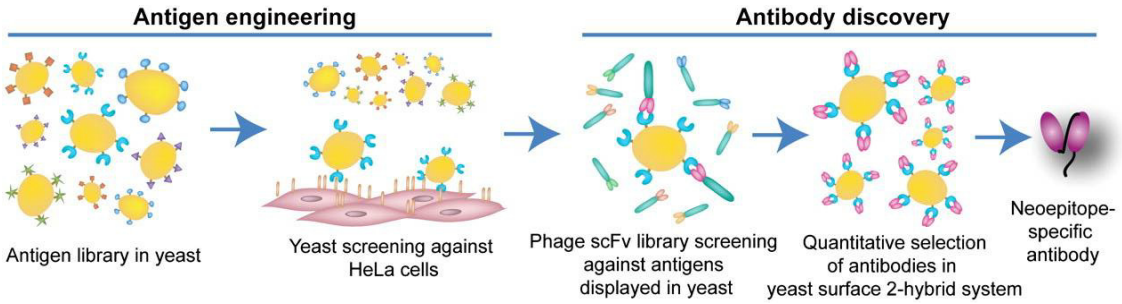

Figure 3.1. Streamlined antibody selection strategy.

A mutagenesis library of antigens expressed in yeast display system [21] is subjected to directed evolution to isolate mutations to induce active conformation, to which a phage library of human single-chain antibody is screened. Final selection of specific antibodies is made in yeast surface 2-hybrid system [20] according to quantitative assessment of monomeric antigen–antibody interactions.

cells progressively increased with successive sorting (Fig 3.2a). High affinity binders from the second sort library were collected and grown in SDCAA plate. Twenty-four clones from the plate were individually tested for binding to HeLa, from which five unique clones containing one or two mutations were isolated. These five clones bound to HeLa better than the second sort library (Fig. 3.3). One highest binder was found to contain Leu substitution for Phe-302. Phe-302 is located in the loop between the β6-strand and the α7-helix (Fig. 3.3b), which was identified as an activation hot spot in Mac-1 (F302W) [18] and its equivalent position as a hot spot in LFA-1 (F292G) [22]. To confirm that the mutation of F302L induced high affinity conformation of the I domain, the I domains with the mutations of F302L and the previously identified I316G [31] were produced in bacteria and tested for binding to ICAM-1, iC3b, and fibronectin using surface plasmon resonance (Fig. 3.2, b and c). The mutation of I316G would disrupt van der Waals interactions of Ile-316 with the neighboring residues in a low affinity conformation (Fig. 3.3e), inducing high affinity conformation [23]. Whereas the wild-type I domain showed little binding to fibronectin and ICAM-1, and low-level binding to iC3b (K_D = 1.8 μM) (Table 3.1), the active mutants of F302L and I316G bound much stronger to all three ligands (Fig. 3.2, b and c). Overall, the F302L exhibited slower kinetics in both association (k_{on}) and dissociation rates (k_{off}) than the I316G, and bound with higher affinity to the ligands (Fig. 3.2, b and c, and Table 3.1).

Selection of antibody library against yeast cells expressing active Mac-1 I domain

Nonspecific binders of phage clones were first depleted by incubation with yeast cells expressing unrelated proteins. The remaining phage clones were then panned against the yeast cells expressing Mac-1 I domain with F302L. The binding of

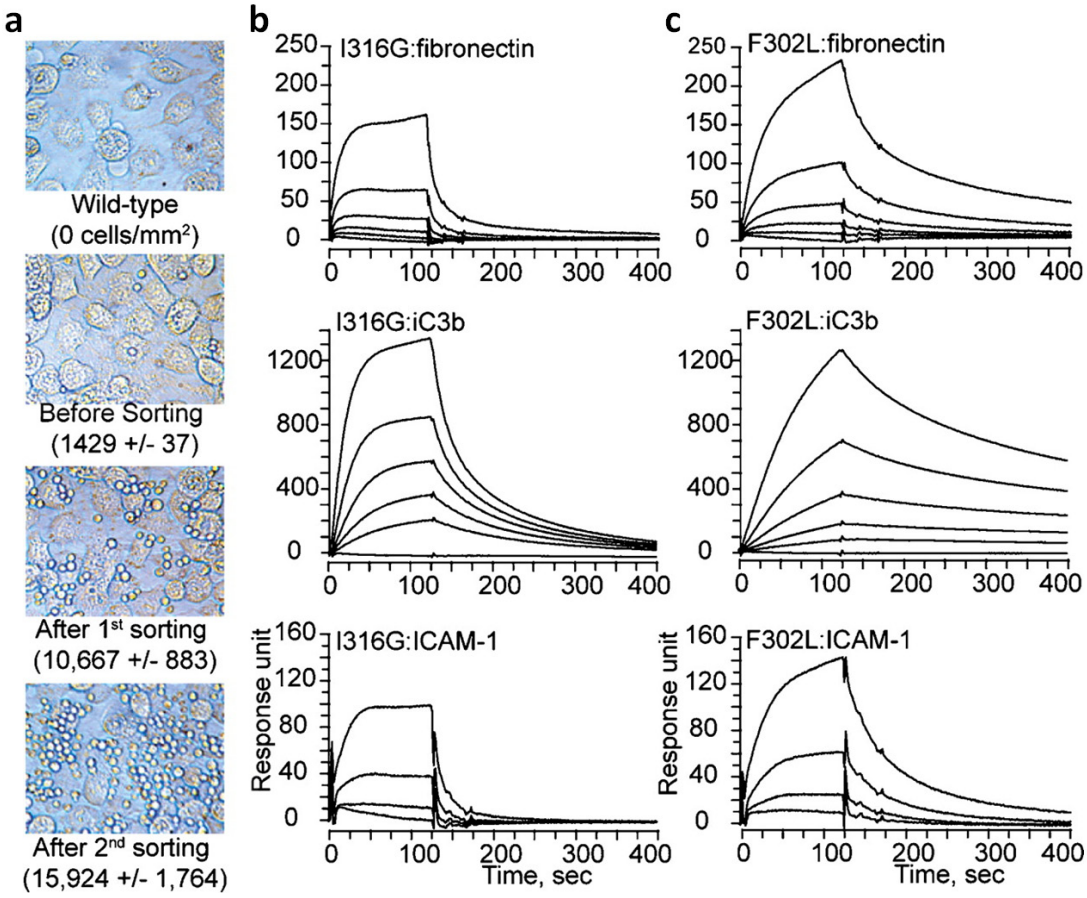

Figure 3.2. Selection of high affinity Mac-1 I domains.

(a) A mutagenesis library of Mac-1 I domain in yeast was screened with HeLa cells to isolate high affinity mutants. Yeast cells appear as small bright spheres in the images. (b&c) SPR measurement of the binding of active I domains (I316G and F302L) to ICAM-1, iC3b, and fibronection. I domains were injected at a series of two-fold serial dilutions starting at 250 nM.

Figure 3.3. Identification of activation mutations in Mac-1 I domain.

(a) From sequence analysis of twelve clones, five unique clones containing one or two mutations were isolated, which contained mutations along α1-helix (H148R, E155G/K, E162K, L164S) and at the loop between the β6 strand and the α7-helix (F302L) (b–e). Mac-1 I domain was drawn in cartoon using PyMOL (DeLano Scientific) with α-helices and β-strands colored in cyan and yellow, respectively. (b&c) The closed (b) and open (c) conformations were modeled based on the crystal structures as described previously [42]. The residues where activation mutations were found and the residues in their vicinity were drawn in sticks. The activation of the I domains by the mutations along the α1-helix has not been isolated before: The activation by E155K/G and presumably by H148R (b) may be due to the disruption of favorable electrostatic attraction, as Glu-155 forms interaction with Lys-306 only in the closed position of the α7-helix (b&c); the insertion of Arg into His-148 and as a result Arg triad (at 148, 151, and 152) would likely to create unfavorable electrostatic interaction in a closed conformation. In the open conformation, the residues at 148, 151, and 152 move away from each other (c). (d&e) L164S would induce high affinity conformation by presumably disrupting the interaction of Leu164 with Ile-316 (e), which creates van der Waals interaction with neighboring hydrophobic residues in the closed position of the α7-helix.

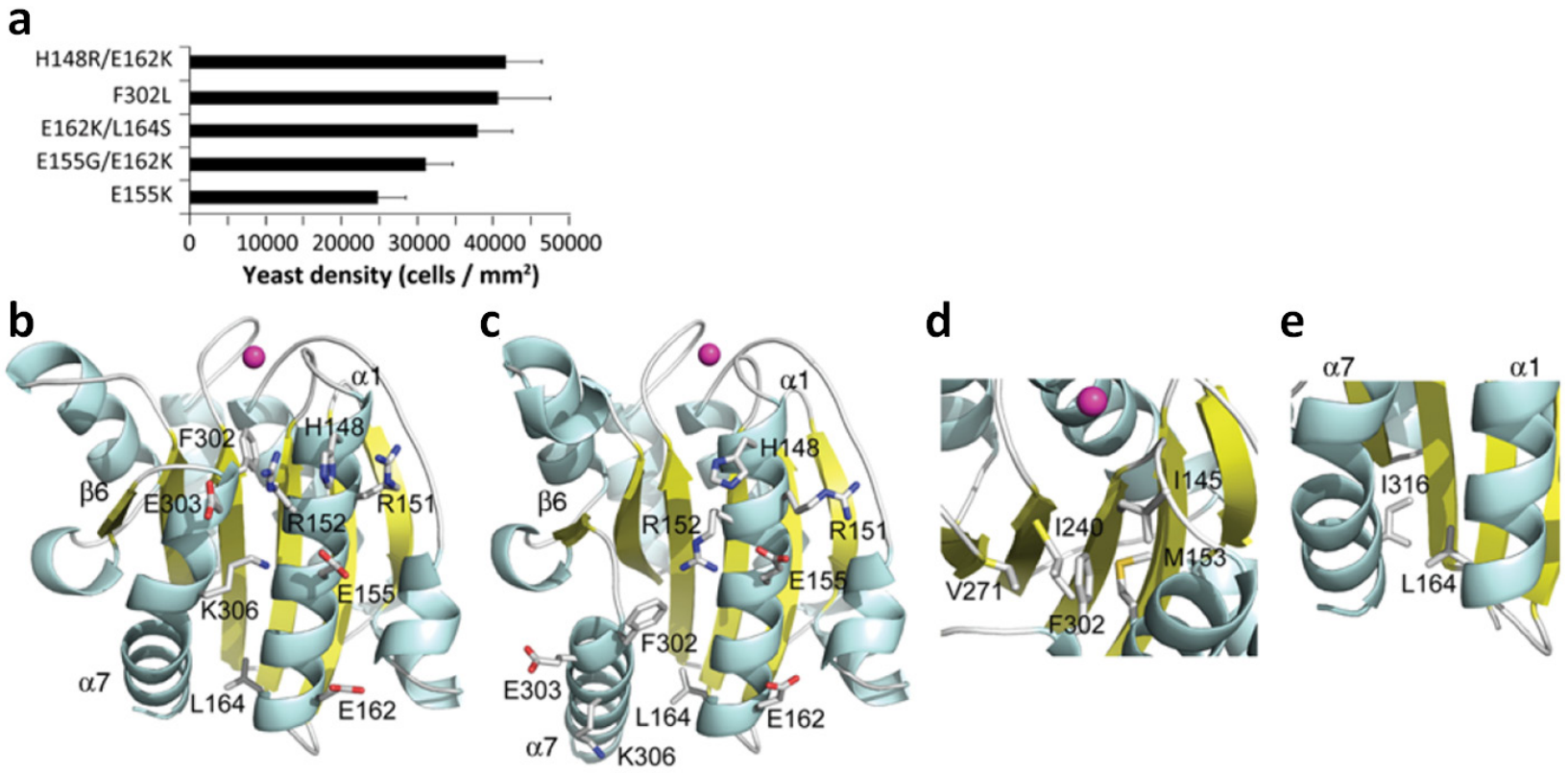
a
H148R/E162K
F302L
E162K/L164S
E155G/E162K
E155K
0
10000
20000
30000
40000
50000
Yeast density (cells / mm²)
b
α1
F302
H148
β6
E303
R151
R152
E155
K306
α7
L164
E162
c
α1
H148
β6
R152
R151
E155
F302
E303
L164
E162
α7
K306
d
I145
I240
M153
V271
F302
e
α7
α1
I316
L164

Table 3.1. SPR measurement of the binding of physiological ligands to the wild-type and active I domain mutants.

		MgCl2		
		ICAM-1	iC3b	fibronectin
WT	k_{on} (M^{-1} s^{-1} × 10^{-3})	ND	ND	ND
	k_{off} s^{-1} × 10^{3}	ND	ND	ND
	K_D (M × 10^{9})	ND	1820 ± 25.4	ND
I316G	k_{on} (M^{-1} s^{-1} × 10^{-3})	92.3 ± 32.7	231.3 ± 11.6	163.0 ± 20.2
	k_{off} s^{-1} × 10^{3}	110.9 ± 55.6	9.69 ± 0.69	53.50 ± 10.6
	K_D (M × 10^{9})	1050 ± 199	41.8 ± 1.43	363 ± 86.8
F302L	k_{on} (M^{-1} s^{-1} × 10^{-3})	61.1 ± 11.8	47.9 ± 4.6	50.9 ± 11.1
	k_{off} s^{-1} × 10^{3}	17.1 ± 2.6	1.63 ± 0.25	9.44 ± 0.20
	K_D (M × 10^{9})	339 ± 110	33.5 ± 1.98	222 ± 42.0

The values are mean ± S.E., estimated from BIAevaluation software from Biacore.

the enriched phage clones to the F302L after each round of sorting was examined by flow cytometry (Fig. 3.4a). The binding of the second sort phage library to F302L was metal-ion dependent (38% vs. 1% with EDTA), indicating that the metal-ion dependent adhesion site (MIDAS) is the key epitope for antibody binding. Positive binding to the wild-type I domain was also observed with the third and fourth round sort. The fourth sort library contained phage clones that reacted with the wild-type I domain with or without the metal-ion. For the final selection of antibodies, we constructed the YS2H vector with the F302L cDNA as the bait and the scFv cDNA as the prey proteins that were cloned from the second and the fourth sort libraries (Fig. 3.4b). In YS2H, the expression of Myc and Flag tag indicates, respectively, the amount of antibody captured by the antigen and the level of antigen expression. Although the second and the fourth sort phage libraries bound comparably to yeast cells (Fig. 3.4a), when the pair of antigen and antibody were expressed in yeast, yeast expressing the second sort antibody library exhibited much lower Myc expression than the fourth sort library (3% vs. 37%) (Fig. 3.4b). This discrepancy may arise from the excess of phage clones used in flow cytometry, which resulted in comparable binding to F302L irrespective of the difference in the percentage of reactive clones in the second vs. the fourth sort library. This is in contrast to Myc expression in YS2H, which reports the percentage of positive clones with mean fluorescence intensity correlating with the antigen–antibody interaction strength. Yeast cells expressing the fourth sort scFv library were grown in SDCAA plate, from which twenty-four clones were individually tested for tag expression. Nine clones among the twenty-four clones displayed positive Myc tag expression; from sequencing, three unique clones were identified. Whereas Flag tag expression was comparable in all three clones (clones 1, 2, and 17 were designated as AM01, AM2, and AM17), the level of Myc expression varied considerably with highest expression seen in clone AM01. Using the first-order

Figure 3.4. Selection of phage library against the F302L displayed in yeast.
(a) A phage library after each round of panning was examined for binding to the F302L and the wild-type I domain using flow cytometry. Unless noted otherwise, open and filled histograms correspond to antibody binding to uninduced and induced cells, respectively. Control indicates yeast cells expressing unrelated proteins. (b) The cDNAs amplified from the second and fourth round sort were introduced into the YS2H vector along with the F302L for final selection of antibodies. (c) Selected individual clones exhibit differential level of Myc expression, correlating with antibody-F302L binding affinity.

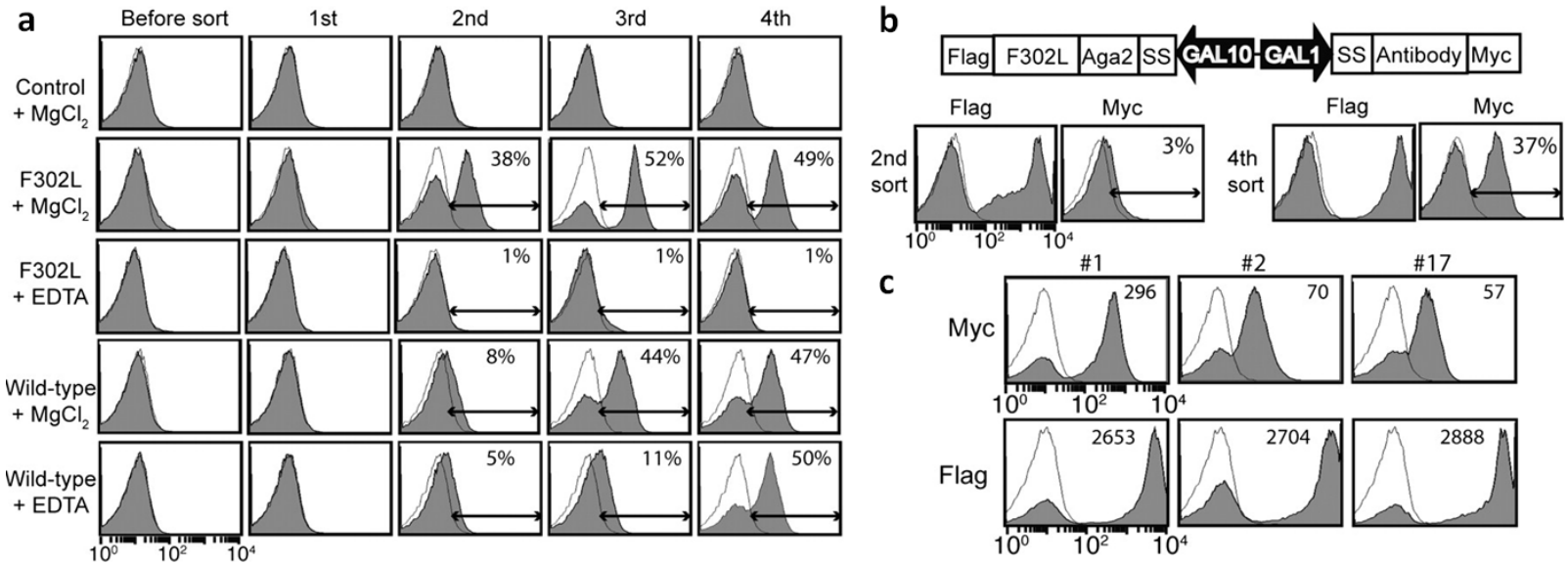
a
Before sort
1st
2nd
3rd
4th
Control + MgCl2
F302L + MgCl2
F302L + EDTA
Wild-type + MgCl2
Wild-type + EDTA
38%
52%
49%
1%
1%
1%
8%
44%
47%
5%
11%
50%
10^0 10^2 10^4
b
Flag
F302L
Aga2
SS
GAL10
GAL1
SS
Antibody
Myc
Flag
Myc
2nd sort
3%
4th sort
37%
c
#1
#2
#17
Myc
296
70
57
Flag
2653
2704
2888

Langmuir binding isotherm, the affinity (K_D) for AM01 and AM17 was determined at 34 nM and 241 nM, respectively. Sequencing analysis revealed that these three clones were identical in the framework regions, differing only in the complementarity determining regions 2 and 3 (CDR2 & CDR3) (Fig. 3.5).

Soluble antibody binding to Mac-1 I domain expressed in yeast

In YS2H, the prey proteins exist on cell surface due to their binding to the bait as well as in culture media; the level of soluble protein in the media was estimated to be around 10 nM for scFv (Fig. 3.6) [20]. Antibody concentration in the media was high enough for flow cytometry application without the need for purification. These antibodies were examined for binding to the active I domain mutants that were induced by different mutations (D132C/K315C [31], F302W, and I316G) to confirm that selected antibodies are activation-specific but not specific to the mutation itself (Fig. 3.7a). Single chain antibodies AM01 and AM17 both bound the F302L in a metal-ion dependent manner (10 mM $MgCl_2$ vs. 10 mM EDTA). AM01 exhibited higher affinity binding than AM17, and bound to other active mutants. To further examine antigen–antibody binding affinity, AM01 and AM17 were expressed from bacteria and used at 1, 5, and 10 μg/ml to label the wild type and the active I domain mutants (Fig. 3.7b). Overall, the binding of purified antibodies to I domains was in good agreement with the antibodies produced in yeast: Whereas AM01 bound the active I domains much higher than the wild type, the binding of AM17 was more specific to the F302L, displaying low-level binding to D132C/K315C, F302W, and I316G and no binding to the wild-type I domain. Without the metal ions, AM01 exhibited much lower binding to the active I domains, whereas binding was undetectable with AM17. It can be hypothesized that although the metal ion in the

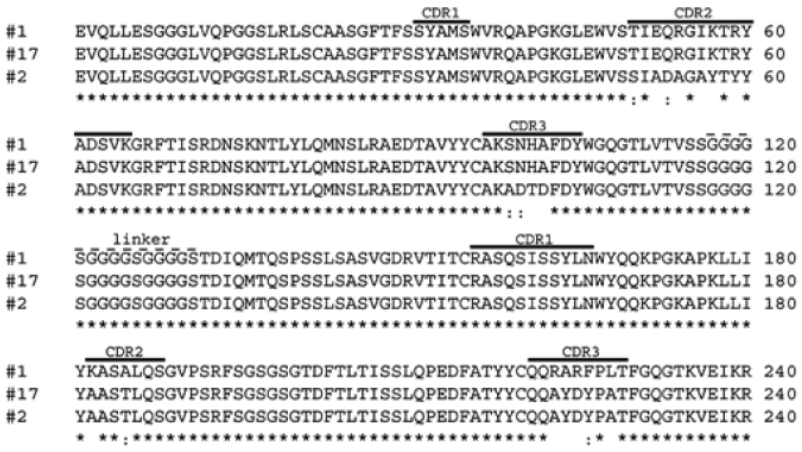

Figure 3.5. Sequence alignment of single-chain antibodies isolated against the Mac-1 high affinity I domain (F302L). Complementarity determining regions (CDRs) and a linker are indicated with a line above the sequence.

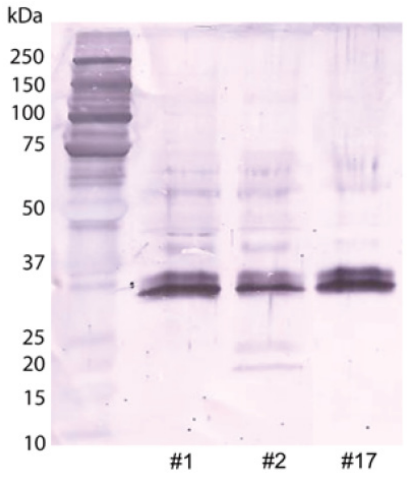

Figure 3.6. Western blot detection of antibodies from yeast culture supernatant. Anti-Mac-1 antibodies were detected with antiHis tag antibody as a primary and HRP-conjugated goat antimouse antibody as a secondary antibody. Each lane was loaded with 30 µl of culture. Assuming 10 ng of scFv (30 kDa) for each band, the amount of antibodies secreted into the media was estimated to be approximately 10 nM (330 µg⁄mL).

Figure 3.7. The measurement of antibody binding to the Mac-1 I domains.
(a) Yeast culture supernatant containing antibodies were used without purification for binding to I domain expressing yeast cells. (b) To further confirm antibody specificity, AM01 and AM17 were produced from bacteria and used at 0–10 μg/mL concentrations for binding to yeast cells expressing I domain variants.

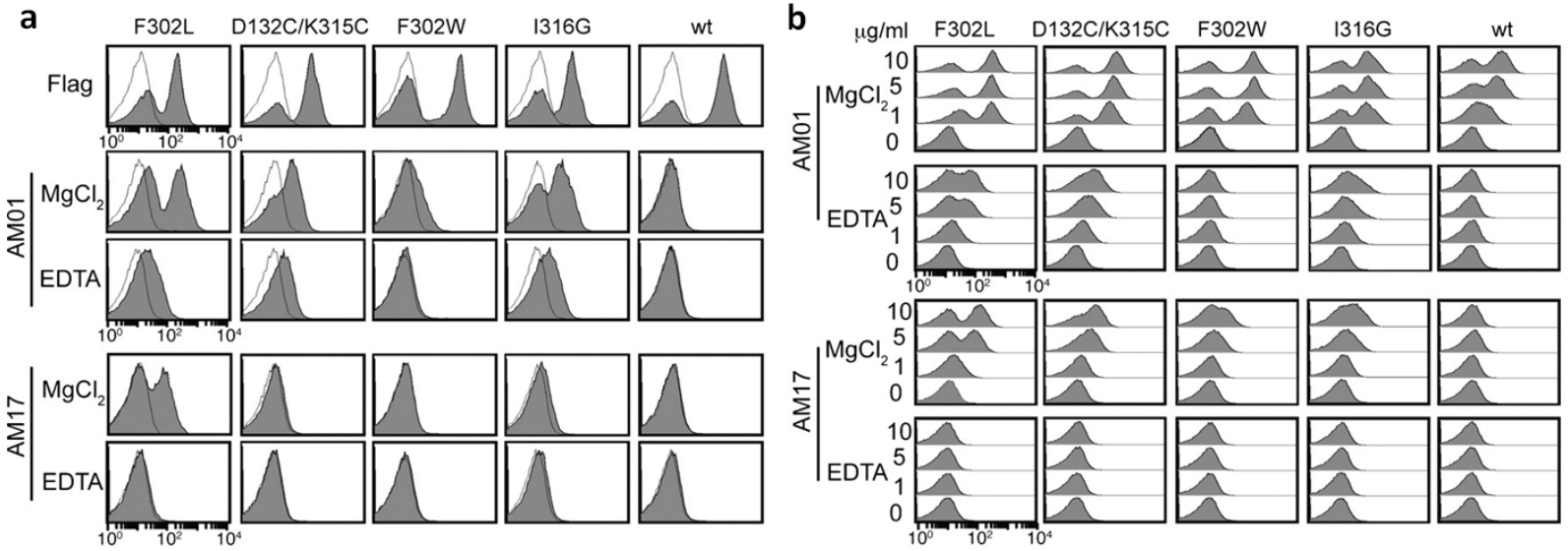
a
F302L
D132C/K315C
F302W
I316G
wt
Flag
AM01
MgCl2
EDTA
AM17
MgCl2
EDTA
10^0
10^2
10^4
b
µg/ml
F302L
D132C/K315C
F302W
I316G
wt
AM01
MgCl2
10
5
1
0
EDTA
10
5
1
0
AM17
MgCl2
10
5
1
0
EDTA
10
5
1
0
10^0
10^2
10^4

MIDAS in the active conformation is a critical epitope for both antibodies, other activation-independent epitopes may contribute to AM01 binding.

Surface plasmon resonance (SPR) measurement of Mac-1 binding to activation-specific or activation-insensitive antibodies

A number of antibodies against the Mac-1 I domain have previously been isolated, some of which react differentially with the activation state of Mac-1. mAb44 was found to bind Mac-1 irrespective of its activation state in a metal-ion independent manner [23]. To compare newly selected AM01 with activation-insensitive mAb44, antibody binding to the wild type and the active I domains (I316G and F302L) was examined by flowing I domains over the SPR chip immobilized with AM01 and mAb44 (Fig. 3.8a). The configuration of antibodies immobilized to the surface and the I domains as analytes was chosen to examine monomeric interaction, which was necessary as AM01 is monovalent whereas mAb44 is divalent. Consistent with AM01 binding to the I domains expressed in yeast cells (Fig. 3.7), AM01 bound the active mutants much higher affinity (K_D = 2 nM) than the wild-type I domain (K_D = 66 nM) with strong dependence on the metal ion (Fig. 3.8a). In contrast to preferential binding of AM01 to active I domains, mAb44 bound better to the wild-type I domain (K_D = 0.4 nM) with little influence by the metal ions (Fig. 3.8a and Table 3.2).

Inhibition of Mac-1 binding to ligands by antibodies

Therapeutic potency of antibody antagonists can be quantified as the concentration of antibody that produces half maximal inhibition of receptor binding to ligands or the half maximal inhibitory concentration (IC_{50}). To measure the potency of inhibition of Mac-1 binding to ligands, Mac-1 I domains (I316G and F302L at 200 nM) mixed with scFv or antibodies (1000 to 62.5 nM) were injected over the SPR chip

Figure 3.8. SPR measurement of the affinity of antibody to I domains and inhibition of I domain-ligand interactions.

(a) Antibodies were immobilized to a Biacore chip, and the I domains were injected at a series of two-fold serial dilutions starting from 12.5 nM in buffer containing either 10 mM $MgCl_2$ or 1 mM EDTA. (b) The I domains at 200 nM were preincubated with the antibodies, ranging from 62.5 to 1000 nM, and this complex was injected into a chip coated with Mac-1 ligands. The solid lines represent the best fit of the model to the data, from which the values of a half maximal inhibitory concentration (IC_{50}) of antibodies were derived.

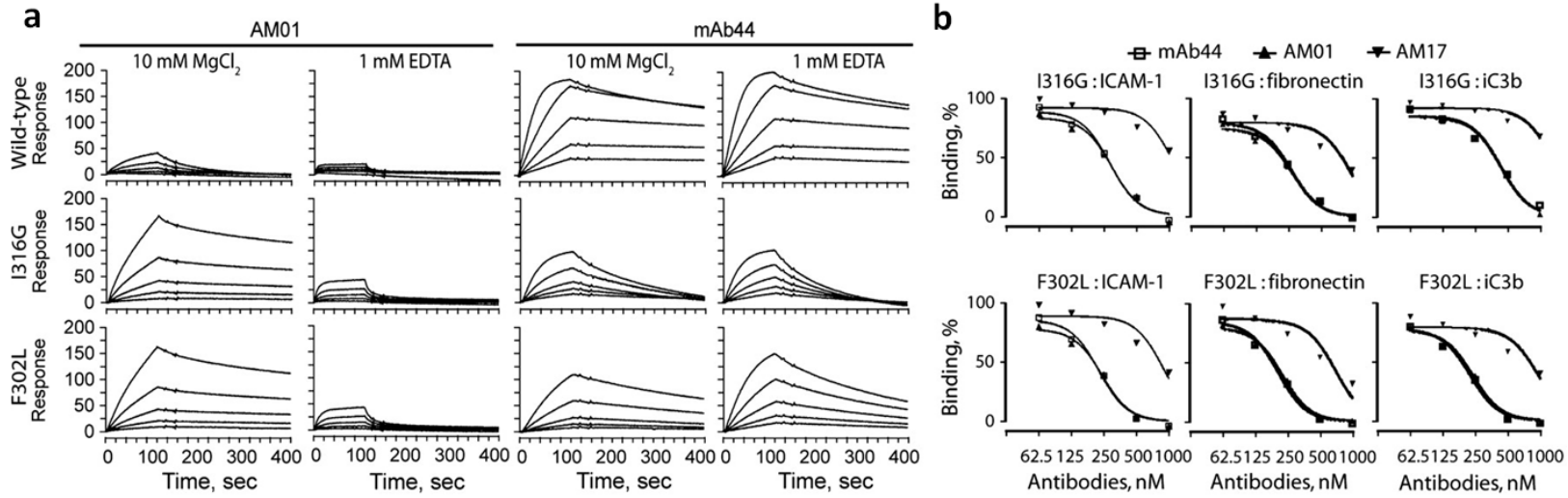
a
AM01
mAb44
10 mM MgCl2
1 mM EDTA
10 mM MgCl2
1 mM EDTA
Wild-type Response
I316G Response
F302L Response
200
150
100
50
0
0 100 200 300 400
Time, sec
b
mAb44
AM01
AM17
I316G : ICAM-1
I316G : fibronectin
I316G : iC3b
F302L : ICAM-1
F302L : fibronectin
F302L : iC3b
Binding, %
100
50
0
62.5 125 250 500 1000
Antibodies, nM

Table 3.2. SPR measurement of the binding of antibodies to the wild-type and active I domain mutants.

		MgCl2		EDTA	
		AM01	mAb44	AM01	mAb44
WT	k_{on} (M^{-1} s^{-1} × 10^{-3})	198.0 ± 8.7	1247.5 ± 17	ND	2290 ± 120
	k_{off} s^{-1} × 10^{3}	12.90 ± 0.4	0.44 ± 0.14	ND	0.87 ± 0.13
	K_D (M × 10^{9})	65.8 ± 4.68	0.358 ± 0.01	ND	0.375 ± 0.04
I316G	k_{on} (M^{-1} s^{-1} × 10^{-3})	477.3 ± 37	1242.9 ± 47	ND	1778.6 ± 54
	k_{off} s^{-1} × 10^{3}	0.93 ± 0.03	5.65 ± 0.53	ND	9.13 ± 0.57
	K_D (M × 10^{9})	1.96 ± 0.09	4.63 ± 0.515	51.5 ± 7.09	5.21 ± 0.457
F302L	k_{on} (M^{-1} s^{-1} × 10^{-3})	463.8 ± 37	464.4 ± 18.2	ND	1217.5 ± 42
	k_{off} s^{-1} × 10^{3}	0.93 ± 0.08	2.06 ± 0.14	ND	2.88 ± 0.15
	K_D (M × 10^{9})	2.01 ± 0.05	4.47 ± 0.349	51.5 ± 7.07	2.36 ± 0.068

The values are mean ± S.E., estimated from BIAevaluation software from Biacore.

coated with ICAM-1, iC3b, and fibronectin (Fig. 3.8a). The observations that AM01 and AM17 binding to the I domains was strongly dependent on the metal ions (Fig. 3.7) suggest that the MIDAS is a critical epitope and antibodies should compete with the ligands for binding to the I domain. Under this condition, the IC_{50} of the antibodies should be proportional to the affinity of the antibody (or inversely proportional to the dissociation constant, K_D) to antigen. The mAb44 and AM01 exhibited comparable inhibitory potency (IC_{50}), whereas 3- to 4-fold higher concentration of AM17 was required to produce comparable inhibition (Fig. 3.7 and Table 3.3). Higher potency of AM01 and mAb44 than AM17 agreed with their higher affinity to the active I domains.

Inhibition of neutrophil adhesion and migration by antibodies

Next, we analyzed the binding of antibodies to neutrophils and inhibition of neutrophil adhesion and migration on fibrinogen-coated surface. To activate integrins without inducing cellular activation (29), neutrophils were treated with 1 mM $MgCl_2$ and 1 mM EGTA to deplete free calcium ions and labeled with AM01 or AM17. Whereas little binding of AM01 and AM17 to neutrophils was observed without EGTA or with EDTA, AM01 binding increased significantly when cells were treated with 1 mM $MgCl_2$ and 1 mM EGTA (Fig. 3.9a). In contrast to its binding to the F302L expressed in yeast, the binding of AM17 to neutrophils was not detected with $MgCl_2$/EGTA activation. This discrepancy was presumably due to the difference in the degree of activation by F302L vs. by the depletion of calcium ions in Mac-1. To evaluate the potency of antibodies in inhibiting neutrophil binding to fibrinogen-coated surface, 96-well V-bottom plate assay was used to measure the amount of detached cells by centrifugal force. In this assay, more cells would accumulate to the V-bottom tip if the affinity between antibody antagonist and Mac-1 is higher.

Table 3.3. SPR measurement of the effectiveness of antibodies (IC_{50}) in inhibition of ligand binding to the I domain.

		mAb44	AM01	AM17
I316G	ICAM-1	284 ± 4	294 ± 5	1097 ± 17
	iC3b	432 ± 7	433 ± 6	1351 ± 19
	fibronectin	271 ± 4	275 ± 4	937 ± 19
F302L	ICAM-1	226 ± 3	242 ± 3	898 ± 18
	iC3b	223 ± 3	237 ± 4	948 ± 21
	fibronectin	203 ± 3	222 ± 3	698 ± 20

The values are in nM concentration. Mean ± 95% confidence interval are shown.

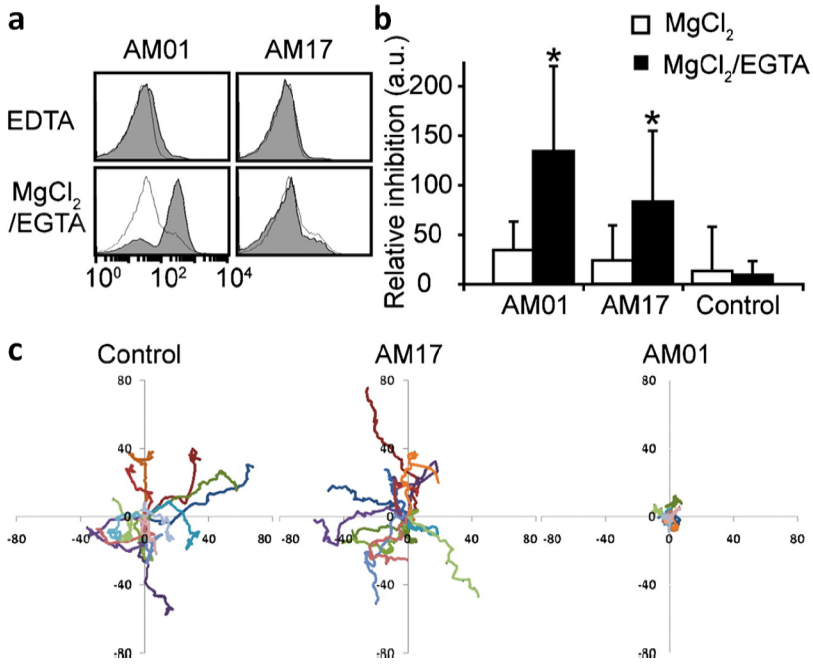

Figure 3.9. Evaluation of antibodies in inhibition of neutrophil adhesion and migration.

(a) Activation-dependent binding of antibodies to neutrophils was examined with immunofluorescence flow cytometry. The histograms represent antiHis antibody binding with (Filled) and without (Open) antibodies against Mac-1. (b) The inhibition of neutrophil adhesion to fibrinogen by antibodies was measured using 96-well V-bottom plate assays. Student's t tests were used to determine statistical significance ($p < 0.05$ for * vs. control). (c) The migration of neutrophils on fibrinogen-coated surface after10 nM fMLP activation was recorded and analyzed. Each line represents the movement of single neutrophils.

Neutrophils were incubated for 15 min at RT in 20 μg/mL of antibodies with or without activation by EGTA, washed, and added to the wells coated with fibrinogen. Whereas the inhibition of neutrophil adhesion to fibrinogen without EGTA activation was not statistically significant, after EGTA activation significant inhibition of neutrophil adhesion was observed by AM01 and AM17 at 40% and 25% (the percent relative inhibition as defined in Methods), respectively (Fig. 3.9b). Incomplete inhibition by antibodies may be due to the activation of Mac-1 after washing out unbound antibodies caused by the force applied to neutrophils during centrifugation of the plate, ligand-induced activation, and nonspecific neutrophil adhesion to the plate. To examine if these antibodies are capable of blocking neutrophil migration after stimulation with 10 nM formyl-Met-Leu-Pro (fMLP), which is the condition that would not only activate integrins but also upregulate Mac-1 expression [4], the migration of activated neutrophils on fibrinogen-coated surface was analyzed. Compared with no antibody control, preincubation of neutrophils with AM01 resulted in highly restricted migration within 15 μm from an initial attachment site. In contrast, AM17 did not significantly inhibit neutrophil migration over control.

Discussion

Antibodies specific to activated cell surface molecules may be used to probe cellular state as well as to target activated cells for the delivery of therapeutic agent [3]. With protein domains expressed on the surface of yeast as an antigen, we demonstrate a streamlined approach applicable to developing activation-specific antibodies against the I domain-containing integrins. Compared to the previous approaches using soluble proteins as antigens [7-8], the use of yeast cells expressing antigen offers several advantages such as obviating the need to purify soluble proteins

and direct estimation of antibody affinity using immunofluorescence flow cytometry. More importantly, antigens displayed in yeast display system can be engineered by directed evolution approach to induce active conformation, which would mimic the conformation induced by activation signals in cells [22]. Compared to rationally designed mutations, directed evolution approach led to mutations more potent in inducing active conformation of Mac-1 I domain, consistent with our previous studies with LFA-1 I domain [22]. Compared to the diversity in cell surface molecules in mammalian cells, the protein antigens expressed in yeast as a fusion to agglutinin would likely represent one of the most abundant cell surface proteins [32]. This can lead to highly efficient selection of specific phage clones, as evidenced by the isolation of positive clones after as few as two rounds of sorting. The use of YS2H for the final stage of antibody selection by quantitative estimation of antigen-antibody affinity was proven effective in identifying single chain antibodies of differing affinity. This method can overcome the problem of selecting phage clones biased toward those expressing multimeric scFv or with higher titer [33].

In contrast to depleting antibody library against the inactive I domains to select for activation-specific antibodies [8], we used yeast cells expressing unrelated proteins to deplete nonspecific binders. Even without the depletion against the inactive I domains, antibodies selected against the active I domain (F302L) (e.g., AM01 and AM17) preferentially bound or were specific to the active I domains induced by various mutations. We also found that a subset of enriched phage clones reacted with the wild-type I domain as well, which are likely to be activation-insensitive. Notably, all the reactive phage clones against the F302L were metal-ion dependent. Structural changes of the integrin I domains coupled to different affinity states have been studied extensively [18, 22, 33]: It involves the rearrangement of the metal-ion coordinating and proximal residues in the MIDAS and the downward displacement of the C-

terminal α7-helix. Therefore, some of the activation-specific antibodies may be specific to the residues in the MIDAS or in the α7-helix, not necessarily requiring the metal ions. The dominance of the metal ion in the MIDAS as an activation-specific epitope may be attributed to unstructured nature of the C-terminal region containing the α7-helix [19, 34] and may also reflect the nature of Mac-1 I domain in recognition of diverse molecules largely dependent on the electrostatic potential in the MIDAS.

The use of YS2H in the final selection of antibodies led to a number antibodies varying in affinities to the active I domain. We have chosen AM01 and AM17 that represented Myc expression highest to lowest among the selected yeast clones. Previously we have demonstrated that the affinity between two interacting proteins in YS2H can be quantitatively estimated from flow cytometry measurement of tag expression. Using the Langmuir isotherm equation, the predicted affinities (K_D) were 34 nM for AM01 vs. 241 nM for AM17 to the F302L. These values closely approximate the SPR data indicating 3- to 4-fold higher concentration of AM17 than AM01 to induce comparable inhibition of the I domain binding to the ligands and the solution affinity of AM01 binding to F302L (K_D = 2 nM). Quantitative selection of antibodies in YS2H based on 1:1 interaction of antigen-antibody can be a powerful method in selecting antibodies of desired affinities to achieve an optimal level of antibody binding to cells and antigens.

The antibodies isolated in this study, such as those that preferentially bind activated Mac-1 can be developed into antagonists targeting aberrantly active leukocytes or to diagnose inflammatory diseases associated with inflamed leukocytes. It is hypothesized that aberrant or excessive infiltration of immune cells, wherein integrin activation may be dysregulated, lead to direct damage to the vasculature and the underlying tissue, and the diseases such as sepsis, cardiovascular disease, and other inflammation-related diseases [35-36]. Among leukocyte-specific integrins, Mac-1

($\alpha_M\beta_2$) is expressed predominantly in phagocytic, myeloid cells such as neutrophils, monocytes, and macrophages, and is distinct in its ability to interact with a wide-range of ligands including ICAMs, fibrinogen, fibronectin, heparin, and iC3b [37]. Due to this reason, the diseases associated with myeloid cells such as ischemia-reperfusion injuries in cerebral and myocardial infarction and sepsis have been targeted with antagonists to β_2 integrins or to Mac-1 [15, 38-39]. To assess potential use of activation-specific antibodies developed in this study, we examined the ability of antibodies to block soluble Mac-1 I domain binding to ICAM-1, fibronectin, and iC3b, and to inhibit neutrophil adhesion and migration over fibrinogen-coated surface. The degree of reduction in neutrophil adhesion and migration was in agreement with the affinity of antibody binding to Mac-1 I domain. Although AM17 was less potent than AM01 due to lower affinity to Mac-1, conversion of scFv AM17 into bivalent immunoglobulins (IgG) may induce sufficiently potent affinity to Mac-1 with little interaction with inactive Mac-1.

Many mammalian proteins consist of multidomains, some of which can be expressed separately in a native conformation retaining modular functions. The use of modular domains expressed in yeast for antibody selection not only overcomes the difficulty with the functional expression of large mammalian molecules but also offers the advantage of narrowing antibody epitopes into specific region to function as agonists or antagonists. Some of the agonistic antibodies against integrins (such as mAbs KIM127 [40] and CBR LFA-1/2 [41]) map to a region in the β_2 subunit that is buried in an inactive conformation but exposed in an active conformation. Therefore, agonistic antibodies can be developed by screening phage library against the domains or the regions that become exposed only in an active conformation. Likewise, antibodies screened against the domains that interact with the ligands may become antagonist antibodies. Furthermore, by tapping into the power of directed evolution

implemented by the yeast display system, the protein domains that undergo conformational change or exhibit allostery can be stabilized into one conformation for selection of conformation-specific antibodies. In summary, the strategy demonstrated in this study can be applicable to the selection of conformation-specific or activation-dependent antibodies against human antigens that are hard to express in solution, highly homologous to those in other mammals for immunization, or that undergo conformational change that needs to be locked into one conformation by mutations.

REFERENCES

1. Tsai CJ, Del Sol A, Nussinov R. Protein allostery, signal transmission and dynamics: a classification scheme of allosteric mechanisms. Mol Biosyst. 2009;5(3):207-16.

2. Shimaoka M, Kim M, Cohen EH, Yang W, Astrof N, Peer D, et al. AL-57, a ligand-mimetic antibody to integrin LFA-1, reveals chemokine-induced affinity up-regulation in lymphocytes. Proc Natl Acad Sci U S A. 2006;103(38):13991-6.

3. Peer D, Zhu P, Carman CV, Lieberman J, Shimaoka M. Selective gene silencing in activated leukocytes by targeting siRNAs to the integrin lymphocyte function-associated antigen-1. Proc Natl Acad Sci U S A. 2007;104(10):4095-100.

4. Diamond MS, Springer TA. A subpopulation of Mac-1 (CD11b/CD18) molecules mediates neutrophil adhesion to ICAM-1 and fibrinogen. J Cell Biol. 1993;120(2):545-56.

5. Elemer GS, Edgington TS. Monoclonal antibody to an activation neoepitope of alpha M beta 2 inhibits multiple alpha M beta 2 functions. J Immunol. 1994;152(12):5836-44.

6. Lu C, Ferzly M, Takagi J, Springer TA. Epitope mapping of antibodies to the C-terminal region of the integrin beta 2 subunit reveals regions that become exposed upon receptor activation. J Immunol. 2001;166(9):5629-37.

7. Gao J, Sidhu SS, Wells JA. Two-state selection of conformation-specific antibodies. Proc Natl Acad Sci U S A. 2009;106(9):3071-6.

8. Huang L, Shimaoka M, Rondon IJ, Roy I, Chang Q, Po M, et al. Identification and characterization of a human monoclonal antagonistic antibody AL-57 that preferentially binds the high-affinity form of lymphocyte function-associated antigen-1. J Leukoc Biol. 2006;80(4):905-14.

9. Eisenhardt SU, Schwarz M, Schallner N, Soosairajah J, Bassler N, Huang D, et al. Generation of activation-specific human anti-alphaMbeta2 single-chain antibodies as potential diagnostic tools and therapeutic agents. Blood. 2007;109(8):3521-8.

10. Kretzschmar T, von Ruden T. Antibody discovery: phage display. Curr Opin Biotechnol. 2002;13(6):598-602.

11. Bowley DR, Jones TM, Burton DR, Lerner RA. Libraries against libraries for combinatorial selection of replicating antigen-antibody pairs. Proc Natl Acad Sci U S A. 2009;106(5):1380-5.

12. Hynes RO. Integrins: bidirectional, allosteric signaling machines. Cell. 2002;110(6):673-87.

13. Yusuf-Makagiansar H, Anderson ME, Yakovleva TV, Murray JS, Siahaan TJ. Inhibition of LFA-1/ICAM-1 and VLA-4/VCAM-1 as a therapeutic approach to inflammation and autoimmune diseases. Med Res Rev. 2002;22(2):146-67.

14. Shimaoka M, Springer TA. Therapeutic antagonists and the conformational regulation of the beta2 integrins. Curr Top Med Chem. 2004;4(14):1485-95.

15. Yonekawa K, Harlan JM. Targeting leukocyte integrins in human diseases. J Leukoc Biol. 2005;77(2):129-40.

16. Schwarz M, Meade G, Stoll P, Ylanne J, Bassler N, Chen YC, et al. Conformation-specific blockade of the integrin GPIIb/IIIa: a novel antiplatelet strategy that selectively targets activated platelets. Circ Res. 2006;99(1):25-33.

17. Lee JO, Rieu P, Arnaout MA, Liddington R. Crystal structure of the A domain from the alpha subunit of integrin CR3 (CD11b/CD18). Cell. 1995;80(4):631-8.

18. Li R, Rieu P, Griffith DL, Scott D, Arnaout MA. Two functional states of the CD11b A-domain: correlations with key features of two Mn2+-complexed crystal structures. J Cell Biol. 1998;143(6):1523-34.

19. Shimaoka M, Xiao T, Liu JH, Yang Y, Dong Y, Jun CD, et al. Structures of the alpha L I domain and its complex with ICAM-1 reveal a shape-shifting pathway for integrin regulation. Cell. 2003;112(1):99-111.

20. Hu X, Kang S, Chen X, Shoemaker CB, Jin MM. Yeast surface two-hybrid for quantitative in vivo detection of protein-protein interactions via the secretory pathway. J Biol Chem. 2009;284(24):16369-76.

21. Boder ET, Wittrup KD. Yeast surface display for screening combinatorial polypeptide libraries. Nat Biotechnol. 1997;15(6):553-7.

22. Jin M, Song G, Carman CV, Kim YS, Astrof NS, Shimaoka M, et al. Directed evolution to probe protein allostery and integrin I domains of 200,000-fold higher affinity. Proc Natl Acad Sci U S A. 2006;103(15):5758-63.

23. Xiong JP, Li R, Essafi M, Stehle T, Arnaout MA. An isoleucine-based allosteric switch controls affinity and shape shifting in integrin CD11b A-domain. J Biol Chem. 2000;275(49):38762-7.

24. Dransfield I, Cabanas C, Craig A, Hogg N. Divalent cation regulation of the function of the leukocyte integrin LFA-1. J Cell Biol. 1992;116(1):219-26.

25. Elphick GF, Sarangi PP, Hyun YM, Hollenbaugh JA, Ayala A, Biffl WL, et al. Recombinant human activated protein C inhibits integrin-mediated neutrophil migration. Blood. 2009;113(17):4078-85.

26. de Wildt RM, Mundy CR, Gorick BD, Tomlinson IM. Antibody arrays for high-throughput screening of antibody-antigen interactions. Nat Biotechnol. 2000;18(9):989-94.

27. Kieke MC, Cho BK, Boder ET, Kranz DM, Wittrup KD. Isolation of anti-T cell receptor scFv mutants by yeast surface display. Protein Eng. 1997;10(11):1303-10.

28. Rao BM, Driver I, Lauffenburger DA, Wittrup KD. Interleukin 2 (IL-2) variants engineered for increased IL-2 receptor alpha-subunit affinity exhibit increased potency arising from a cell surface ligand reservoir effect. Mol Pharmacol. 2004;66(4):864-9.

29. Kim YS, Bhandari R, Cochran JR, Kuriyan J, Wittrup KD. Directed evolution of the epidermal growth factor receptor extracellular domain for expression in yeast. Proteins. 2006;62(4):1026-35.

30. Lee HW, Kim TI, Chan KH, Kwon MH, Kim JS, Jin M, et al. Inducing rigid local structure around the zinc-binding region by hydrophobic interactions enhances the homotrimerization and apoptotic activity of zinc-free TRAIL. Biochem Biophys Res Commun. 2007;362(3):766-72.

31. McCleverty CJ, Liddington RC. Engineered allosteric mutants of the integrin alphaMbeta2 I domain: structural and functional studies. Biochem J. 2003;372(Pt 1):121-7.

32. Dranginis AM, Rauceo JM, Coronado JE, Lipke PN. A biochemical guide to yeast adhesins: glycoproteins for social and antisocial occasions. Microbiol Mol Biol Rev. 2007;71(2):282-94.

33. Shimaoka M, Lu C, Palframan RT, von Andrian UH, McCormack A, Takagi J, et al. Reversibly locking a protein fold in an active conformation with a disulfide bond: integrin alphaL I domains with high affinity and antagonist activity in vivo. Proc Natl Acad Sci U S A. 2001;98(11):6009-14.

34. Zhang H, Casasnovas JM, Jin M, Liu JH, Gahmberg CG, Springer TA, et al. An unusual allosteric mobility of the C-terminal helix of a high-affinity alphaL integrin I domain variant bound to ICAM-5. Mol Cell. 2008;31(3):432-7.

35. Hansson GK. Inflammation, atherosclerosis, and coronary artery disease. N Engl J Med. 2005;352(16):1685-95.

36. Libby P. Inflammation in atherosclerosis. Nature. 2002;420(6917):868-74.

37. Diamond MS, Garcia-Aguilar J, Bickford JK, Corbi AL, Springer TA. The I domain is a major recognition site on the leukocyte integrin Mac-1 (CD11b/CD18) for four distinct adhesion ligands. J Cell Biol. 1993;120(4):1031-43.

38. Harlan JM, Vedder NB, Winn RK, Rice CL. Mechanisms and consequences of leukocyte-endothelial interaction. West J Med. 1991;155(4):365-9.

39. Curley GP, Blum H, Humphries MJ. Integrin antagonists. Cell Mol Life Sci. 1999;56(5-6):427-41.

40. Stephens P, Romer JT, Spitali M, Shock A, Ortlepp S, Figdor CG, et al. KIM127, an antibody that promotes adhesion, maps to a region of CD18 that includes cysteine-rich repeats. Cell Adhes Commun. 1995;3(5):375-84.

41. Petruzzelli L, Maduzia L, Springer TA. Activation of lymphocyte function-associated molecule-1 (CD11a/CD18) and Mac-1 (CD11b/CD18) mimicked by an antibody directed against CD18. J Immunol. 1995;155(2):854-66.

42. Jin M, Andricioaei L, Springer TA. Conversion between three conformational states of integrin I domains with a C-terminal pull spring studied with molecular dynamics. Structure. 2004;12(12):2137-47.

CHAPTER 4

COMPLEX STRUCTURE OF ENGINEERED MODULAR DOMAINS DEFINING MOLECULAR INTERACTION BETWEEN ICAM-1 AND INTEGRIN LFA-1

Summary

Intermolecular contacts between integrin LFA-1 ($\alpha_L\beta_2$) and ICAM-1 exist solely within single domains called α I domain of the integrin and the first domain (D1) of ICAM-1. We previously engineered the I domain into high affinity while preserving the native sequence in the C-terminal α7-helix, whose downward displacement is linked to allosteric activation of integrins. We also identified mutations in D1, converting hydrogen bond networks into vdW contacts at solvent-excluded core and enabling the domain to functionally fold on its own. To examine the structural basis leading to folding of D1 and its binding to I domain, we solved the crystal structure of their complex. Backbone of β-sandwich fold in contact with I domain is closely superimposable, with deviations limited to the N-terminal loops that interact with HRV. The finding that α7-helix is positioned downward further supports the allostery in I domain and global conformational rearrangements of integrins in signaling.

Introduction

Integrins are noncovalently associated αβ heterodimeric cell surface receptors that mediate cell-cell and cell-extracellular matrix adhesions, and signaling bidirectionally across the plasma membrane. Integrins play important roles in

development, immune cell trafficking and responses, and homeostasis [1-3]. One of the major leukocyte integrins is the lymphocyte function-associated antigen (LFA)-1, which provides interactions necessary for immunological synapse formation and adhesion to endothelial cells [4]. Ligands of LFA-1 include intercellular adhesion molecules (ICAMs; ICAM-1, -2, -3, -4, and -5) [5] and junctional adhesion molecule (JAM)-1 [6], both of which are members of the immunoglobulin superfamily (IgSF) receptors. As one of the most biologically important ligands for LFA-1, ICAM-1 is expressed at a low constitutive level in diverse types of cells and tissues, while its expression is greatly upregulated as a response to inflammation [7], and in some tumors and their stroma [8-9]. The interaction of LFA-1 and ICAM-1 is contained within the single domains called α I domain in LFA-1 and the first N-terminal domain (D1) of ICAM-1. ICAM-1 is also subverted as a receptor for human rhinovirus (HRV), while the epitope within D1 for HRV binding is distinct from that of the LFA-1 binding site [10].

Previous structural studies have indicated that I domains of both α and β chains exhibit low to high affinity to their ligands [11-12]. Distinct allosteric conformational changes have been observed between the top of the I domains, known as the metal ion-dependent adhesion site (MIDAS), and the C-terminal α7-helix. The downward motion of the α7-helix has been hypothesized to cause a change in the coordination to the metal ion of the residues in the MIDAS, leading to a higher affinity conformation [13]. For integrins containing α I domains, the downward 'pull' of the α7-helix is coupled to global conformational rearrangements of integrins, and more specifically, to opening of the integrin headpiece and allostery in the integrin □ I domain [14]. Structural changes in integrin is linked to its bidirectional cell signaling across the plasma membrane, termed "outside-in" and "inside-out" signalings [3]. The LFA-1 α I domain is functionally expressed in isolation, but it does not retain affinity to

physiologic ligands and requires allosteric activation. Structural linkage between the MIDAS and the α7-helix, *i.e.* allostery in α I domains, has been demonstrated by rationally designed mutational studies [11, 15] and by a molecular simulation study [16]. However, no previous crystal structures of α I domains in complex with physiological ligands were obtained with the native sequence in the α7-helix and the neighboring residues, which would be necessary to examine natively induced conformation of the α7-helix without mutation-induced bias or perturbation. Compared to the rationally designed activating mutations in the LFA-1 α I domain, we previously reported an application of directed evolution to select active forms of the I domain from a library through a selective pressure for binding to ICAM-1 [17]. Several point mutations at different places away from the α7-helix were found to induce higher affinity through a decrease in the dissociation rate from ICAM-1.

The ectodomain of ICAM-1 contains five Ig-like domains with D1 solely responsible for interactions with LFA-1 and HRV. The binding sites in D1 for LFA-1 and HRV, however, are distinct. The loops at the N-terminal face of D1 interact with HRV by docking into a region known as the canyon [10, 18], whereas the residues within the β-strands make contact with the I domain [11]. Despite the modular nature of many IgSF domains, D1 does not fold on its own unless it is expressed with the second domain [10, 19]. In an attempt to stabilize in physiologic fold, we have previously engineered D1 by directed evolution [20]. A set of extensive and concurrent mutations in D1 were necessary to express D1 alone that is competent for binding to the LFA-1 I domain and conformation-specific antibodies. We have previously noted that D1 contains a hydrogen bond network in the core of the domain and that the mutations selected for the native conformation were those converting it to hydrophobic, van der Waals (vdW) contacts. The engineered D1 retained interaction with the I domain, comparable as seen with the wild-type ICAM-1. However, full-

length ICAM-1 containing the mutations found in D1 exhibited lower binding to HRV [20], implying that conversion of the hydrogen bond network into vdW contacts may be responsible for reduced binding to the virus.

Here we report the crystal structure of the complex between the engineered LFA-1 I domain and ICAM-1 D1. Distinct from the previous studies [11, 15, 21], we used a high-affinity I domain mutant with one substitution (F265S), located in the β5-α6 loop, while preserving the native sequence for the β6-α7 loop, the α7-helix, and the residues in close contact with the α7-helix. The crystal structure herein shows that the α7-helix is indeed displaced downward, comparable to the open conformations previously observed in α_M and α_2 I domains [22-23]. Furthermore, despite *in vitro* refolding of bacterially-expressed ICAM-1 D1, which contained extensive mutations and lacked contact with D2, the backbone structure is closely superimposable to the previously solved structures in the context of D1D2 fragments expressed in mammalian systems.

Experimental Procedures

Protein production and crystallization condition

The LFA-1 I domain (Asn-129 - Tyr-307 with a mutation F265S) and ICAM-1 D1 (Gln-1 - Thr-85 with mutations Q1M, T2V, I10T, T23A, P38V, P63V, S67A, and T78A) were expressed in E. coli, refolded, and purified as previously described [20]. Equal molar of the I domain and D1 were mixed in the presence of 1 mM $MgCl_2$ to form the complex, purified by size exclusion and ion exchange columns, and concentrated to ~18 mg/ml. The condition for crystallization, identified using Crystal Screen HT (Hampton Research), was with 0.4 M sodium formate, 0.1 M sodium cacodylate, and 14% PEG6000 at pH 5.75 at 4 °C.

Data collection and molecular replacement

The diffraction data were collected at Cornell High Energy Synchrotron Source (CHESS) Beamline F1 and processed with HKL2000 for integration and scaling. Molecular replacement (PHASER) was used to determine the structure [24]. Previous complex structures of ICAM and I domain (PDB codes 1MQ8 and 3BN3) were used as search models and refinement. The structure was refined with Refmac5 (CCP4) to R = 21.76% and R_{free} = 23.36%. The model was validated with COOT and PDB validation server.

Structure alignments and analysis

Previous structures of the α_M (1IDO) [22], α_2 (1DZI) [23], and α_L (3F74) [25] I domains were superimposed to the α_L I domain of our structure (3TCX) based on residues in the α6-helix (α_M: 278-288 ; α_2: 294-304; α_L: 268-278) (Fig. 4.1c). Previous complex structures of α_L I domain with ligands, which included ICAM-1 D1D2 (1MQ8) [11], ICAM-3 D1 (1T0P) [15], and ICAM-5 D1D2 (3BN3) [21], were superimposed to the α_L I domain of our structure (3TCX) using residues in the central β-sheet (129-140, 164-181, 231-237). Previous wild-type ICAM-1 D1 structures (1IAM [10], 1IC1 [19], and 1MQ8) were superimposed to the ICAM-1 D1 of our structure (3TCX) using the residues in the β-strands (2-5, 8-11, 15-23, 30-34, 38-42, 50-57, 61-68, and 73-83). A model structure of ICAM-1 D1 bound to HRV16 was constructed by aligning the HRV16 coat protein (1AYM) [26] and ICAM-1 structures (residues 1-80) to the corresponding cryo-EM Cα coordinates of ICAM-1 D1D2 bound to HRV (1D3E) [27] (Fig. 4.3f). All the molecular graphic figures herein were made using PyMOL (DeLano, W.L.).

Accession numbers

The coordinates of our complex structure have been deposited to the RCSB with the PDB code 3TCX. Previous structures used in this study for comparisons include 3F74 (α_L I domain) [25], 1IDO (α_M I domain), 1DZI (α_2 I domain in complex with collagen), 3BN3 (α_L I domain in complex with ICAM-5 D1D2), 1MQ8 (α_L I domain in complex with ICAM-1 D1D2), 1T0P (α_L I domain in complex with ICAM-3 D1), 1IAM (ICAM-1 D1D2) [10], 1IC1 (ICAM-1 D1D2),1D3E (cryo-EM of HRV16 with ICAM-1 D1D2), and 1AYM (HRV16 coat protein).

Results

Structural evidence for the open position of the α7-helix in the LFA-1 I domain in complex with ICAM-1 D1

In an attempt to obtain a physiological high affinity conformation of the α7-helix, we chose the I domain with single substitution of Ser for Phe-265, located in the β5-α6 loop (Fig. 4.1a), with no other mutations in succeeding residues of Gln-266 to the terminal residue Tyr-307. ICAM-1 D1 was previously engineered with seven mutations to achieve native fold on its own with the affinity to the I domain comparable to that with the wild-type ICAM-1 D1D2 or D1-D5 [20]. The complex structure shows docking of Glu-34 in ICAM-1 D1 to a divalent metal ion (Mg^{2+}) of the MIDAS (Fig. 4.1a), identical to the previous integrin-ligand complex structures [11, 15, 21, 23]. Compared to previous crystals with one or two ICAM-1 D1D2 molecules or complexes per asymmetric unit (1MQ8, 1IAM, and 1IC1), a total of 14 complexes per asymmetric unit with a large unit cell dimension were found in our structure (Table 4.1). One reason for a large number of molecules in one asymmetric unit cell may be ascribed to the interaction between two D1 fragments at the

Figure 4.1. Overall structure of the complex and comparison with the α7-helices of I domains from different α subunits.

(a) Ribbon diagram of the engineered α_L I domain (pale yellow), containing a substitution of F265S, in complex with the engineered domain 1 (D1) of ICAM-1 (light purple). The residues coordinating to the metal ion in the MIDAS, Ser-139, Ser-141, and Thr-206 in I domain and Glu-34 in ICAM-1 D1 are shown as stick models. The Mg^{2+} ion is shown as a pink sphere. (b) The electron density map, drawn together with cartoon or stick models, shows an open conformation of the β6-strand and the α7-helix. The three hydrophobic residues (Leu-289, Phe-292, and Leu-295; cyan) are shown in stick models. (c) In comparison to the previous open structures of the I domains of different α subunits, α_M (1IDO; blue) [22] and α_2 (1DZI; green) [23], the α7-helix in our structure (3TCX; magenta) shows a comparable extent of downward displacement, away from the closed structure seen in the wild-type α_L I domain (3F74; yellow) [25].

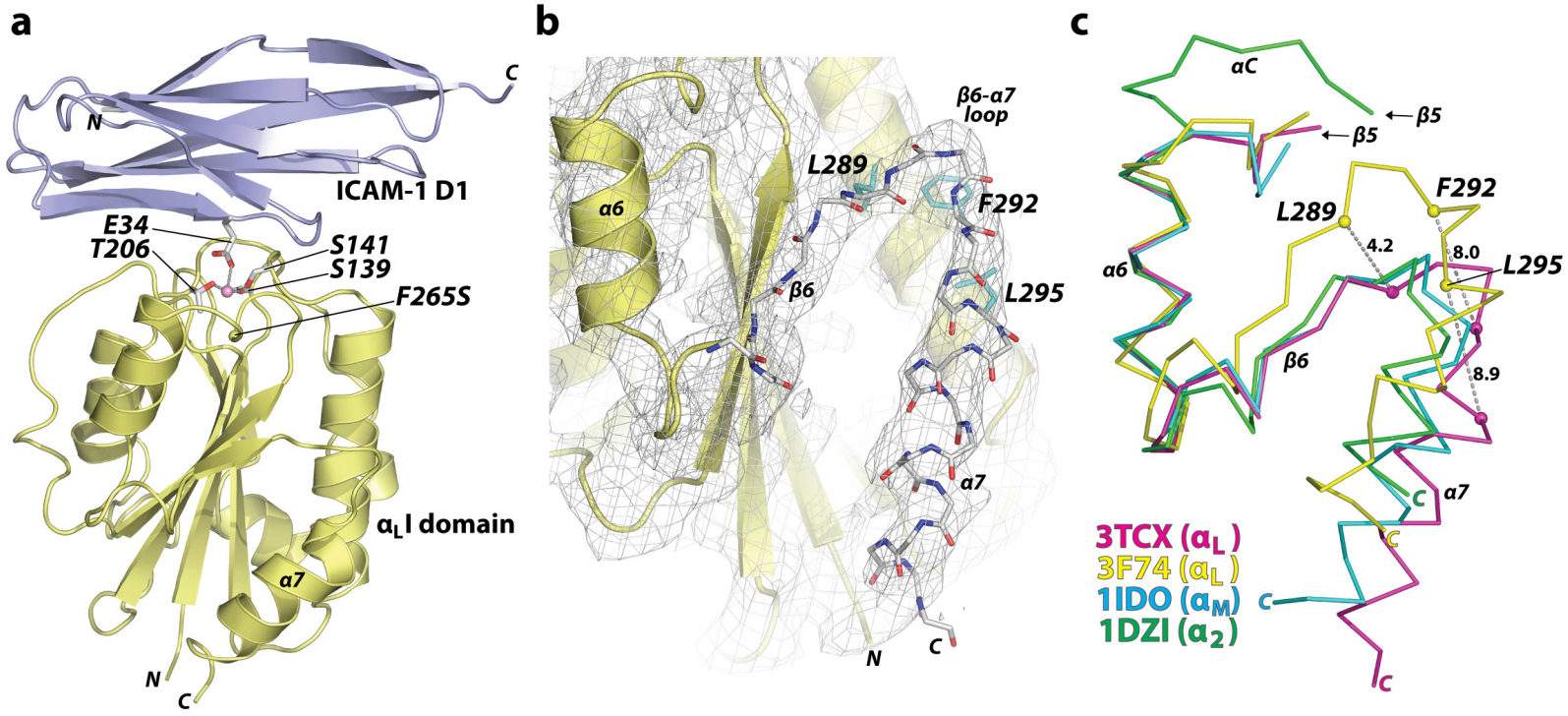
a
N
C
ICAM-1 D1
E34
T206
S141
S139
F265S
αLI domain
α7
N
C
b
β6-α7
loop
L289
F292
α6
β6
L295
α7
N
C
c
αC
β5
β5
L289
F292
4.2
8.0
L295
α6
β6
8.9
α7
C
C
C
C
3TCX (αL)
3F74 (αL)
1IDO (αM)
1DZI (α2)

Table 4.1. Data Collection and Refinement Statistics

Space group	$P2_12_12_1$
a (Å)	104.041
b (Å)	166.334
c (Å)	299.372
Molecules/asymmetric unit	14
Resolution (Å)	50-3.6
Unique reflections	58846
Completeness (%)	96.2 (83.9)
R_{sym} (%)	12.4 (48.6)
I/σ(I)	14.6 (1.7)
Redundancy	5.5 (2.2)
R_{work}/R_{free} (%)	21.76 (23.36)
Ramachandran Plot (favored/allowed/outlier %)	87.0/13.0/0
Average B factor (Å^2)	
ICAM-1 D1	54.502
LFA-1 I domain	58.377
ICAM-1 D1 + LFA-1 I domain	57.191
Rmsd from ideal values	
Bond lengths (Å)	0.013
Bond angles (°)	1.418

Number in parentheses are for the highest resolution shell.

C-terminal face, which is naturally not exposed if D2 is present. Even with the native sequence in the α7-helix and its preceding β6-α7 loop, the I domain was found in an open conformation with the α7-helix positioned downward, away from the closed state found in the wild-type (Fig. 4.1, b and c). The backbone structure of the β6-strand and the α7-helix shown with electron density was found in the open state (Fig. 4.1b). The β6-strand and the α7-helix contain three hydrophobic residues, Leu-289, Phe-292, and Leu-295, which in concert determine the position of the α7-helix (closed, intermediate, or open) and the corresponding low or high affinity conformations of the MIDAS. Compared to the previous structures of the α7-helix displacements in the α_M and α_2 I domains, the α_L I domain in our crystal structure exhibited a comparable extent of downward displacement (Fig. 4.1c).

Comparison with the previous structures of high-affinity LFA-1 I domain variants in complex with physiologic ligands

The LFA-1 I domain has previously been cocrystallized with ICAM-1 D1D2 [11], ICAM-3 D1 [15], and ICAM-5 D1D2 [21] (Fig. 4.2, a-c). All of the I domain structures were closely superimposable at the structurally invariant central β-sheet, with most deviations found in the β5-α6 loop, β6-α7 loop, and α7-helix. The affinity of the I domain to ICAM-5 was at least 10-fold weaker than to ICAM-1, and the I domain with two point mutations of F265S/F292G were necessary to form a stable complex for crystallization (Fig. 4.2a) [21]. However, the α7-helix was found flipped upward pivoting on Gly-292 in the β6-α7 loop and the vacated space was then occupied with the α7-helix belonging to a neighboring I domain (Fig. 4.2a). This unnatural conformation of the α7-helix would be attributed to a greater flexibility in dihedral angles along the peptide backbone around Gly substituted for Phe-292. However, compared to the current I domain containing only F265S, the backbone

Figure 4.2. Comparison with the previous complex structures of the α_L I domain with ligands.

(a-c) Superimposed to the current α_L I domain and ICAM-1 D1 structure (3TCX; magenta) are the previously solved complex structures of (a) high affinity (HA) α_L I domain containing two substitutions, F265S and F292G, with ICAM-5 D1D2 (3BN3; yellow) [21], (b) intermediate affinity (IA) α_L I domain containing, L161C and F299C, with ICAM-1 D1D2 (1MQ8; blue) [11], and (c) high affinity (HA) α_L I domain containing K287C and K294C, with ICAM-3 D1 (1T0P; green) [15]. The acidic residues of the ICAMs (Glu-37 in ICAM-5, Glu-34 in ICAM-1, and Glu-37 in ICAM-3) docking into the I domains and the Mg^{2+} ions are shown as stick and spheres, respectively. The β5-α6 and β6-α7 loops are circled with dotted lines.

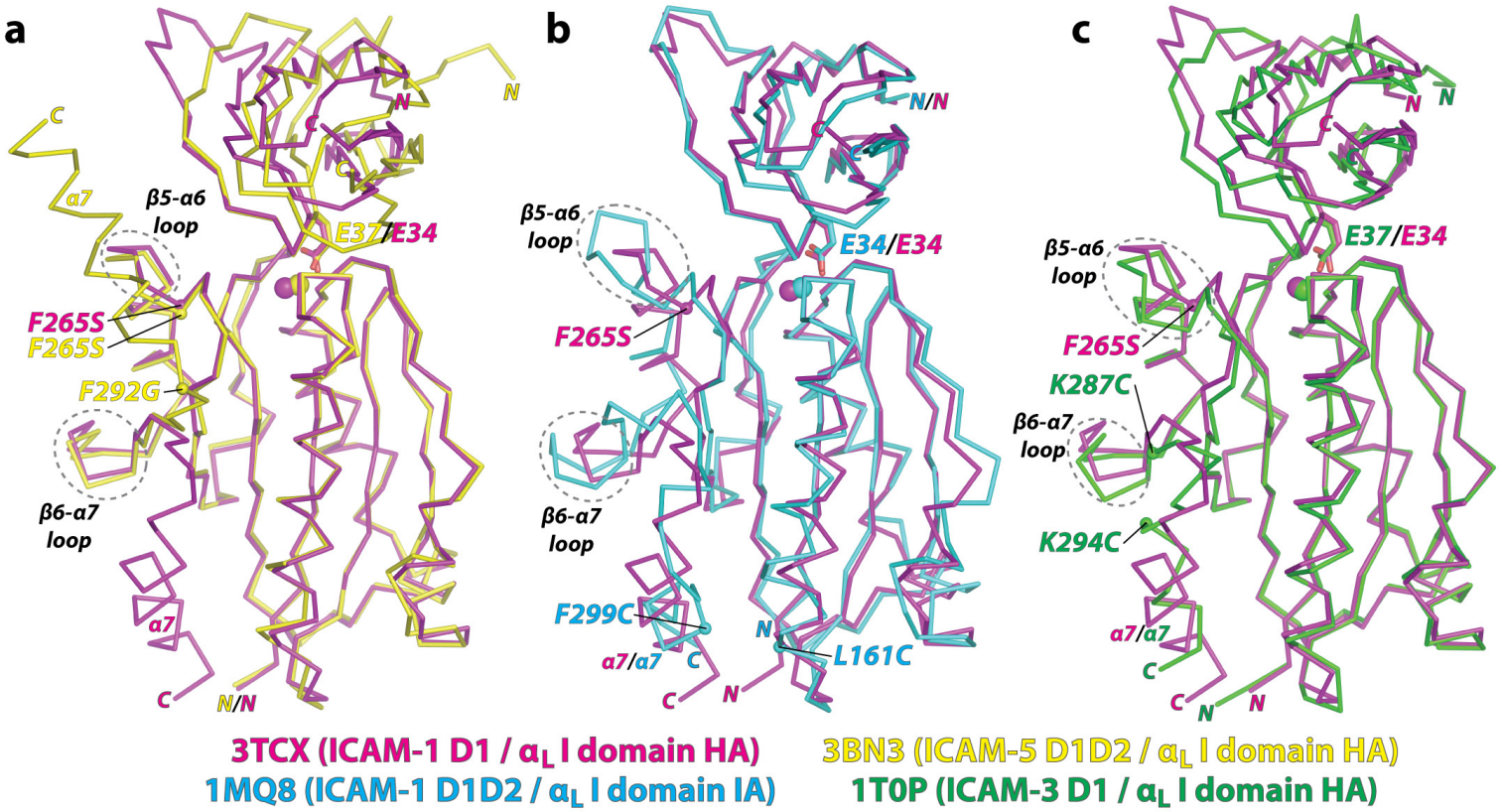
a
b
c
C
α7
β5-α6
loop
N
N
E37/E34
F265S
F265S
F292G
β6-α7
loop
α7
C
N/N
N/N
E34/E34
F265S
F299C
α7/α7
L161C
K287C
K294C
α7/α7
3TCX (ICAM-1 D1 / αL I domain HA)
1MQ8 (ICAM-1 D1D2 / αL I domain IA)
3BN3 (ICAM-5 D1D2 / αL I domain HA)
1T0P (ICAM-3 D1 / αL I domain HA)

structure of the F265S/F292G mutant from Asn-129 to Leu-289, and thus excluding the backbone affected by the flipped helix, was closely superimposable with 0.6 Å root-mean-square deviation (RMSD) between Cα atoms. In complexes with ICAM-1 D1D2 and ICAM-3 D1, the I domain contained two introduced cysteines to lock the α7-helix in intermediate and open positions, respectively (Fig. 4.2, b and c) [11, 15]. Compared to these disulfide bridge mutants, the β5-α6 loop of our structure was more closely superimposable to that in the high affinity mutant (K287C/K294C; 1T0P) than that in the intermediate affinity mutant (L161C/F299C; 1MQ8) (Fig. 4.2, b and c). At the same time, the β6-α7 loop of our structure is also more closely superimposable to that in 1T0P than that in 1MQ8, implying that our structure adopted a fully open position of the α7-helix but without mutations (Fig. 4.2, b and c), providing a structural evidence that the downward, displaced α7-helix conformation is physiologically relevant.

Structure of the engineered ICAM-1 D1 single domain in comparison with the previous wild-type structures

Unlike the modular expression of the I domain, functional expression of D1 alone was achieved only after the introduction of seven mutations (T2V/A, I10T, T23A, P38V/A, P63V, S67A, T78A) into Gln1-Thr85 sequence, identified previously by the combination of directed evolution and rational design approaches [20]. Except for the mutations P38V and I10T, the remaining five mutations, which were all substituted with non-polar amino acids, were located in solvent-excluded regions (Fig. 4.3, a-c). Substitutions of T2V, T23A, and S67A would disrupt the hydrogen bond interactions near the N-terminal face of the domain and create hydrophobic,

Figure 4.3. Hydrogen bond networks in the protein core of ICAM-1 and implications to the binding of ICAM-1 D1 to HRV and to the α_L I domain.

(a) Positions of the mutations found in D1 (magenta) are shown with superimposed previous wild-type ICAM-1 D1D2 structure (1IAM in yellow) shown with solvent-accessible surface plot (grey) [10]. (b) Hydrogen bond network formed by Thr-2, Thr-23, Ser-67, and Ser-74 at the N-terminal protein core is shown in grey dotted lines from the wild-type ICAM-1 structure (1IAM). Substitutions of T2V, S67A, and T23A in D1 are indicated. (c) A hydrogen bond between Pro-6 and Thr-78 is shown with a dotted line. Substitutions of P63V and T78A found in D1 are indicated. (d) Previous ICAM-1 D1D2 structures (1IAM in yellow, 1IC1 in blue [19], 1MQ8 in green [11]) were superimposed to D1 (3TCX in magenta). The loops, B-C, D-E, and F-G, are circled with dotted lines. (e) The distances between the Cα atoms (dotted lines in magenta) of the triad Thr-2, Thr-23, and Ser-67, and the Cα distance between Pro-28 to Thr-23 in previous structures are compared with those in D1 mutant. (f) The superimposed ICAM-1 structures with the HRV were modeled based on the cryo-EM Cα coordinates of ICAM-1 D1D2 bound to HRV16 (1D3E [27] and 1AYM [26]). (g) The superimposed D1 structures are shown with the αL I domain shown as solvent-accessible surface.

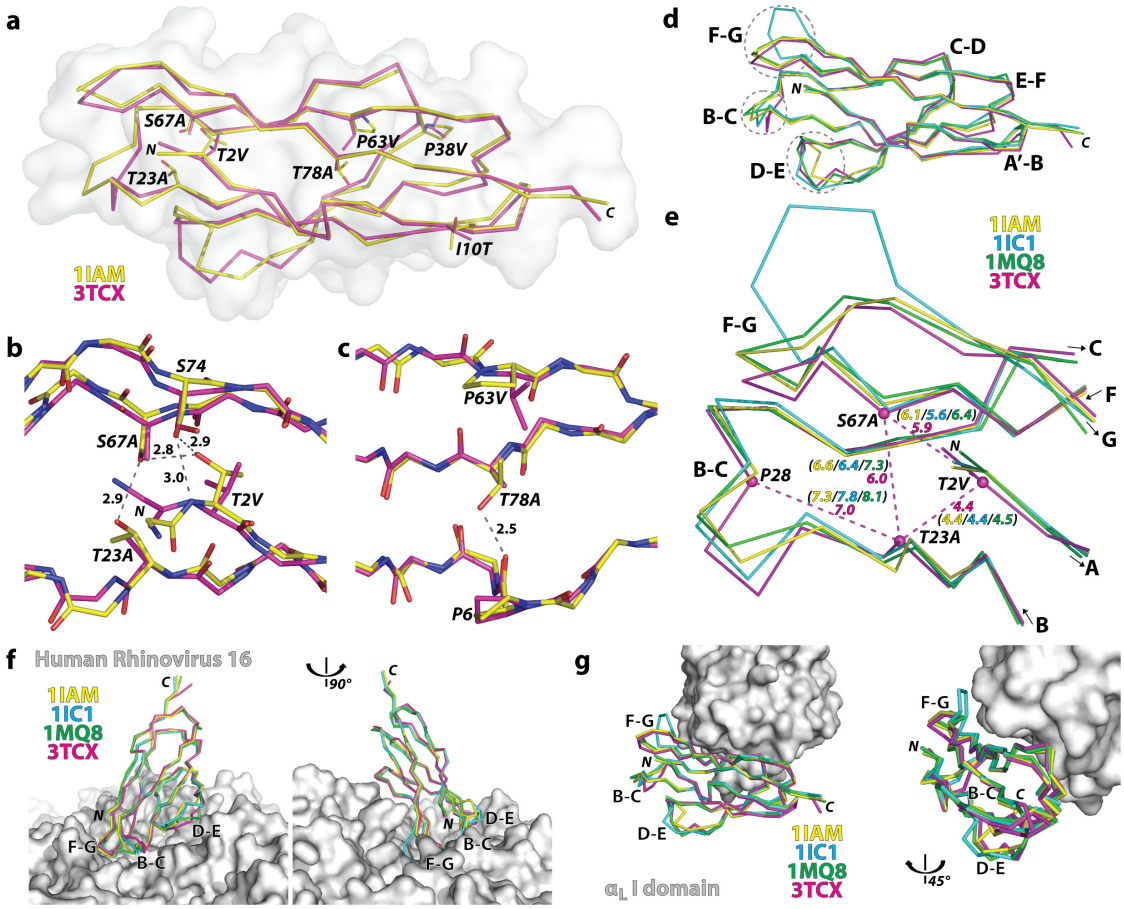
a
S67A
N
T2V
T23A
T78A
P63V
P38V
C
I10T
1IAM
3TCX
b
S74
S67A
2.8
2.9
3.0
2.9
N
T2V
T23A
c
P63V
T78A
2.5
P6
d
F-G
C-D
E-F
N
B-C
C
D-E
A'-B
e
1IAM
1IC1
1MQ8
3TCX
F-G
C
F
G
S67A
(6.1/5.6/6.4)
5.9
N
B-C
P28
(6.6/6.4/7.3)
6.0
T2V
(7.3/7.8/8.1)
7.0
4.4
(4.4/4.4/4.5)
T23A
A
B
f
Human Rhinovirus 16
1IAM
1IC1
1MQ8
3TCX
C
N
D-E
F-G
B-C
90°
C
N
D-E
B-C
F-G
g
F-G
N
B-C
C
D-E
1IAM
1IC1
1MQ8
3TCX
αL I domain
F-G
N
B-C
C
45°
D-E

vdW contacts (Fig. 4.3b). Substitutions of P63V and T78A also create new vdW contacts in the protein core (Fig. 4.3c). In addition to these critical mutations for native folding, Gln-1 was mutated into Met to avoid an extra residue being appended to the N-terminal [28], which can grossly compromise ICAM-1 binding to HRV [4].

The backbone structure of the mutant D1 along the β-strands was closely superimposable to those of the wild-type in the context of D1D2 fragments, crystals of which were obtained by ICAM-1 fragment itself (0.5 Å RMSD to 1IAM & 0.7 Å RMSD to 1IC1) or in complex with the LFA-1 I domain (0.6 Å RMSD to 1MQ8) (Fig. 4.3d). The largest deviation of the mutant D1 from the wild-type structures as well as the largest among the wild-type structures were found at the F-G, B-C, and D-E loops that together create the contours of the N-terminal face (Figs. 4.3d and 4.4). These loops are in close contact with HRV as seen in the model structure generated from cryo-EM electron density (Fig. 4.3f) [27, 29]. From our previous observation that the mutations into the triad forming a hydrogen bond network are responsible for the reduced binding to HRV [20], it can be speculated that our vdW forming mutations would have affected the flexibility in the N-terminal loops, necessary for fitting into the viral capsid [30]. We noted that Cα-Cα distances among Thr-2, Thr-23, and Ser-67 in the wild-type structures were slightly shortened in the D1 mutant with T2V, T23A, and S67A substitutions (Fig. 4.3e). The substitutions of the residues with smaller side chains (T23A and S67A) in turn would have affected the interaction with the neighboring residues, thus placing the B-C loop closer toward the protein core (Fig. 4.3e). However, the interface with the I domain is contained within the region where the backbone of D1 is closely superimposable to that in the wild-type, unaffected by the deviation seen in the loops (Figs. 4.3g and 4.4).

Figure 4.4. Differences in Cα positions for the superimposed structures of the first N-terminal domain of ICAM-1.

The plot of Cα-Cα distances from the previous wild-type ICAM-1 D1D2 structures (1IAM [10], 1MQ8 [11], and 1IC1 [19]) relative to our D1 structure (3TCX) is shown. Also, the Cα- Cα distances among the wild-type ICAM-1 D1D2 structures are plotted (1IAM to 1MQ8, 1IC1 to 1IAM, and 1MQ8 to 1IC1). Putative interacting residues of ICAM-1 D1 with HRV16 capsid as well as the residues in close contact with the α_L I domain are indicated with brackets and corresponding residue numbers. Arrow bars indicate the residues that form the β-strands in ICAM-1 D1.

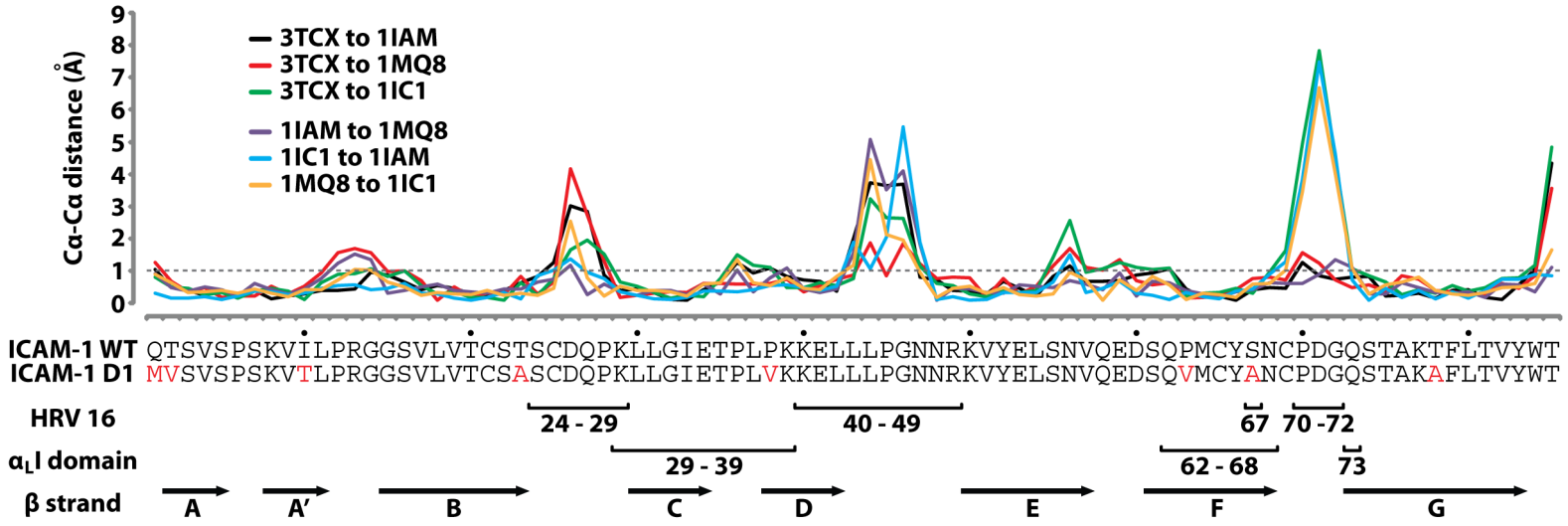
Cα-Cα distance (Å)
9
8
7
6
5
4
3
2
1
0
3TCX to 1IAM
3TCX to 1MQ8
3TCX to 1IC1
1IAM to 1MQ8
1IC1 to 1IAM
1MQ8 to 1IC1
ICAM-1 WT QTSVSPSKVILPRGGSVLVTCSTSCDQPKLLGIETPLPKKELLLPGNNRKVYELSNVQEDSQPMCYSNCPDGQSTAKTFLTVYWT
ICAM-1 D1 MVSVSPSKVTLPRGGSVLVTCSASCDQPKLLGIETPLVKKELLLPGNNRKVYELSNVQEDSQVMCYANCPDGQSTAKAFLTVYWT
HRV 16
24 - 29
40 - 49
67
70 -72
αLI domain
29 - 39
62 - 68
73
β strand
A
A'
B
C
D
E
F
G

Discussion

Here we report the crystal structure of the LFA-1 I domain in complex with ICAM-1 D1, which have been engineered for high affinity and native fold, respectively. A point mutation in the LFA-1 I domain (F265S), which resulted in an increase in affinity to ICAM-1 by ~10,000 fold over the wild-type I domain [17], was sufficient to trigger allosteric shifting of the MIDAS into a high affinity metal ion coordination and the downward displacement of the α7-helix. Using a comprehensive, systematic approach to isolate mutations that would enhance protein fold, we have previously engineered a functional ICAM-1 D1 alone, fully active regarding its interaction with LFA-1 and less active with HRV [20]. Although as many as seven mutations were necessary to achieve functional D1 in isolation, our crystal structure revealed little perturbation in the conformation of β-strands forming two faces of β-sandwich structure.

Structural basis of allosteric switching of the integrin I domains to the conformation that is competent for ligand binding has been studied extensively. Conformational allostery in the α7-helix was first evidenced in the α_M I domain structure with the glutamic acid of the neighboring I domain coordinating to the metal ion in the MIDAS [22], which was associated with the downward displacement of the α7-helix compared to the later structures of the wild-type α_M I domain [31]. The first ligand complexed structure of the I domain was the α_2 I domain bound to collagen mimetic peptide, exhibiting a similar piston-like pulldown of the α7-helix [23]. However, due to the low affinity state of the wild-type LFA-1 I domain, previous complex structures with ICAMs required a pair of cysteines or the mutation (e.g., F292G) that would directly affect the position of α7-helix. With the native sequence of the α7-helix and the neighboring residues, the crystal structure of the I domain in

complex with native ligand in this study further underscores the intrinsic mobility of the α7-helix and how the I domain allostery is coupled to a global conformation change of integrin from low to high affinity states to their ligands.

ICAM-1 consists of five Ig-like domains in its extracellular region, from which D1 is solely responsible for the molecular contacts with the LFA-1 I domain and HRV. Despite an extensive set of mutations in D1, the majority of which would convert the hydrogen bond interaction into vdW contacts, D1 mutant was found to retain native conformation of β-strands and β-sandwich fold with the largest deviation localized to the loops that form the N-terminal face of the Ig-like fold. The flexible nature of the loops in D1, analogous to the complementarity determining region (CDR) in antibodies [32], was also pronounced among the crystal structures of the wild-type ICAM-1 D1D2 with as much as 1.1, 2.9, and 4.8 Å RMSD between Cα distances in B-C, D-E, and F-G loops, respectively, whereas the rest of the domain differed by less than 0.6 Å RMSD. Although the stable D1 mutant retained its interaction with conformation-specific antibodies and the LFA-1 I domain, the full-length ICAM-1 D1-D5 containing the mutations found in D1 displayed lower binding to HRV [20]. In addition to the proposed role of the complementarity of the charge distribution on the interface between ICAM-1 and HRV [33], the flexible nature of the loops and hydrogen bond network present in the N-terminal face of ICAM-1 may also be critical to the recognition of over 90 different serotypes of rhinovirus by ICAM-1. The insight gained from the crystal structure of the engineered ICAM-1 D1 and its comparison with the wild-type structures, i.e., the importance of hydrogen bond network in the protein core that determines the conformation of the CDR-like loops for interaction with HRV, may guide us to design a functional D1 that retains full binding potential to the virus.

REFERENCES

1. Springer TA, Wang JH. The three-dimensional structure of integrins and their ligands, and conformational regulation of cell adhesion. Adv Protein Chem. 2004;68:29-63.

2. Luo BH, Carman CV, Springer TA. Structural basis of integrin regulation and signaling. Annu Rev Immunol. 2007;25:619-47.

3. Hynes RO. Integrins: bidirectional, allosteric signaling machines. Cell. 2002;110(6):673-87.

4. Marlin SD, Springer TA. Purified intercellular adhesion molecule-1 (ICAM-1) is a ligand for lymphocyte function-associated antigen 1 (LFA-1). Cell. 1987;51(5):813-9.

5. Gahmberg CG. Leukocyte adhesion: CD11/CD18 integrins and intercellular adhesion molecules. Curr Opin Cell Biol. 1997;9(5):643-50.

6. Ostermann G, Weber KS, Zernecke A, Schroder A, Weber C. JAM-1 is a ligand of the beta(2) integrin LFA-1 involved in transendothelial migration of leukocytes. Nat Immunol. 2002;3(2):151-8.

7. Dustin ML, Rothlein R, Bhan AK, Dinarello CA, Springer TA. Induction by IL 1 and interferon-gamma: tissue distribution, biochemistry, and function of a natural adherence molecule (ICAM-1). J Immunol. 1986;137(1):245-54.

8. Nelson H, Ramsey PS, Donohue JH, Wold LE. Cell adhesion molecule expression within the microvasculature of human colorectal malignancies. Clin Immunol Immunopathol. 1994;72(1):129-36.

9. Kelly CP, O'Keane JC, Orellana J, Schroy PC, 3rd, Yang S, LaMont JT, et al. Human colon cancer cells express ICAM-1 in vivo and support LFA-1-dependent lymphocyte adhesion in vitro. Am J Physiol. 1992;263(6 Pt 1):G864-70.

10. Bella J, Kolatkar PR, Marlor CW, Greve JM, Rossmann MG. The structure of the two amino-terminal domains of human ICAM-1 suggests how it functions as a rhinovirus receptor and as an LFA-1 integrin ligand. Proc Natl Acad Sci U S A. 1998;95(8):4140-5.

11. Shimaoka M, Xiao T, Liu JH, Yang Y, Dong Y, Jun CD, et al. Structures of the alpha L I domain and its complex with ICAM-1 reveal a shape-shifting pathway for integrin regulation. Cell. 2003;112(1):99-111.

12. Xiao T, Takagi J, Coller BS, Wang JH, Springer TA. Structural basis for allostery in integrins and binding to fibrinogen-mimetic therapeutics. Nature. 2004;432(7013):59-67.

13. Shimaoka M, Takagi J, Springer TA. Conformational regulation of integrin structure and function. Annu Rev Biophys Biomol Struct. 2002;31:485-516.

14. Takagi J, Petre BM, Walz T, Springer TA. Global conformational rearrangements in integrin extracellular domains in outside-in and inside-out signaling. Cell. 2002;110(5):599-11.

15. Song G, Yang Y, Liu JH, Casasnovas JM, Shimaoka M, Springer TA, et al. An atomic resolution view of ICAM recognition in a complex between the binding domains of ICAM-3 and integrin alphaLbeta2. Proc Natl Acad Sci U S A. 2005;102(9):3366-71.

16. Jin M, Andricioaei I, Springer TA. Conversion between three conformational states of integrin I domains with a C-terminal pull spring studied with molecular dynamics. Structure. 2004;12(12):2137-47.

17. Jin M, Song G, Carman CV, Kim YS, Astrof NS, Shimaoka M, et al. Directed evolution to probe protein allostery and integrin I domains of 200,000-fold higher affinity. Proc Natl Acad Sci U S A. 2006;103(15):5758-63.

18. Oliveira MA, Zhao R, Lee WM, Kremer MJ, Minor I, Rueckert RR, et al. The structure of human rhinovirus 16. Structure. 1993;1(1):51-68.

19. Casasnovas JM, Stehle T, Liu JH, Wang JH, Springer TA. A dimeric crystal structure for the N-terminal two domains of intercellular adhesion molecule-1. Proc Natl Acad Sci U S A. 1998;95(8):4134-9.

20. Owens RM, Gu X, Shin M, Springer TA, Jin MM. Engineering of single Ig superfamily domain of intercellular adhesion molecule 1 (ICAM-1) for native fold and function. J Biol Chem. 2010;285(21):15906-15.

21. Zhang H, Casasnovas JM, Jin M, Liu JH, Gahmberg CG, Springer TA, et al. An unusual allosteric mobility of the C-terminal helix of a high-affinity alphaL integrin I domain variant bound to ICAM-5. Mol Cell. 2008;31(3):432-7.

22. Lee JO, Rieu P, Arnaout MA, Liddington R. Crystal structure of the A domain from the alpha subunit of integrin CR3 (CD11b/CD18). Cell. 1995;80(4):631-8.

23. Emsley J, Knight CG, Farndale RW, Barnes MJ, Liddington RC. Structural basis of collagen recognition by integrin alpha2beta1. Cell. 2000;101(1):47-56.

24. McCoy AJ. Solving structures of protein complexes by molecular replacement with Phaser. Acta Crystallogr D Biol Crystallogr. 2007;63(Pt 1):32-41.

25. Zhang H, Astrof NS, Liu JH, Wang JH, Shimaoka M. Crystal structure of isoflurane bound to integrin LFA-1 supports a unified mechanism of volatile anesthetic action in the immune and central nervous systems. FASEB J. 2009;23(8):2735-40.

26. Hadfield AT, Lee W, Zhao R, Oliveira MA, Minor I, Rueckert RR, et al. The refined structure of human rhinovirus 16 at 2.15 A resolution: implications for the viral life cycle. Structure. 1997;5(3):427-41.

27. Kolatkar PR, Bella J, Olson NH, Bator CM, Baker TS, Rossmann MG. Structural studies of two rhinovirus serotypes complexed with fragments of their cellular receptor. EMBO J. 1999;18(22):6249-59.

28. Sherman F, Stewart JW, Tsunasawa S. Methionine or not methionine at the beginning of a protein. Bioessays. 1985;3(1):27-31.

29. Olson NH, Kolatkar PR, Oliveira MA, Cheng RH, Greve JM, McClelland A, et al. Structure of a human rhinovirus complexed with its receptor molecule. Proc Natl Acad Sci U S A. 1993;90(2):507-11.

30. Xiao C, Tuthill TJ, Bator Kelly CM, Challinor LJ, Chipman PR, Killington RA, et al. Discrimination among rhinovirus serotypes for a variant ICAM-1 receptor molecule. J Virol. 2004;78(18):10034-44.

31. Lee JO, Bankston LA, Arnaout MA, Liddington RC. Two conformations of the integrin A-domain (I-domain): a pathway for activation? Structure. 1995;3(12):1333-40.

32. Yin J, Beuscher AEt, Andryski SE, Stevens RC, Schultz PG. Structural plasticity and the evolution of antibody affinity and specificity. J Mol Biol. 2003;330(4):651-6.

33. Bella J, Rossmann MG. ICAM-1 receptors and cold viruses. Pharm Acta Helv. 2000;74(2-3):291-7.

CHAPTER 5

TUNABLE PHYSIOLOGIC INTERACTIONS OF ADHESION MOLECULES FOR INFLAMED CELL-SELECTIVE DRUG DELIVERY

Summary

Dysregulated inflammatory responses contribute to the pathogenesis of various diseases. Therapeutic efficacy of most anti-inflammatory agents, however, fall short against resilient immune and inflammatory diseases, whereas long-term and high-dose systemic administration can cause adverse side effects. Site-directed drug delivery systems would thus render safer and more effective treatments by increasing local dosage and minimizing systemic toxicity. Nonetheless, achieving clinically effective targeted delivery to the inflammatory sites has been difficult due to diverse cellular players involved in the immune responses and endogenous target markers being expressed at basal levels. Here we exploit a physiological interaction between two cell adhesion molecules, called intercellular adhesion molecule (ICAM)-1 and lymphocyte function associated antigen (LFA)-1, to deliver a potent anti-inflammatory and anti-oxidative drug, celastrol, specifically and comprehensively to inflamed cells. We found that affinity and avidity adjusted inserted (I) domain, the major binding site of LFA-1 integrin, on the surface of liposomes greatly enhanced the specificity toward lipopolysaccharides (LPS)-treated or inflamed endothelial cells (HMEC-1) and

This chapter was originally published in Biomaterials (Kang, S., Park, T., Chen, X., Dickens, G., Lee, B., Lu, K., Rakhilin, N., Daniel, S., and Jin, M.M. *Biomaterials*. 2011;32(13):3487-98. © 2011 Elsevier.), and is reprinted with permission. The following is the detailed contribution of authors: Kang S and Jin MM designed research; Kang S, Park T, Chen X, Dickens G, Lee B, Lu K, Rakhilin N, Daniel S, and Jin MM performed research; Kang S and Jin MM analyzed data; and Kang S, Daniel S, and Jin MM wrote the paper.

monocytes (THP-1) via ICAM-1 overexpression, reflecting inherent affinity and avidity modulation of these two molecules in physiology. Targeted delivery of celastrol to inflamed HMEC-1 and THP-1 cells protected them from recurring challenges of LPS, resulting in reduced expression of pro-inflammatory mediators as well as suppression of inflammation-induced cell proliferation. Targeted delivery also potently blocked the adhesion of THP-1 cells to inflamed HMEC-1 cells, forming a critical barrier to immune cell accumulation and to aggravating inflammatory signals. Our results demonstrate affinity and avidity of targeting moieties on nanoparticles as important design parameters to ensure specificity and avoid toxicities. We anticipate that tunable physiologic interactions such as those examined in this study could be used for designing effective drug carriers for *in vivo* applications and contribute to treating a broad spectrum of immune and inflammatory diseases.

Introduction

Imbalance between pro- and anti-inflammatory responses of host immune system contributes to the pathogenesis of various human diseases of modern society [1]. In particular, prolonged and excessive inflammation, which comprises persistently reinitiating acute and chronic inflammatory responses between non-immune (epithelium, endothelium, etc) and immune cells, has been implicated in cardiovascular diseases [2], obesity [3], neurodegenerative diseases [4], and cancer [5]. Subsequently, anti-inflammatory agents such as corticosteroids, nonsteroidal anti-inflammatory drugs, cyclo-oxygenase-2-selective inhibitors, and statins have been used clinically to treat acute and chronic inflammatory diseases [6-9]. Long-term and high-dose enteral or parenteral administration of these drugs, however, have been limited due to adverse systemic side effects that included gastrointestinal disturbances,

renal, ocular and liver toxicities, skeletal and muscle damages, and increased risk of cardiovascular diseases [10-13].

Current advances in site-directed drug delivery systems [14] would thus contribute much benefit towards safer and more effective clinical use of anti-inflammatory agents. Numerous studies have targeted drug carriers to the endogenous molecules of endothelium such as ICAM-1 [15-16], vascular cell adhesion molecule (VCAM)-1 [17-18], platelet endothelial cell adhesion molecule (PECAM)-1 [19], E- and P-selectins [20-21], and $\alpha_v\beta_3$ integrin [22-23], which belong to a family of cell adhesion molecules. Some of the cell adhesion molecules such as E-selectins and $\alpha_v\beta_3$ integrin are more exclusively expressed in vascular endothelium, while others may be present in both non-immune and immune cells. The difference in their response to inflammation is also observed in terms of the levels of induction as well as their basal expression prior to inflammation. ICAM-1 has been of particular interest for its superior inducible and localized expression upon inflammatory stimuli both in immune and non-immune cells such as endothelial, smooth muscle, epithelial cells, fibroblasts, lymphocytes, and myeloid cells [24-25]. Specific delivery of drug carriers or nanoparticles to inflamed cells has traditionally been achieved by molecular interactions with cell surface molecules created by attaching antibodies or short peptides to the surface of nanoparticles [26-27]. However, most prior approaches have failed to address affinity and avidity modulation as important design criteria for efficient nanoparticle binding to target cells, which will be drastically different from those for free molecule binding due to much larger detachment force on nanoparticles caused by hydrodynamic stress *in vitro* and *in vivo*. Alternative to non-native interactions, the use of physiological ligands or their engineered variants [28-30] conjugated to nanoparticles at an optimal density for tunable affinity and avidity may

prove advantageous in regard to ensuring specificity against target receptors and a lower risk of unwanted immune response.

In any attempt to deliver drugs via ICAM-1 targeting, one needs to ensure specific delivery of drug carriers to inflamed cells but not to normal cells, given the observation that ICAM-1 is broadly expressed in the body albeit at much lower levels than post exposure to inflammatory stimuli [31]. In order to design drug carriers against ICAM-1 to be robust and amenable to fine-control in terms of affinity and avidity, we have chosen a targeting moiety based on a native molecule called the inserted or I domain, derived from a physiological receptor to ICAM-1 called lymphocyte function associated antigen (LFA)-1 integrin [25, 28]. In contrast to commonly used monoclonal antibodies (~150 kDa) against ICAM-1 for targeting, LFA-1 I domain is small (~20 kDa) and suitable for a low-cost, large-scale production in bacteria, and can be modified for optimal affinity to ICAM-1 and facile conjugation to drug carriers. Among various nanoparticles suitable for drug delivery, liposomes have been used in this study, which have been approved for clinical use to take advantage of diverse functionalized phospholipids and large compartments for encapsulation of both hydrophilic and hydrophobic molecules. To the surface of liposomes, high-affinity LFA-1 I domain (Id-HA) was attached via non-covalent, His-tag binding to nickel ions chelated onto phospholipid molecules.

As a model anti-inflammation drug, we incorporated celastrol, a quinone methide triterpene, into the liposomes. Celastrol possesses potent anti-inflammatory, anti-oxidative, and anti-proliferative activities via the inhibition of NF-κB signaling and proteasome activity [32-34]. We emphasized the delivery of celastrol selectively to inflamed cells without causing cytotoxicity while maintaining potent therapeutic effect. To implement this, the density of Id-HA on the surface of liposomes was adjusted for optimal dose and specificity. We showed that targeted delivery of

liposomes encapsulating celastrol to active endothelial cells potently blocked the migration of monocytes, forming a key barrier to immune cell accumulation and to aggravating inflammatory responses. The results in this study demonstrate that the physiologic interaction between ICAM-1 and LFA-1 I domain could be of a great clinical use for inflamed cell-specific targeted delivery and may contribute for safer and more aggressive treatments with anti-inflammatory agents against a broad range of severe inflammatory and immune diseases.

Experimental Procedures

Cell Culture

Human dermal microvascular endothelial cells (HMEC-1) were obtained from the Center for Disease Control. HMEC-1 were cultured in MCDB 131 medium (Invitrogen) supplemented with 10% FBS (Atlanta Biologicals), 10 mM L-glutamine, Pen-strep (100 units/ml penicillin and 100 μg/ml streptomycin), 1 μg/ml hydrocortisone (MP Biomedicals), and 10 ng/ml recombinant human epidermal growth factor (Invitrogen). HMEC-1 were trypsinized when confluent, and gently centrifuged and washed to remove residual trypsin before plating. Human monocytic leukemia THP-1 cells (ATCC) were grown in RPMI 1640 medium (Invitrogen) with 10% FBS and Pen-strep. HeLa cells were propagated in Advanced DMEM medium (Invitrogen) containing 10% FBS and 2 mM L-glutamine, and Pen-strep. Mouse brain microvascular endothelial cells (bEnd.3, ATCC) were maintained in Advanced DMEM medium supplemented with 4 mM L-glutamine, Pen-strep, and 10% FBS. For induction of inflammation, HMEC-1, THP-1, or bEnd.3 cells were treated with 1 μg/ml of LPS (*E. coli.* 026:B6, Sigma). All mammalian cells were maintained at 37 °C in a 5% CO_2 humidified incubator.

Production of I domains and GFP-Id-HA fusion protein

The wild-type (WT), D137A, and F265S/F292G mutants of LFA-1 I domains (Id-WT, Id-D137A, and Id-HA) were produced as previously described [28, 30]. Briefly, the I domains (Asn129 to Tyr307) followed by a stop codon were subcloned into pET28a vector (Novagen) between NheI and XhoI for expression with a His-tag at the N-terminal. The I domains were expressed in *Escherichia coli* BL21 (DE3) cells (Novagen) as inclusion bodies. Cells were initially grown to OD600 of 0.4-0.5 and induced with 1 mM IPTG (isopropyl-β-D-thiogalactoside) for 6 h at 37 °C. To isolate the inclusion bodies, cells were resuspended in washing buffer (50 mM Tris-Cl (pH 8.0), 23% (w/v) sucrose, 1 mM EDTA, 0.5% (v/v) Triton X-100) and sonicated. Inclusion bodies were washed by repeating cycles of centrifugation, removal of supernatant, and sonication until pure pellets were obtained. Inclusion bodies were then solubilized in denaturing buffer (50 mM Tris-Cl (pH 8.0), 6 M guanidine HCl) and diluted in refolding buffer (50 mM Tris-Cl (pH 8.0), 15% glycerol, 1 mM $MgCl_2$) to a volume such that the final concentration of guanidine HCl was less than 25 mM. Refolded proteins were concentrated and subjected to gel filtration chromatography using Superdex S200 column in HBS (20 mM HEPES, 140 mM NaCl, pH 7.4) connected to AKTA Purifier (GE Healthcare). Some of the I domains were conjugated to Alexa Fluor 488 (AF488, Invitrogen) according to the instruction of the vendor. For GFP-Id-HA fusion protein, eGFP (Val2 to Lys239) [35] was first inserted into pET28a vector between NheI and BamHI and then Id-HA (Asn129 to Tyr307) followed by a stop codon was placed between BamHI and XhoI. GFP-Id-HA was produced from soluble fractions in BL21 cells. Cells were grown to OD600 of 0.4-0.5, induced with 1 mM IPTG at 25 °C for 6 h and recovered by centrifugation. Cells were then resuspended and sonicated in NTA (nitrilotriacetic acid) binding buffer (50 mM

NaH_2PO_4 (pH 8.0), 300 mM NaCl, 10 mM imidazole). Soluble proteins were separated from cell debris by centrifugation, purified by flowing the supernatant through a Ni-NTA column (Novagen) and gel filtration chromatography using S200 column.

Immunofluorescence flow cytometry and microscopy

Antibodies used for this study include anti-ICAM-1 monoclonal antibody (mAb) LB-2 (Santa Cruz) and anti-VCAM-1 mAb P3C4 (Developmental Studies Hybridoma Bank). If necessary, phycoerythrin (PE)-labeled goat anti-mouse IgG (Santa Cruz) was used for the detection of primary mAbs. For flow cytometric analysis (Beckman Coulter EPICS XL-MC), cells were trypsinized, washed with ice-chilled labeling buffer (PBS (pH 7.4), 0.5% (w/v) BSA, 10 mM $MgCl_2$), and incubated on ice for 20 min. Antibodies and proteins were used at 10 μg/ml in 200 μl of the labeling buffer and were incubated with cells on ice for 30 min. Cells were washed twice in 500 μl of the labeling buffer between each step of labeling when secondary antibodies were needed. After final washing, cells were resuspended in 300 μl of the labeling buffer and subjected to flow cytometer. For immunofluorescence microscopy, HMEC-1 were fixed with 3.7% paraformaldehyde for 30 min, washed and labeled with mAbs LB-2 or P3C4 in labeling buffer (PBS, 1% BSA, 0.02% (v/v) Tween 20) on a rocker at room temperature for 2 h. DAPI (4',6-diamidino-2-phenylindole, Invitrogen) was used at 300 nM in PBS for 10 min for nucleus staining. To estimate fluorescence and nuclei density from DAPI staining, microscopic images of 4 random spots were acquired and processed by Image-Pro Plus (Media Cybernetics) for automated intensity measurement and object counting. Similarly, confluent bEnd.3 cells were incubated with AF488 conjugated Id-HA. Stained cells were washed and imaged with a fluorescence microscope (Zeiss Axio Observer Z1).

For confocal microscopy (Leica TCS SP2), HeLa cells were labeled with 10 μg/ml of mAb LB-2 or GFP-Id-HA in 200 μl of labeling buffer on ice for 30 min.

LFA-1 or Mac-1 I domain-displaying yeast binding to HMEC-1

Mammalian cell surface binding of yeast cells displaying various I domains was performed as previously described [35]. In short, yeast cells expressing WT or activated mutants of LFA-1 and Mac-1 I domains were washed and resuspended in washing buffer (PBS (pH 7.4), 0.5% BSA, 10 mM $MgCl_2$). 300 μl of yeast cell suspension containing approximately $5x10^7$ cells was applied to each well of confluent HMEC-1 in a 24 well plate. Yeast cells were allowed to bind to HMEC-1 for 1 h at room temperature. Cells were then washed with washing buffer by gentle shaking on an orbital shaker for 15 min.

Preparation of I domain coupled liposomes

Liposomes were prepared by the thin lipid film method followed by the sonication and extrusion method [36]. Phospholipid (Avanti Polar Lipids) mixture was prepared by mixing 52.5 mol % DPPC (1,2-dipalmitoyl-*sn*-glycero-3-phosphocholine), 12.5 mol % DPPE (1,2-dipalmitoyl-*sn*-glycero-3-phosphoethanolamine), 20 mol % cholesterol, 5 mol % PEG1000-PE (1,2-dimyristoyl-*sn*-glycero-3-phosphoethanolamine-N-[methoxy(polyethylene glycol)-1000]), and 10 mol % DOGS-NTA(Ni) (1,2-dioleoyl-*sn*-glycero-3-[(N-(5-amino-1-carboxypentyl)iminodiacetic acid)succinyl]) in chloroform. Chloroform in the lipid mixture in a round bottom flask was then evaporated with nitrogen gas to form a lipid film. Lipid films were rehydrated with HBS (20 mM HEPES, 140 mM NaCl, pH 7.4) containing 10 mM FITC (fluorescein isothiocyanate) or 1 mM celastrol. Rehydrated multilamellar vesicular (MLV) liposomes were then sonicated (Misonix Sonicator

3000) and extruded 10 times through 100 nm polycarbonate membranes (Nuclepore, Whatman). Extruded unilamellar vesicular (ULV) liposomes were supplemented with 10 mM $NiCl_2$ and collected by centrifugation at 35,000 rpm for 2 h. Supernatant was removed, leaving a final volume of approximately 500 μl. Pelleted liposomes were gently sonicated (Branson Sonified 150), filtered through 0.2 μm centrifugal filters, and subjected to S200 column (GE Healthcare) in HBS. Liposome diameters were measured using dynamic light scattering (Zetasizer Nano-S, Malvern Instruments). Encapsulation efficiency of FITC was estimated by fluorescence (excitation 490 nm/emission 520 nm) and celastrol by absorbance at 425 nm (extinction coefficient, 10,063 M^{-1} cm^{-1}) after lipid solubilization with 1% (v/v) Triton X-100. Liposomes encapsulating FITC or celastrol were mixed with I domains and incubated on ice for 30 min for spontaneous coupling. For all couplings, a mass ratio of I domains to liposomes was 20% unless otherwise stated. Coupling efficiency of His-tagged I domains to liposomes was estimated by sucrose gradient flotation assay. Liposome/I domain mixture was diluted to final 30% (w/v) sucrose, layered with 20% sucrose solution, and centrifuged at 35,000 rpm for 2 h. After centrifugation, top fractions were collected and estimated for protein concentrations by Lowry method (Bio-Rad DC Protein Assay Kit).

Liposome delivery into endothelium and monocytes

HMEC-1 or THP-1 cells were initially grown to confluence in 24-well plates and treated with 1 μg/ml LPS for 24 h to induce inflammation. The liposome/I domain mixtures were adjusted to a final volume of 300 μl with prewarmed complete growth media containing 10% FBS and added to cells. HMEC-1 or THP-1 cells were treated with the preassembled liposomes or other control treatments at 37 °C for 30 min and washed twice with complete growth media. At 36 to 48 h after incubation, cells were

challenged again with 1 μg/ml LPS for 3 h for quantitative PCR gene expression analysis or 24 h for THP-1 cell adhesion assay. For cell viability assays, HMEC-1 in 24-well plates were treated with basal media containing 0.5 mg/ml of MTT (3-(4,5-Dimethylthiazol-2-yl)-2,5-diphenyltetrazolium bromide) for 4 h at 37 ºC. Blue formazan products were solubilized with DMSO and the absorbance was measured at 570 nm with a plate reader (Infinite M1000, TECAN).

Real-time quantitative RT-PCR

Total RNA was extracted using TRI Reagent (Ambion). Briefly, cells in 24-well plates were given 200 μl TRI Reagent for each well. Homogenized lysates were mixed with 40 μl of chloroform and centrifuged for 15 min at 12,000 x g. 80 μl of the colorless upper aqueous phase was carefully collected and mixed with 200 μl isopropanol. Samples were loaded to spin columns (Zymo-Spin II, Zymo Research) and washed twice with 500 μl ethanol. RNA was eluted with 30 μl of RNase-free water (UltraPure, Invitrogen). 500 ng of total RNA was reverse-transcribed at 25 °C for 10 min, 37 °C for 2 h, and 85 °C for 5 min using a reverse transcription kit (High Capacity cDNA RT Kits, Applied Biosystems) in a thermal cycler (GeneAmp PCR System 2700, Applied Biosystems). 2 μl of the cDNA product was used for real-time gene amplification analysis. Master mix 2X qPCR kit (Sybr Green 2x Master Mix, Bio-Rad) was used to amplify the specified genes for quantitative PCR (MyiQ iCycler, Bio-Rad). Gene expression was normalized to a house keeping gene ATP5J. Intron spanning primers were designed from the National Institute of Health qPrimerDepot using accession codes of NM_000201 (ICAM-1), NM_001078 (VCAM-1), NM_002982 (MCP-1), NM_000575 (IL-1α), NM_000594 (TNF-α), NM_000450 (E-selectin), NM_001250 (CD40) and NM_001003703 (ATP5J).

THP-1 cell adhesion assay

THP-1 cells were suspended at 10^6 cells/ml in complete growth media containing 10% FBS and labeled with 2 μg/ml BCECF-AM (2,7-bis-(2-carboxyethyl)-5-(and-6)-carboxyfluorescein acetoxymethyl ester, Invitrogen) for 30 min at 37 ºC. BCECF labeled THP-1 cells were washed and resuspended at $2x10^6$ cells/ml in growth media. 300 μl of the THP-1 cell suspension was applied to each well of HMEC-1 in 24-well plates and allowed to bind for 30 min at 37 ºC. Cells were repeatedly washed with complete growth media until THP-1 cells on resting HMEC-1 were cleared. THP-1 cells were then imaged by a fluorescence microscope and lysed with a lysis buffer (PBS (pH 7.4), 1% (v/v) Triton X-100) by vigorously shaking the plate for 1 h at room temperature. Fluorescence (excitation 490 nm/emission 535 nm) of the cell lysates was measured by a plate reader.

Statistical analysis

Data were expressed as mean ± standard deviation (S.D.) of at least quadruplicate samples. Statistical analysis of data was carried out using GraphPad Prism 5. Unpaired student's t-test was used to determine statistical significance in comparison to matching controls (Figs. 5.1 and 5.2). One-way ANOVA was used to compare mean responses among different liposome and control treatments (Figs. 5.6 and 5.7), followed by Tukey's post-hoc test to determine statistical significance.

Results

Detection of temporal upregulation of ICAM-1 in endothelium and monocytes

Upregulated expression of ICAM-1 is associated with almost all cellular players in acute and chronic inflammation [24]. Diversity of the cellular components

and their complex inflammatory signaling network present a challenge to developing an effective anti-inflammatory therapy. We used HMEC-1 and THP-1 representing major non-immune and immune cells, respectively, that constitute an inflammatory milieu. To induce inflammation, cells were treated with LPS that activate NF-κB dependent inflammatory signaling pathways [37]. In resting HMEC-1 and THP-1 cells, ICAM-1 expression was below the detection limit with anti-ICAM-1 mAb LB-2 (Fig. 5.1a). LPS treatment gradually induced ICAM-1 expression in both HMEC-1 and THP-1 cells, peaking at 12-24 h (Fig. 5.1a). We then tested whether a physiologic counter-receptor for ICAM-1, the I domain from human LFA-1 integrin containing two activating mutations (F265S/F292G) (abbreviated as Id-HA) [28, 30], would detect a comparable temporal induction of ICAM-1. To measure Id-HA binding to ICAM-1 without any additional labels, Id-HA was expressed as a fusion to GFP (GFP-Id-HA) and tested for its binding to HeLa cells with constitutive expression of ICAM-1 (Fig. 5.1b). ICAM-1 staining with Id-HA in HeLa was comparable to mAb LB-2, shown by confocal microscopy (Fig. 5.1c). The temporal induction of ICAM-1 in HMEC-1 and THP-1 cells measured by flow cytometry using GFP-Id-HA was in good agreement with ICAM-1 staining with mAb LB-2 (Fig. 5.1e). We also found that human Id-HA cross-reacts with murine ICAM-1, confirmed with mouse brain microvascular endothelial cells (bEnd.3) after LPS treatment (Fig.5.1d). Cross-reactivity of Id-HA with murine ICAM-1 will be of significant advantage as the identical formulation can be applied to both human cells and mouse models in preclinical studies.

Suppression of various pro-inflammatory mediators by celastrol

Celastrol is a plant derived quinone methide triterpene (Fig. 5.2a), long been known for potent anti-inflammatory, anti-oxidative, and anti-proliferative activities.

Figure 5.1. Inflammation-induced upregulation of ICAM-1 in HMEC-1 and THP-1 cells.

(a) Confluent HMEC-1 and THP-1 cells were exposed to LPS (1 μg/ml) for 0 - 24 h. ICAM-1 expression and nuclei were detected by immunofluorescence staining with mAb LB-2 and DAPI, respectively (scale bar, 50 μm). (b) A model structure of the fusion protein GFP-Id-HA is shown as a ribbon diagram. (c) ICAM-1 expression in HeLa cells was detected by confocal microscopy with GFP-Id-HA and mAb LB-2 staining (scale bar, 20 μm). (d) bEnd.3 cells were treated with LPS for 24 h and labeled with Id-HA conjugated to AF488 to assess cross-reactivity of human LFA-1 I domain with murine ICAM-1 (scale bar, 50 μm). (e) GFP-Id-HA was used to detect upregulated expression of ICAM-1 in LPS-treated HMEC-1 and THP-1 cells. The data are presented as the average values of fluorescence intensity (F.I.) with error bars indicating S.D. (*$p < 0.05$, unpaired Student's t-test compared to control group, n=4).

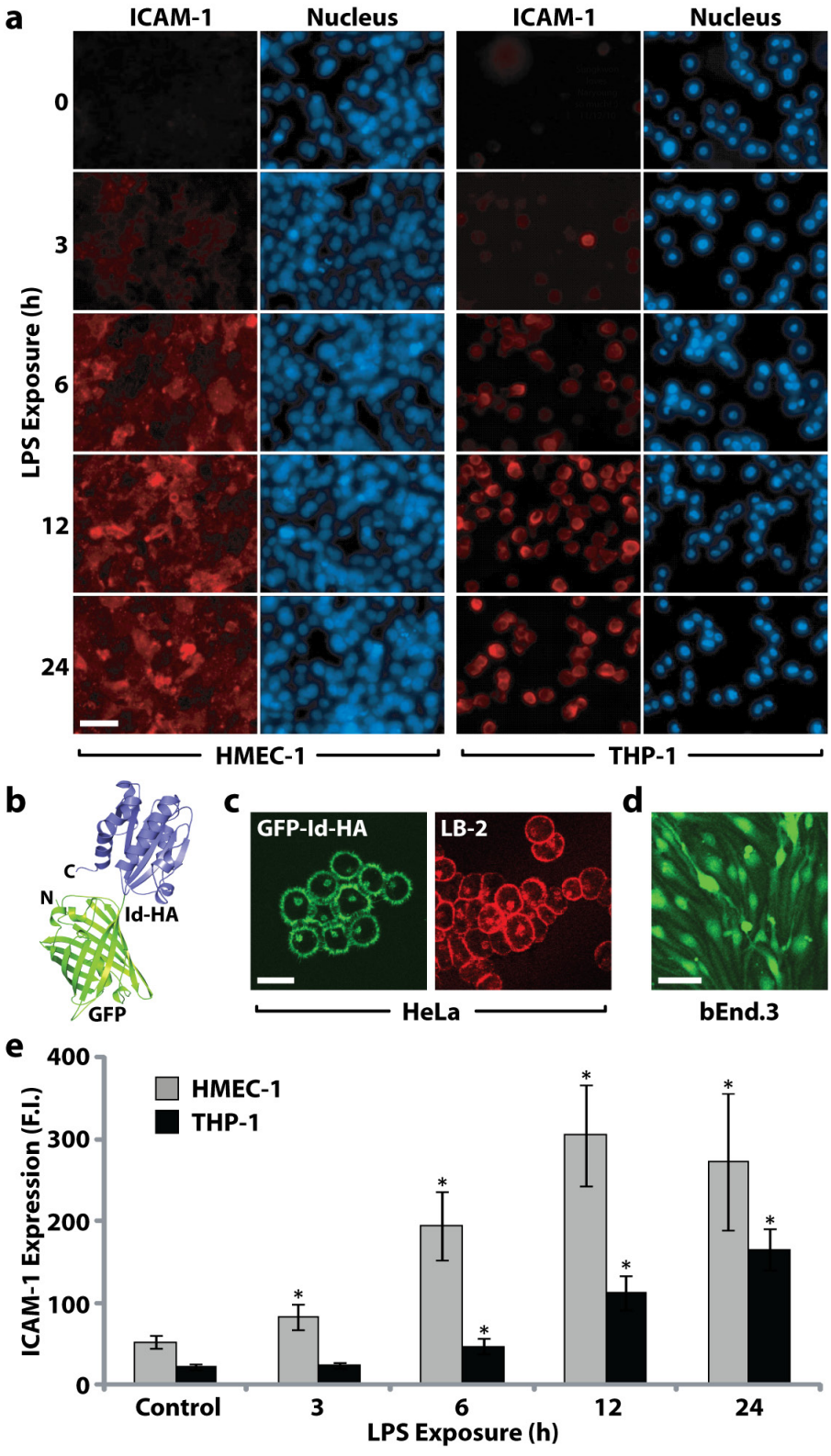
a
ICAM-1
Nucleus
ICAM-1
Nucleus
0
3
6
12
24
LPS Exposure (h)
HMEC-1
THP-1
b
C
N
Id-HA
GFP
c
GFP-Id-HA
LB-2
HeLa
d
bEnd.3
e
400
300
200
100
0
ICAM-1 Expression (F.I.)
HMEC-1
THP-1
Control
3
6
12
24
LPS Exposure (h)

Figure 5.2. Reversal of pro-inflammatory markers by celastrol in HMEC-1 and THP-1 cells.

(a) The chemical structure of celastrol. (b&c) Quantitative RT-PCR was performed to measure various LPS-induced pro-inflammatory gene expression. HMEC-1 (b) and THP-1 cells (c), pretreated either with or without 1 μM celastrol for 3 h, were challenged with LPS (1 μg/ml) for 3 h before gene expression analysis. (d&e) Protein expression of cell adhesion molecules ICAM-1 (mAb LB-2) and VCAM-1 (mAb P3C4) was evaluated by flow cytometry. HMEC-1 (d) or THP-1 (e) cells were pretreated with 0.04 - 1 μM celastrol for 3 h and challenged with LPS (1 μg/ml) for 12 or 24 h to assess inhibition of ICAM-1 and VCAM-1 expression. The data represent the average values of fluorescent intensity (F.I.) (*$p < 0.05$, unpaired Student's t-test compared to the LPS group (d&c) or to control group (d&e), n=4).

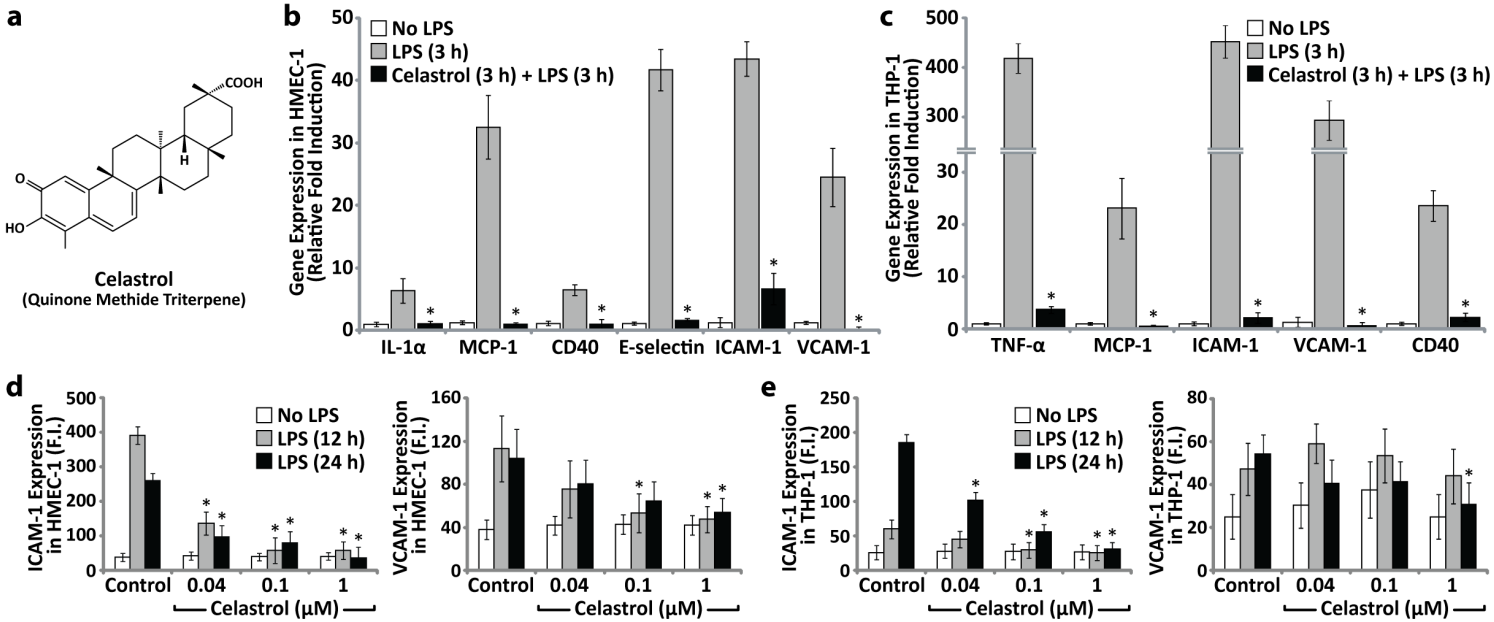
a
COOH
O
H
HO
Celastrol
(Quinone Methide Triterpene)
b
No LPS
LPS (3 h)
Celastrol (3 h) + LPS (3 h)
Gene Expression in HMEC-1
(Relative Fold Induction)
IL-1α
MCP-1
CD40
E-selectin
ICAM-1
VCAM-1
c
Gene Expression in THP-1
(Relative Fold Induction)
TNF-α
MCP-1
ICAM-1
VCAM-1
CD40
d
ICAM-1 Expression
in HMEC-1 (F.I.)
No LPS
LPS (12 h)
LPS (24 h)
VCAM-1 Expression
in HMEC-1 (F.I.)
Control
0.04
0.1
1
Celastrol (μM)
e
ICAM-1 Expression
in THP-1 (F.I.)
VCAM-1 Expression
in THP-1 (F.I.)

Previous studies have shown celastrol as a potent antagonist of proteasomes and NF-κB signaling [32-34]. To examine whether celastrol can be used as a model drug for the suppression of inflammation in both HMEC-1 and THP-1 cells, we first assessed its inhibitory effect on LPS-induced gene expression of various pro-inflammatory mediators by quantitative real-time PCR (Fig. 5.2, b and c). LPS treatment highly upregulated various cytokines, chemokines, and cell surface molecules in both HMEC-1 and THP-1 cells compared with their resting states (Fig. 5.2, b and c). In HMEC-1, interleukin (IL)-1α, monocyte chemotactic protein (MCP)-1, CD40, E-selectin, ICAM-1, and VCAM-1 were greatly upregulated as early as 3 h treatment with LPS (Fig. 5.2b). Similarly in THP-1 cells, tumor necrosis factor (TNF)-α, MCP-1, ICAM-1, VCAM-1, and CD40 were highly upregulated (Fig. 5.2c). Relative fold inductions of ICAM-1 and VCAM-1 were much larger for THP-1 cells than HMEC-1 (Fig. 5.2, b and c), partly due to their lower levels in THP-1 at a resting state. Pretreatment with celastrol at 1 μM for 3 h, however, potently blocked LPS-induced expression of pro-inflammatory markers in both HMEC-1 and THP-1 cells (Fig. 5.2, b and c). To examine if the suppression of pro-inflammatory markers at the mRNA level would reduce cell surface expression of cell adhesion molecules, which in effect would form a critical barrier to cell-cell adhesion and monocyte migration, we measured ICAM-1 and VCAM-1 expression by flow cytometry (Fig. 5.2, d and e). Pretreatment of HMEC-1 with celastrol for 3 h significantly inhibited both ICAM-1 and VCAM-1 expression in a dose-dependent manner, restoring to their basal levels with 100 nM of celastrol (Fig. 5.2d). In THP-1 cells, a similar trend was observed, resulting in nearly complete inhibition of ICAM-1 expression with as low as 100 nM celastrol (Fig. 5.2e). In contrast to as much as 10-fold increase in fluorescence intensity measured for ICAM-1 in both cell lines, VCAM-1 expression was less prominent with only 3-fold induction (Fig. 5.2, d and e). Also, inhibition of VCAM-1

expression in THP-1 cells was less potent as significant reduction was detected only with 1 μM celastrol (Fig. 5.2e).

Ni-NTA liposome as a drug carrier with tunable assembly with targeting moieties

Ni-NTA phospholipids (10 mol % DOGS-NTA(Ni)) were included in pegylated liposomes to assemble with polyhistidine (6xHIS) tagged moieties, which would enable coupling of liposome nanoparticles with LFA-1 I domain variants at a predefined coating density and in a correct orientation. Unilamellar vesicles encapsulating desired drug or dye molecules were formulated by the hydration of thin lipid film in drug/dye-containing solutions, followed by the sonication and extrusion method (Fig. 5.3a). Liposomes encapsulating FITC or celastrol (denoted as liposome(FITC) and liposome(celastrol)) were separated from free molecules by gel filtration chromatography using size exclusion column (Fig. 5.3, a and b), where small molecules such as FITC and celastrol eluted much later than nanoparticles (Fig. 5.3b). Liposomes were then mixed with Id-HA and subjected to centrifugation through a gradient of sucrose (20 to 30%, w/v), where Id-HA coated liposomes would float to the top of the gradient and unconjugated Id-HA remain at the bottom of the tube. The top fractions of the sucrose gradient were collected and measured for protein concentrations. Only when both liposomes and Id-HA were premixed, proteins were present at the top fractions (Fig. 5.3c). The size of liposomes before or after assembly with Id-HA was measured by dynamic light scattering (DLS). The diameter of the liposomes before protein conjugation was ~107 nm, which increased to ~115 nm after coupling with Id-HA, corresponding closely to a single layer of I domain ~4 nm in size. Encapsulation efficiencies (weight of drug/weight of phospholipid) of celastrol and FITC were estimated to be 0.8% and 1.5%, respectively (Fig. 5.3d).

Figure 5.3. Ni-NTA liposome for spontaneous assembly with the I domains. (a) The schematic depicts the process of formulating targeted liposome, highlighting the steps of thin lipid film hydration, extrusion of multilamellar vesicles (MLV) to unilamellar vesicles (ULV), payload encapsulation, purification, and spontaneous assembly with His-tagged targeting moieties. (b) The elution profiles of FITC or celastrol containing liposome from S200 size exclusion column are shown. (c) The amount of proteins assembled with Ni-NTA liposome was measured from the top fractions after sucrose gradient flotation assay. (d) Encapsulation efficiencies of FITC (1.5%) and celastrol (0.8%) were measured from the weight ratio of the payload to phospholipids.

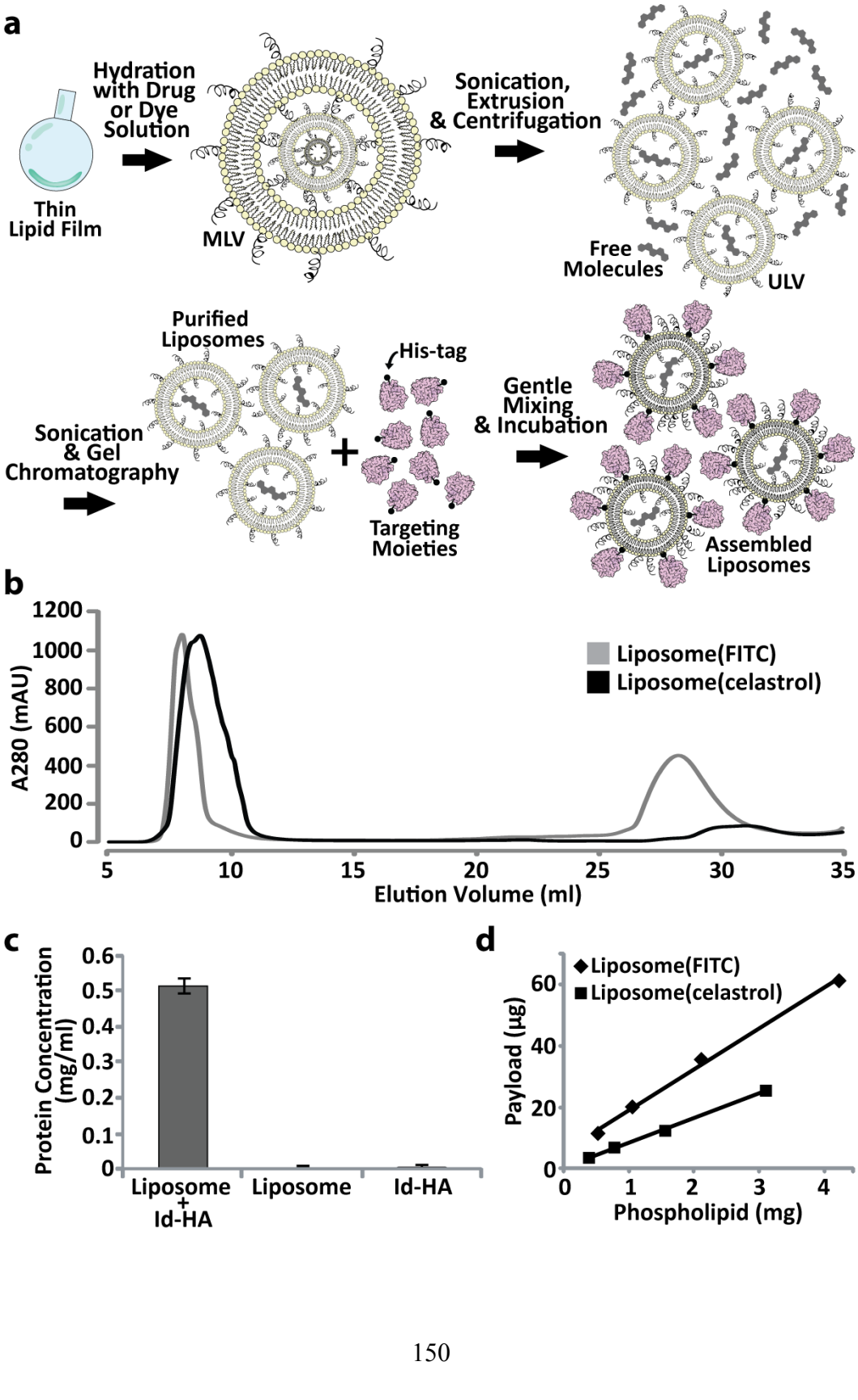
a
Hydration with Drug or Dye Solution
Thin Lipid Film
MLV
Sonication, Extrusion & Centrifugation
Free Molecules
ULV
Purified Liposomes
His-tag
Sonication & Gel Chromatography
Targeting Moieties
Gentle Mixing & Incubation
Assembled Liposomes
b
A280 (mAU)
Liposome(FITC)
Liposome(celastrol)
Elution Volume (ml)
c
Protein Concentration (mg/ml)
Liposome + Id-HA
Liposome
Id-HA
d
Liposome(FITC)
Liposome(celastrol)
Payload (µg)
Phospholipid (mg)

Specific targeting of inflamed cells by tunable affinity and avidity of I domain and ICAM-1 interactions

Structurally and functionally homologous I domains from two different β_2 integrins, LFA-1 ($\alpha_L\beta_2$) and Mac-1 ($\alpha_M\beta_2$), both interact with ICAM-1 [25, 38]. A number of mutations have been isolated to increase their binding affinity to ICAM-1, mimicking activation signals transmitted to the I domain by the neighboring domains in full-length integrins [28, 35]. To test the specificities of LFA-1 and Mac-1 I domains, they were expressed on yeast cell surface in their wild-type (WT) or with activating mutations (F265S/F292G for LFA-1 [28] and F302L for Mac-1 [35]). Yeast cells expressing the WT of LFA-1 or Mac-1 I domains failed to bind strongly to HMEC-1 cells even after LPS-induced ICAM-1 expression (Fig. 5.4a). While the binding of yeast cells expressing LFA-1 Id-HA was specific to LPS-treated HMEC-1, yeast cells expressing Mac-1 Id-HA bound to both resting and LPS-treated HMEC-1. This indicates the presence of other ligands to Mac-1 such as fibrinogen, heparin, and ICAM-2 [38-39], which may be constitutively expressed and not dependent on LPS-induced inflammation.

We then examined whether the affinity and avidity could be fine-tuned for inflamed cell-specific targeted delivery of liposomes (Fig. 5.4, b and c). Liposome(FITC) assembled with LFA-1 I domain variants (Id-WT, Id-HA, or Id-D137A) or without a targeting moiety were incubated with LPS-treated HMEC-1 (Fig. 5.4b). The mutation D137A abolishes the metal ion coordination in the MIDAS and inactivates I domain binding to ligands [40]. The maximum delivery of liposome(FITC) was observed when coupled with Id-HA, whereas much lower binding was achieved with Id-WT (Fig. 5.4b). As expected, liposomes coated with Id-D137A or without a moiety did not bind to LPS-treated HMEC-1 cells. To examine

Figure 5.4. Targeted delivery by tunable affinity and avidity of targeting moieties on liposomes.

(a) The wild-type or the active I domains of LFA-1 or Mac-1 integrins displayed on yeast cells were examined for binding to either resting or LPS-treated HMEC-1 (scale bar, 50 μm). (b) Microscopic fluorescence images of LPS-treated HMEC-1 after 30 min incubation with nanoparticles assembled with LFA-1 I domain variants (Id-WT, Id-HA, and Id-D137A) or without a targeting moiety are shown (scale bar, 50 μm). (c) Liposome(FITC) assembled with mass ratios of Id-HA to phospholipids ranging from 10 to 40% were incubated with LPS-treated HMEC-1 for 30 min to fine-tune avidity interaction to overexpressed ICAM-1 (scale bar, 100 μm).

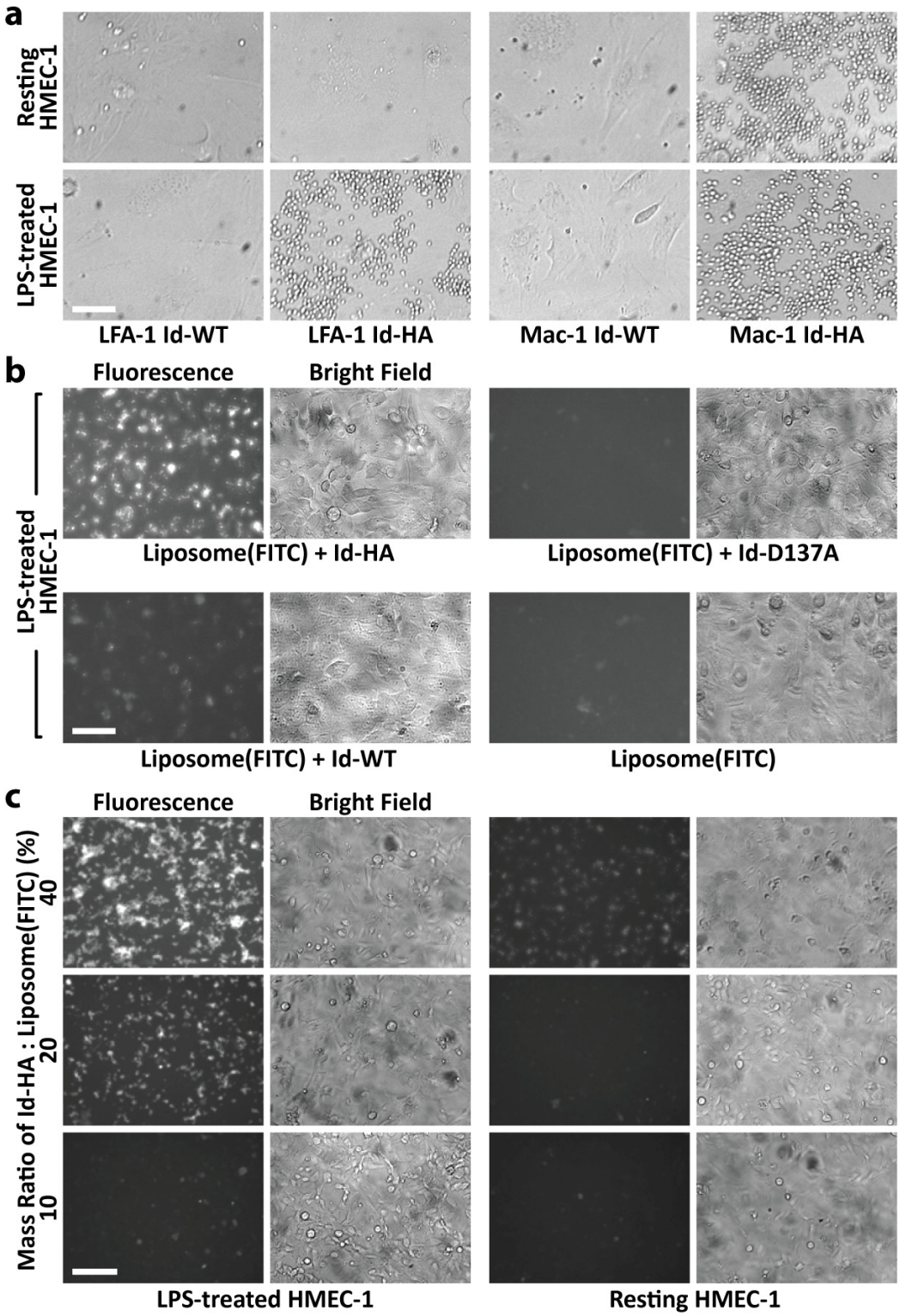
a
Resting HMEC-1
LPS-treated HMEC-1
LFA-1 Id-WT
LFA-1 Id-HA
Mac-1 Id-WT
Mac-1 Id-HA
b
Fluorescence
Bright Field
LPS-treated HMEC-1
Liposome(FITC) + Id-HA
Liposome(FITC) + Id-D137A
Liposome(FITC) + Id-WT
Liposome(FITC)
c
Fluorescence
Bright Field
Mass Ratio of Id-HA : Liposome(FITC) (%)
40
20
10
LPS-treated HMEC-1
Resting HMEC-1

the avidity effect of interactions between the Id-HA and ICAM-1 on the efficiency of liposome delivery and specificity to inflamed cells, liposome nanoparticles were coupled with a varying amounts of Id-HA in the range of 10 to 40% mass ratio (w/w) of protein to phospholipid (Fig. 5.4c). Liposomes coated with ~40% (w/w) Id-HA showed a highest level of delivery to active HMEC-1, which was also associated with significant binding to resting HMEC-1. At 20% Id-HA, although the level of binding to LPS-treated HMEC-1 was reduced, liposome delivery to resting HMEC-1 was not detectable. When the mass ratio of Id-HA to phospholipids was further reduced to 10%, liposome delivery to LPS-treated HMEC-1 was only faintly detectable. These results highlight the importance of the ability to fine-tune both affinity and avidity of targeting moieties in delivering nanoparticles to differentially expressed endogenous cell surface molecules.

Optimal concentration of celastrol that is anti-inflammatory but not cytotoxic

In order to find an optimal dosage of celastrol that effectively elicits therapeutic efficacy with minimum cytotoxicity, we examined dose-dependent suppression of pro-inflammatory markers and cell viability of HMEC-1. To better mimic *in vivo* condition where the target cells may be exposed to nanoparticles for a relatively short time due to the clearance of nanoparticles from the body, 30 min incubation with celastrol or liposome(celastrol) was applied to LPS-treated HMEC-1 or THP-1 cells (Fig. 5.5). Celastrol began to show a dose-dependent inhibitory effect on gene expression of VCAM-1, ICAM-1, and MCP-1 with as low as 10 nM concentration, with a steady increase in inhibition with an increase in drug dose (Fig. 5.5, a and b). We then evaluated the corresponding cell viability of LPS-treated HMEC-1 after treatment with celastrol at various concentrations (Fig. 5.5c). Cell viability was significantly reduced starting with 10 μM celastrol treatment for 30 min.

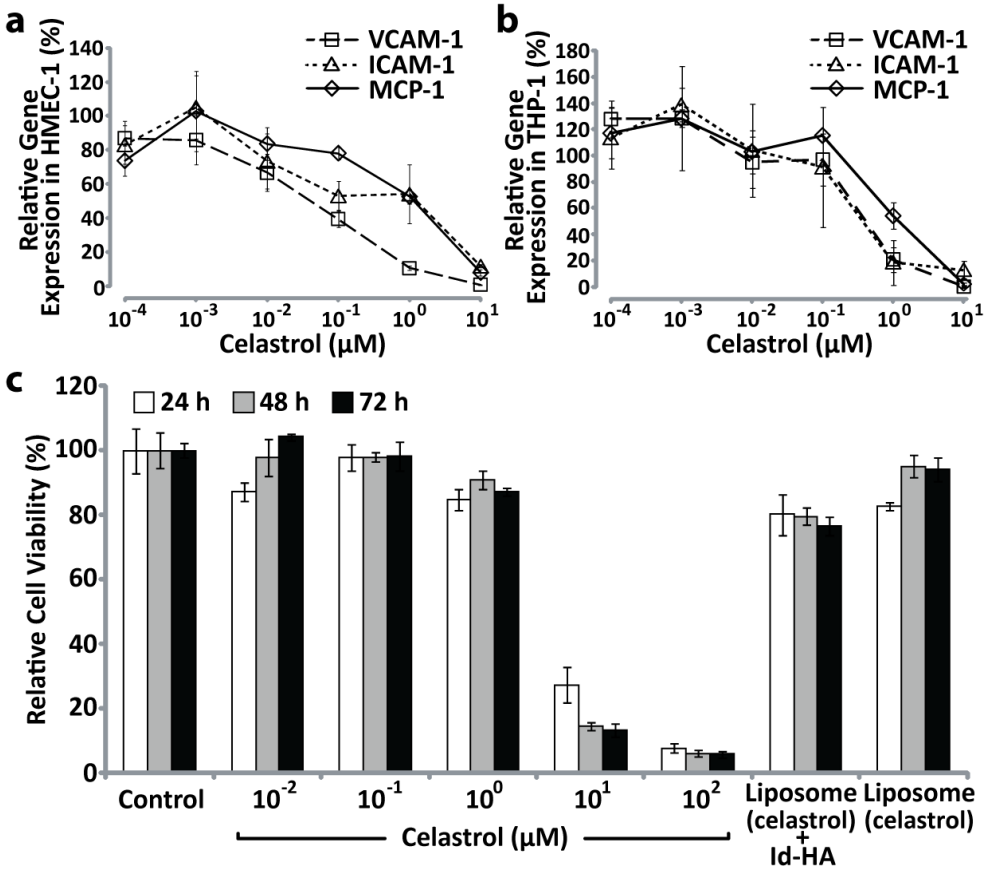

Figure 5.5. Optimal dosage of celastrol that is anti-inflammatory but not cytotoxic. (a&b) Dose-dependent anti-inflammatory effect of celastrol was evaluated by qPCR analysis for LPS-induced pro-inflammatory gene expression. HMEC-1 (a) and THP-1 cells (b) were incubated with celastrol (100 pM - 10 μM for 30 min), challenged with LPS (1μg/ml, 3 h) 36 h after celastrol treatment, and examined for inhibition of gene expression of VCAM-1, ICAM-1, and MCP-1. Data are presented as the percentage of gene expression relative to LPS-treated, no celastrol control groups (n=4). (c) The effect of celastrol treatment on cell viability of LPS-treated HMEC-1 was evaluated at 72 h. Liposome containing ~1 μM celastrol assembled with or without Id-HA was also evaluated for cell viability (n=4).

Treatment with 1 μM celastrol, however, did not produce any significant cytotoxic effect (Fig. 5.5c). We also evaluated the cytotoxicity of liposome containing 1 μM celastrol. Liposome(celastrol) coupled with ~20% (w/w) Id-HA or without a targeting moiety did not produce significant cell death in HMEC-1 for (Fig. 5.5c).

Suppression of pro-inflammatory gene expression by targeted delivery of celastrol

A mass ratio of ~20% Id-HA to phospholipid and a dosage of celastrol at ~1 μM were chosen for the specificity towards inflamed cells and for the lack of cytotoxicity. With these conditions, we examined the inhibitory effect of targeted delivery of liposome(celastrol) on pro-inflammatory marker expression in HMEC-1 and THP-1 cells. To simulate the reinitiating loop of inflammatory signals in the milieu of endothelium/immune cells and to examine the efficacy of targeted delivery on inhibition of inflammation therein, both HMEC-1 and THP-1 cells were first treated with LPS for 24 h before liposome(celastrol) delivery (Fig. 5.6a). At 36-48 h after 30 min treatment of liposome(celastrol), cells were then challenged with LPS for another 3 h, followed by gene expression analysis (Fig. 5.6a). In both HMEC-1 and THP-1 cells, targeted delivery of liposome(celastrol) was as effective or superior to the same dosage of free celastrol (Fig. 5.6b). The inhibitory effect of liposome(celastrol) in HMEC-1 cells was dependent on specific molecular interaction with ICAM-1, evidenced by the lack of inhibition when coupled with Id-D137A (Fig. 5.6b). In THP-1 cells, a maximum inhibition of pro-inflammatory marker expression was seen with liposome(celastrol) coated with Id-HA, although some level of inhibition was also observed with non-targeted delivery with Id-D173A (Fig. 5.6b). This may be attributed to the non-specific uptake of liposomes by THP-1 cells that differentiate into macrophage-like phenotype upon inflammatory stimuli, exhibiting phagocytic activities independent of molecular interactions [41].

Figure 5.6. Suppression of pro-inflammatory gene expression by targeted delivery of celastrol.

(a) The timeline shows the sequence of the treatment with LPS, celastrol delivery, and gene analysis by qPCR. (b) Gene expression of ICAM-1, MCP-1, and IL-1α was examined to assess therapeutic efficacy of targeted delivery of celastrol. Liposome containing ~1 μM celastrol coupled with Id-HA or Id-D137A or free celastrol at 0.5 or 1 μM were delivered to HMEC-1 and THP-1 cells (one-way ANOVA followed by Tukey's post-hoc test, *$p < 0.05$, **$p < 0.01$, and ***$p < 0.001$, n=4).

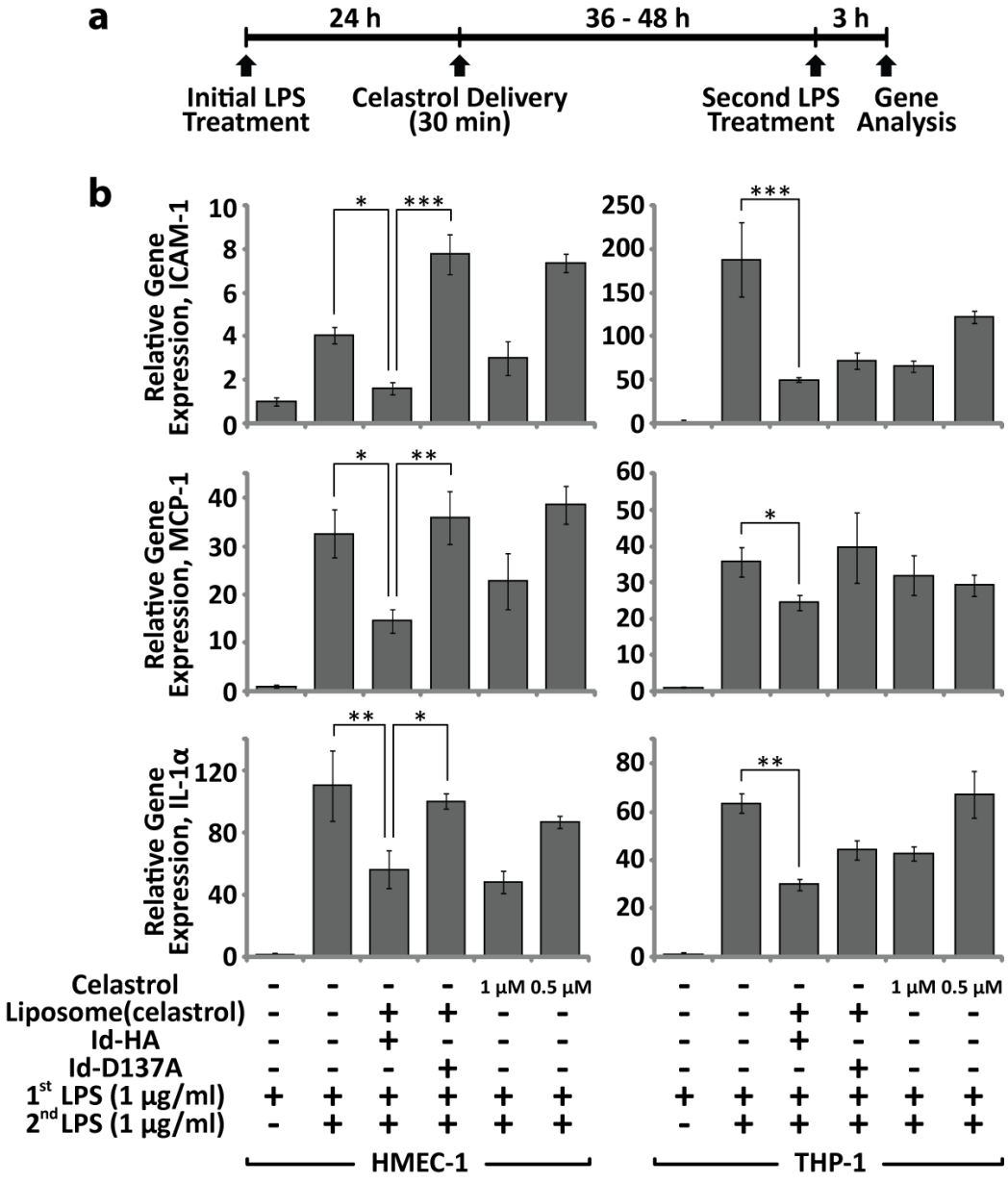
a
24 h
36 - 48 h
3 h
Initial LPS Treatment
Celastrol Delivery (30 min)
Second LPS Treatment
Gene Analysis
b
Relative Gene Expression, ICAM-1
Relative Gene Expression, MCP-1
Relative Gene Expression, IL-1α
Celastrol
Liposome(celastrol)
Id-HA
Id-D137A
1st LPS (1 μg/ml)
2nd LPS (1 μg/ml)
1 μM 0.5 μM
HMEC-1
THP-1

Potent inhibition of monocyte adhesion to the endothelium by targeted delivery of celastrol

Inhibition of the continuing accumulation of immune cells to inflamed vasculature will be an important measure that anti-inflammatory therapies should demonstrate. As a functional assay to measure the efficacy of targeted delivery of liposome(celastrol), we examined the attenuation of cell surface expression of ICAM-1 and the inhibition of THP-1 cell adhesion to HMEC-1. Similarly as before, HMEC-1 were treated with LPS for 24 h before liposome(celastrol) delivery, followed by a second LPS challenge 36-48 h after the delivery (Fig. 5.7a). The measurements of ICAM-1 expression and THP-1 adhesion were performed 24 h after the second LPS challenge to allow sufficient time for cells to respond at the protein level (Fig. 5.7a). The amount of ICAM-1 expression measured by mAb LB-2 was significantly lower with the targeted delivery of liposome(celastrol) coupled with Id-HA than free celastrol (Fig. 5.7b). Liposome(celastrol) coupled with Id-D137A produced little suppression of ICAM-1 expression compared with free celastrol, implying a minimum non-specific uptake of liposomes by HMEC-1 and a minimum escape of encapsulated celastrol from the liposomes (Fig. 5.7b). LPS-induced proliferation [42] of HMEC-1 was also significantly inhibited by targeted delivery of liposome(celastrol) evidenced by cell density (Fig. 5.7c). However, free celastrol of equal concentration did not exhibit the anti-proliferative effect of the drug and failed to inhibit endothelial proliferation followed by LPS injury (Fig. 5.7c). The levels of ICAM-1 suppression on HMEC-1 surface also led to a proportional decrease in the adhesion of THP-1 cells to HMEC-1, i.e., a maximum inhibition seen with Id-HA coated liposome(celastrol) followed by free celastrol, while no change was observed with Id-D137A coated liposomes (Fig. 5.7, d and e). Enhanced inhibition of ICAM-1 expression and THP-1

Figure 5.7. Potent inhibition of HMEC-1 proliferation and THP-1 adhesion by targeted delivery of celastrol.

(a) The timeline shows the sequence of the treatment with LPS, celastrol delivery, and the measurements of anti-inflammatory effect at the protein level and immune cell accumulation. (b) The amount of ICAM-1 expression in HMEC-1 after targeted delivery of liposome(celastrol) was assessed by staining with mAb LB-2 (*$p < 0.001$, n=4). (c) The effect of targeted delivery of liposome(celastrol) was also tested for its ability to inhibit LPS-induced proliferation of HMEC-1 or increase in cell density, estimated by the number of nuclei (identified with DAPI) per microscopic field ($1.5x10^5$ μm^2) (*$p < 0.001$, n=4). (d) Representative microscopic fluorescence images show BCECF-labeled THP-1 cell adhesion to LPS-treated HMEC-1 after delivery of celastrol (scale bar, 100 μm). (e) Fluorescence of whole lysates of adhered BCECF-labeled THP-1 cells was measured (*$p < 0.001$, n=6). (B,C,&E) One-way ANOVA followed by Tukey's post-hoc test was performed to obtain statistical significance.

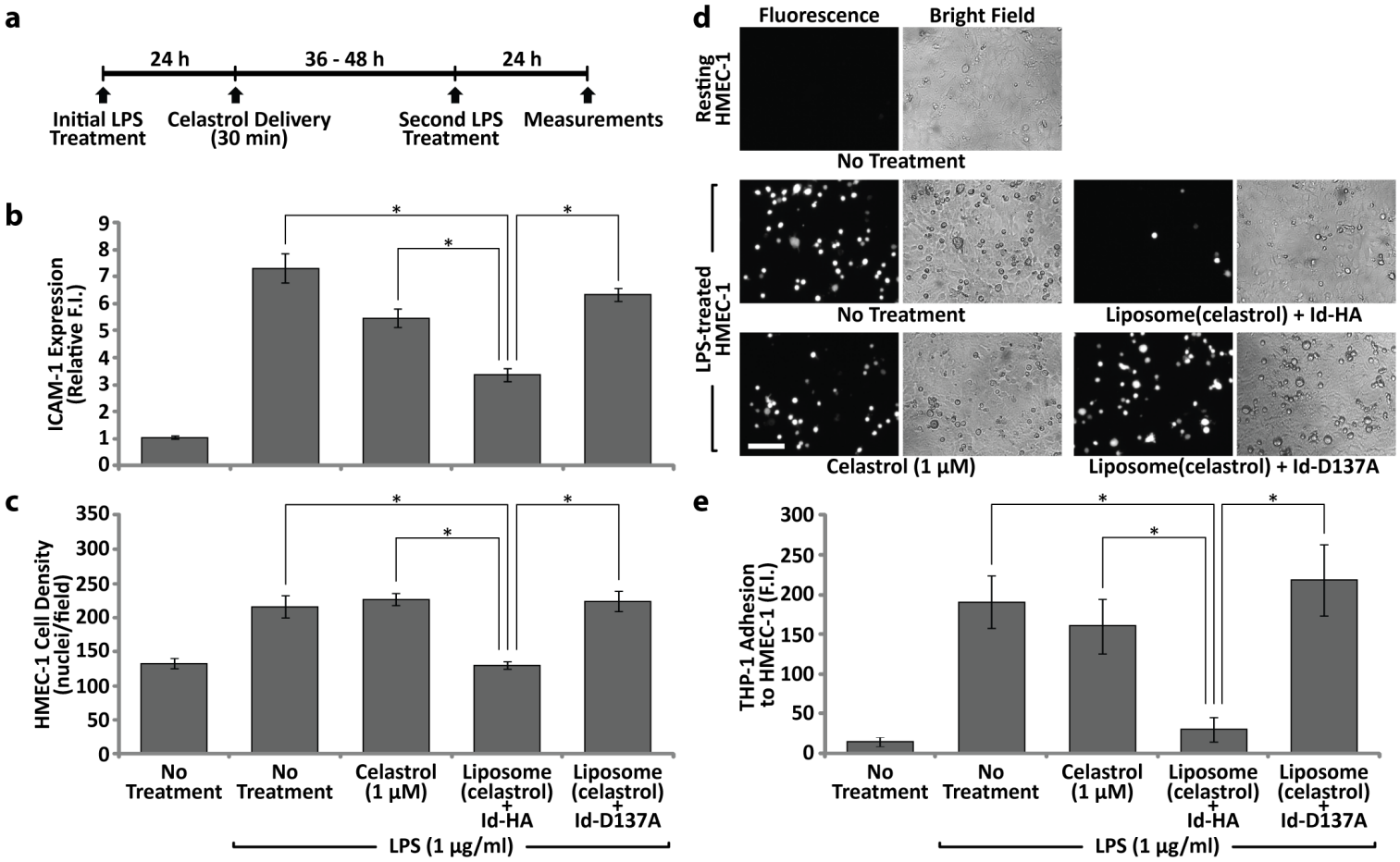
a
24 h
36 - 48 h
24 h
Initial LPS Treatment
Celastrol Delivery (30 min)
Second LPS Treatment
Measurements
b
ICAM-1 Expression (Relative F.I.)
c
HMEC-1 Cell Density (nuclei/field)
No Treatment
No Treatment
Celastrol (1 μM)
Liposome (celastrol) + Id-HA
Liposome (celastrol) + Id-D137A
LPS (1 μg/ml)
d
Fluorescence
Bright Field
Resting HMEC-1
No Treatment
LPS-treated HMEC-1
No Treatment
Liposome(celastrol) + Id-HA
Celastrol (1 μM)
Liposome(celastrol) + Id-D137A
e
THP-1 Adhesion to HMEC-1 (F.I.)
No Treatment
No Treatment
Celastrol (1 μM)
Liposome (celastrol) + Id-HA
Liposome (celastrol) + Id-D137A
LPS (1 μg/ml)

cell adhesion by Id-HA coated liposome(celastrol) as compared with free celastrol may be due to more potent suppression of ICAM-1 gene expression (Fig. 5.6b) and reduction of ICAM-1 surface density (Fig. 5.7b) impelled by the binding and subsequent internalization of Id-HA coated liposome(celastrol).

Discussion

Comprehensive inflamed cell-specific targeted delivery may contribute to a more effective clinical use of potent anti-inflammatory drugs against a broad spectrum of immune and inflammatory diseases. The challenge of targeting overexpressed endogenous molecules for selective delivery is that these molecules may also be present in cells outside of the disease sites. In addition, diverse cellular players that together form reciprocal inflammatory signals pose another challenge to delivery strategies targeting only either immune or non-immune cells. Thus ensuring specificity as well as the spectrum of cellular components that drug carriers can influence should be considered as two important factors for an effective treatment for immune and inflammatory diseases. In this study, we investigated a strategy to address both issues of specificity and comprehensive targeting by the choice of ICAM-1, which is greatly upregulated broadly over both non-immune and immune cells under inflammation, and exploiting its physiological interaction with LFA-1 integrin for inflamed cell-specific delivery of anti-inflammatory agents. This design criteria led us to use liposomal nanoparticles coated at a tunable density with the LFA-1 I domain, of which a collection of engineered variants are available for differing affinity to ICAM-1 in the range of mM to nM K_D [28]. Our ICAM-1 targeting strategy, therefore, mimics to a great extent an intrinsic behavior of leukocytes that bind selectively to the

inflammatory sites by modulating affinity and avidity of integrins [43] for targeting inflammation.

Preferential and comprehensive delivery of celastrol, a potent anti-inflammatory, anti-oxidative, and anti-proliferative drug [32-34], was demonstrated against the cell lines of endothelium (HMEC-1) and monocytes/macrophages (THP-1), which displayed dramatic upregulation of ICAM-1 after LPS challenge. Unlike soluble monomeric molecule binding to ICAM-1, multivalent interactions will be required for effective binding of nanoparticles of ~100 nm in diameter to resist thermal diffusion and detachment force exerted by fluid-induced shear stress. This is to some extent analogous to the binding and the entry of human rhinoviruses (a non-enveloped viral particle with ~35 nm diameter capsid), which shows little binding to cells with basal levels of ICAM-1 expression, but becomes rapidly internalized into cells after upregulated expression of ICAM-1 by cytokines or other pro-inflammatory agents [44]. The requirement for multivalency interaction was supported by the observation that a higher coating density of the I domain on FITC-containing liposomes led to an increase in fluorescence intensity in HMEC-1. At the highest coating density of I domain, a low level of fluorescence began to show up even in resting HMEC-1 without LPS challenge. Previously, we have reported a correlation between the intrinsic affinity of the I domain (due to different mutations) to ICAM-1 and the efficiency of nanoparticle delivery into ICAM-1 overexpressing tumor cells [30]. In the current study, we used either the wild-type or active I domain containing F265S/F292G and varied the coating density of the I domains to ensure selective delivery against inflamed cells. The versatility of our ICAM-1 targeting strategy by virtue of affinity and avidity modulation is absent in most previous approaches based on monoclonal antibodies or short peptides with largely uncharacterized affinities to ICAM-1. Also, chemical conjugation methods were used to attach targeting moieties

to nanoparticles, which unavoidably resulted in aggregation and uncertainty in the number of functional molecules per particle. The ability to fine-tune the avidity by simple mixing of the I domains and liposomes at varying ratios as well as the affinity by the use of different I domain variants (e.g., F292A (K_D ~10 mM), F292G (K_D ~100 nM), and F265S/F292G (K_D ~6 nM)) will likely be more critical for *in vivo* studies, which would involve different disease types or severity of inflammation and ICAM-1 expression, and different rheology and hemodynamic forces in arteries versus peripheral blood vessels.

The inhibitory effect on pro-inflammatory gene expression by targeted delivery *in vitro* was in general more effective than free celastrol at equal dosage (1 μM). Non-specific uptake of free celastrol or many other small molecule compounds in this matter will probably be due to the hydrophobic nature of the compounds, which would aggregate in aqueous solution and be taken up by cells [45]. In contrast, the inhibitory effect of celastrol encapsulated in liposome was dependent on the specific molecular interactions of ICAM-1 with Id-HA, evidenced by the lack of inhibition with Id-D137A coated liposome. *In vivo* benefit and efficacy of selective delivery of anti-inflammatory drugs via liposomes will more likely be pronounced in a clinical perspective, considering many problems associated with parenteral administration of hydrophobic and poorly water-soluble drugs such as low absorption and bioavailability, and side-effects due to non-selective, systemic cytotoxicity. Furthermore, targeted delivery to ICAM-1 may not only directly compete with ICAM-1 specific cell adhesion molecules for immune cell adhesion to inflamed vascular endothelium but also reduce surface density of ICAM-1 by causing multivalent clustering and subsequent internalization of ICAM-1 [46]. Such potent inhibition of immune cell accumulation, inflamed cell-selective intracellular delivery of the drug, and alleviation of pro-inflammatory signals *in vivo* for the treatment of acute and

chronic inflammatory diseases would be difficult to achieve with free celastrol. Moreover, considering anti-proliferative and cytotoxic effects at higher dosage of celastrol, applications of ICAM-1 directed delivery may be extended to neovasculatures in tumors and proliferative immune cells in atherosclerotic lesions without significant adverse systemic side effects.

Cell surface molecules that are induced under inflammation and therefore have been used for targeted delivery of imaging agents and drugs include E- and P-selectins, ICAM-1, and VCAM-1. Although VCAM-1 has been more frequently chosen as a marker for inflamed vasculature, our studies clearly show several advantages of targeting ICAM-1 due to its higher degree of induction in both non-immune and immune cells, rendering an opportunity to deliver anti-inflammatory agents to the greater part of the cellular culprits in inflammatory diseases. Such properties of ICAM-1 greatly supports the use of the physiologic counter-receptors to ICAM-1 for inflamed cell-specific targeted drug delivery. Among the major integrin receptors against ICAM-1 such as LFA-1 and Mac-1, we found that active Mac-1 I domain exhibited binding to resting endothelium, indicating the presence of high affinity inflammation-independent ligands for Mac-1. Despite the fact that quiescent HMEC-1 constitutively expresses other physiologic ligands of LFA-1 such as ICAM-2 [47], inflammation-specific delivery of Id-HA coated liposomes is consistent with the observation that LFA-1 integrin has at least 10-fold higher affinity to ICAM-1 than to other ICAM members. Another cell adhesion molecule called junctional adhesion molecule (JAM)-1 redistributes from cell junctions to the accessible apical surface of endothelial cells under inflammation, which may also contribute to adhesion and transmigration of leukocytes through its putative interaction with LFA-1 [48]. Although little is known in regard to the affinity of LFA-1 to JAM-1 and if the I domain variants engineered for high affinity to ICAM-1 would also bind better to

JAM-1, the use of LFA-1 I domain may be extended to targeting JAM-1 to potentiate inflammation-specific delivery.

In summary, our study demonstrates the importance of specificity, affinity, and avidity of targeting moieties on nanoparticles as important design parameters for selective drug carriers. Specific delivery of nanoparticle carriers should therefore optimize molecular interactions from all these perspectives, rather than focusing only on monomeric affinity between two interacting, soluble molecules. The optimization of molecular interactions can be facilitated greatly with tunable physiologic interactions such as those in LFA-1 I domain and ICAM-1 in this study, resulting in preferential to specific binding of nanoparticles to inflamed HMEC-1 and THP-1 cells with little delivery into resting cells. Targeting ICAM-1 via its interaction with LFA-1 I domain would thus enable comprehensive treatments against a broad range of immune and inflammatory diseases.

REFERENCES

1. Nathan C, Ding A. Nonresolving inflammation. Cell. 2010;140(6):871-82.

2. Libby P. Inflammation in atherosclerosis. Nature. 2002;420(6917):868-74.

3. Hotamisligil GS. Inflammation and metabolic disorders. Nature. 2006;444(7121):860-7.

4. Glass CK, Saijo K, Winner B, Marchetto MC, Gage FH. Mechanisms underlying inflammation in neurodegeneration. Cell. 2010;140(6):918-34.

5. Coussens LM, Werb Z. Inflammation and cancer. Nature. 2002;420(6917):860-7.

6. FitzGerald GA, Patrono C. The coxibs, selective inhibitors of cyclooxygenase-2. N Engl J Med. 2001;345(6):433-42.

7. Jain MK, Ridker PM. Anti-inflammatory effects of statins: clinical evidence and basic mechanisms. Nat Rev Drug Discov. 2005;4(12):977-87.

8. Patrono C, Garcia Rodriguez LA, Landolfi R, Baigent C. Low-dose aspirin for the prevention of atherothrombosis. N Engl J Med. 2005;353(22):2373-83.

9. Rhen T, Cidlowski JA. Antiinflammatory action of glucocorticoids--new mechanisms for old drugs. N Engl J Med. 2005;353(16):1711-23.

10. Ridker PM, Cushman M, Stampfer MJ, Tracy RP, Hennekens CH. Inflammation, aspirin, and the risk of cardiovascular disease in apparently healthy men. New Engl J Med. 1997;336(14):973-9.

11. Schacke H, Docke WD, Asadullah K. Mechanisms involved in the side effects of glucocorticoids. Pharmacol Therapeut. 2002;96(1):23-43.

12. Fitzgerald GA. Coxibs and cardiovascular disease. N Engl J Med. 2004;351(17):1709-11.

13. Hanai J, Cao P, Tanksale P, Imamura S, Koshimizu E, Zhao J, et al. The muscle-specific ubiquitin ligase atrogin-1/MAFbx mediates statin-induced muscle toxicity. J Clin Invest. 2007;117(12):3940-51.

14. Allen TM, Cullis PR. Drug delivery systems: entering the mainstream. Science. 2004;303(5665):1818-22.

15. Muzykantov VR. Targeting of superoxide dismutase and catalase to vascular endothelium. J Control Release. 2001;71(1):1-21.

16. Muro S, Dziubla T, Qiu WN, Leferovich J, Cui X, Berk E, et al. Endothelial targeting of high-affinity multivalent polymer nanocarriers directed to intercellular adhesion molecule 1. J Pharmacol Exp Ther. 2006;317(3):1161-9.

17. Kelly KA, Allport JR, Tsourkas A, Shinde-Patil VR, Josephson L, Weissleder R. Detection of vascular adhesion molecule-1 expression using a novel multimodal nanoparticle. Circ Res. 2005;96(3):327-36.

18. Voinea M, Manduteanu I, Dragomir E, Capraru M, Simionescu M. Immunoliposomes directed toward VCAM-1 interact specifically with activated endothelial cells--a potential tool for specific drug delivery. Pharm Res. 2005;22(11):1906-17.

19. Kozower BD, Christofidou-Solomidou M, Sweitzer TD, Muro S, Buerk DG, Solomides CC, et al. Immunotargeting of catalase to the pulmonary endothelium alleviates oxidative stress and reduces acute lung transplantation injury. Nature Biotechnology. 2003;21(4):392-8.

20. Spragg DD, Alford DR, Greferath R, Larsen CE, Lee KD, Gurtner GC, et al. Immunotargeting of liposomes to activated vascular endothelial cells: A strategy for site-selective delivery in the cardiovascular system. P Natl Acad Sci USA. 1997;94(16):8795-800.

21. Ehrhardt C, Kneuer C, Bakowsky U. Selectins-an emerging target for drug delivery. Adv Drug Deliv Rev. 2004;56(4):527-49.

22. Arap W, Pasqualini R, Ruoslahti E. Cancer treatment by targeted drug delivery to tumor vasculature in a mouse model. Science. 1998;279(5349):377-80.

23. Sugahara KN, Teesalu T, Karmali PP, Kotamraju VR, Agemy L, Girard OM, et al. Tissue-Penetrating Delivery of Compounds and Nanoparticles into Tumors. Cancer Cell. 2009;16(6):510-20.

24. Dustin ML, Rothlein R, Bhan AK, Dinarello CA, Springer TA. Induction by Il-1 and Interferon-Gamma - Tissue Distribution, Biochemistry, and Function of a Natural Adherence Molecule (Icam-1). Journal of Immunology. 1986;137(1):245-54.

25. Marlin SD, Springer TA. Purified Intercellular-Adhesion Molecule-1 (Icam-1) Is a Ligand for Lymphocyte Function-Associated Antigen-1 (Lfa-1). Cell. 1987;51(5):813-9.

26. Dunehoo AL, Anderson M, Majumdar S, Kobayashi N, Berkland C, Siahaan TJ. Cell adhesion molecules for targeted drug delivery. J Pharm Sci. 2006;95(9):1856-72.

27. Simone E, Ding BS, Muzykantov V. Targeted delivery of therapeutics to endothelium. Cell Tissue Res. 2009;335(1):283-300.

28. Jin M, Song G, Carman CV, Kim YS, Astrof NS, Shimaoka M, et al. Directed evolution to probe protein allostery and integrin I domains of 200,000-fold higher affinity. Proc Natl Acad Sci U S A. 2006;103(15):5758-63.

29. Phan UT, T Waldron T, Springer TA. Remodeling of the lectin-EGF-like domain interface in P- and L-selectin increases adhesiveness and shear resistance under hydrodynamic force. Nat Immunol. 2006;7(8):883-9.

30. Park S, Kang S, Veach AJ, Vedvyas Y, Zarnegar R, Kim JY, et al. Self-assembled nanoplatform for targeted delivery of chemotherapy agents via affinity-regulated molecular interactions. Biomaterials. 2010;31(30):7766-75.

31. Almenarqueralt A, Duperray A, Miles LA, Felez J, Altieri DC. Apical Topography and Modulation of Icam-1 Expression on Activated Endothelium. Am J Pathol. 1995;147(5):1278-88.

32. Lee JH, Koo TH, Yoon H, Jung HS, Jin HZ, Lee K, et al. Inhibition of NF-kappa B activation through targeting I kappa B kinase by celastrol, a quinone methide triterpenoid. Biochem Pharmacol. 2006;72(10):1311-21.

33. Yang HJ, Chen D, Cui QZC, Yuan X, Dou QP. Celastrol, a triterpene extracted from the Chinese "Thunder of God Vine," is a potent proteasome inhibitor and suppresses human prostate cancer growth in nude mice. Cancer Res. 2006;66(9):4758-65.

34. Mu TW, Ong DST, Wang YJ, Balch WE, Yates JR, Segatori L, et al. Chemical and biological approaches synergize to ameliorate protein-folding diseases. Cell. 2008;134(5):769-81.

35. Hu X, Kang S, Lefort C, Kim M, Jin MM. Combinatorial libraries against libraries for selecting neoepitope activation-specific antibodies. Proc Natl Acad Sci U S A. 2010;107(14):6252-7.

36. Szoka F, Olson F, Heath T, Vail W, Mayhew E, Papahadjopoulos D. Preparation of unilamellar liposomes of intermediate size (0.1-0.2 mumol) by a combination of reverse phase evaporation and extrusion through polycarbonate membranes. Biochim Biophys Acta. 1980;601(3):559-71.

37. Chow JC, Young DW, Golenbock DT, Christ WJ, Gusovsky F. Toll-like receptor-4 mediates lipopolysaccharide-induced signal transduction. J Biol Chem. 1999;274(16):10689-92.

38. Diamond MS, Staunton DE, Marlin SD, Springer TA. Binding of the Integrin Mac-1 (Cd11b/Cd18) to the 3rd Immunoglobulin-Like Domain of Icam-1 (Cd54) and Its Regulation by Glycosylation. Cell. 1991;65(6):961-71.

39. Xie J, Li R, Kotovuori P, Vermot-Desroches C, Wijdenes J, Arnaout MA, et al. Intercellular adhesion molecule-2 (CD102) binds to the leukocyte integrin CD11b/CD18 through the A domain. J Immunol. 1995;155(7):3619-28.

40. Lupher ML, Harris EAS, Beals CR, Sui LM, Liddington RC, Staunton DE. Cellular activation of leukocyte function-associated antigen-1 and its affinity are regulated at the I domain allosteric site. Journal of Immunology. 2001;167(3):1431-9.

41. Takashiba S, Van Dyke TE, Amar S, Murayama Y, Soskolne AW, Shapira L. Differentiation of monocytes to macrophages primes cells for lipopolysaccharide stimulation via accumulation of cytoplasmic nuclear factor kappa B. Infect Immun. 1999;67(11):5573-8.

42. Penn MS, Chisolm GM. Relation between Lipopolysaccharide-Induced Endothelial-Cell Injury and Entry of Macromolecules into the Rat Aorta Invivo. Circ Res. 1991;68(5):1259-69.

43. Stewart M, Hogg N. Regulation of leukocyte integrin function: Affinity vs avidity. J Cell Biochem. 1996;61(4):554-61.

44. Subauste MC, Jacoby DB, Richards SM, Proud D. Infection of a Human Respiratory Epithelial-Cell Line with Rhinovirus - Induction of Cytokine Release and Modulation of Susceptibility to Infection by Cytokine Exposure. Journal of Clinical Investigation. 1995;96(1):549-57.

45. Johnson JLH, He Y, Yalkowsky SH. Prediction of precipitation-induced phlebitis: A statistical validation of an in vitro model. J Pharm Sci. 2003;92(8):1574-81.

46. Muro S, Wiewrodt R, Thomas A, Koniaris L, Albelda SM, Muzykantov VR, et al. A novel endocytic pathway induced by clustering endothelial ICAM-1 or PECAM-1. J Cell Sci. 2003;116(8):1599-609.

47. Staunton DE, Dustin ML, Springer TA. Functional cloning of ICAM-2, a cell adhesion ligand for LFA-1 homologous to ICAM-1. Nature. 1989;339(6219):61-4.

48. Weber C, Fraemohs L, Dejana E. The role of junctional adhesion molecules in vascular inflammation. Nature Reviews Immunology. 2007;7(6):467-77.

CHAPTER 6

VIRUS-LIKE PARTICLES FOR SYSTEMIC AND INFLAMMATION-SPECIFIC TARGETED DELIVERY OF LARGE GENETIC CONTENTS

Summary

Systemic and target-specific delivery of large genetic materials has been difficult to achieve. While viruses effortlessly deliver kilobase-long genome into cells, a clinical use of viral vectors has been hindered due to the mismatch between the native tropism and the therapeutic need or the difficulties in engineering for a new epitope, and serious safety concerns. Nonviral vectors, in contrast, are limited by low gene transfer efficiency in parenteral applications and inherent cytotoxicity. Here we devised a polyanionic peptide (PAP) for expression as a fusion to targeting moieties and attachment to cationic nonviral vectors by electrostatic self-assembly. We fused PAP to the binding domain of integrin $\alpha_L\beta_2$ to target its ligand, ICAM-1, and formed plasmid bearing particles using cationic polymer polyethyleneimine (PEI). Assembled nanoparticles delivered genes like viruses, as it packaged large genetic contents, bound specifically to target molecules, elicited receptor-mediated endocytosis, and escaped endosomal pathway. Molecular interaction-mediated delivery was resistant to the presence of serum and resulted in higher gene transfer efficiency without the associated toxicity of PEI. Furthermore, by targeting ICAM-1, virus-like particles were inflammation-specific, delivering genes only to LPS treated inflamed cells both *in vitro* and *in vivo*. Simplicity and versatility of the platform may open up opportunities for multifaceted products with improved efficiency and safety that can be translated into the clinic.

Introduction

Viruses have evolved ways to efficiently deliver their genetic materials into cells, which are as large as multiples of kilobase-long nucleic acids. The use of viral gene delivery vectors for clinical applications [1-6], however, poses serious safety issues, including pathogenicity by insertional mutagenesis [7] and anaphylactic response to the virus [8-9]. On the other hand, nonviral synthetic cationic vectors suffer from inherent cytotoxicity [10-11] and are severely limited due to a low gene transfer efficiency in systemic parenteral applications, as negatively charged glycosaminoglycans in circulation [12] can neutralize the positive charge of cationic vectors, necessary for binding to cell surfaces [13-14].

To achieve cell type- or cell-state specific targeted systemic delivery, it often requires the use of complex molecules such as antibodies and proteins that specifically bind to target molecules. However, systemic site-directed targeted delivery of large nucleic acid molecules has had limited success, and in fact, studies have been mostly constrained to the delivery of small nucleic acids such as siRNA [15-18]. While viruses have the ability to effortlessly evade through the barriers of gene delivery, i.e., cell entry through the membrane and escape from lysosomal nuclease degradation, engineering the viral tropism for site-directed delivery to a range of different targets [19-21] is a difficult process that often leads to loss of viral function. Nonviral vectors are capable of delivering large content of nucleic acids such as plasmids, but modifications for targeting moieties have been mostly confined within chemical attachments of small molecules [22], peptides [23], and several types of proteins [24-25], which would inevitably affect original physicochemical properties of the vectors.

In this study, we devised a polyanionic peptide (PAP) comprised of 18 randomly ordered glutamic and aspartic acids that can be expressed as a fusion to

proteins to mediate electrostatic attachment to cationic transfection agents. Polyethyleneimine (PEI) was used as a scaffold to hold both a large amount of nucleic acid and targeting moieties. PEI has been extensively studied as a cationic polymer-mediated gene delivery agent, and has been considered to have relatively high gene transfer efficiency [26]. PEI has all primary, secondary, and tertiary amines that are not fully protonated under physiological pH [27]. However, it becomes fully protonated at low pH, such as in late endosomes, attracting protons and raising osmotic pressure that eventually bursts the vesicles and releases nucleic acid payload, which process has been termed as the proton sponge effect [28].

Intercellular adhesion molecule (ICAM)-1 is a cell surface molecule that mediates leukocyte attachment to various types of cells under inflammation [29-30] and often colocalizes at various disease sites [31-32]. ICAM-1 is also subverted as a receptor for the major human rhinoviruses (HRV) [33], by which multimeric clustering of ICAM-1 via the virus particle can promote rapid endocytosis [34-35]. We have previously engineered the major ligand binding domain (I domain) of the physiologic receptor for ICAM-1, integrin $\alpha_L\beta_2$, into a high affinity mutant [36]. The I domain is a globular Rossmann fold protein of approximately the size of a single-chain variable-fragment antibody. We previously used the high affinity I domain to deliver drugs [37-38] and imaging contrast agents [39] specifically to inflamed endothelial cells and immune cells, and to cancer cells and their stroma.

Here we show that by fusing PAP to the I domain (PAP-Id) we were able to convert PEI into a molecular interaction-dependent gene delivery platform based on their stepwise electrostatic self-assembly, which creates nanoparticles that mimic the processes involved in viral infection. Similarly as to how cell entry is gained by HRV, our virus-like particles were also able to mediate endocytosis by multivalent clustering of ICAM-1 via the I domain. Because the attachment of targeting moieties is a self-

assembling process, we were able to precisely control the moiety density or avidity, optimal for efficient endocytosis and gene transfer. Not only did the association of plasmid/PEI particles with PAP-Id decreased the inherent cytotoxicity of PEI, it also enabled the delivery to be resistant to the presence of serum. Similarly as acid catalyzed conformational change in HRV capsid leads to penetration of the membrane, endosomal escape of virus-like particles is elicited by the proton sponge effect. Moreover, by targeting ICAM-1, we were able to deliver genes specifically to inflamed endothelial cells and immune cells both *in vitro* and systemically *in vivo*.

Experimental Procedures

Cell culture conditions

HeLa, bEnd.3, RAW 264.7 (ATCC), and primary mouse lung cells were cultured in Advanced DMEM medium (Invitrogen) containing 2 mM L-glutamine, Pen-step (100 units/ml penicillin and 100 μg/ml streptomycin), and 10% FBS (endotoxin free, PAA Laboratories). Primary mouse lung cells were harvested from fetus lungs of mouse strain Gt(ROSA)26Sor$^{tm4(ACTB\text{-}tdTomato,\text{-}EGFP)Luo}$ (Jackson Laboratory). Lungs were aseptically minced and digested in 1 mg/ml collagenase A (Roche) for 3 h at 37 °C, which were then filtered through 70 μm nylon mesh cell strainer and washed twice in complete media for culture. HMEC-1 (Center for Disease Control) was propagated in MCDB 131 medium (Invitrogen) supplemented with 10% FBS, 10 mM L-glutamine, Pen-strep, 1 μg/ml hydrocortisone (MP Biomedicals), and 10 ng/ml human epidermal growth factor (Invitrogen). THP-1 cells (ATCC) were cultured in RPMI 1640 medium (Invitrogen) with 10% FBS and Pen-strep. Endothelial cells and primary mouse lung cells were trypsinized when confluent, and

washed to remove residual trypsin before plating. All mammalian cells were maintained at 37 °C in a 5% CO_2 humidified incubator.

Protein construction, design, and purification

Wild-type LFA-1 I domain sequence (Asn-129 to Tyr-307) followed by a stop codon was subcloned into pET28a vector (Novagen) between BamH1 and Xho1. QuickChange (Stratagene) site-directed mutagenesis was used to create F265S/F292G and D137A mutants. For GFP-Id, a superfolder GFP [40] was inserted between Nhe1 and BamH1. To construct PAP-Id, complementary primers encoding 5'-ctagcgaggatgaagatgaggaagacgaagaagatgaagaggacgaagaggacgaggatg-3' and 5'-gatccatcctcgtcctcttcgtcctcttcatcttcttcgtcttcctcatcttcatcctcg-3' were annealed and directly ligated between Nhe1 and BamH1. Constructs were transformed into *E. coli* BL21 (DE3) cells (Novagen) for production of the fusion proteins (Fig. 6.4). Overnight starter culture was used to inoculate a larger Luria Bertani medium at 1:40 volume ratio and was grown at 37 °C to OD600 of 0.4-0.5 (~2 h). Then cells were induced with freshly prepared 1 mM isopropyl-*β*-D-thiogalactopyranoside at 25 °C overnight (~15 h). Cells were recovered by centrifugation, and sonicated in buffer A (50 mM NaH_2PO_4, 300 mM NaCl, 10 mM imidazole, protease inhibitor cocktail (ProteCEASE-EDTA free, G-Biosciences)) with pH adjusted to 8.0 for GFP-Id and 6.0 for PAP-Id. Soluble fraction of GFP-Id was purified by passage over a Ni-NTA column (Pierce). Insoluble fraction of PAP-Id was washed in buffer A with 4 cycles of sonication and super-centrifugation at 20,000g for 30 min. Protein pellet was then solubilized in buffer B (buffer A plus 6 M guanidine HCl, pH 8.0) and purified by Ni-NTA. GFP-Id was eluted in buffer C (50 mM NaH_2PO_4, 300 mM NaCl, 250 mM imidazole, pH 8.0) and PAP-Id in buffer D (buffer C plus 6 M guanidine HCl, pH 8.0).

Eluted proteins were then subjected to gel filtration chromatography using Superdex S200 column in PBS connected to AKTA Purifier (GE Healthcare).

Electrostatic self-assembly of virus-like particles and the bearing plasmids

For any given mass ratios, plasmid and PEI (branched, M_W 25,000, Sigma-Aldrich) were each diluted in 1 volume of PBS (pH 7.4), and PAP-Id in 2 volumes of PBS. Solutions containing plasmid and PEI were first vortex mixed and incubated at room temperature for 40 min. Plasmid/PEI mixture was then gently mixed with PAP-Id solution and incubated at room temperature for 40 min. Vector for GFP expression (pGFP) was constructed by subcloning a complete Kozak consensus sequence and enhanced GFP sequence followed by a stop codon between EcoRI and BglII of pAAV-MCS vector (AAV Helper-Free System, Agilent Technologies). Vectors for expression of diphtheria toxin A (pDTA) and Cre recombinase (pCRE) were obtained from Addgene, originally named as PGK-DTA-bpA [41] (plasmid 13440) and pLOX-CW-CRE [42] (plasmid 12238), respectively. All components used for assembly of virus-like particles, including plasmids, PAP-Id, PEI, and PBS, were filter sterilized through 0.2 μm centrifugal or syringe filters before assembly.

In vitro delivery of virus-like particles

Cells were grown in 24-well plates to confluence and pretreated with complete media containing 1 μg/ml of LPS (*Escherichia coli,* 026:B6, Sigma) to induce inflammation. Each well received virus-like particles prepared with 0.4 μg of plasmid and the relative mass and volumes of PEI and PAP-Id. Final virus-like particles were then mixed with an equal volume of FBS and incubated at room temperature for 40 min before delivery to cells. After delivery, cells were washed twice with media, followed by addition of fresh complete media.

In vivo delivery of virus-like particles

Eight to ten-week-old female BALB/c mice (Jackson Laboratory) were used. All administrations performed in this study were parenteral and given intravenously, using 29G × 0.5" insulin syringes via lateral tail vein route injections. To induce systemic inflammation, 20 μg/mouse of LPS (*Escherichia coli,* 026:B6, Sigma) in PBS (pH 7.4) was injected. Virus-like particles bearing 10 μg/mouse of plasmid was formed in a mass ratio of the components (plasmid:PEI:PAP-Id) fixed to 1:6:16 in a final volume of 200 μl. Virus-like particles were supplemented with 1 mM $MgCl_2$ before injection. All animal procedures were approved by the Cornell University IACUC and were conducted in accordance with recommendations in the Guide for the Care and Use of Laboratory Animals published by the National Institutes of Health.

Immunofluorescence for imaging and flow cytometric analysis

Mean fluorescence intensity and percentage of GFP-positive cells were quantified by flow cytometry (Beckman Coulter EPICS XL-MC). After *in vitro* delivery of virus-like particles for GFP expression, cells were trypsinized, washed with washing buffer (PBS, 0.5% BSA, pH 7.4), and subjected to flow cytometer. Total fluorescence was quantified by lysing cells with 1% (v/v) Triton X-100 in PBS and measuring with a fluorescence plate reader. Confocal microscopy (Zeiss LSM 710) was used to assess endocytosis of virus-like particles and protein expression in HeLa cells. PAP-Id was conjugated to Alexa Fluor 555 (succinimidyl ester, Invitrogen) and pGFP was labeled with Cy5 (Label IT Nucleic Acid Labeling Kit, Mirus Bio). HeLa cells were grown in 35 mm glass bottom dishes (0.16-0.19 mm cover glass, In Vitro Scientific) and fixed in 3.7% formaldehyde for 1 h at different time points after delivery of fluorophore-labeled virus-like particles. Expression of ICAM-1 in mouse

lungs were assessed by GFP-Id-HA. Lungs were collected at different time points after systemic LPS treatment (20 μg/mouse, *Escherichia coli,* 026:B6, Sigma) and were minced and digested in 1 mg/ml collagenase A (Roche) for 3 h at 37 °C. Singlet lung cells were prepared by passage through 70 μm nylon mesh cell strainer and incubation with red blood cell lysis buffer (eBiosciences) for 5 min on ice. Cells were then washed and labeled for ICAM-1 with 10 μg/ml GFP-Id-HA in ice-cold labeling buffer (PBS, 0.5% BSA, 10 mM $MgCl_2$, pH 7.4) for 1 h. Cells were then labeled with either rat IgG anti-mouse CD31 (1:20, BD Pharmingen) or rat IgG anti-mouse F4/80 (1:50, Abcam) for 1 h, followed by goat anti-rat IgG-PE (Santa Cruz) as secondary antibody for 1 h. For detection of GFP expression after delivery of virus-like particles bearing pGFP, singlet lung cells were fixed with 3.7% formaldehyde for 1 h and permeabilized with 1% (v/v) Triton X-100 for 30 min. Permeabilized cells were then labeled with rabbit IgG anti-GFP antibody (1:20, Invitrogen) for 1h, followed by goat anti-rabbit IgG-PE (1:100, Santa Cruz) for 1 h. Cells were then labeled for CD31 and F4/80 similarly as described, followed by goat anti-rat IgG-FITC (1:100, Santa Cruz) for 1h.

Immunohistology of lung tissue sections

Dissected lung tissues were embedded and frozen in OCT compound. Cryostat sections (10 μm) were fixed in 3.7% formaldehyde for 1 h and permeabilized in 1% (v/v) Triton X-100 for 1 h at room temperature. Sections were washed with 0.1% (v/v) Tween-20 PBS (PBST) and blocked with 1% BSA in PBST for 1 h at room temperature. For GFP immunostaining, sections were incubated with rabbit IgG anti-GFP antibody (1:20, Invitrogen) in PBST for 2 h at room temperature. After washing with PBST, sections were incubated with Rhodamine Red-X goat anti-rabbit IgG (1:50, Invitrogen) in PBST for 1 h at room temperature. Sections were then washed and labeled similarly for either rat IgG anti-mouse CD31 (1:20, BD Pharmingen) or

rat IgG anti-mouse F4/80 (1:50, Abcam) followed by goat anti-rat IgG-FITC (1:50, Santa Cruz) as secondary antibody. Slides were finally washed with PBST and mounted with Vectashield mounting medium (Vector Laboratories) for fluorescence imaging. Images were obtained by a confocal microscope (Zeiss LSM 710).

Real-time quantitative PCR

Total RNA from harvested lungs were extracted using TRI Reagent (Ambion). Briefly, one mouse lung (~150 mg) was homogenized in 1 ml of TRI Reagent solution followed by brief sonication. Homogenized lysates were mixed with 200 µl chloroform and centrifuged at 12,000g for 15 min. 400 µl of colorless upper aqueous phase was collected and mixed with 500 µl isopropanol and loaded to spin columns (Zymo-Spin II, Zymo Research). 1 µg of eluted RNA was converted to cDNA using a reverse transcription kit (High Capacity cDNA RT kits, Applied Biosystems) in a thermal cycler (GeneAmp PCR System 2700, Applied Biosystems). Real-time gene amplification analysis (MyiQ iCycler, Bio-Rad) was performed using a qPCR kit (Sybr Green 2× Master Mix, Bio-Rad) for mRNA expression of GFP relative to CYC1 housekeeping gene expression. Primer sequences for GFP was used as previously reported [43] and CYC1 (NM_025567) was obtained from the Mouse qPrimerDepot of the National Cancer Institute.

Quantification of cell viability

Cell viability of HeLa cells treated with virus-like particles bearing pDTA was analyzed by trypan blue exclusion test. Cells were incubated with 0.2% trypan blue for 5 min and microscopic images were taken at random places of culture wells. Viable cells that excluded trypan blue and nonviable cells with blue cytoplasm were counted per given image field for analysis. Rest of viability studies was quantified by MTT (3-

(4,5-Dimethylthiazol-2-yl)-2,5-diphenyltetrazolium bromide) assay. Cells were incubated with basal media containing 0.5 mg/ml MTT for 4 h at 37 °C. Blue formazan products were solubilized in DMSO and quantified by absorbance at 570 nm.

Statistical Analysis

Data were expressed as mean ± standard deviation (S.D.) of at least quadruplicate samples. Statistical analysis of data was carried out using GraphPad Prism 5. Unpaired student's *t*-test was used to determine statistical significance in comparison to matching controls. One-way ANOVA was used to compare mean responses among different groups, followed by Tukey's post-hoc test to determine statistical significance.

Results

Molecular interaction-specific targeted gene delivery of virus-like particles

Virus-like particles were designed to mimic the components of non-enveloped viruses such as HRV and its entry into specific range of host cells (Fig. 6.1a). Virus-like particles were assembled in a sequential manner: first PEI and DNA plasmids were mixed together, to which proteins were added. The ratio of protein, DNA, and PEI was adjusted to have positive charges in PEI are not completely neutralized such that proteins are attached to DNA/PEI particles through strong electrostatic attraction between PAP and PEI (Fig. 6.1b). When added to cells with ICAM-1 expression, the particles attach to cells through I domain binding and subsequent clustering of ICAM-1, which would be then rapidly internalized into cells.

Figure 6.1. Cell entry, endosomal escape, and gene expression of virus-like particles. (a) HRV gains cell entry by binding and clustering ICAM-1, which is upregulated on inflamed cell surfaces. Acid-catalyzed conformational change in the viral capsid (violet) forms a pore in the membrane of late endosomes and releases the RNA genome that leads to the production of more viruses (green). (b) Self-assembly of virus-like particles is mediated by stepwise electrostatic interactions among negatively charged nucleic acids, positively charged PEI, and polyanionic peptide fused I domain (PAP-Id). Virus-like particles similarly gain cell entry by multivalent ICAM-1 clustering-mediated endocytosis. A decrease in pH in late endosome fully protonates PEI, which creates osmotic pressure and eventually bursts the vesicle. Plasmid payloads that have escaped endosomal nuclease degradation lead to the expression of encoding genes. (c) Confocal images were taken to track PAP-Id-HA conjugated to Alexa Fluor 555 (red), pGFP labeled with Cy5 (blue), and GFP expression in HeLa cells. Virus-like particles were self-assembled at its optimal mass ratio of pGFP:PEI:PAP-Id-HA adjusted to 1:6:16. Cells were fixed at time points of 3, 24, and 48 h after delivery of virus-like particles and were imaged by confocal microscopy. Colocalization of red and blue appears in magenta in merged image. Focal plane was set to go through the cells to capture virus-like particles inside cells. Dotted lines mark the cell boundaries. Scale bar, 20 μm. (d) Z-stack confocal images were also taken to show the presence of virus-like particles inside cells. Dotted lines indicate the top surface of cells. Scale bar, 10 μm.

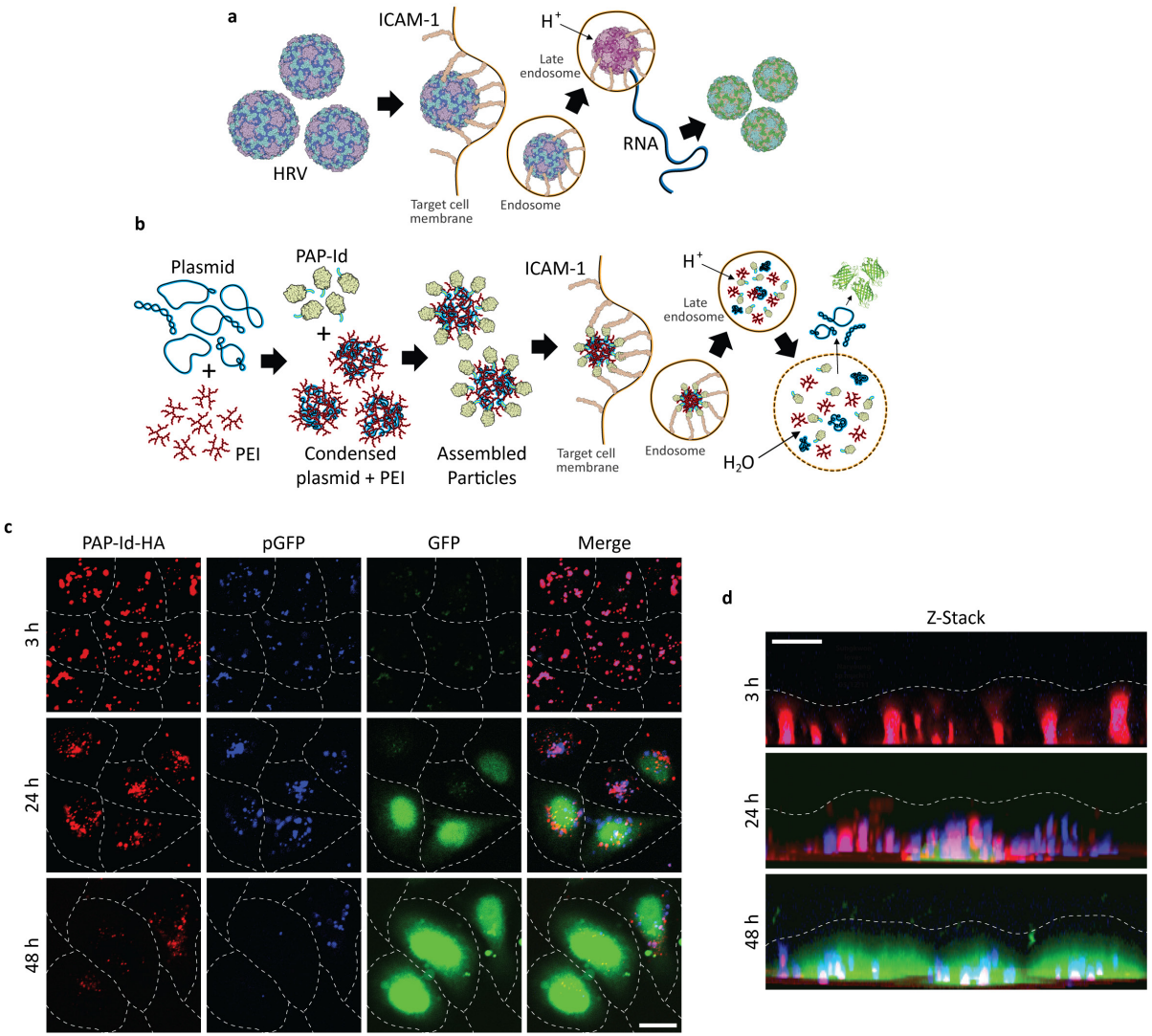
a
ICAM-1
H+
Late endosome
HRV
RNA
Target cell membrane
Endosome
b
Plasmid
PAP-Id
ICAM-1
H+
Late endosome
PEI
Condensed plasmid + PEI
Assembled Particles
Target cell membrane
Endosome
H2O
c
PAP-Id-HA
pGFP
GFP
Merge
3 h
24 h
48 h
d
Z-Stack
3 h
24 h
48 h

To visualize virus-like particles throughout the process of cell entry, endosomal escape, and gene expression, we fluorescently labeled pGFP and PAP-Id-HA to track the particles in HeLa cells by confocal microscopy. Virus-like particles were constructed using Cy5 labeled pGFP and Alexa Fluor 555 conjugated PAP-Id-HA at a mass ratio determined to be within an optimal range for delivery (1:6:16 for pGFP:PEI:PAP-Id-HA; see Fig. 6.3). We then delivered the fluorescently labeled virus-like particles to HeLa cells in the presence of serum, and fixed the cells at 3, 24, and 48 h after delivery. At 3 h post delivery, virus-like particles were found mostly inside cells confirmed by confocal microscopic and Z-stack images with (Fig. 6.1, c and d). PAP-Id-HA (red) and pGFP (blue) appeared to be in complex with each other, evidenced by colocalization of red and blue colors in the merged image. At 24 h post delivery, some cells began to express GFP, which coincided with the observation that the components of virus-like particles appeared to dissociate from each other. At 48 h, most cells expressed GFP, while much of the components of virus-like particles were no longer detectable.

In virus-like particles assembled without PEI, PAP-Id-HA would not associate with pGFP, and remained on cell surface (Fig. 6.2, a and b) while pGFP would be outside of cells. This is consistent with the requirement for the clustering of ICAM-1 necessary for ICAM-1 mediated endocytosis, which was not triggered by monomeric interaction between I domain and ICAM-1. In the absence of pGFP, in contrast, PAP-Id-HA/PEI particles entered the cells (Fig. 6.2b). In addition, pGFP/PEI particles assembled without PAP-Id-HA showed much less amount of plasmids inside cells (Fig. 6.2b).

Determining optimal ratios of protein, DNA, and PEI for efficient gene delivery

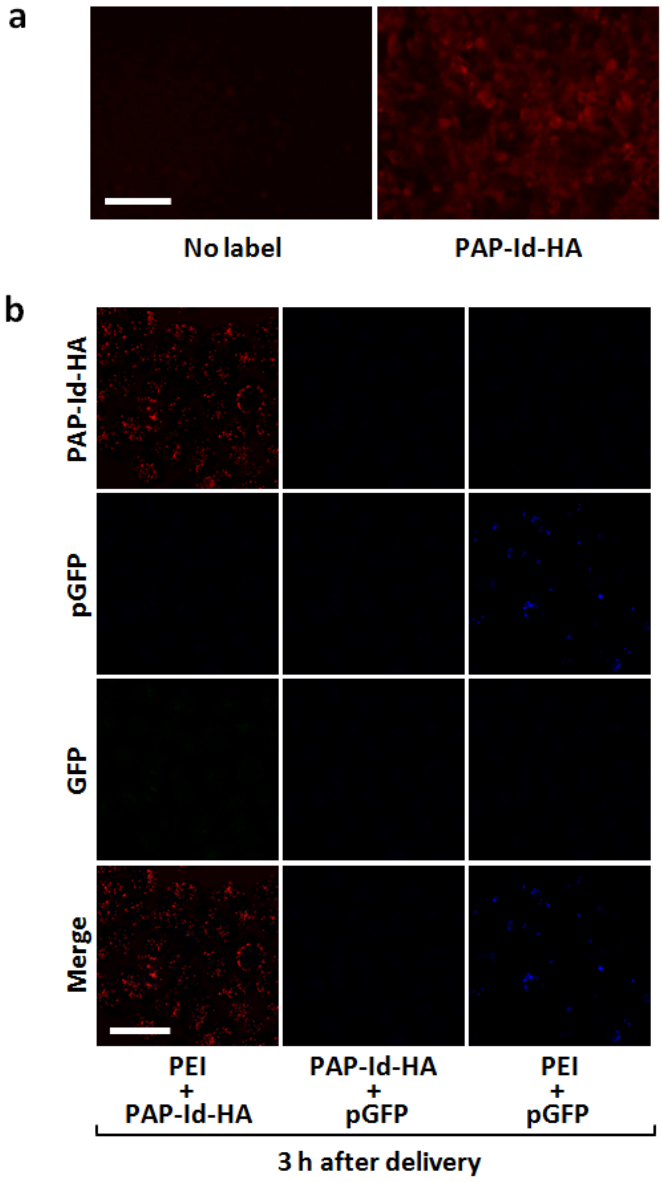

Figure 6.2. Controls for confocal imaging of virus-like particles.

(a) Fluorescence microscope image of HeLa cells labeled with PAP-Id-HA conjugated to Alexa Fluor 555. Scale bar, 100 μm. (b) Confocal images of HeLa cells were taken at 3 h post delivery for the uptake of virus-particles (formed with PEI and PAP-Id-HA, or PAP-Id-HA and pGFP, or PEI and pGFP) in the presence of serum. PAP-Id-HA was conjugated to Alexa Fluor 555 and is shown in red. pGFP was labeled with Cy5 and is shown in blue. Scale bar, 50 μm.

In an effort to assemble virus-like particles for the highest gene transfer efficiency with minimum cytotoxicity, we varied the mass ratios of individual components and examined the efficiency of gene expression and cytotoxicity associated with particles (Fig. 6.3). Two versions of PAP-Ids were used, one with the I domain engineered for high affinity (HA) with double mutations F265S/F292G [36] (denoted as PAP-Id-HA) and the other with a loss-of-function mutation D137A [44] (PAP-Id-D137A) (Fig. 6.4, a and c). With the fixed amount of the plasmid encoding enhanced GFP under cytomegalovirus (CMV) promoter (denoted as pGFP). we varied the amount of PEI ranging from 3 to 8 mass ratios of PEI to plasmids. To the mixture of pGFP/PEI particles, PAP-Id-HA or PAP-Id-D137A were added at mass ratios varying from 2 to 32 of proteins to plasmids (Fig. 6.3a). As additional controls and for comparison to conventional transfection methods, pGFP/PEI particles were used without proteins. Assembled virus-like particles were delivered to HeLa cells, which constitutively express a high level of ICAM-1. Gene transfer efficiency was assessed by several different readouts, i.e., total fluorescence measured from cell lysates, and mean fluorescence intensity and the percentage of GFP-positive cells measured by flow cytometry. Virus-like particles formulated with the mass ratios of 4-8 fold higher excess of PAP-Id-HA and PEI over pGFP led to overall highest measures of total fluorescence and highest percentage of GFP positive cells (Fig. 6.3a). While the total fluorescence reached as high as 20 fold with PAP-Id-HA over the controls that omitted PEI and over 80% GFP-positive cells, notably virus-like particles assembled with PAP-Id-D137A did not show any sign of GFP expression. Particles assembled without the I domains, essentially identical to conventional PEI-based transfection method, led to significantly reduced levels of GFP expression, which was then almost completely abolished in the presence of serum (Fig. 6.3a).

Figure 6.3. Molecular interaction-specific gene delivery of virus-like particles. (a) Virus-like particles bearing pGFP were delivered to HeLa cells with varying mass ratios among components: plasmid, PEI, and PAP-Id. Two-fold serial dilutions of PAP-Id-HA (high affinity) was probed to titrate for optimal gene transfer efficiency. PAP-Id-D137A (no affinity) was used as a negative control as the loss-of-function mutation abrogates the interaction with ICAM-1. Heatmap in green shows the total fluorescence measured by a microplate reader after cell lysis, in yellow shows the mean fluorescence intensity measured by flow cytometry, and in white is the percentage of GFP-positive cells (n=4). Fluorescence values are shown in relative fold difference compared to the negative control that assembled without PEI. (b) Virus-like particles bearing pDTA (diphtheria toxin subunit A) were delivered to HeLa cells in a similar manner with varying mass ratios between components. Trypan blue exclusion assay was used to stain nonviable cells. Solid bars are the counts of viable cells and hollow bars are the nonviable cells counted per image field (n=4). Data represent mean ± S.D.

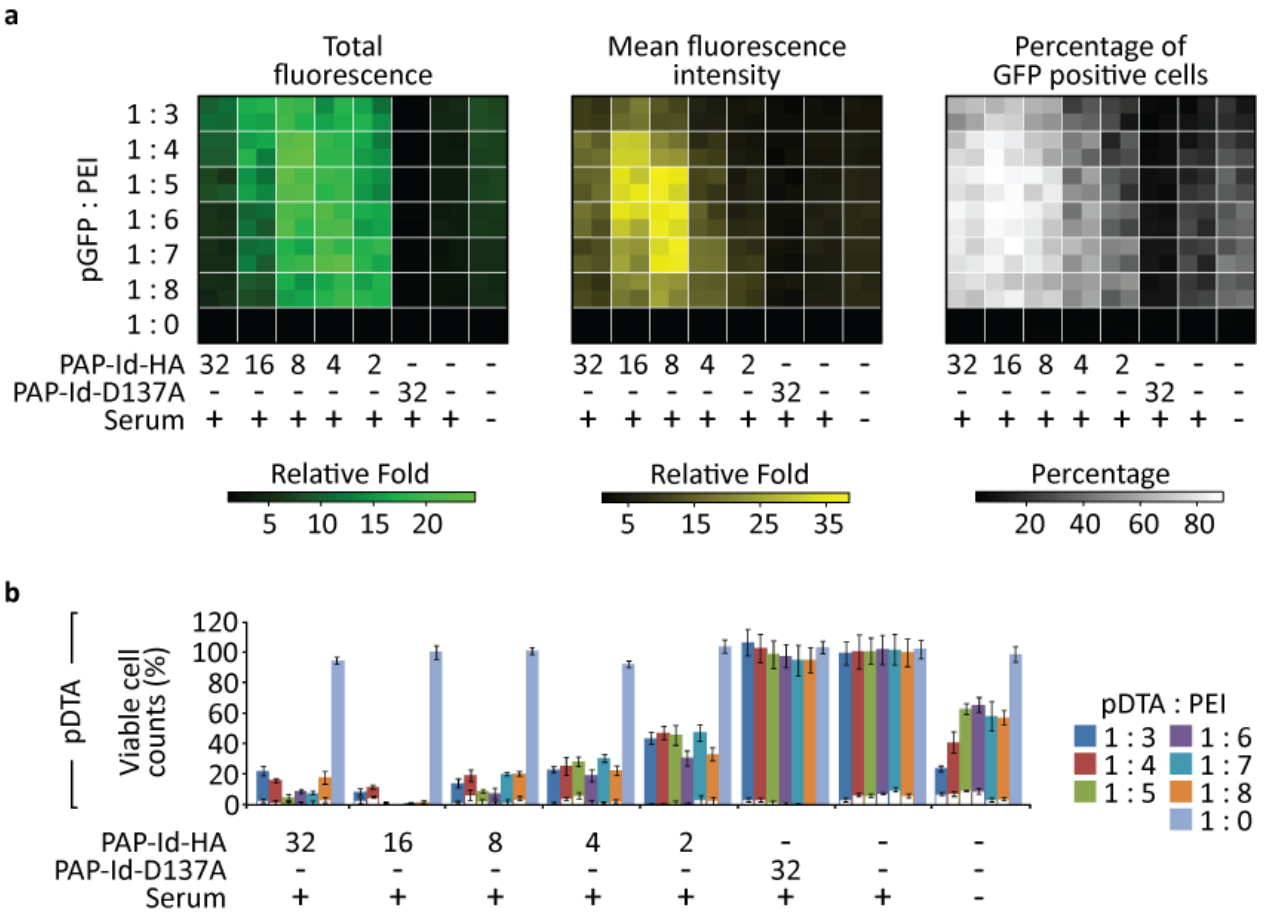
a
Total fluorescence
Mean fluorescence intensity
Percentage of GFP positive cells
pGFP : PEI
1 : 3
1 : 4
1 : 5
1 : 6
1 : 7
1 : 8
1 : 0
PAP-Id-HA 32 16 8 4 2 - - -
PAP-Id-D137A - - - - - 32 - -
Serum + + + + + + + -
Relative Fold
5 10 15 20
Relative Fold
5 15 25 35
Percentage
20 40 60 80
b
pDTA
Viable cell counts (%)
120
100
80
60
40
20
0
PAP-Id-HA 32 16 8 4 2 - - -
PAP-Id-D137A - - - - - 32 - -
Serum + + + + + + + -
pDTA : PEI
1 : 3
1 : 4
1 : 5
1 : 6
1 : 7
1 : 8
1 : 0

a < PAP-Id-HA >

MGSSHHHHHHSSGLVPRGSHMASEDEDEEDEEDEEDEEDEDGSNVDLVFLFDGSMSL
QPDEFQKILDFMKDVMKKLSNTSYQFAAVQFSTSYKTEFDFSDYVKRKDPDALLKHVK
HMLLLTNTFGAINYVATEVFREELGARPDATKVLIIITDGEATDSGNIDAAKDIIRYIIGIGK
HSQTKESQETLHKFASKPASEFVKILDTGEKLKDLFTELQKKIY.

b < GFP-Id-HA >

MGSSHHHHHHSSGLVPRGSHMASVSKGEELFTGVVPILVELDGDVNGHKFSVRGEGE
GDATIGKLTLKFICTTGKLPVPWPTLVTTLTYGVQCFSRYPDHMKQHDFFKSAMPEGYV
QERTISFKDDGKYKTRAVVKFEGDTLVNRIELKGTDFKEDGNILGHKLEYNFNSHNVYIT
ADKQKNGIKANFTVRHNVEDGSVQLADHYQQNTPIGDGPVLLPDNHYLSTQTVLSKD
PNEKRDHMVLHEYVNAAGITTLGMDELYKGSNVDLVFLFDGSMSLQPDEFQKILDFM
KDVMKKLSNTSYQFAAVQFSTSYKTEFDFSDYVKRKDPDALLKHVKHMLLLTNTFGAIN
YVATEVFREELGARPDATKVLIIITDGEATDSGNIDAAKDIIRYIIGIGKHSQTKESQETLHK
FASKPASEFVKILDTGEKLKDLFTELQKKIY.

c

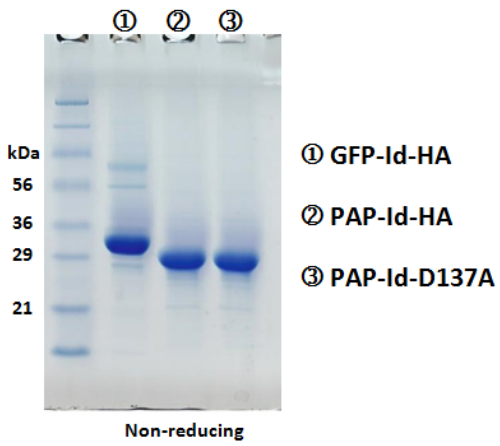

Figure 6.4. Characterizations of I domain fusion proteins.

(a&b) Single letter amino acid sequences and domain demarcations of the fusion proteins, GFP-Id-HA (a) and PAP-Id-HA (b). (c) Coomassie blue staining of size exclusion column purified GFP-Id-HA, PAP-Id-HA, and PAP-Id-D137A ran through SDS-PAGE in non-reducing condition.

To demonstrate ICAM-1 specific delivery of functional genes, we then assembled the particles with the plasmid encoding a catalytic domain (subunit A) but not the receptor-binding domain of diphtheria toxin [45] (pDTA), which would limit a potent cell killing to those transfected but not neighboring non-transfected cells. Cell death mediated by pDTA-encapsulating virus-like particles would thus indicate that our delivery system was able to compensate for the missing functions of the modified toxin: cell binding/entry and endosomal escape. Potent cytotoxicity in HeLa cells was evident at the mass ratios optimized for the highest delivery efficiency with pGFP (Fig. 6.3b). In contrast to highly efficient and ICAM-1 dependent cell killing by PAP-Id-HA mediated delivery, pDTA/PEI particles or the particles assembled with PAP-Id-D137A were completely ineffective in delivering the plasmids in the presence of serum, providing an evidence that Id-HA but not PEI was responsible for specific targeting of ICAM-1.

Inflammation-specific gene delivery to endothelial cells and monocytes/macrophages

Major cellular culprits of inflammatory diseases [46-47] are endothelial cells that line the luminal surface of blood vessels, and immune cells that actively elicit immune responses. Cell surface expression of ICAM-1 is highly upregulated during the course of acute and chronic inflammation, which makes ICAM-1 a specific target against inflammatory diseases. We chose human dermal microvascular endothelial cells (HMEC-1) and human acute monocytic leukemia cells (THP-1) as representative cellular models. As a model of inflammation, HMEC-1 and THP-1 were treated with endotoxin lipopolysaccharides (LPS) (Fig. 6.5a) that can initiate nuclear factor kappa B (NF-κB) transcription factor dependent inflammatory response [48]. Virus-like particles formulated with a fixed mass ratio of pGFP to PEI at 1:6 and varying

Figure 6.5. Inflammation-specific targeted delivery to endothelial cells and monocyte/macrophages.

(a) Timeline shows the sequence of LPS treatment, virus-particle delivery, and the measurements in human cell lines. (b&c) Virus-like particles were formed with varying mass ratios of the components, plasmid, PEI, and PAP-Id and were delivered to either normal or LPS treated endothelial cells, HMEC-1 (b), and monocytes, THP-1 (c). Two-fold serial dilutions of PAP-Id-HA was used for assessment of avidity dependent efficiency of ICAM-1-mediated endocytosis and gene delivery. PAP-Id-D137A was used as a negative control. Cells were analyzed for mean fluorescence intensity and percentage of GFP-positive cells by flow cytometry (n=4). Cell viability was measured by MTT assay (n=4). (d) Timeline shows a similar sequence of treatments and virus-like particle delivery to mouse cell lines. (e&f) Similarly, gene transfer efficiency and the associated toxicity in endothelial cells, bEnd.3 (e), and macrophages, RAW 264.7 (f), were assessed by mean fluorescence intensity and percentage of GFP-positive cells (n=4), and cell viability (n=4). Data represent mean ± S.D.

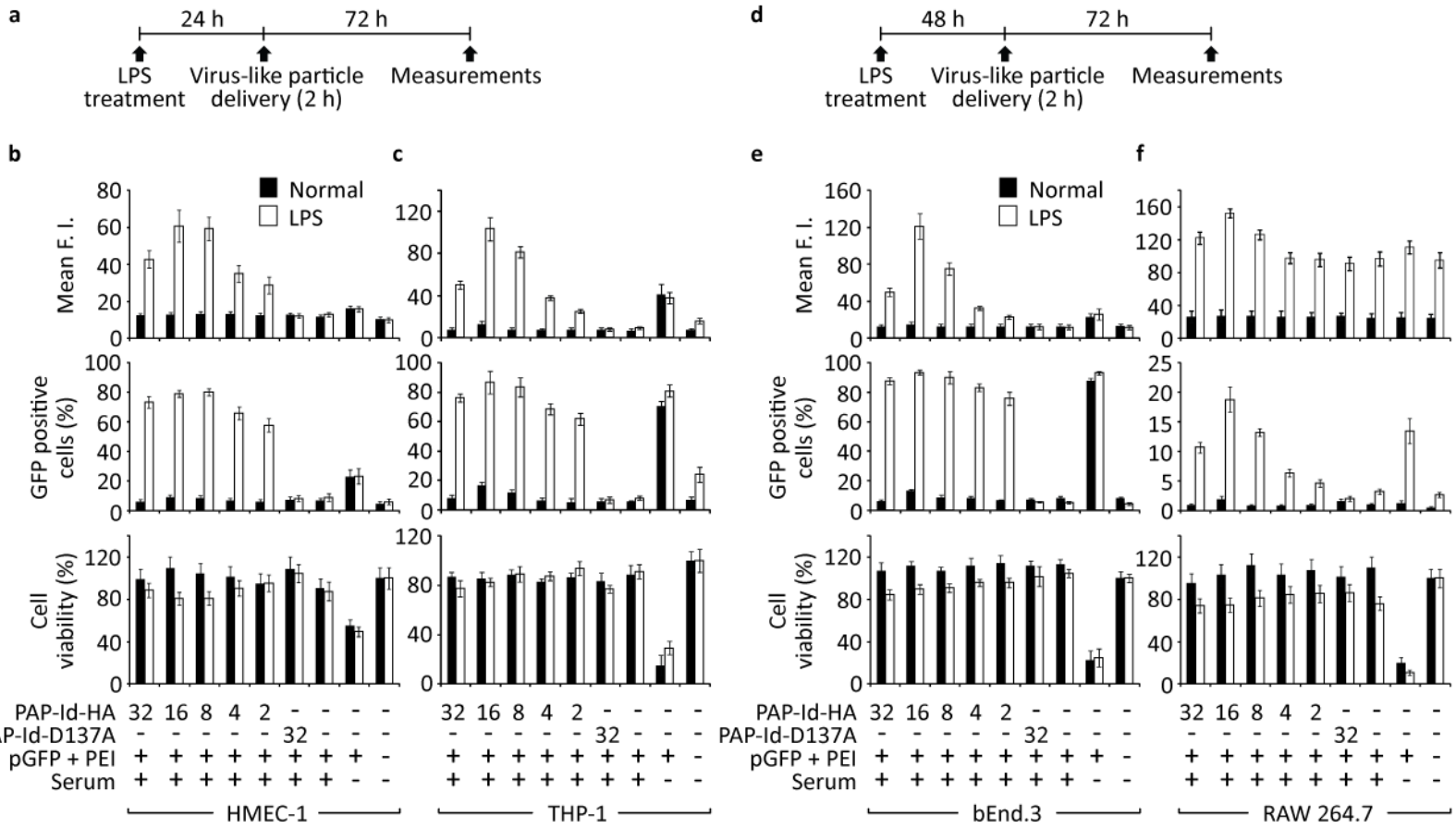
a
24 h
72 h
LPS treatment
Virus-like particle delivery (2 h)
Measurements
d
48 h
72 h
LPS treatment
Virus-like particle delivery (2 h)
Measurements
b
c
e
f
Normal
LPS
Mean F. I.
GFP positive cells (%)
Cell viability (%)
PAP-Id-HA 32 16 8 4 2 - - - -
PAP-Id-D137A - - - - - 32 - - -
pGFP + PEI + + + + + + + + -
Serum + + + + + + + - -
HMEC-1
THP-1
bEnd.3
RAW 264.7

amounts of proteins were delivered to either normal or LPS treated HMEC-1 (Fig. 6.5b) and THP-1 cells (Fig. 6.5c). Mean fluorescence intensity and the percentage of GFP-positive cells measured from the group with PAP-Id-HA showed a significant increase, only for LPS treated cells (Fig. 6.5, b and c, and Fig. 6.6, a and b). pGFP/PEI particles also transfected cells and resulted in slight increase in HMEC-1 and significant increase in THP-1. However, gene transfer efficiencies were much lower than PAP-Id-HA mediated delivery and were not specific to LPS treated group. Conventional pGFP/PEI transfection was almost completely blocked by serum or PAP-Id-D137A. Notably, pGFP/PEI transfection caused cell death as high as 90%, whereas PAP-Id-HA preserved the viability of cells, both in HMEC-1 and THP-1.

One of the major advantages of using the I domain for targeted delivery is that it cross-reacts with murine ICAM-1 [38-39], enabling same targeting moiety to be used for preclinical animal studies. Similarly, we chose two types of cells, mouse brain microvascular endothelial cells (bEnd.3) and mouse leukemic monocyte macrophage cells (RAW 264.7), to study inflammation-specific delivery of virus-like particles bearing pGFP. Overall, the induction of ICAM-1 in murine cells in response to LPS was slower than in human cells (Fig. 6.7, a and b), and accordingly we delivered virus-like particles at 48 h post LPS treatment (Fig. 6.5d). Similarly, mean fluorescence intensity and percentage of GFP-positive cells for both bEnd.3 and RAW 264.7 were significantly higher in the group that were treated with LPS and received virus-like particles formed with PAP-Id-HA (Fig. 6.5, e and f, and Fig. 6.8, a and b). pGFP/PEI resulted in up to 90% GFP-positive in bEnd.3, irrespective of LPS treatment. RAW 264.7 after treatment with LPS became enlarged and autofluorescent, resulted in an increase in MFI across all conditions. Nonetheless, PAP-Id-HA mediated delivery resulted in significant increase in fluorescence and as much as 20%

Figure 6.6. Inflammation-specific gene delivery to human endothelial cells and monocytes.

(a&b) Representative fluorescence and light microscope images and flow cytometric measurements (shown as dot plots, side scatter (SSC) vs. FL1) for GFP expression after virus-like particle delivery to either normal or LPS treated HMEC-1 (a) and THP-1 (b). Virus-like particles were formed with pGFP. Images and dot plot for PAP-Id-HA is shown only for the case with mass ratio of 16. Scale bar, 50 μm. Percentage of cells in the regions gated for GFP expression are indicated.

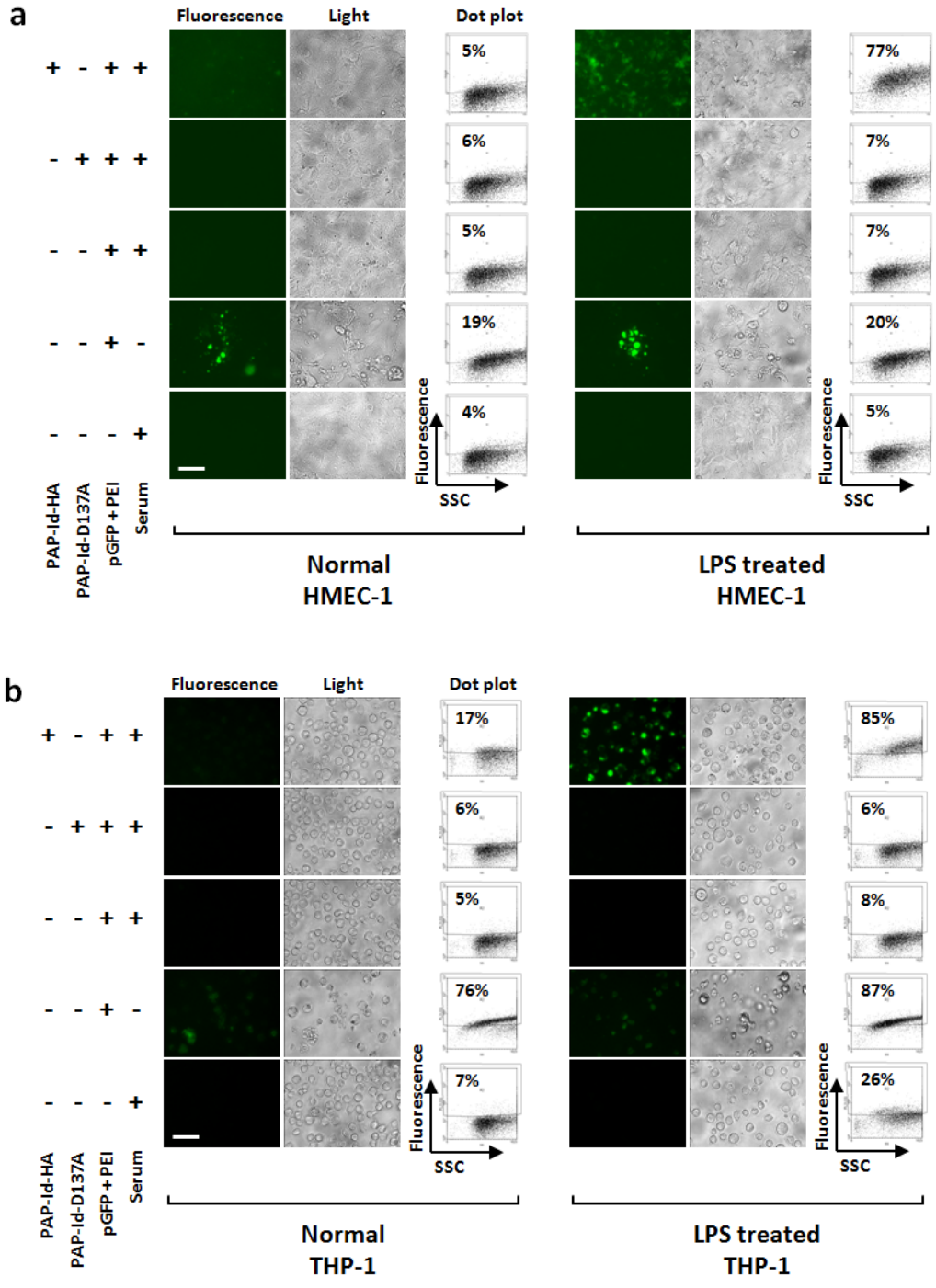
a
Fluorescence
Light
Dot plot
+ - + +
- + + +
- - + +
- - + -
- - - +
PAP-Id-HA
PAP-Id-D137A
pGFP + PEI
Serum
5%
6%
5%
19%
4%
77%
7%
7%
20%
5%
Fluorescence
SSC
Normal HMEC-1
LPS treated HMEC-1
b
Fluorescence
Light
Dot plot
+ - + +
- + + +
- - + +
- - + -
- - - +
PAP-Id-HA
PAP-Id-D137A
pGFP + PEI
Serum
17%
6%
5%
76%
7%
85%
6%
8%
87%
26%
Fluorescence
SSC
Normal THP-1
LPS treated THP-1

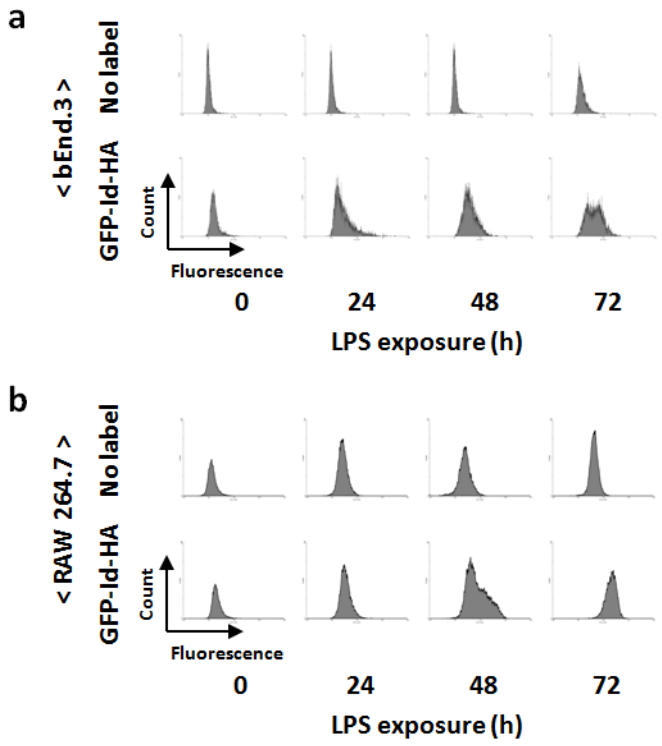

Figure 6.7. ICAM-1 expression in mouse endothelial cells and macrophages. (a&b) GFP-Id-HA was used to probe LPS-induced ICAM-1 expression in bEnd.3 (a) and RAW 264.7 (b) at 24, 48, and 72 hour post treatment time points, measured by flow cytometry. Autofluorescence of cells without label is also shown.

Figure 6.8. Inflammation-specific gene delivery to mouse endothelial cells and macrophages.

(a&b) Representative fluorescence and light microscope images and flow cytometric measurements (shown as dot plots, side scatter (SSC) vs. FL1) for GFP expression after virus-like particle delivery to either normal or LPS treated bEnd.3 (a) and RAW 264.7 (b). Virus-like particles were formed with pGFP. Images and dot plot for PAP-Id-HA is shown only for the case with mass ratio of 16. Scale bar, 50 μm. Percentage of cells in the regions gated for GFP expression are indicated.

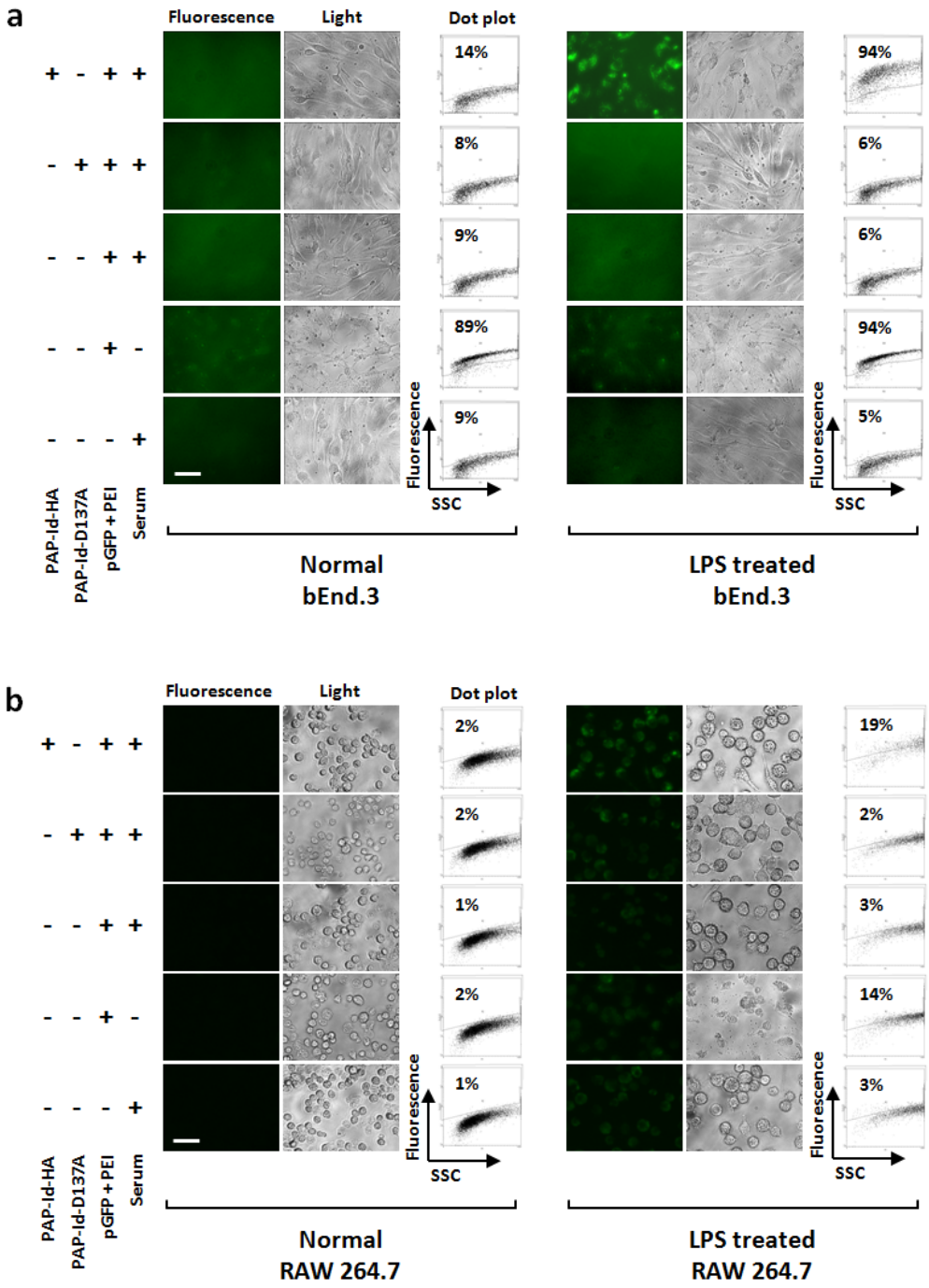
a
Fluorescence
Light
Dot plot
14%
8%
9%
89%
9%
94%
6%
6%
94%
5%
Fluorescence
SSC
PAP-Id-HA
PAP-Id-D137A
pGFP + PEI
Serum
Normal
bEnd.3
LPS treated
bEnd.3
b
Fluorescence
Light
Dot plot
2%
2%
1%
2%
1%
19%
2%
3%
14%
3%
Fluorescence
SSC
PAP-Id-HA
PAP-Id-D137A
pGFP + PEI
Serum
Normal
RAW 264.7
LPS treated
RAW 264.7

cells were GFP-positive. In comparison to other cell types, in LPS treated RAW 264.7cells, pGFP/PEI particles in the absence of serum resulted in high MFI and ~15% GFP-positive cells, ascribed to nonspecific uptake by activated macrophages. PAP-Id-HA mediated delivery preserved cell viability, while non-specific pGFP/PEI transfection caused significant cell death in both cell lines.

Inflammation-specific targeted gene delivery of virus-like particles in vivo

Gene delivery has the potential to treat many diseases, which may require or benefit much from systemic and targeted treatments via intravenous routes. Major hurdle of cationic gene delivery systems for such applications is that the electrostatic interaction with target cell surfaces can be inhibited by negatively charged glycosaminoglycans in blood serum. We chose to study the delivery of virus-like particles to the lung, where endothelial cells comprise a large portion of tissue composition. We also confirmed that cell surface expression of ICAM-1 is highly upregulated in lung after systemic LPS treatment (Fig. 6.9). We first studied gene delivery to primary mouse lung cells cultured *in vitro*, harvested from a mouse strain engineered such that exogenous Cre recombinase expression would result in constitutive expression of GFP by excision of the transcriptional STOP region flanked by *lox*P sites. We formed virus-like particles with a plasmid encoding Cre recombinase as a fusion to nuclear localization signal under the CMV promoter. Similarly, cells were treated with LPS and received virus-like particles (Fig. 6.10a), formed with a fixed ratio of pCRE to PEI (1:6) and with varying amounts of PAP-Id (Fig. 6.10b). PAP-Id-HA mediated delivery was specific to LPS treated cells, evidenced by increased mean fluorescence intensity (Fig. 6.10b and Fig. 6.11). Percentage of GFP-positive cells for the cases that were delivered to normal cells reached as high as 40%, given that even a low copy number of Cre recombinase can

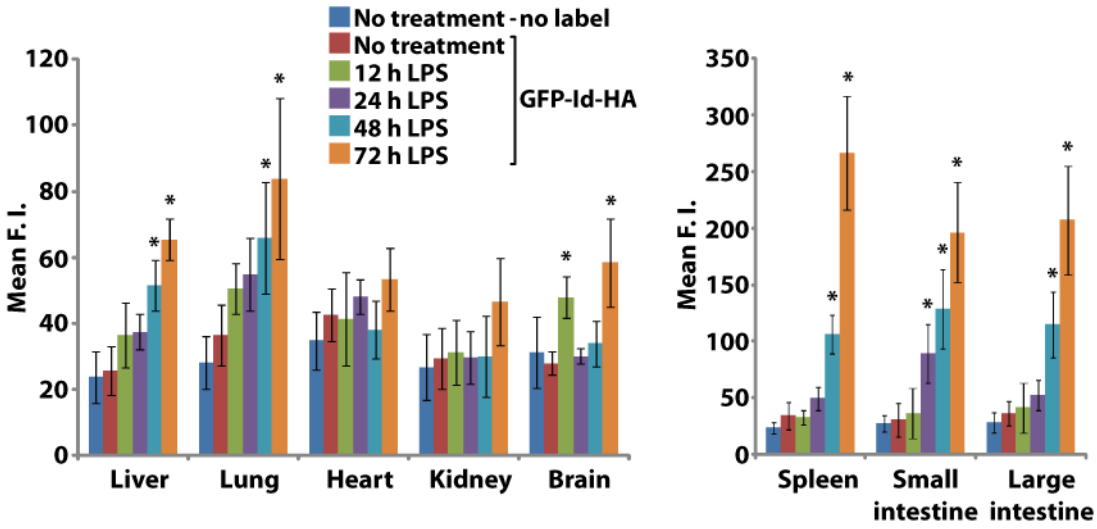

Figure 6.9. LPS-induced ICAM-1 expression in mouse organs. Collagenase-digested organs, collected at different time points (■ 12, ■ 24, ■ 48, and ■ 72 h) after systemic LPS treatments, were labeled with GFP-Id-HA. Organs were also collected from non-treated mice for measurement of autofluorescence (■ no treatment - no label) and the basal level expression of ICAM-1 (■ no treatment - GFP-Id-HA). Mean fluorescence intensities measured by flow cytometry are shown in bar graph with error bars indicating S.D. (*$p < 0.05$, unpaired Student's *t*-test compared to no treatment, GFP-Id-HA labeled control group, n = 4)

Figure 6.10. Systemic and inflammation-specific targeted gene delivery to mouse lung.

(a) Timeline shows the sequence of treatments for virus-like particle delivery to primary mouse lung cells in culture. Lung cells were harvested from a mouse strain engineered for constitutive expression of GFP after Cre recombinase-mediated *lox*P-STOP-*lox*P excision. (b) Virus-like particles were assembled with pCRE (Cre recombinase) and varying mass ratios of PEI and PAP-Id, and were delivered to either normal or LPS treated primary mouse lung cells. Data represent mean ± S.D. (c&d) Cell surface expression of ICAM-1 in CD31-positive endothelial cells (c), and F4/80-positive monocyte/macrophages (d) in mouse lung was detected by I domain fused to GFP (GFP-Id-HA) (n=4). Percentage of cells in each quadrant is shown. (e) Timeline shows the sequence of treatments, injections, and data collection of *in vivo* systemic application of virus-like particles bearing pGFP. Mass ratio of the components of virus-like particles was fixed to 1:6:16 (pGFP:PEI:PAP-Id). Virus-like particles were injected intravenously via lateral tail vein route into either normal or LPS-treated mice (BALB/c). (f) Lungs were collected and analyzed for GFP mRNA expression by qPCR. Expression was normalized to CYC1 and shown as relative fold difference as compared to PAP-Id-D137A case (n=4). PAP-Id-HA mediated delivery to LPS treated group was statistically significant among all groups. Data represent mean ± S.D. (*$p < 0.05$, One-way ANOVA followed by Tukey's post-hoc test). (g) Flow cytometric histograms show GFP expression assessed by immunostaining of fixed/permeabilized collagenase-digested lung cells (n=4). (h&i) Lung cells were dual labeled for GFP and CD31 or F4/80, and were analyzed the percentage of GFP-positive cells (black dots) within CD31-positive (h) or F4/80-positive subset (i) (yellow region and dotted box).

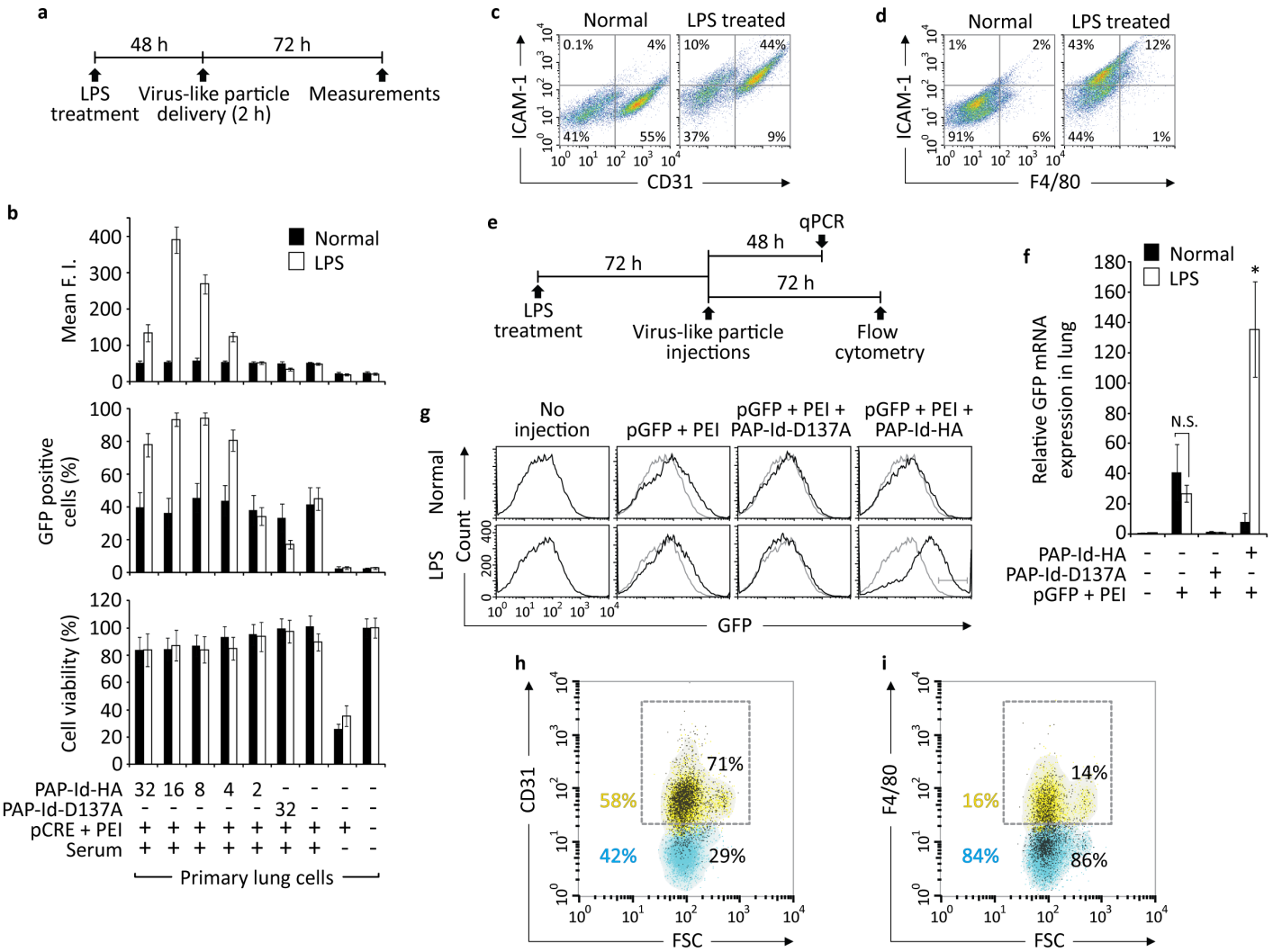
a
48 h
72 h
LPS treatment
Virus-like particle delivery (2 h)
Measurements
b
Normal
LPS
Mean F. I.
GFP positive cells (%)
Cell viability (%)
PAP-Id-HA 32 16 8 4 2 - - - -
PAP-Id-D137A - - - - - 32 - - -
pCRE + PEI + + + + + + + + -
Serum + + + + + + + - -
Primary lung cells
c
Normal
LPS treated
ICAM-1
CD31
0.1%
4%
41%
55%
10%
44%
37%
9%
d
Normal
LPS treated
ICAM-1
F4/80
1%
2%
91%
6%
43%
12%
44%
1%
e
qPCR
48 h
72 h
72 h
LPS treatment
Virus-like particle injections
Flow cytometry
f
Normal
LPS
Relative GFP mRNA expression in lung
N.S.
*
PAP-Id-HA - - - +
PAP-Id-D137A - - + -
pGFP + PEI - + + +
g
No injection
pGFP + PEI
pGFP + PEI + PAP-Id-D137A
pGFP + PEI + PAP-Id-HA
Normal
LPS
Count
GFP
h
CD31
FSC
71%
58%
42%
29%
i
F4/80
FSC
14%
16%
84%
86%

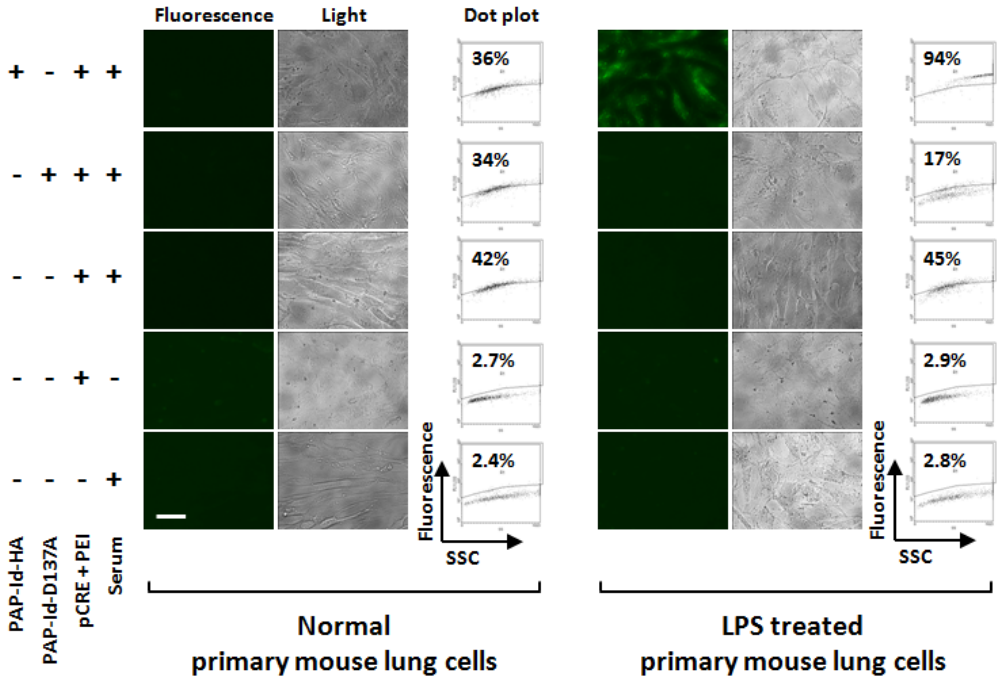

Figure 6.11. Inflammation-specific gene delivery to primary mouse lung cells. Representative fluorescence and light microscope images and flow cytometric measurements (shown as dot plots, side scatter (SSC) vs. FL1) for GFP expression after virus-like particle delivery to either normal or LPS treated primary mouse lung cells. Primary mouse lung cells were harvested from a mouse strain engineered for constitutive expression of GFP after excision of *lox*P flanked transcriptional STOP region by exogenous Cre recombinase. Virus-like particles were formed with pCRE. Images and dot plot for PAP-Id-HA is shown only for the case with mass ratio of 16. Scale bar, 50 μm. Percentage of cells in the regions gated for GFP expression are indicated.

result in excision of *lox*P-STOP-*lox*P. PAP-Id-HA mediated delivery to LPS treated cells, however, was more efficient, reaching as much as 90% GFP-positive cells. Conventional transfection of pCRE/PEI in serum free media consistently resulted in a significant loss of cell viability, whereas PAP-Id-HA mediated delivery did not.

We questioned what types of cells within blood-accessible region, in reach of virus-like particles for targeted delivery, would have the most upregulated expression of ICAM-1. Expression of ICAM-1 was upregulated predominantly in CD31-positive cells, which consist of mainly endothelial cells and small percentages of platelets, monocytes/macrophages, and a subset of T-cells (Fig. 6.10c and Fig. 6.12a). As for more specific cell type, we looked at ICAM-1 expression in F4/80-positive myeloid lineage macrophages, which participate critically in inflammatory diseases including atherosclerosis and cancer (Fig. 6.10d and Fig. 6.12b). Although LPS was delivered intravenously, some CD31/F4/80-negative cells that have induced ICAM-1 should include pneumocytes, which may have been exposed to LPS-triggered inflammation cascades. We injected virus-like particles bearing pGFP via the lateral tail vein route, either to normal or LPS treated mice (BALB/c). Relative amount of GFP mRNA expression was analyzed at 48 h post injection (Fig. 6.10e). The pattern of GFP mRNA expressions in the lung was similar to that in primary lung cells *in vitro*, such that PAP-Id-HA mediated delivery was specific to LPS treated group, whereas pGFP/PEI without the Id had a lower gene transfer efficiency irrespective of the induction of inflammation (Fig. 6.10f). Similarly, gene delivery by virus-like particles formulated with PAP-Id-D137A was completely inhibited. Virus-like particle delivery for GFP expression in the lung was also assessed at 72 h post delivery (Fig. 6.10e) by immunostaining of fixed/permeabilized collagenase-digested lung cells (Fig. 6.10g and Fig. 6.13, a and b). PAP-Id-HA mediated delivery was specific to LPS treated group, resulting in nearly 15% of the entire population are GFP-positive, while

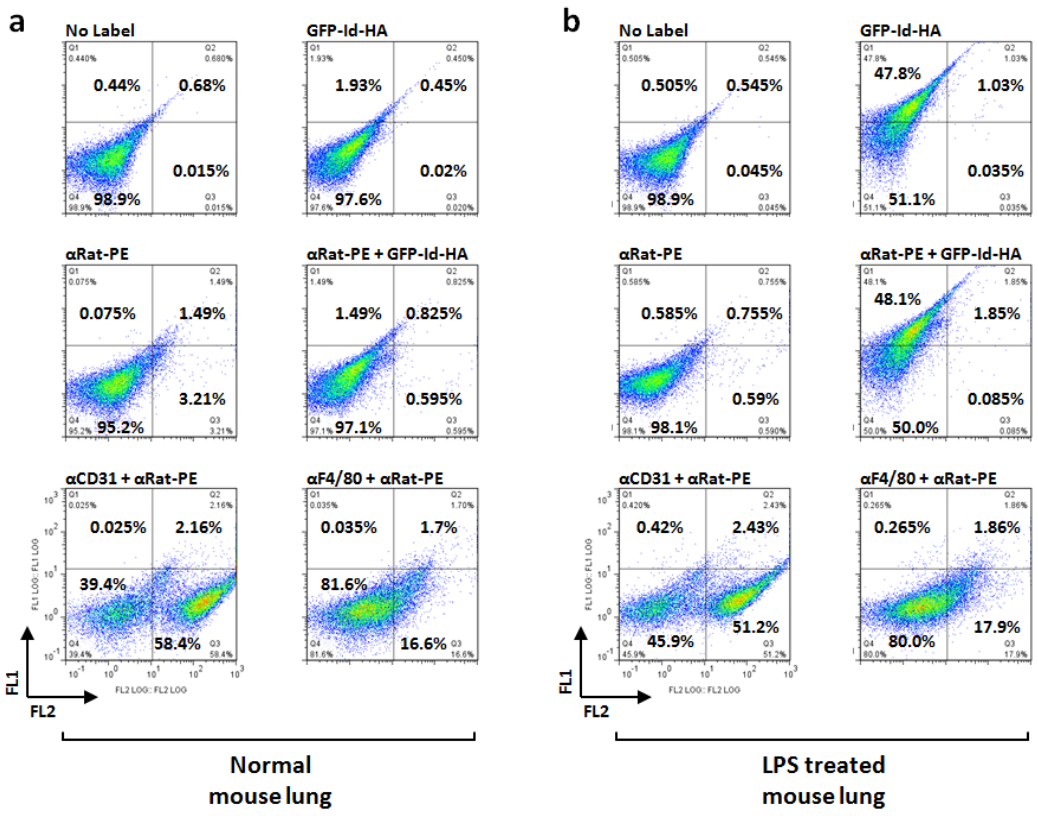

Figure 6.12. Single-color and secondary antibody controls for detection of ICAM-1 expression in CD31 or F4/80-positive cells in lung.

(a&b) Collagenase-digested lungs from normal (a) or systemic LPS treated mice (b) were labeled for ICAM-1 (GFP-Id-HA), CD31 (rat IgG), and F4/80 (rat IgG). Goat anti-rat IgG conjugated with PE was used as a secondary antibody. Fluorescence measured by flow cytometry is shown as dot plots (FL2 vs. FL1). Percentage of cells in each quadrant gated for GFP-positive cells and for CD31 or F4/80-positive cells are indicated.

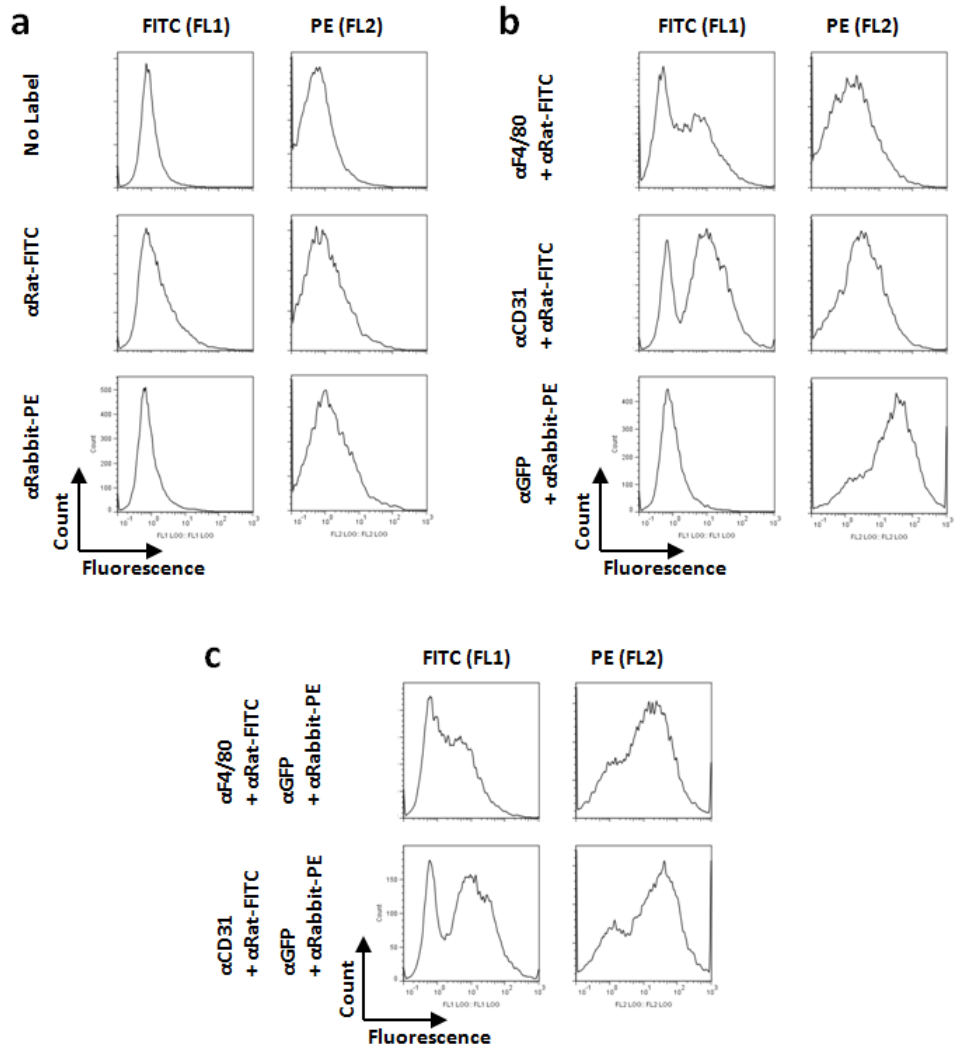

Figure 6.13. Single-color and secondary antibody controls for detection of GFP expression in lung.

Collagenase-digested lungs, collected from mice treated with systemic LPS and injected for virus-like particles formed with pGFP and PAP-Id-HA, were fixed and permeabilized for detection of GFP expression by immunofluorescence flow cytometry. (a) Secondary antibody controls for goat anti-rat IgG-FITC and goat anti-rabbit IgG-PE. (b) Single-color controls labeled for F4/80, CD31, and GFP. (c) Samples that were dual labeled for GFP and CD31 or F4/80.

conventional pGFP/PEI transfection was associated with much less GFP-positive cells without specificity toward inflammatory conditions. We further analyzed for the types of cells that were targeted by PAP-Id-HA mediated delivery (Fig. 6.10, h and i). GFP-positive cells were mostly found within CD31-positive cells, comprising up to approximately 71% of the GFP-positive subset, consistent with the high level of ICAM-1 expression observed in those cells (Fig. 6.10h and Fig. 6.13c). Gene delivery to F4/80-positive cells was also assessed, resulting in about 14% of the GFP-positive cells found within the F4/80-positive subpopulation (Fig. 6.10i and Fig. 6.13c).

Discussion

In this study we have shown that, by using a polyanionic peptide, cationic transfection agent PEI can be converted into moiety/target interaction-dependent gene delivery system without chemical modification or conjugation. We targeted ICAM-1, via the engineered high affinity I domain, to specifically deliver nucleic acid payload to inflammatory state of cells. The particles behave like viruses because, a) large nucleic acid molecules are packaged by PEI-mediated condensation, b) fully assembled particles can specifically bind to cell surface receptors, c) particles can elicit receptor mediated endocytosis, d) escape endosomal degradation attributed to the proton sponge effect of PEI, and e) express the payload gene with high efficiency.

Striking specificity of virus-like particles to ICAM-1 overexpression, or inflammation, was consistently observed in this study. This is analogous to the previous studies that showed how HRV infectivity can be enhanced after cells were treated with inflammatory cytokines such as TNF-α that upregulate the expression of ICAM-1 [49]. Additionally, the given barriers in gene delivery [50], which comprise the hurdles for genetic content to reach target cells, gain entry through the membrane,

escape lysosomal nuclease degradation, may have provided a threshold for expression strictly in LPS treated inflammatory conditions. This goes parallel with the observation that the gene transfer efficiency of virus-like particles was largely dependent on coating density or avidity of PAP-Id, as it would determine the dynamics of multimeric interaction with ICAM-1 and ultimately the efficiency of endocytosis.

Molecular interaction-dependent uptake of plasmid/PEI particle resulted in a remarkable recovery of cell viability close to the normal state of the cells. We speculate that nonspecific interaction of plasmid/PEI particles with cell surfaces would drive uncontrolled uptake of the densely charged particles that eventually leads to cell death. In contrast, molecular interaction-dependent uptake, or receptor mediated endocytosis, is an active cellular process that can be controlled and handled by cells. We also think that the improved viability contributes significantly to the more efficient gene transfer of PAP-Id mediated delivery as compared to toxicity-laden conventional transfection of plasmid/PEI. Low gene transfer efficiency of plasmid/PEI in the presence of serum, on the other hand, requires high-dose injection of these toxic particles, which leads to serious systemic toxicity in subject mice. In contrast, virus-like particles required as low as 10 μg of plasmid for successful gene transfer and were well tolerated for days, emphasizing the advantage of targeted delivery via receptor/ligand interaction for systemic applications.

Virus-like particles delivered genes mostly to CD31-positive cells in lung. CD31-positive cells in lung would predominantly be comprised of pulmonary endothelial cells that line the luminal surface of blood vessels. While lung is also comprised of epithelial cells, but were out of reach from virus-like particles for gene delivery. With the given size of virus-like particles, we expect that targeted cells would mostly reside in the blood accessible stroma as opposed to the parenchyma

without routes for the particles to reach. However, the endothelium as well as immune cells such as monocytes have been implicated to play critical roles in the pathology of inflammatory diseases, especially in the cases of atherosclerosis [47], psoriasis, and arthritis [51]. The ability to deliver genes to these types of cells should provide immense therapeutic opportunity, even without the access to the parenchyma. For diseases characterized by leaky vasculatures, such as cancer, virus-like particles should also provide much more specificity by molecular interaction-dependent delivery together with passive targeting, as it can freely access the cancerous parenchyma and adhere specifically to antigens for receptor-mediated endocytosis.

Apart from the ability of viruses to efficiently evade into host cells, they also have evolved mechanisms for their genome to self-replicate, elude the immune system by synthesizing viral cytokine homologues, and gene expression or viral life cycles to be dependent on specific host cellular component or activity. The use of more advanced genetic materials, such as plasmids with promoters for improved expression or cell type specific expression, mechanisms for self-replication/integration, or functions that can be activated under disease-associated cellular activities, may further improve virus-like particles with enhanced gene transfer efficiency, specificity, and safety. We anticipate that such simplicity and versatility of the system may open up opportunities for rapid assessments of multifaceted virus-like particles formed with a range of different targeting moieties and payloads, all of which can be easily formulated by self-assembly, and contribute to successful translation of nonviral vectors into the clinic.

REFERENCES

1. Hacein-Bey-Abina S, Hauer J, Lim A, Picard C, Wang GP, Berry CC, et al. Efficacy of gene therapy for X-linked severe combined immunodeficiency. N Engl J Med. 2010;363(4):355-64.

2. Bainbridge JW, Smith AJ, Barker SS, Robbie S, Henderson R, Balaggan K, et al. Effect of gene therapy on visual function in Leber's congenital amaurosis. N Engl J Med. 2008;358(21):2231-9.

3. Christine CW, Starr PA, Larson PS, Eberling JL, Jagust WJ, Hawkins RA, et al. Safety and tolerability of putaminal AADC gene therapy for Parkinson disease. Neurology. 2009;73(20):1662-9.

4. Manno CS, Pierce GF, Arruda VR, Glader B, Ragni M, Rasko JJ, et al. Successful transduction of liver in hemophilia by AAV-Factor IX and limitations imposed by the host immune response. Nat Med. 2006;12(3):342-7.

5. Mendell JR, Campbell K, Rodino-Klapac L, Sahenk Z, Shilling C, Lewis S, et al. Dystrophin immunity in Duchenne's muscular dystrophy. N Engl J Med. 2010;363(15):1429-37.

6. Breitbach CJ, Burke J, Jonker D, Stephenson J, Haas AR, Chow LQ, et al. Intravenous delivery of a multi-mechanistic cancer-targeted oncolytic poxvirus in humans. Nature. 2011;477(7362):99-102.

7. McCormack MP, Rabbitts TH. Activation of the T-cell oncogene LMO2 after gene therapy for X-linked severe combined immunodeficiency. N Engl J Med. 2004;350(9):913-22.

8. Yang YP, Nunes FA, Berencsi K, Furth EE, Gonczol E, Wilson JM. Cellular-Immunity to Viral-Antigens Limits E1-Deleted Adenoviruses for Gene-Therapy. P Natl Acad Sci USA. 1994;91(10):4407-11.

9. Yang YP, Li Q, Ertl HCJ, Wilson JM. Cellular and Humoral Immune-Responses to Viral-Antigens Create Barriers to Lung-Directed Gene-Therapy with Recombinant Adenoviruses. J Virol. 1995;69(4):2004-15.

10. Lv H, Zhang S, Wang B, Cui S, Yan J. Toxicity of cationic lipids and cationic polymers in gene delivery. J Control Release. 2006;114(1):100-9.

11. Luo D, Saltzman WM. Synthetic DNA delivery systems. Nat Biotechnol. 2000;18(1):33-7.

12. Staprans I, Felts JM. Isolation and characterization of glycosaminoglycans in human plasma. J Clin Invest. 1985;76(5):1984-91.

13. Moret I, Esteban Peris J, Guillem VM, Benet M, Revert F, Dasi F, et al. Stability of PEI-DNA and DOTAP-DNA complexes: effect of alkaline pH, heparin and serum. J Control Release. 2001;76(1-2):169-81.

14. Ruponen M, Yla-Herttuala S, Urtti A. Interactions of polymeric and liposomal gene delivery systems with extracellular glycosaminoglycans: physicochemical and transfection studies. Biochim Biophys Acta. 1999;1415(2):331-41.

15. Kumar P, Ban HS, Kim SS, Wu H, Pearson T, Greiner DL, et al. T cell-specific siRNA delivery suppresses HIV-1 infection in humanized mice. Cell. 2008;134(4):577-86.

16. Peer D, Park EJ, Morishita Y, Carman CV, Shimaoka M. Systemic leukocyte-directed siRNA delivery revealing cyclin D1 as an anti-inflammatory target. Science. 2008;319(5863):627-30.

17. Song E, Zhu P, Lee SK, Chowdhury D, Kussman S, Dykxhoorn DM, et al. Antibody mediated in vivo delivery of small interfering RNAs via cell-surface receptors. Nat Biotechnol. 2005;23(6):709-17.

18. Davis ME, Zuckerman JE, Choi CH, Seligson D, Tolcher A, Alabi CA, et al. Evidence of RNAi in humans from systemically administered siRNA via targeted nanoparticles. Nature. 2010;464(7291):1067-70.

19. Waehler R, Russell SJ, Curiel DT. Engineering targeted viral vectors for gene therapy. Nat Rev Genet. 2007;8(8):573-87.

20. Maheshri N, Koerber JT, Kaspar BK, Schaffer DV. Directed evolution of adeno-associated virus yields enhanced gene delivery vectors. Nat Biotechnol. 2006;24(2):198-204.

21. Douglas JT, Rogers BE, Rosenfeld ME, Michael SI, Feng M, Curiel DT. Targeted gene delivery by tropism-modified adenoviral vectors. Nat Biotechnol. 1996;14(11):1574-8.

22. Lee RJ, Huang L. Folate-targeted, anionic liposome-entrapped polylysine-condensed DNA for tumor cell-specific gene transfer. J Biol Chem. 1996;271(14):8481-7.

23. Erbacher P, Remy JS, Behr JP. Gene transfer with synthetic virus-like particles via the integrin-mediated endocytosis pathway. Gene Ther. 1999;6(1):138-45.

24. Ogris M, Brunner S, Schuller S, Kircheis R, Wagner E. PEGylated DNA/transferrin-PEI complexes: reduced interaction with blood components,

extended circulation in blood and potential for systemic gene delivery. Gene Ther. 1999;6(4):595-605.

25. Wagner E, Zenke M, Cotten M, Beug H, Birnstiel ML. Transferrin-polycation conjugates as carriers for DNA uptake into cells. Proc Natl Acad Sci U S A. 1990;87(9):3410-4.

26. Boussif O, Lezoualc'h F, Zanta MA, Mergny MD, Scherman D, Demeneix B, et al. A versatile vector for gene and oligonucleotide transfer into cells in culture and in vivo: polyethylenimine. Proc Natl Acad Sci U S A. 1995;92(16):7297-301.

27. Godbey WT, Wu KK, Mikos AG. Poly(ethylenimine) and its role in gene delivery. J Control Release. 1999;60(2-3):149-60.

28. Akinc A, Thomas M, Klibanov AM, Langer R. Exploring polyethylenimine-mediated DNA transfection and the proton sponge hypothesis. J Gene Med. 2005;7(5):657-63.

29. Dustin ML, Rothlein R, Bhan AK, Dinarello CA, Springer TA. Induction by IL 1 and interferon-gamma: tissue distribution, biochemistry, and function of a natural adherence molecule (ICAM-1). J Immunol. 1986;137(1):245-54.

30. Marlin SD, Springer TA. Purified intercellular adhesion molecule-1 (ICAM-1) is a ligand for lymphocyte function-associated antigen 1 (LFA-1). Cell. 1987;51(5):813-9.

31. Albelda SM, Smith CW, Ward PA. Adhesion molecules and inflammatory injury. FASEB J. 1994;8(8):504-12.

32. van de Stolpe A, van der Saag PT. Intercellular adhesion molecule-1. J Mol Med (Berl). 1996;74(1):13-33.

33. Tomassini JE, Graham D, DeWitt CM, Lineberger DW, Rodkey JA, Colonno RJ. cDNA cloning reveals that the major group rhinovirus receptor on HeLa cells is intercellular adhesion molecule 1. Proc Natl Acad Sci U S A. 1989;86(13):4907-11.

34. Grunert HP, Wolf KU, Langner KD, Sawitzky D, Habermehl KO, Zeichhardt H. Internalization of human rhinovirus 14 into HeLa and ICAM-1-transfected BHK cells. Med Microbiol Immunol. 1997;186(1):1-9.

35. Muro S, Wiewrodt R, Thomas A, Koniaris L, Albelda SM, Muzykantov VR, et al. A novel endocytic pathway induced by clustering endothelial ICAM-1 or PECAM-1. J Cell Sci. 2003;116(Pt 8):1599-609.

36. Jin M, Song G, Carman CV, Kim YS, Astrof NS, Shimaoka M, et al. Directed evolution to probe protein allostery and integrin I domains of 200,000-fold higher affinity. Proc Natl Acad Sci U S A. 2006;103(15):5758-63.

37. Park S, Kang S, Veach AJ, Vedvyas Y, Zarnegar R, Kim JY, et al. Self-assembled nanoplatform for targeted delivery of chemotherapy agents via affinity-regulated molecular interactions. Biomaterials. 2010;31(30):7766-75.

38. Kang S, Park T, Chen X, Dickens G, Lee B, Lu K, et al. Tunable physiologic interactions of adhesion molecules for inflamed cell-selective drug delivery. Biomaterials. 2011;32(13):3487-98.

39. Chen X, Wong R, Khalidov I, Wang AY, Leelawattanachai J, Wang Y, et al. Inflamed leukocyte-mimetic nanoparticles for molecular imaging of inflammation. Biomaterials. 2011;32(30):7651-61.

40. Cabantous S, Terwilliger TC, Waldo GS. Protein tagging and detection with engineered self-assembling fragments of green fluorescent protein. Nat Biotechnol. 2005;23(1):102-7.

41. Soriano P. The PDGF alpha receptor is required for neural crest cell development and for normal patterning of the somites. Development. 1997;124(14):2691-700.

42. Cudre-Mauroux C, Occhiodoro T, Konig S, Salmon P, Bernheim L, Trono D. Lentivector-mediated transfer of Bmi-1 and telomerase in muscle satellite cells yields a duchenne myoblast cell line with long-term genotypic and phenotypic stability. Hum Gene Ther. 2003;14(16):1525-33.

43. Zou K, Yuan Z, Yang Z, Luo H, Sun K, Zhou L, et al. Production of offspring from a germline stem cell line derived from neonatal ovaries. Nat Cell Biol. 2009;11(5):631-6.

44. Huth JR, Olejniczak ET, Mendoza R, Liang H, Harris EA, Lupher ML, Jr., et al. NMR and mutagenesis evidence for an I domain allosteric site that regulates lymphocyte function-associated antigen 1 ligand binding. Proc Natl Acad Sci U S A. 2000;97(10):5231-6.

45. Choe S, Bennett MJ, Fujii G, Curmi PM, Kantardjieff KA, Collier RJ, et al. The crystal structure of diphtheria toxin. Nature. 1992;357(6375):216-22.

46. Coussens LM, Werb Z. Inflammation and cancer. Nature. 2002;420(6917):860-7.

47. Ross R. Atherosclerosis--an inflammatory disease. N Engl J Med. 1999;340(2):115-26.

48. Chow JC, Young DW, Golenbock DT, Christ WJ, Gusovsky F. Toll-like receptor-4 mediates lipopolysaccharide-induced signal transduction. J Biol Chem. 1999;274(16):10689-92.

49. Subauste MC, Jacoby DB, Richards SM, Proud D. Infection of a human respiratory epithelial cell line with rhinovirus. Induction of cytokine release and modulation of susceptibility to infection by cytokine exposure. J Clin Invest. 1995;96(1):549-57.

50. Whitehead KA, Langer R, Anderson DG. Knocking down barriers: advances in siRNA delivery. Nat Rev Drug Discov. 2009;8(2):129-38.

51. Folkman J. Angiogenesis in cancer, vascular, rheumatoid and other disease. Nat Med. 1995;1(1):27-31.

CHAPTER 7

CONCLUSIONS AND FUTURE DIRECTIONS

Integrins and their ligands are among the most important cell adhesion molecules in metazoa. They provide the molecular basis of cell adhesion and play critical roles in embryogenesis, development, hemostasis, wound healing, and everyday maintenance of a healthy immune system. They have also been implicated in various pathological conditions and represent important therapeutic targets.

In this dissertation, I have demonstrated my efforts on integrin engineering for therapeutic development. One of the major breakthroughs presented in this work was the engineering of the α_M I domain into a high affinity state to its ligands, which led to the subsequent discovery of an activation-specific antibody that has potential therapeutic use. This was possible because we have also developed the novel protein engineering platform YS2H, which facilitated the process of antigen engineering and antibody discovery. Our integrin engineering studies eventually led to obtaining a crystal structure of the complex between LFA-1 I domain and ICAM-1 D1, engineered for high affinity and native folding, respectively. While the crystal structure provided us with further structural evidence of the allostery in the I domain and the nature of ICAM-1 D1 folding, it also attested to the power of my protein engineering platform for modulating protein function and folding. The specificity and affinity of LFA-1 I domain to ICAM-1 provide ways to specifically target therapeutics to the sites of inflammation. I demonstrated inflammation-dependent targeted delivery of anti-inflammatory drug compounds as well as plasmids, using the engineered LFA-1 I domain for high affinity and avidity binding to upregulated expression of ICAM-1. From these studies I have realized that the extent of

multimeric and avidity interactions is a critical component in the design of targeted delivery systems. Especially for gene delivery systems, my studies highlighted the importance of achieving intracellular delivery and the endosomal escape for efficient and functional delivery of the gene payloads.

One of my major goals in developing targeted delivery systems has been to establish a facile, yet versatile, and multifaceted platform that can be used by many scientists and physicians. Currently the field of targeted delivery is overflowing with newly invented ingenious products, crossing various disciplines in the fields of chemical engineering, protein engineering, cell and molecular biology, immunology, virology, and many more. Various drug and gene delivery systems are in clinical trials, while some are already being used in the clinics. However, I believe that there is yet a need for a platform that can be more approachable and implemented by many scientists at ease without the requirement of esoteric techniques or special knowledge about the system. This is because most current systems often involve complicated procedures or uncommon materials that make it difficult for other scientists to adapt for different applications. As described in Chapter 6, the self-assembly system to create virus-like particles that can be used for systemic and site-directed targeted gene delivery only requires to bacterially produce a targeting moiety as a fusion to a polyanionic peptide. I envision that such easy and multifunctional systems will become the major tools for biomedical research for the development of targeted therapeutics against debilitating diseases, and will greatly aid the translation of targeted delivery systems into the clinic.

Future directions

Throughout the studies, I have pondered ways to make targeted delivery systems safer in clinical settings. In this dissertation, I have focused my attention to the delivery of anti-inflammatory drugs and genes to autoimmune and inflammatory diseases, where the off-target effect may not raise a major safety concern. However, when the purpose of delivery systems is to elicit cytotoxic cell death in target cells by delivering cancer drugs, associated side effects due to off-targeting become a serious safety issue. I envision that if two distinct antigens are present on target cells, one could prepare targeted delivery vehicles directed separately to each antigen, such that only cells that have taken up both vehicles are killed. This would amplify the therapeutic effect at the overlapping sites that are targeted by the two carriers, and minimize the off target side-effects outside of the targets. For example, two chemotherapeutic drugs that have cumulative or synergistic effects could be delivered with a system that targeted ICAM-1 and VCAM-1. Such targeted delivery would provide more potent anti-tumor cytotoxicity to cells co-expressing ICAM-1 and VCAM-1, while minimizing toxicity to cells that express only one antigen. Use of such delivery systems, would allow synergistic chemotherapeutics or payloads to be used more effectively. In the case of gene delivery systems, payloads can be engineered to be dependent on each other for their efficacy, such as combinatorial cytokines or fragments of a toxin designed for split protein-like association.

Current studies and work on targeted delivery systems do not take the affinity and avidity of the targeting moiety into careful consideration. Counter-intuitive to the notion that antibody with the highest affinity to the target antigen would result in the best therapeutic outcome, recent studies have demonstrated that low to medium affinity interaction could be more advantageous for targeted delivery systems [1-3]. This is perhaps attributed to the fact that the efficiency of immunotargeting of drug/gene carriers is not only determined by single interactions between the targeting

moiety and the target. It is also affected by multimeric binding of the carriers that creates the avidity effect, as emphasized throughout this dissertation. When targeting endogenous molecules such as ICAM-1, which many cell types constitutively express at a low level, the use of delivery systems that target ligand with a low affinity/high avidity interaction may provide a safer therapeutic approach than a high affinity/low avidity interaction. One of the advantages to using the LFA-1 I domain for targeted delivery is that the affinity of the I domain can be modulated by the position and the type of amino acid for substitution [4]. The self-assembling targeted delivery systems presented in this dissertation also enable fine-tuning of the multivalent interaction or avidity. To this end, I would investigate the modulation of affinity and avidity of targeted delivery systems *in vivo* using different mutants of I domain, not only for the specific accumulation at target sites, but also for minimal off-target delivery into irrelevant tissues and organs.

For a more immediate research direction, I would apply virus-like particles for therapeutic gene delivery in an *in vivo* disease model. Within the context of my current research, I am particularly interested in developing treatments for atherosclerosis because inflammation plays central roles in the pathophysiology of the disease. As I briefly summarized in Chapter 1, localized upregulated expression of ICAM-1 is found on endothelial cells and myeloid cells present within atherosclerotic lesions. Prolonged inflammatory responses of activated endothelial cells and accumulated myeloid cells, leads to prolonged production of pro-inflammatory mediators that exacerbate disease progression [5]. Antioxidant treatments reduce the oxidative stress elicited by the pro-inflammatory mediators, and restore the efficient emigration of lipid-laden foam cells from atherosclerotic lesions into the lymph nodes, with concomitant regression of plaques [6-7]. Other studies have shown that endothelial cell-specific inhibition of NF-κB activity prevents atherogenesis [8].

Hence investigation of the use of virus-like particles for delivery of therapeutic genes, such as anti-inflammatory cytokines and protein inhibitors of NF-κB, or shRNAs against pro- inflammatory mediators, specifically to plaque forming myeloid and endothelial cells in mouse models of atherosclerosis (e.g. ApoE-null mutation, B6.129P2-*Apoe*^{tm1Unc}) would be of great interest as a follow-up study.

Chronic inflammation is associated with the development and progression of dysplasia [9]. This is related to the epigenetic changes in tumor cells as well as the surrounding inflammatory stroma, leading to abnormal expression of growth factors, cytokines and chemokines, and the production of free radicals such as reactive oxygen and nitrogen species. Inflammatory tumor stroma has been implicated for the presence of upregulated expression of ICAM-1 [10-12], providing a great therapeutic opportunity for my inflammation-specific virus-like particles. Delivery of genes designed to reduce inflammation may reduce the factors that predispose to the development and progression of cancer. During my studies with virus-like particles for the delivery of diphtheria toxin gene, I realized that diphteria toxin might be used to kill ICAM-1-overexpressing tumors. Along with the efforts to create safer delivery schemes, the use of virus-like particles for epigenetic correction or cytotoxic removal of tumors and the stroma may greatly contribute to the current clinical cancer therapeutics.

REFERENCES

1. Adams GP, Schier R, McCall AM, Simmons HH, Horak EM, Alpaugh RK, et al. High affinity restricts the localization and tumor penetration of single-chain Fv antibody molecules. Cancer Res. 2001;61(12):4750-5.

2. Mammen M, Choi SK, Whitesides GM. Polyvalent interactions in biological systems: Implications for design and use of multivalent ligands and inhibitors. Angew Chem Int Edit. 1998;37(20):2755-94.

3. Yu YJ, Zhang Y, Kenrick M, Hoyte K, Luk W, Lu YM, et al. Boosting Brain Uptake of a Therapeutic Antibody by Reducing Its Affinity for a Transcytosis Target. Sci Transl Med. 2011;3(84).

4. Jin M, Song G, Carman CV, Kim YS, Astrof NS, Shimaoka M, et al. Directed evolution to probe protein allostery and integrin I domains of 200,000-fold higher affinity. Proc Natl Acad Sci U S A. 2006;103(15):5758-63.

5. Hansson GK, Robertson AK, Soderberg-Naucler C. Inflammation and atherosclerosis. Annu Rev Pathol. 2006;1:297-329.

6. Curtiss LK. Reversing atherosclerosis? N Engl J Med. 2009;360(11):1144-6.

7. Park YM, Febbraio M, Silverstein RL. CD36 modulates migration of mouse and human macrophages in response to oxidized LDL and may contribute to macrophage trapping in the arterial intima. J Clin Invest. 2009;119(1):136-45.

8. Gareus R, Kotsaki E, Xanthoulea S, van der Made I, Gijbels MJ, Kardakaris R, et al. Endothelial cell-specific NF-kappaB inhibition protects mice from atherosclerosis. Cell Metab. 2008;8(5):372-83.

9. Coussens LM, Werb Z. Inflammation and cancer. Nature. 2002;420(6917):860-7.

10. Kelly CP, O'Keane JC, Orellana J, Schroy PC, 3rd, Yang S, LaMont JT, et al. Human colon cancer cells express ICAM-1 in vivo and support LFA-1-dependent lymphocyte adhesion in vitro. Am J Physiol. 1992;263(6 Pt 1):G864-70.

11. Maurer CA, Friess H, Kretschman B, Wildi S, Muller C, Graber H, et al. Over-expression of ICAM-1, VCAM-1 and ELAM-1 might influence tumor progression in colorectal cancer. International Journal of Cancer. 1998;79(1):76-81.

12. Hayes SH, Seigel GM. Immunoreactivity of ICAM-1 in Human Tumors, Metastases and Normal Tissues. Int J Clin Exp Patho. 2009;2(6):553-60.

APPENDIX 1

DIRECTED EVOLUTION TO ENGINEER β_1 INTEGRIN I-LIKE DOMAIN INTO HIGH AFFINITY STATES

This appendix describes the preliminary results and analyses of β_1 I-like domain engineering. The I-like domain from β_1 integrin subunit was engineered via directed evolution implemented by yeast surface display system, similarly as described in Chapter 3 for the engineering of α_M I domain. The final goal of this study has been to use the engineered high affinity I-like domain as a platform to develop function-blocking, therapeutic antibodies that specifically or preferentially antagonize the active conformation of β_1 integrins.

Although the engineering of LFA-1 I domain was successfully implemented by selecting active mutants through monomeric binding to ICAM-1 or AL57 [1-2], we failed to enrich active mutants of α_M I domain and β_1 I-like domain using the same strategy. In fact, active mutants of LFA-1 I domain were enriched by labeling of the yeast cell library with either ICAM-1-human-IgG or AL57-human-IgG, followed by superparamagnetic microbeads conjugated to anti-human-IgG, for selection through magnetic-activated cell sorting (MACS) [1]. The underlying assumption of the system is that activating mutations in the domain would elicit sufficient affinity for binding to the physiologic ligands in a monomeric, one-to-one fashion, so that the microbeads can stably select binders by magnetic force. However, we found that α_M I domain and β_1 I-like domain rather required higher avidity, multimeric interaction with ligands for stable binding, as it is also the case for the leukocytes that utilize these integrins for adhesion and migration [3-5]. Therefore, we hypothesized that the sorting of the yeast libraries of α_M I domain and β_1 I-like domain needed to be panned through a system

that can provide multimeric interaction with physiologic ligands. To this end, we enriched the binders by sorting the libraries against HeLa cells, whose cell surface is rich in numerous ligands for both integrins, including fibronectin, ICAM-1, and VCAM-1 (data not shown).

Initially, the yeast cell library of β_1 I-like domain did not show any significant binding to HeLa cells (Fig. A1.1a). However, the presence of yeast cells that remained bound to HeLa cell surface after washing was evident from the second sort, which then we analyzed for the prevailing mutations of individual clones after the third sort (Fig. A1.1, a and b). To rationalize the effect of mutations found from the enriched library, we constructed a model structure of β_1 I-like domain, based on the existing crystal structure of complete ectodomain of $\alpha_{IIb}\beta_3$ integrin [6] (Fig. A1.1c). After structural interpretations of the mutations, we concluded that mutations D137N, M153V, E169K, D259N, and I351T were the corresponding hot spots that resulted in activated states of the I-like domain. Interestingly, we also found that a stop codon mutation preceding the α7-helix of the I-like domain resulted in an increased number of yeast cells bound to HeLa, though it was not statistically significant (Fig. A1.1b). Mutants we found in b1 I-like domain were either at least equally comparable or much more strengthened in their binding to HeLa cell surface, as compared to the rationally designed active mutants, D137A, D138A, and T339C/A342C. These rationally designed substitutions were determined by sequence homology, based on previous biochemical and structural studies that demonstrated activation by the point mutations and disulfide bond in full length integrins β_7 and β_3 [7-8].

We also constructed a model structure for high affinity conformation of β_1 I-like domain, based on the existing crystal structure of the β_3 integrin in which the hybrid domain was extended by ligand mimetic compounds for active open conformation of the integrin [9-10] (Fig. A1.2a). By comparing the model structures,

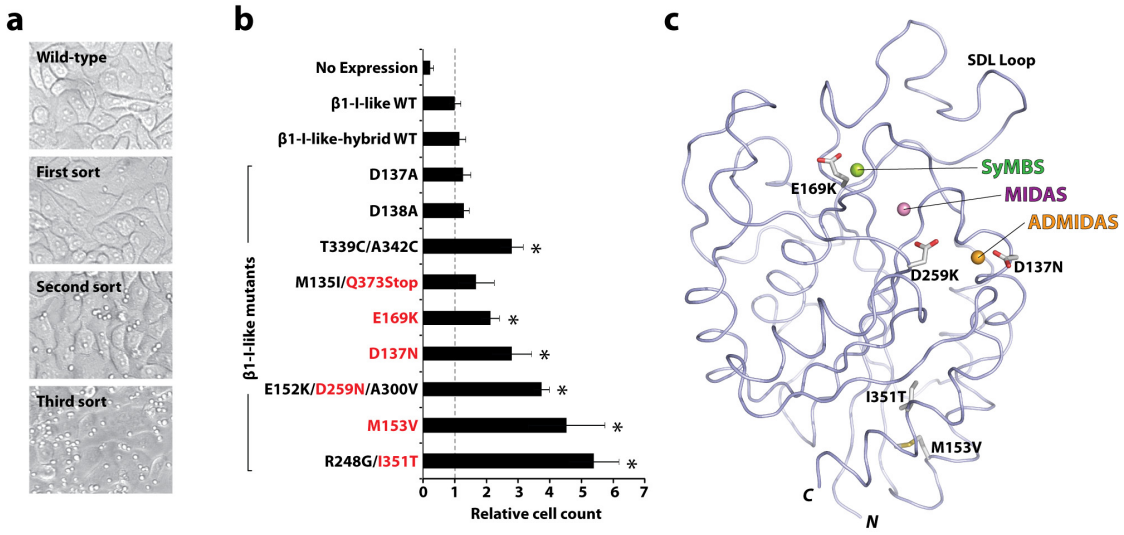

Figure A1.1. Enrichment of active mutants of β_1 I-like domain by directed evolution. (a) Yeast cells expressing the wild-type of the β_1 I-like domain or its mutagenesis library were sorted against HeLa cells surface up to third round of sorting. In the microscopic images, larger cells in the background are HeLa cells and smaller spherical cells are yeast cells. (b) Individual clones after the third sort were analyzed for binding to HeLa cells. Microscopic images were taken at random regions and were counted and normalized to the numbers of yeast cells bound in the wild-type case. Putative hot spots for activation, or the responsible substitution mutations that resulted in higher binding, are indicated in red. (c) Model structure of β_1 I-like domain is shown with the putative activating mutations. The three metal ion binding sites of I-like domain is indicated, SyMBS (green), MIDAS (purple), and ADMIDAS (orange). The specificity-determining loop (SDL) as well as the N- and C-terminus are also indicated.

for inactive and active states of β_1 I-like domain, we further analyzed the discovered mutations and categorized them into two groups: 1) activation by mutating the residues that coordinate the metal ion binding sites, and 2) activation by mutation in the hydrophobic socket that stabilizes the α7-helix of the I-like domain. Substitution of D137N, E169K, and D259N directly affected the metal ion binding sites of the I-like domain (Fig. A1.2, b-d). Unlike I domains, I-like domains possess three metal ion binding sites, denoted as SyMBS, MIDAS, and ADMIDAS. MIDAS provides the major binding site, whereas SyMBS and ADMIDAS render positive and negative regulatory roles in ligand binding [6] (Fig. A1.2, a-d). Asp-137 is one of the side chains that coordinate the ADMIDAS, and similarly as the rationally designed substitution D137A, directed evolution enriched yeasts that had D137N mutation. Intriguingly, we have selected a mutant with E169K, where Glu-169 residue participates in coordinating to the SyMBS that has been hypothesized to positively regulate the affinity of the MIDAS. In any of the previous I domain engineering studies, we have never encountered a direct mutation into the residues coordinating the MIDAS [1]. However, we found a substitution into Asp-259, which participates in the MIDAS. Based on the model structures and the previous crystals of other homologous I-like domains, we find that Asp-259 participates in both the MIDAS and ADMIDAS of the active conformation. Indeed, the metal ion coordination of Asp-259 is at a secondary shell, through a water molecule in the primary shell which is also held by Asp-130. Hence, we speculate that the substitution of D259N minimally affects the MIDAS, as ? can complete the coordination to the metal ion. A second mode of activation we found was at influencing rigidity or fluidity of the α7-helix (Fig. A1.2e). This type of allosteric switch has been demonstrated in α_M I domain, by mutating evolutionarily conserved Ile-316 in the α7-helix, which inserts into a hydrophobic socket, into the residues with smaller side chains [11-12]. The substitution I351T in

Figure A1.2. Rationalization of the effect of activating mutations in β_1 I-like domain. (a) Ribbon diagram shows the superimposed inactive and active model structures of β_1 I-like domain. The largest structural deviation between the inactive and active structures are colored yellow (inactive) and magenta (active). Distinct structural features, including SDL loop, α1-helix, β6-α7 loop, and α1-helix, and the three metal ion binding sites, SyMBS, MIDAS, and ADMIDAS, are indicated. (b) Sequence alignment between β_3 and β_1 I-like domains are shown in single letter amino acid sequences. The residues that coordinate the three metal ion binding sites are shaded with matching colors of SyMBS (green), MIDAS (purple), and ADMIDAS (orange). (c&d) Detailed conformational changes in the residues coordinating the three metal ion binding sites, between the inactive (c) and inactive conformations (d). Mutations discovered from directed evolution are shown in red. (e) The neighboring residues that form a hydrophobic socket for the allosteric switches found in the α7-helix, M153V and I351T, are shown.

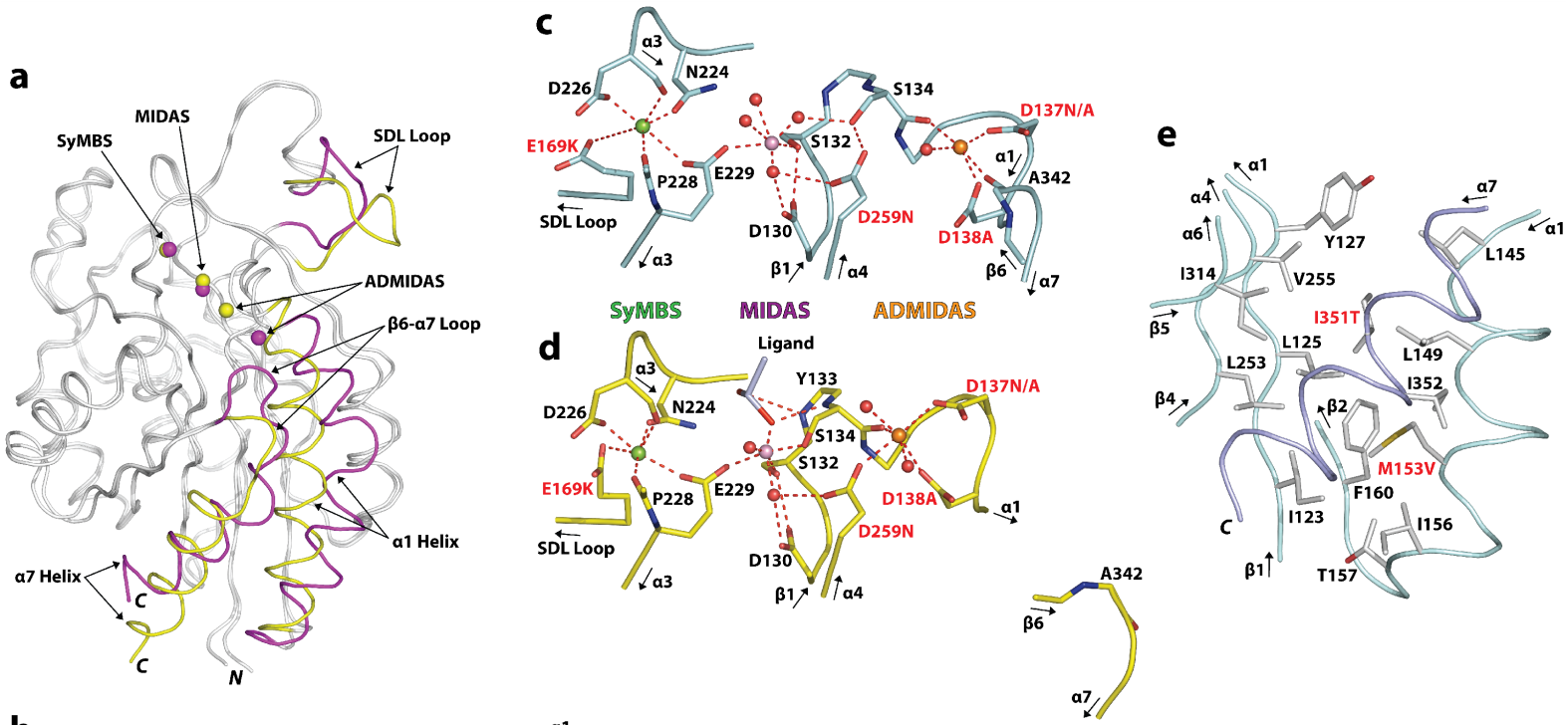

b

α1

β_3 109 DYPVDIYYLMDLSYSMKDDLWSIQNLGTKLATQMRKLTSNLRIGFGAFVDKPVSPYMYISPPEALENPCYDMKTTCLPMFGYKHVLTLTD

β_1 120 DYPIDLYYLMDLSYSMKDDLENVKSLGTDLMNEMRRITSDFRIGFGSFVEKTVMPYISTTP-AKLRNPCTSE-QNCTSPFSYKNVLSLTN

β_3 199 QVTRFNEEVKKQSVSRNRDAPEGGFDAIMQATVCDEKIGWRNDASHLLVFTTDAKTHIALDGRLAGIVQPNDGQCHVGSDNHYSASTTMD

β_1 208 KGEVFNELVGKQRISGNLDSPEGGFDAIMQVAVCGSLIGWRN-VTRLLVFSTDAGFHFAGDGKLGGIVLPNDGQCHLE-NNMYTMSHYYD

β_3 289 YPSLGLMTEKLSQKNINLIFAVTENVVNLYQNYSELIPGTTVGVLSMDSSNVLQLIVDAYGKIR

β_1 296 YPSIAHLVQKLSENNIQTIFAVTEEFQPVYKELKNLIPKSAVGTLSANSSNVIQLIIDAYNSLS

SyMBS
MIDAS
ADMIDAS

α7

β_1 I-like domain is analogous to I316G in aM I domain, as the mutation replaced Ile into a polar residue that would disrupt stable docking into the similarly positioned hydrophobic socket (Fig. A1.2e). Likewise, the substitution M153V would affect the interaction with the residues neighboring the α7-helix, thereby increasing the chance of the helix being displaced downward for higher affinity (Fig. A1.2e).

We then combined the two modes of activations, by adding the mutations found in the metal ion sites to the mutation in the α7-helix, I351T. The resulting double mutants, D137N/I351T, E169K/I351T, and D259N/I351T, were displayed on yeast and tested for binding to HeLa cells, and to surface-immobilized physiologic ligands, MAdCAM-1, fibronectin, and VCAM-1 (Fig. A1.3). We also included rationally designed mutations to create two more double mutants, D137A/I351T and D138A/I351T. The overall effect of the combination of the two types of mutations on ligand affinity were additive, such that all of the double mutants rendered more binders than single mutants. The binding of yeast cells expressing the double mutants to HeLa cell surface resulted in an increase of 3-fold in the numbers of binders than the single mutant I351T, and 20-fold compared to the wild-type (Fig. A1.3a). Purified ligands of β_1 I-like domain were immobilized on plastic surface and yeast cells were allowed to bind (Fig. A1.3b). Double mutants that used substitutions found from directed evolution were generally more potent binders than the ones rationally designed. For MAdCAM-1, the double mutants led to an increase of 10-fold in binding than the wild-type (Fig. A1.3b). For fibronectin and VCAM-1, the double mutants had about 6-fold and 20-fold higher binding than the wild-type, respectively (Fig. A1.3b).

Our results clearly indicated that β_1 I-like domain was engineered for higher affinity. The mutations identified by directed evolution are in accordance with the structural insights provided by other biochemical and crystal studies of homologous

Figure A1.3. Ligand binding of yeasts expressing double mutants of I-like domains. (a) Yeast cells expressing double mutants of β_1 I-like domains, D137A/I351T, D138A/I351T, D137N/I351T, E169K/I351T, and D259N/I351T, were tested for binding to HeLa cell surface. Other β_1 I-like domains, wild-type and the single mutant I351T, were also included for comparison. As controls, yeast cells expressing α_L I domain wild-type and active mutant K287C/K294C, and α_M I domain wild-type and active mutants, D132C/K315C and F302L, were included. (b) Double mutants of β_1 I-like domains were analyzed for binding to surface immobilized physiologic ligands, including MAdCAM-1, fibronectin, and VCAM-1. The data are presented as the average values of number of counted cells normalized to the wild-type, with error bars indicating S.D. (*$p < 0.05$, unpaired Student's t-test compared to control group, n=3).

a
Relative binding to HeLa
0
5
10
15
20
25
30
No Expression
αL-I-domain WT
αL-I-domain K287C/K294C
αM-I-domain WT
αM-I-domain D132C/K315C
αM-I-domain F302L
β1-I-like WT
β1-I-like I351T
β1-I-like D137A/I351T
β1-I-like D138A/I351T
β1-I-like D137N/I351T
β1-I-like E169K/I351T
β1-I-like D259N/I351T
b
Relative binding to VCAM-1
0
5
10
15
20
25
30
35
Relative binding to fibronectin
0
1
2
3
4
5
6
7
8
9
Relative binding to MAdCAM-1
0
2
4
6
8
10
12
14
No Expression
β1-I-like WT
β1-I-like I351T
β1-I-like D137A/I351T
β1-I-like D138A/I351T
β1-I-like D137N/I351T
β1-I-like E169K/I351T
β1-I-like D259N/I351T

integrins. Modular expression of I-like domain in bacterial expression system has been attempted before [13], but the study has neglected the biochemical and functional analysis, such as with conformational antibodies and ligands [14]. We are currently investigating a way to functionally produce the engineered I-like domains in a soluble form. Also, we note that there is a lack of antibodies directed to β_1 I-like domain. Our flow cytometric data have indicated that the previously known function-blocking antibody AIIB2 [15-16] does not show binding to β_1 I-like domain. The antibody, however, bound to yeast cells when β_1 I-like domain was expressed together with hybrid domain, suggesting that the antibody may target integrin β_1 by inhibiting the extension of the hybrid domain for activation. The remaining work involves using more detailed and comprehensive biochemical analysis, such as with surface plasmon resonance, to analyze the interaction of the double mutants of β_1 I-like domain and the ligands. We also anticipate that high affinity mutants will be useful in screening human antibody libraries to select for activation-specific function-blocking antibodies against β_1 integrins.

REFERENCES

1. Jin M, Song G, Carman CV, Kim YS, Astrof NS, Shimaoka M, et al. Directed evolution to probe protein allostery and integrin I domains of 200,000-fold higher affinity. Proc Natl Acad Sci U S A. 2006;103(15):5758-63.

2. Hu X, Kang S, Chen X, Shoemaker CB, Jin MM. Yeast surface two-hybrid for quantitative in vivo detection of protein-protein interactions via the secretory pathway. J Biol Chem. 2009;284(24):16369-76.

3. van Kooyk Y, Figdor CG. Avidity regulation of integrins: the driving force in leukocyte adhesion. Curr Opin Cell Biol. 2000;12(5):542-7.

4. Carman CV, Springer TA. Integrin avidity regulation: are changes in affinity and conformation underemphasized? Curr Opin Cell Biol. 2003;15(5):547-56.

5. Stewart M, Hogg N. Regulation of leukocyte integrin function: affinity vs. avidity. J Cell Biochem. 1996;61(4):554-61.

6. Zhu J, Luo BH, Xiao T, Zhang C, Nishida N, Springer TA. Structure of a complete integrin ectodomain in a physiologic resting state and activation and deactivation by applied forces. Mol Cell. 2008;32(6):849-61.

7. Chen J, Salas A, Springer TA. Bistable regulation of integrin adhesiveness by a bipolar metal ion cluster. Nat Struct Biol. 2003;10(12):995-1001.

8. Luo BH, Takagi J, Springer TA. Locking the beta(3) integrin I-like domain into high and low affinity conformations with disulfides. Journal of Biological Chemistry. 2004;279(11):10215-21.

9. Springer TA, Zhu J, Xiao T. Structural basis for distinctive recognition of fibrinogen gammaC peptide by the platelet integrin alphaIIbbeta3. J Cell Biol. 2008;182(4):791-800.

10. Xiao T, Takagi J, Coller BS, Wang JH, Springer TA. Structural basis for allostery in integrins and binding to fibrinogen-mimetic therapeutics. Nature. 2004;432(7013):59-67.

11. Xiong JP, Li R, Essafi M, Stehle T, Arnaout MA. An isoleucine-based allosteric switch controls affinity and shape shifting in integrin CD11b A-domain. J Biol Chem. 2000;275(49):38762-7.

12. Hu X, Kang S, Lefort C, Kim M, Jin MM. Combinatorial libraries against libraries for selecting neoepitope activation-specific antibodies. Proc Natl Acad Sci U S A. 2010;107(14):6252-7.

13. Baneres JL, Roquet F, Martin A, Parello J. A minimized human integrin alpha(5)beta(1) that retains ligand recognition. J Biol Chem. 2000;275(8):5888-903.

14. Takagi J, DeBottis DP, Erickson HP, Springer TA. The role of the specificity-determining loop of the integrin beta subunit I-like domain in autonomous expression, association with the alpha subunit, and ligand binding. Biochemistry. 2002;41(13):4339-47.

15. Humphries MJ. Integrin structure. Biochem Soc Trans. 2000;28(4):311-39.

16. Takada Y, Puzon W. Identification of a regulatory region of integrin beta 1 subunit using activating and inhibiting antibodies. J Biol Chem. 1993;268(23):17597-601.